THE UNIVERSITY OF HULL

BIOARTIFICIAL SCAFFOLDS FABRICATION AND THEIR USE FOR IN VITRO TESTING OF WOUND HEALING DEVICES

being a Thesis submitted for the Degree of

PhD Medical Engineering

in the University of Hull

by

Nicola Mandolini, MSc

08/2023

Abstract

In the last decades Negative Pressure Wound Therapy (NPWT) has shown its efficacy in wound healing, applying continuous or intermittent subatmospheric pressure to the wound surface by means of dressing systems. While there is general consensus that positive effects originate from a complex interplay of mechanisms such as deformations and exudate removal, uncertainty persists about the optimal mode of application and the consequences of this therapy at a cellular level. A better understanding of the skin mechanobiology in response to therapeutic stimuli using a bioreactor system can help to individualize future wound therapies in a reproducible and controlled environment.

This thesis proposed the fabrication of *in vitro* 3D skin models aiming to reproduce the relationship that occurs between cell types and skin substrate and investigated their use in a bioreactor in order to obtain new knowledge of NPWT mechanisms. Freeze-drying and electrospinning were considered to be the best methodologies to obtain homogenous and standardized 3D structures that were favourable for the purpose.

Highly porous pure collagen and collagen-based scaffolds were firstly created using the freeze-drying technique. Various cross-linking methods were assessed and directly compared to establish the most suitable to improve mechanical stability and physical properties. Meanwhile, fibrous structures that could resemble the topography of the extra cellular matrix (ECM) were produced with the electrospinning system using toxic-free solutions and an in-house-developed rotating collector. The prospect to fabricate a hybrid bilayer scaffold, combining the two techniques was also investigated and discussed.

Primary human skin fibroblasts were cultured on these structures and cell interaction and viability were evaluated through assays and microscopy techniques.

Lastly, a proof-of-concept bioreactor for NPWT investigation was designed and tested on the freeze-dried scaffolds demonstrating the feasibility of this research approach.

Results showed that blending methodology used in the freeze-drying can lead to scaffolds with unique physical properties while cross-linking has influence on substrate stiffness that guides cell response.

With regard to the electrospinning, the use of the rotating collector was found to be promising in obtaining a bimodal fibre distribution resulting in porous and orientated membranes that simulate the orientation of collagen fibres in the dermis of human skin and could be beneficial for cell infiltration.

To conclude, this study laid the groundwork for further development of these bioartificial scaffolds with improved properties that could be used as skin models and combined in a negative-pressure cell culture system with the aim to advance the understanding of NPWT biological mechanism and its clinical efficacy.

TABLE OF CONTENTS

LIST OF FIGURES

LIST OF TABLES

LIST OF ABBREVIATIONS

ε: Porosity/strain

σ: Stress

Φ: Water Uptake

AAc: Acetic Acid

ATR-FTIR: Attenuated Total Reflection - Fourier Transform Infrared

CL: Collagen

CT: Chitosan

CTRL: Control

DAPI: 4',6-diamidino-2-phenylindole

E: Young's / Elastic modulus

ECM: Extra Cellular Matrix

EDC-NHS: 1-Ethyl-3-(3-dimethylaminopropyl) carbodiimide / N-hydroxy succinimide

EtOh: Ethanol

GA: Glutaraldehyde

GAA: Glacial Acetic Acid

GAV: Glutaraldehyde Vapours

HDF: Human Dermal Fibroblasts

LMW: Low Molecular Weight

M: Molarity

MMW: Medium Molecular Weight

mQ: Milli-Q water

MTS: 3-(4,5-dimethylthiazol-2-yl)-5-(3-carboxymethoxyphenyl)-2-(4-sulfophenyl)-2H-tetrazolium

n: number of samples

NP: Negative Pressure

NPWT: Negative Pressure Wound Therapy

NXl: Non-crosslinked

PBS: Phosphate Buffered Saline

PCL: Poly(caprolactone)

PEO: Poly (ethylene oxide)

PVA: Poly (vinyl alcohol)

rpm: revolutions per minute

RT: room temperature

SEM: Scanning Electron Microscopy

UTS: Ultimate Tensile Strength

UV: ultraviolet

v/v: volume/volume

w/v: Weight/Volume

WU: water uptake

ACKNOWLEDGEMENTS

I feel grateful and proud to have reached the point where I can thank all the people that supported me during this challenging yet very worthwhile journey.

First of all, I would like to sincerely thank Dr Louise France for the opportunity to work in her research group and for her valuable supervision and continuous support. I would like to extend my thanks to technicians, collaborators and postdocs for their contribution and help during these years. To name few of them: Stuart, Mike and Simon in the Mechanical Engineering workshop for their assistance on my PhD project, Dr. Elizabeth Roberts for training and help with cell culture and Dr. Bongkot Ngamsom (Por) for sharing with me her knowledge and contagious positive energy.

A special thanks go to Peter Lobo-Kazinczi for his valuable advice and Garry Robinson for the SEM analysis and much more. They are two warm-hearted people always up for a chat that made me feel welcome every time I was with them.

Huge thank you to Noemi and Ana Maria, wonderful friends with whom I shared unforgettable moments.

Finally, the most important thank you is for my wife Vanessa, for her unconditional love and encouragement throughout these years. I could not imagine finishing my PhD without you on my side.

CHAPTER 1 Introduction

1.1 Motivation

The advent of skin tissue engineering has revolutionised not only the way wounds can be treated but also the way wound healing can be studied. One of the main applications consists in growing relevant cells in a template, known as a scaffold, to eventually have a viable three-dimensional tissue that can be manipulated and utilised in *in vitro* studies. In this context, although extensive clinical research has been done on Negative Pressure Wound Therapy (NPWT) demonstrating its beneficial effect on wound treatment [1], its mechanism of action at a cellular level remains still unknown and basic *in vitro* studies using cultured scaffolds could shed light on this research gap.

This doctoral thesis describes work which attempts to establish bioartificial scaffolds that hold features similar to the skin and are suitable to be utilised in studies that evaluate the effect of compressive and suction forces applied by NPWT on cells. In this respect, the development of an appropriate *in vitro* cell culture system combined with these scaffolds will enable to study the mechanism of NPWT under conditions similar to those used in clinical practice and have a better understanding of its efficacy from a perspective of cell behaviour.

1.2 Research aims and objectives

This section describes the individual aims that were defined to achieve the scope of the study introduced in the previous section. The first aim is to assess if bioartificial scaffolds manufactured with specific techniques and materials, possess properties similar to the skin and required for this application. The second aim is to develop an *in vitro* system that allows the application of therapeutical NPWT on the aforementioned scaffolds.

1.2.1 Aim I: Design and characterization of porous and fibrous scaffolds

The success or failure of a biomaterial is affected by chemical, physical and mechanical properties that interfere with cell-surface interaction, an important determinant of cell fate. Polymers, a sequence of repeating units, of natural or synthetic origin are mostly used in

tissue engineering for their material properties that allow them to be shaped into scaffolds. Furthermore, polymer blends offer the advantage to combine individual characteristics resulting in scaffolds with the desired features [2].

Collagen is the major component of the extracellular matrix (ECM) and is the most used biomaterial in skin tissue engineering applications [3]. Although it can be harvested from various animal sources, the preservation of its structural features during extraction and manufacturing process is crucial to maintain the physiological cellular response. Preparation of collagen by suspension or dissolution in water-based solvents can avoid denaturation of the protein. As a consequence, freeze drying method (Section 2.5.4.1) has been widely investigated in tissue engineering as a technique that will allow to obtain highly porous scaffolds by sublimination of the ice-crystals. Other advantages of this fabrication method are control over the pore size and structure and possibility to combine water soluble polymers in the solution.

Since elastin, the other most abundant protein in skin, is extremely difficult to blend as highly insoluble polymer, improving elasticity of collagen freeze-dried scaffolds and achieving physical properties similar to the dermal layer of the skin can be obtained by blending water-soluble polymers. Chitosan and polyvinyl alcohol (PVA), a natural and synthetic polymer respectively, have previously been blended with collagen due to their structural and biological properties [4]. Romanova et al. [5] studied the effect of chitosan as modifying component for skin tissue engineering concluding that chitosan stimulates fibroblasts activity only when used as an additive in collagen scaffolds, probably associated with improvement of mechanical properties. These findings were also demonstrated by Tangsadthakun et al. [6] that elucidated the role of chitosan molecular weight in collagen blends showing that scaffolds containing 30% of low-molecular-weight chitosan promoted and accelerated cell proliferation. With regard to collagen and PVA blends, elastic appearance and good interaction between the materials were shown when content of PVA was lower than 20% [7, 8] While these studies simply investigated mechanical and rheological properties, Choi et al. [9] also demonstrated the biocompatibility nature of PVA/gelatin porous scaffolds at different concentrations.

Although scaffold properties can be improved by blending, freeze-dried porous structures still require further physical/chemical crosslinking to enhance stability and mechanical properties [10]. In this respect, there is a lack of systematic and detailed studies on the influence of different cross-linking treatments on sponge porous scaffolds fabricated by

freeze-drying from blends of collagen-chitosan and collagen-PVA with a volume ratio that mimics *in vivo* ratio of collagen and elastin.

For this reason, in Chapter 3, the following objectives are pursued:

1. To develop collagen and collagen-based scaffolds in a reproducible and controllable way, with a homogeneous and porous topography that can host skin fibroblasts.
2. To understand if the addition of low amount of chitosan and PVA in collagen scaffolds can lead to biomaterials with improved properties.
3. To determine the effect of several cross-linking treatments on the physical and mechanical properties of these scaffolds.
4. To evaluate fibroblast viability and attachment on the produced scaffolds (Section 5.2).

While freeze dried scaffolds can provide a porous environment for cellular integration permitting fluid interchange and waste removal, the main structural components of the dermal layer of the skin are fibres. Electrospinning technique (Section 2.5.4.2) has been used for many years for fabrication of fibrous scaffolds aiming to mimic the structure of the dermis. Through the action of an external electric field, a polymer solution can be drawn in fibres by changing parameters such as flow rate, applied voltage and distance from the collector. The limitations of collagen in electrospinning are represented by the use of organic solvents that are toxic to cells as well as to humans and that may denature the protein structure. In addition, the low mechanical properties, rapid degradation and its poor spinnability shifted the attention to synthetic polymers that can also be dissolved in green solvents or water-based solutions. Polymers such as polycaprolactone (PCL), polyethylene oxide (PEO) and chitosan have been blended and electrospun [11, 12] demonstrating good suitability for tissue engineering applications. Design modifications, processing conditions and interactions between these polymers and different solvent systems could lead to production of scaffolds with unique properties caused by alterations in their orientation and morphologies. Hence, proper control over fabrication is essential to achieve a balance between mechanical and biological properties for skin tissue engineering applications.

For this reason, in Chapter 4, the following objectives are pursued:

1. To assess the spinnability of PCL, PEO and chitosan blends in low-toxic solutions.
2. To assess if the use of an in-house electrospinning rotating target can facilitate the fabrication of fibrous membranes and generate scaffold with enhanced properties.

3. To evaluate the morphology, physiochemical and mechanical properties of these fabricated scaffolds.
4. To assess fibroblast interaction with these fibrous membranes.

1.2.2 Aim II: Fabrication of a platform to assess skin scaffolds under therapeutical NPWT

Although there is general consensus that negative pressure leads to improved would healing, its optimal application mode is not much supported in the literature. The scarcity of studies on this topic is mainly due to the difficulty in reproducing NPWT *in vitro* considering its complex mechanism of action. Researchers have tried to develop special negative pressure cell culture chambers in which NPWT was delivered to cells attached to plastic substrates [13] or seeded in fibrin matrix [14]. The possibility to test clinical application of NPWT *in vitro* on bioartificial scaffolds for studying the link between NPWT stimulation and biological response still need to be investigated.
For this reason, in Chapter 5, the following objectives are pursued:

1. To produce a bilayer scaffold combining electrospinning and freeze drying to make use of the advantages offered by both techniques to better mimic skin structure.
2. To determine cellular biocompatibility of clinical relevant scaled-up scaffolds performing *in vitro* cell culture studies and scanning electron microscope analysis.
3. To design an easy-to-use, proof-of-concept bioreactor that can allow application of clinical NPWT on bioartificial scaffolds cultured with skin fibroblasts.

1.3 Thesis overview

This thesis consists of seven chapters. Chapter 1 gives a brief explanation about motivation for this work, describes its aims and objectives and the thesis structure. Chapter 2 covers the literature review leading to project requirements while Chapters 3, 4 and 5 contain the experimental work of this doctoral thesis. In Chapter 3, the fabrication of porous collagen scaffolds using the freeze-drying method is described with particular interest to the reproducibility of the methodology. The addition of natural and synthetic polymers, chitosan and polyvinyl alcohol respectively, to collagen and the effect of four crosslinking methods on the morphology and mechanical properties of these low-density structures are studied and discussed. In Chapter 4, the use of electrospinning is investigated to create

fibrous structures starting from low-toxic solutions of PCL, PEO-CT and PCL-CT collecting fibres on an in-house-built rotating disk and on a static platform. Morphological, physical and mechanical characterization of these membrane is performed to understand the influence of the rotating disk on average fibre diameter, distribution and arrangement of fibres. The effect of these morphological features is also evaluated with respect to skin fibroblasts behaviour. Chapter 5 is dedicated to assessing cell behaviour on freeze-dried and bilayer scaffolds and to the fabrication of an easy-to-use proof-of-concept bioreactor that can be combined with single use NPWT device. Its efficacy is tested on porous scaffolds cultured with human dermal fibroblasts. In Chapter 6, a general discussion is presented to summarise results and findings. Lastly, in Chapter 7 conclusions are drawn and future directions for continuing this work provided.

CHAPTER 2 Research background

2.1 Anatomy and physiology of skin

2.1.1 Structure

Skin is undoubtedly the largest part of the body. It has distinct functions such as providing protection to underlying structures, representing a mechanical barrier against environmental agents and pathogens and being responsible for thermoregulation and fluid homeostasis of human body preventing dehydration.

The skin can be considered as the supporting area for all external forces that act on the body. It is composed of three layers (Figure 2.1):

- *Epidermis*

Epidermis consists of 4 sublayers, *basalis*, *spinosum*, *granulosum* and *corneum* that in totality have a thickness ranging between 75 and 150 μm (up to 600 μm on palms/soles).

The outermost layer is known as *stratum corneum*, composed of dead cells called 'corneocytes' because the primary cell type of the epidermis, the keratinocyte, undergoes a process known as cornification. From the innermost layer *stratum basalis*, new generated living cells move toward the surface differentiating and ending to form the *stratum corneum*. These cells are continuously sloughed off from the skin surface by the rubbing or washing process.

The epidermis is an avascular layer that only obtains nutrients from dermis. Cells adhere tightly to each other by complex membrane-associated plaques called desmosomes providing a barrier against atmospheric factors. Also, these bonds occur between keratinocytes and the basement membrane (BM) that separates and adheres epidermis and dermis together. Composed mostly of collagen IV, the basal lamina is a complex molecular structure resembling a sheet-like substratum.

In addition to keratinocytes (95%), the epidermis also houses melanocytes, fabricators of pigment, Langerhans cells, sentinels against invaders and Merkel cells, associated with the sense of touch and the discrimination of shapes and textures. Moreover, the epidermis contains a subpopulation of slow-cycling stem cells that are possibly of critical importance to the regenerative potential of human skin.

- *Dermis*

Underneath the epidermis, anchored to basement membrane by collagen VII fibrils and fibrillin-rich microfibril bundles, lays a connective tissue named *dermis*. Its thickness varies significantly across the body, but it is between 15 to 40 times thicker than the epidermis (3-5 mm). Although structurally complex, two regions in the dermis can be distinguished: *stratum papillare* and *stratum reticulare*. Both the layers are composed of proteins such as collagen and elastin arranged in an intricate fibrous structure of extracellular matrix (ECM) that harbours specialized cells.

The diameter of collagen fibres ranges from 2 μm to 15 μm; they are smaller in the papillary dermis that is dominated by collagen III, whereas in the reticular dermis dominated by collagen I they are sensitively larger. Overall, the ratio of collagen I to collagen III is 4:1. Similar to collagen, elastic fibres tend to be smaller in the papillary dermis and thicker in the reticular dermis.

The ground substance that forms the interfibrous milieu is composed mainly of glycosaminoglycan (GAGs) that are classified in four categories: hyaluronic acid, chondroitin sulphate/dermatan sulphate, heparan sulphate and heparin and keratan sulphate. These molecules are covalently linked to peptide chains, except for hyaluronic acid, to form high-molecular-weight complexes called proteoglycans. The main function of this layer is to absorb stress and strain. However, once injured it is not capable of true regeneration in postnatal life. In contrast to the epidermis, the dermis heals through a process known as scarring.

What makes dermis complex is the presence of several structures such as plexus of blood vessels, lymph vessels, nerve endings, glands, sense receptors and hair follicles and distinct types of cells. Fibroblast is the major cell type of the dermis, responsible for both the synthesis and the degradation of dermal proteins but other cell types associated with the vascular, lymphatic and nervous systems are abundant.

- *Hypodermis*

Subcutaneous fat tissue or hypodermis consists of loose connective tissue and cells, mainly adipocytes (50%). Hypodermis carries out three essential functions: attaching the dermis to the muscles and bones, it minimizes mechanical injury to skin (energy-absorbing layer), controls the body temperature and it is an energy reservoir where lipids can be easily accessed and catabolized on demand.

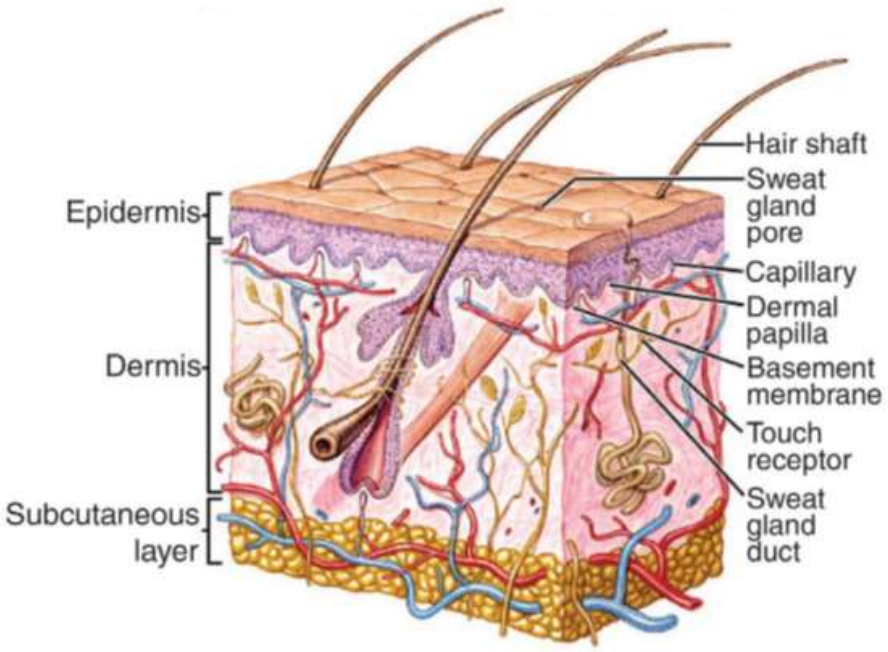

Figure 2. 1 Representative image of the structure of human skin showing the three layers and the complexity of the thicker dermal layer with hair follicles, sweat glands and capillary vessels [15].

2.1.2 Factors affecting skin structure and behaviour

During life, skin aspect changes not only aesthetically but structural and functional alterations take place as well. This affects mechanical properties of the skin and it is a factor to consider in skin studies.

The most studied factor that affects skin aspects is the age. Changes in Young's modulus make evident the decline of skin function with age becoming thinner, stiffer and less flexible [16]. This is associated with alterations that occur in the ECM such as a reduction in collagen, elastin network and a decrease in viscoelastic properties of ground substance [17]. Mechanical and morphological changes are also related to individual factors such as if the subject is a smoker or has genetic diseases. Another external element is the exposure to ultraviolet (UV) radiations that damage and degrade collagen fibres. Even the race counts. Although data have mostly been obtained from Caucasians, studies have demonstrated that the African skin was thicker and lower in lipid and water content whereas Asian skin resulted to be the thinnest and the highest in lipid and water content [18].

Another significant factor is the location of the skin. Despite similar collagen concentration across the body, structure influences the elastic modulus with collagenous framework that anchor the skin with different patterns [19].

2.1.3 Mechanical properties

Skin has a non-linear, viscoelastic, anisotropic behaviour due to multi-layered composition. Every layer holds distinctive characteristics but the behaviour of skin during mechanical tests can be considered similar to a homogeneous material [20].

The mechanical properties of the skin are closely related to composition and organization of the dermis, therefore dependent on the spatial arrangement, morphology, and cross-linked density of collagen fibrils, orientated in a wavy way allowing stretch but not overstretch, and on elastin fibres that provide elastin recoil strength [21]. The need to understand mechanical properties of the skin has led to perform tests using experimental techniques and studying how it responds to various mechanical loading. It is convenient to separate mechanical tests in two categories, those carried out *ex vivo* and those *in vivo*. *Ex vivo* experiments are usually performed measuring uniaxial or biaxial stress and strain in tensile tests. While for uniaxial tests the material is cut into strips or dog-bone shaped specimens, for biaxial tests square samples are clamped in a machine that exerts stretching in two directions independently. On the other hand, *in vivo* tests are largely based on indentation, suction, torsion methods. Suction refers to the measurements of skin elevation by applying vacuum of 50-500 mbar through a circular aperture. Torsion tests apply constant torque on the skin reducing the effect of underlying tissues and anisotropic behaviour.

The best method or gold standard is still not defined. Despite the tissue is not in its natural environment, uniaxial tensile test remains the most convenient and used in research. The main advantage is the possibility to study ultimate failure stress and control the size of the skin sample that in *in vivo* tests has an undefined geometry. Furthermore, it allows to measure the viscous properties of the skin in hysteresis, relaxation and creep experiments.

2.1.3.1 Stress-Strain relationship

The stress-strain curve describes how the studied material deforms under applied stresses and information such as elastic modulus (Young's modulus) (E) that is the amount of stress (force per unit area) required to produce a given amount of strain (stretching), can be

extrapolated. The relationship between stress-strain of the skin reported in Figure 2.2 is obtained applying variable force to the excised tissue and measuring the strain.

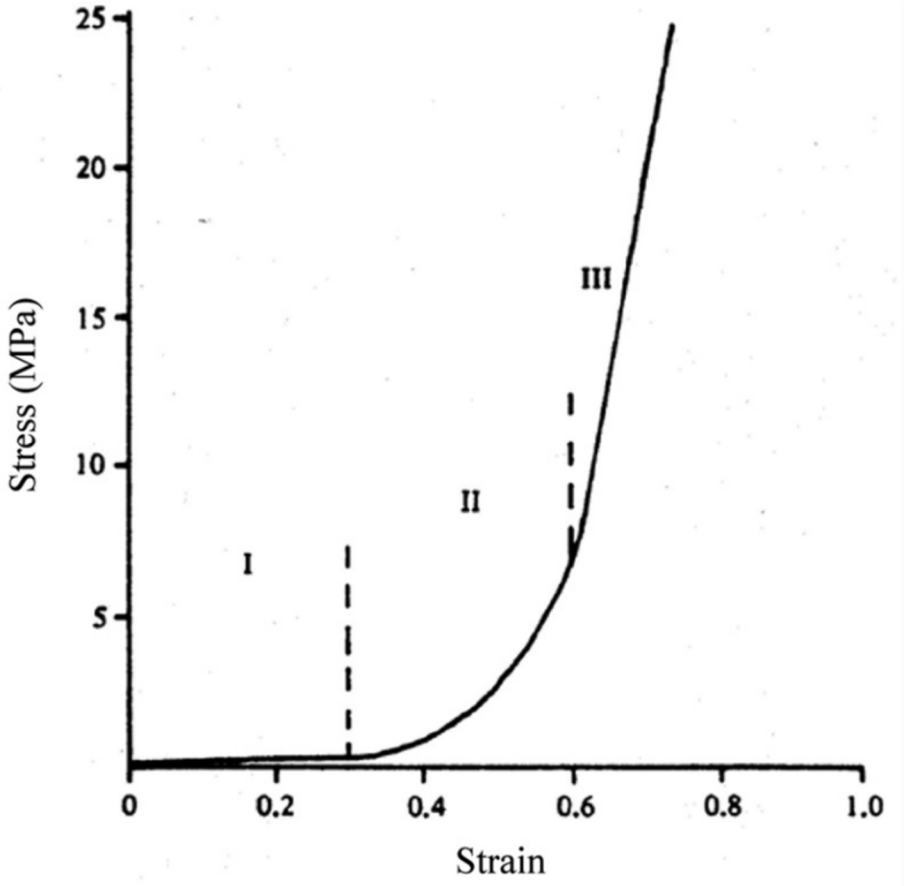

Figure 2. 2 General relationship stress-strain for skin showing the three stages in which collagen fibres in wavy configuration (I) are getting aligned (II) until reaching the maximum stiffness (III) [22].

The curve can be divided into three distinctive phases. In the first stage, the stress-strain relation is almost linear where elastin fibres are responsible for the skin stretching whereas the collagen contribution can be neglected. The Young's modulus is calculated in this phase before the yield point, from which the material will no longer deform elastically. In the second phase, due to straightening of the wavy collagen bundles, similarly to springs, there is an increase of resistance. Then in the last phase, collagen fibres are aligned and gradually break until reaching the ultimate tensile strength.

Even though there is variability in methods and samples, from *in vivo* and *ex vivo* tensile tests it is possible to range the elastic modulus of decellularized skin between 1 and 10^2 MPa [6] while ultimate tensile strength is reported to be in a range of 1 to 16 MPa [24] with values that increase with increasing strain rates and with respect to Langer's lines

[25]. Independently from strain rate, it is recognized that skin exhibits anisotropic behaviour.

2.2 Wound overview

2.2.1 Types and classification

The term “wound”, in brief, is used to describe a break of the skin’s integrity. There is a wide variety of wounds that classify based on aetiology (burns, arterial and venous ulcers, diabetic ulcers, pressure ulcers and traumatic) and on the severity of tissue damage, with involvement of muscle, bone, nerve and whether infection is present.
Wounds can be also categorized based on morphology, partial or full thickness depending on the layers involved. The first one is confined to epidermis and dermis whereas a full thickness wound extend underneath the dermis. Wounds at a certain depth (1/3 of the dermis) heal showing no visible scar while full-thickness wounds heal exclusively with scarring and wound contraction, leading to cosmetic and functional defects.
During wound assessment is important to evaluate the time wounds take to heal. Based on timing, it is possible to further classify *acute* wounds that show signs of normal healing after a brief period of time, and *chronic* wounds that fail to heal in more than a month requiring continuous management.

2.2.2 Wound healing

The process of wound healing involves a series of complex interactions between cells, the ECM, cytokines and growth factors. These are described in a series of stages (Figure 2.3), which often overlap:

1. *Haemostasis*. It is the process in which bleeding stops after the injury. Vascular permeability is initially increased to permit cells to migrate from disrupted blood vessel to the nearby tissue and a temporary fibrin clot forms acting as ECM for cell migration. Vasoconstriction follows in response to signals from trapped cells within the clot. Thus, coagulation occurs as platelets aggregate with fibrin, which is deposited in the wound following its conversion from fibrinogen, a soluble protein. Platelets trigger inflammatory response by the release of vasodilator growth factors that attract neutrophils, signalling the beginning of inflammation.

2. *Inflammation*. In this second overlapping step, blood vessels start to dilate and inflammatory cells, mainly macrophages, reach the injury site removing debris and rising the exudate level. This phase lasts for approximately 4 days.
3. *Proliferation*. It occurs 3-5 days after the injury and lasts up to 3 weeks. Fibroblasts that migrated into the fibrin matrix, produce new ECM while the clot is degraded by enzymes and angiogenesis takes place. As the number of macrophages decreases, various growth factors are secreted by fibroblasts, endothelial cells, and keratinocytes. During the proliferative phase, wound closure occurs through three simultaneous processes: reepithelialisation, ECM formation and contraction. The last two events are the result of fibroblasts migration in the wound site that inducted by certain grow factors, differentiate in myofibroblasts, cells that provide the contractile force.
4. *Remodelling*. Following wound closure, remodelling is the final phase of the process in which collagen fibres and blood vessels formed during proliferation phase are no longer necessary and are removed by apoptosis.

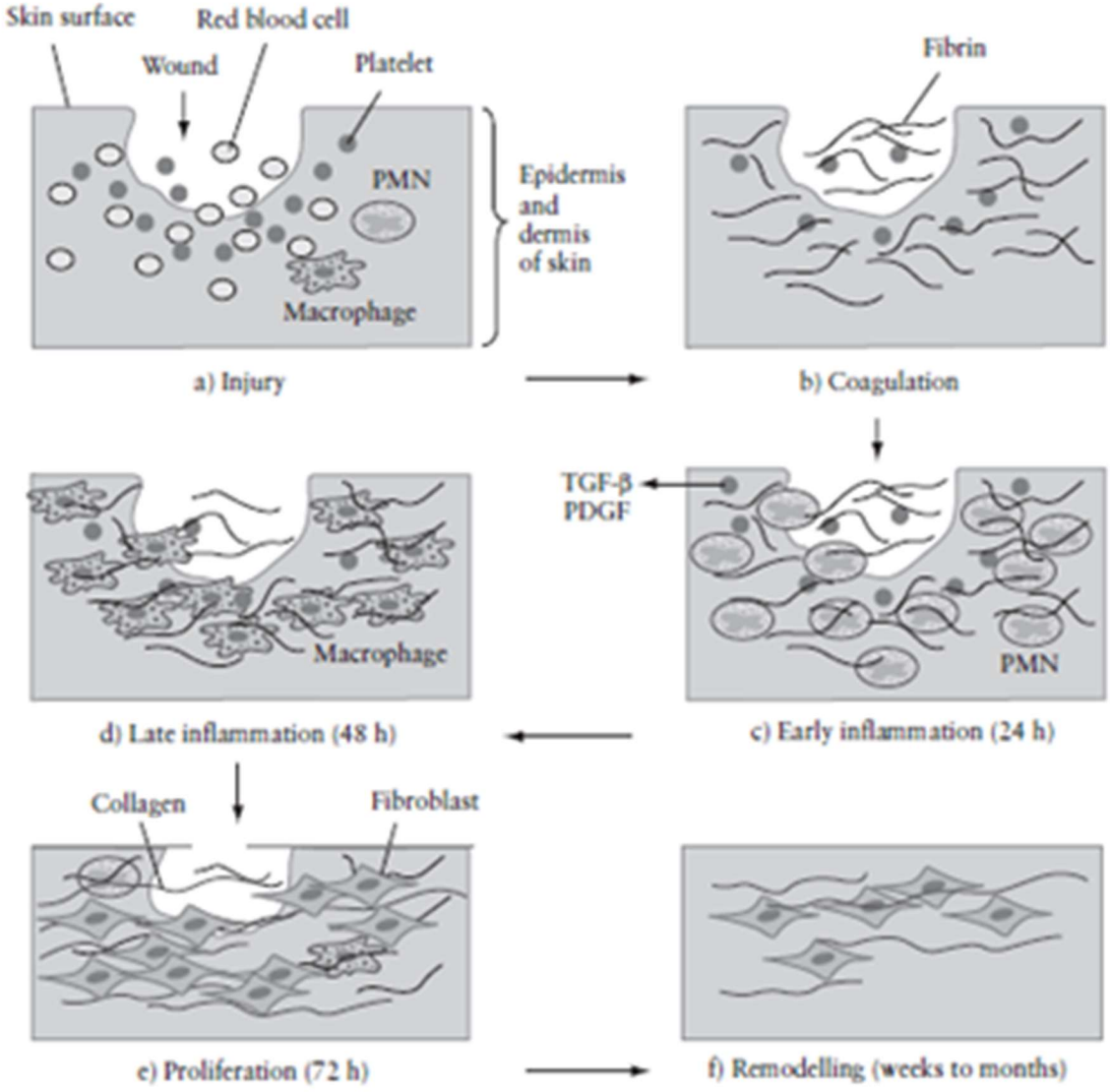

Figure 2. 3 The phases of wound healing following cutaneous injury (a). Vasoconstriction and coagulation (b) are followed by inflammation phase with factors and signals released from platelets (c) and macrophages replacing neutrophils (PMN) (d); these cells release growth factors attracting fibroblasts (e) that synthesize collagen to finally obtain structure reorganisation and wound closure (f) [26].

The phases described above refer to the *repair* process, a physiological adaptation in which skin, after tissue loss, re-establish continuity by synthesis of scar tissue and contraction without restoration of the normal tissue.

2.3 Wound healing devices

2.3.1 Negative Pressure Wound Therapy

Negative Pressure Wound Therapy (NPWT) is a widely accepted advanced technique that can accelerate wound healing by delivering negative pressure (NP). The term "negative" indicates pressure values that are below atmospheric pressure. Other terms used are sub-atmospheric pressure, vacuum assisted closure (VAC) or micro deformational wound therapy.

The traditional system that permits to apply NP is composed of five elements: a porous material as a filler placed into the wound (foam or gauze), a gas semipermeable adhesive drape to isolate wound environment, a suction tube (drainage) connected to the suction device and an exudate-collecting reservoir (Figure 2.4 A). However, in the last years, single use NPWT devices have been developed to offer improved clinical performances as well as a portable and lightweight alternative to the traditional system (Figure 2.4 B). These devices have an enhanced dressing system that allow exudate evaporation, eliminating the use of a canister and offer the possibility to be utilised without the filler.

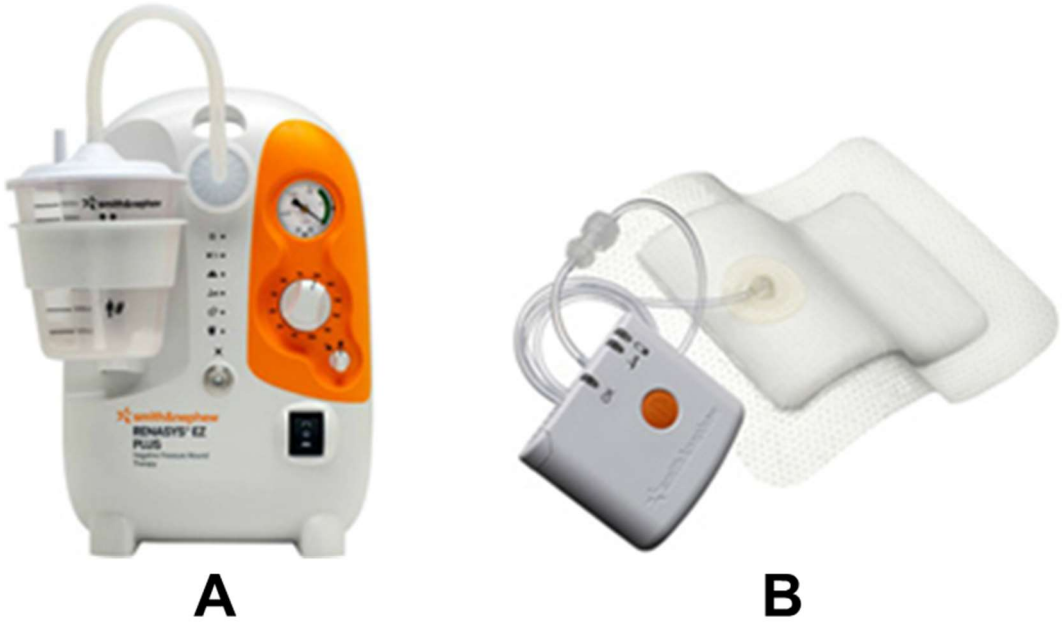

Figure 2. 4 Overview of Smith and Nephew's NPWT devices, traditional system RENESYS (A) and single use PICO (B).

The NPWT refers to any device that can apply vacuum to the wound resulting in a series of primary and secondary effects that enhance wound healing [1]. The role of the filler is to facilitate pressure transmission on the wound bed while the adhesive drape seals the wound maintaining a sterile and moist environment. The pressure of vacuum therapy usually ranges between 50 and 150 mm Hg and can be applied in a continuous and/or intermittent mode until the wound is closed.

In the last 20 years, the efficacy of NPWT in wound healing has been confirmed but no unifying theory exists on mechanism of action. To demonstrate clinical evidence and to support clinicians choosing parameters to enhance NPTW efficacy, more research is needed.

2.3.1.1 Mechanical forces

The mechanism of NPWT acts in primary and secondary mechanisms and involves a series of forces (Figure 2.5) that permit to achieve wound healing.

At the macroscale, primary forces are applied leading to wound deformation known as wound shrinkage. Here, centripetal forces and tension exert onto the wound's margins and their extent depends on the mobility of the area and on the attachment to the underlying structures. The extent of contraction is largely dependent on the deformability of the wound [27]. The optimal setting by which a better contraction occurs is debatable but an intermittent pressure ranging between 50-75 mm Hg has been showed to reach a maximum area reduction [28, 29].

Simultaneously, deformations also occur at the microscale level. The topography of the wound filler is transmitted by the pressure and distributed evenly to the wound bed, causing mechanical stress and strain that skin cells perceive and convert into chemical and electrical signals in a process named mechanotransduction.

Compression forces through the filler have demonstrated to be essential for stimulation of angiogenesis bringing an increase in micro vascularization. Blood flow which delivers oxygen and vital nutrients while removing waste products is essential for wound healing [30]. However, these changes are not uniform. Numerous studies reported a decrease in blood flow in proximity of the wound but an increase distally from the edges of the wound [31].

Also, NP application has the function to remove large amount of potentially toxic fluid, exudate, at certain rates generating shear and hydrostatic forces that are sensed by cells while maintaining an insulated and moist environment.

In this context, it is evident that NPWT application plays a critical role in regulating tissue growth [32], influencing cell behaviour in terms of differentiation, proliferation and migration [27]. Therefore, stresses and strains to the wound bed can be regulated by four factors:

1) Levels of pressure applied and frequency. One pressure level cannot fit all types of wounds and cannot be maintained for the whole cycle of treatment, suggesting that optimal pressure cycle waveforms should be optimized. Level of negative pressure from 50 to 120 mm Hg are effective on the therapy but for pain relief it should be reduced to 50-75 mm Hg [29].

2) Morphology of the filler. The tissue distends into the foam pores experiencing high tension or dilatation whereas regions in contact with foam struts experience compressive strains [33].

3) Constitutive behaviour of the filler material. Strut deformations, frictional interaction and resulting constraints on the tissue surface depend on intrinsic material properties of the dressing.

4) Tissue response. Response of the tissue bed itself that changes over time due to continuous remodelling of ECM.

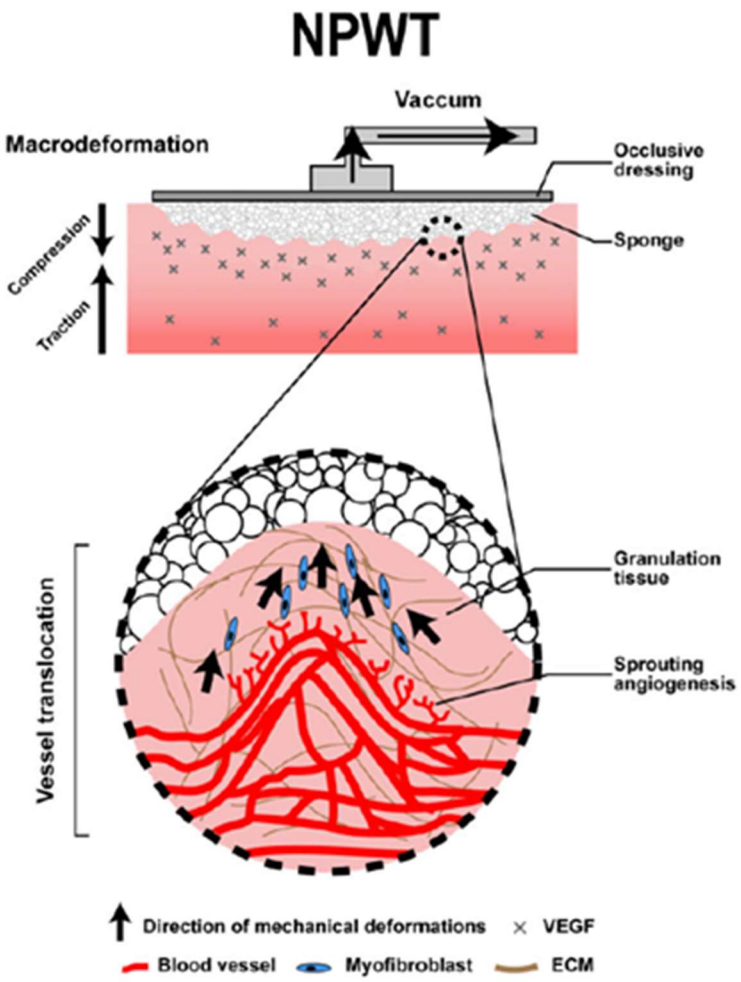

Figure 2. 5 Summary of proposed mechanism(s) involved in NPWT: tissue deformation and interaction between the dressing and the wound surface [34].

2.3.2 Electrical Stimulation

Since researchers have discovered that a decrease in electric current produced by wounds during the injury phase may be linked to a resulting stationary phase in wound healing process, electrical stimulation has been used to support and promote repair and regeneration phase. It has been approved at the beginning of the new century and since then, it has been gaining growing acceptance although more evidence is still needed.

During the healing process, wounds create an electric field around the injury site with a gradient that decreases when moving away from the wound. The current can be maintained using an occlusive dressing, but it gradually diminishes in intensity as the wound is unprotected or starts to heal.

Undamaged skin has an electrical potential generated by movements of ions Na^+, K^+ and Cl^- across the cell's membrane. The sum of these potentials is called trans-epithelial potential (TEP) and is typically few dozens of mV but following an injury, a flow of current generates an electric field named 'current of injury' (Figure 2.6) [35].

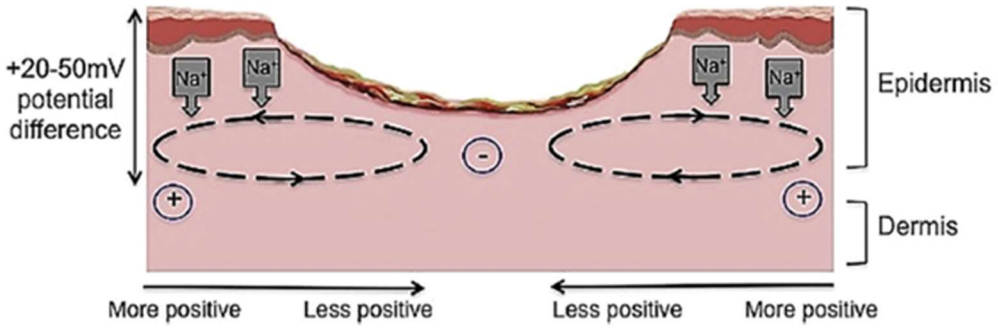

Figure 2. 6 Current of injury. From initial transcutaneous endogenous electrical potential of 20-50 mV, current of injury is generated through epidermal disruption [35].

Various forms of electrical stimulation are available and they are applied by tissue pin, dressing electrodes or wireless devices. The most used modalities included alternating current (AC), high- or low-voltage pulsed current (HVPC, LVPC), and low-intensity direct current (LIDC). Pulsed currents consist in a brief but recurring stimulus followed by a period of non-stimulation (< 1 ms). Low-intensity currents (LIC) are considered to resemble the currents produced by the human body with intensity inferior or equal to 1 mA. Electrical stimulation (ES) has been reported to promote and accelerate wound healing although it is not excluded the possibility that wound healing occurs naturally considering the long-time frame needed to assess results. Moreover, the variability in the parameters of ES application and the differences in types of wounds do not permit to draw a conclusion to the optimal ES for wound healing.

For these reasons, researchers are beginning to use electrical stimulation *in vitro* [36] to provide insights into the cellular and physiological mechanism by which ES enhances wound healing.

2.4 Introduction to Tissue Engineering

Tissue Engineering (TE) can be defined as a multidisciplinary field involving biology, chemistry, medicine and engineering that through the understanding of structure and function of tissues and organs aims to heal, maintain, restore or enhance them combining cells, biomaterials, and biologically active molecules.

Despite engineering efforts to reproduce components and function of human tissues, the biological system is extremely complex, versatile and adaptive.

The topic of TE is incredibly broad in scope and there are strategies that can be adopted in the TE field. However, the use of scaffolds which permit cell attachment, migration and proliferation with subsequent tissue formation for *in vitro* and *in vivo* studies is the most investigated. Skin has been at the forefront of TE and some of the first successful medical products have emerged from this field.

2.5 Wound models

With the aim to obtain new knowledge of the complexity of wound healing process and assist formulation of hypotheses, the use of a model is strictly necessary. The choice of the model depends upon several factors such as type of investigation, relevant parameters and desired outcomes.

Until few decades ago, research on wounds was only based on animal models. Although these studies have been valuable, ethical issues and cost has diverted the research field towards *in vitro* models that constitute an alternative and a method to study and screen treatments before starting *in vivo* experiments.

During recent years due to the advantages that *in vitro* models have over *in vivo* ones, the awareness of how they may play an important role in the investigation of treatments and potential therapeutic solutions has increased. Nevertheless, animal models represent an exact replicate of a clinical situation and enable to understand basic mechanisms present in the wound healing cascade. A list of advantages and limitations in using *in vitro* models to investigate wound healing process is reported in Table 2.1

In 2D wound healing assays, wound closure is simulated creating defects in cell monolayers grown on various substrates to study migration, proliferation and protein synthesis [37]. However, these models are representative neither of complexity of the wound healing process nor the behaviour of cells.

Hence, the use and development of 3D *in vitro* models that allow to study in a reliable and reproducible way the mechanism of healing, cell-cell and cell-matrix interactions is necessary [38].

Table 2. 1 Advantages and disadvantages of in vitro wound healing models.

Advantages	Disadvantages
• Rapid, simple, cost-effective process • Involvement of minimal ethical issues • Homogeneity of models and reproducibility (enhancing statistical significance) • Analysis of contribution that a single group of cells has and examination of single tissue components • Manipulation of the model (using different cell lines and revised parameters)	• Limited investigation, not involve whole body • Limited clinical relevance (impossibility to truly replicate the structure and function) • Results based on healthy organisms

2.5.1 3D *in vitro* skin models

To date, in addition to clinical purposes, the interest in using 3D tissue engineered skin models has become established to reduce animal experimentation and diminish the research costs. The advantage of *in vitro* studies lays on the possibility to control tissue characteristics and monitor the formation of substrate-cell architecture in order to examine cell behaviour and molecular response.

Although fabrication of skin models that closely resemble native tissues has been carried out using various techniques and materials, there is still a need to create valuable scaffolds that can be used for functional tissue engineering or to advance the understanding of certain mechanism of action. 3D *in vitro* models typically involve the combination of cells and a 3D structure intending to mimic the native environment. There are clearly differences between these models and native skin but research is still interested in engineered scaffold to investigate and assess aspects of skin biology [39]. Many factors should be considered to select which model and parameters are relevant for the study such as type of investigation, mechanical properties and biological characteristics.

The constructs used for wound healing model are essentially skin-like structures that are mechanically, thermally or electrically damaged to generate a partial or full-thickness

wound. Despite several attempts to standardize the fabrication process of equivalent skin tissue [26-28], a 3D skin model that can cover all types of investigation is still to be made. The main issue lies in the fact that the composition and structure of these models is much simplified compared to the native tissues (Figure 2.7), due to the absence of skin adnexa (hair follicles, sweat glands, etc).

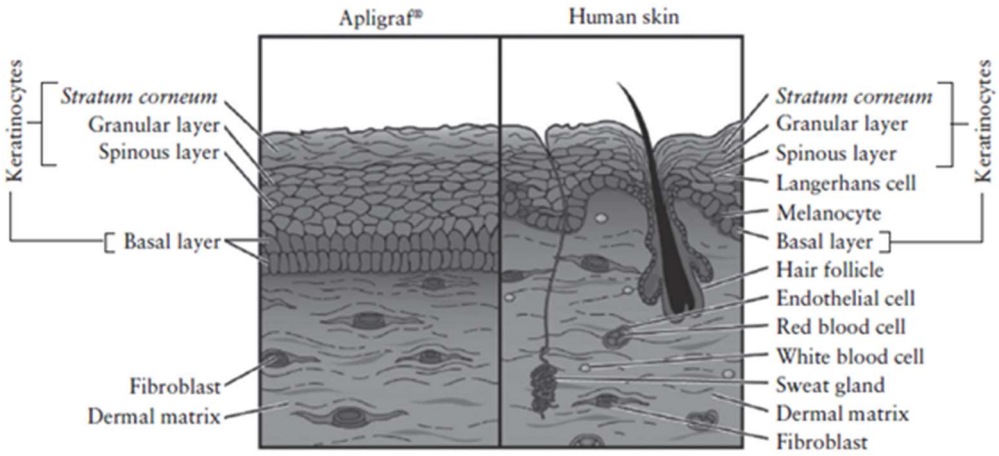

Figure 2. 7 Comparison between an example of artificial skin and normal skin [26].

Skin models can be derived from human tissue (autologous or allogeneic), nonhuman tissue (xenographic), fabricated as composite co-culture or from synthetic and natural materials. A brief synthesis of advantages and disadvantages of each source used for skin models is given in Table 2.2.

Table 2. 2 Characteristics of various sources used to create skin scaffold.

	Advantages	Disadvantages
Human and nonhuman tissue	• Native Architecture	• Limited availability • Risk of infection and immunological rejection • Source variability • Sterilizability
Composite co-culture	• Control of structural features • Biological function	• Source variability • Simplified version of ECM
Synthetic and natural materials	• Complete control of the structure • No risk of disease transmission • Reproducibility • Sterilizability	• Homogeneity • Inability to reproduce biological interactions

Bioengineering skin scaffold can be broadly divided into epidermal, dermal and dermo-epidermal substitutes [43]. They are used to provide the barrier function, aid to wound closure and to promote healing of the wound. Most dermal equivalents in current use are frequently presented as "dermal regeneration templates", structures that can host fibroblasts and endothelial cells to generate "neodermis".

On the market, there are many commercially available skin substitutes and they are mainly projected and developed to promote wound healing through tissue integration and regeneration acting as active wound dressing.

Some examples of these equivalent models of skin are reported in Table 2.3.

Table 2. 3 Some examples of commercially available skin scaffold and their composition.

Dermo-epidermal	
Apligraf®	Human fibroblasts and keratinocytes in bovine collagen I sponge
OrCel®	Human fibroblasts and keratinocytes in bovine collagen I sponge
Integra ®	Bovine collagen I and chondroitin-6-sulfate crosslinked with polysiloxane pseudoepidermis
Dermal	
Alloderm®	Lyophilized cadaveric skin deprived of epidermis and cellular component
AlloDerm®	Allogeneic acellular human dermis
Biobrane®	Silicon membrane bonded to porcine collagen coated nylon mesh
Dermagraft®	Fibroblasts in a biosynthetic polyglycol acid mesh cryopreserved
EZ Derm™	Porcine dermal crosslinked collagen
Hyalograft 3D™	Hyaluronic acid membrane with laser-perforated micro holes with human fibroblasts
KaroDerm™	Human acellular dermis
Pelnac™	Silicon fortified atelocollagen type I from porcine tendon
Permacol™	Porcine dermis derived collagen and elastin acellular matrix
SureDerm®	Human acellular lyophilized dermal tissue
Terudermis®	Bovine dermal type I collagen thermal crosslinked and silicone
Transcyte®	Human fibroblasts in nylon mesh coated with bovine collagen and bonded to a silicon membrane
Xenoderm®	Freeze-dried porcine dermis

2.5.2 Requirements for skin scaffold

Scaffolds can be defined as porous 3D support systems suitable for cell growth but in order to successfully design an 'ideal' scaffold to achieve the purpose of the project, some features and characteristics need to be met [44, 45]:

a. Being biocompatible and non-toxic allowing cell integration; in case of implantable scaffold, it should not cause a body reaction, being non-immunogenic, non-inflammatory with low risk of disease transmission. In addition, it should be made of biodegradable or bioresorbable material that do not degrade into cytotoxic products in the body and do not induce immune rejection.

b. Having an architecture and composition as similar as possible to the skin. Proper porosity is needed to ensure cellular infiltration and vascularisation, as well as an adequate permeability for infusion of nutrients and effusion of waste products. Small pores do not allow cellular infiltration, or, in contrast, excessively large pores do not maintain the proper cellular interactions. An average pore diameter of 20–120 mm is established to be suitable for cells to infiltrate into the scaffold [29].
   It has to be considered that skin is a layered structure with different morphological features in each layer. Different types of substrates can affect adherence, migration, proliferation and signalling of cells. The scaffold architecture should not only mimic the porous and fibrous architecture of dermal components but should also support the development of the epithelial layer.
c. Possessing adequate mechanical properties to match the intended site of implantation and allow clinical manipulation. It does not require to be equivalent to healthy tissue but at least to have sufficient mechanical strength and stiffness to support and transmit the same forces such as stress and wound contraction.
d. Having an appropriate surface chemistry to favour cellular attachment, differentiation, proliferation and consequent migration into the matrix.
e. Being easily fabricated with tight control over important micro and nanostructures within the scaffold architecture, being manipulable into a variety of shapes and sizes and cost-effective.
f. Being sterilizable.

Fundamentally, the goal of skin tissue engineering scientists is to fulfil as many of these criteria when constructing skin scaffolds.

2.5.3 Potential biomaterials for skin tissue engineering

Biomaterials are generally materials that are used in biomedical and tissue engineering applications. They include metals, ceramics, polymers, and composites, a combination of those. Polymers consists of long-chain molecules composed of small repeating units linked together by covalent bonds. Materials used to fabricate matrix for therapeutic application are often absorbable or degradable in the body. Those for skin scaffolds range from natural to synthetic and a proper choice involves a consideration of the different properties. Natural matrices are characterized by interactive properties, such as cell adhesiveness with low toxicity and low chronic inflammatory response. Synthetic matrices, on the other

hand, are manufactured to allow better handling of material properties, such as geometrics, strength, degradation, and permeability.
In the next sections some natural and synthetic materials are described and a table to summarise the main reasons for using them, is given at the end (Table 2.4).

2.5.3.1 Natural materials

Natural matrices can be obtained either by decellularization of an existing anatomical structure or using isolated components and reassembling them into a scaffold. These materials can have human, animal or vegetal origins and they offer the advantages of low toxicity, reduced immunogenicity and limited inflammatory response. Their ability to interact with cells by focal adhesion has also made the use of these material a fundamental point in designing biomimetic scaffolds. Some biomaterials used for skin scaffold fabrication are listed below.

Collagen
Collagen is a major protein of connective tissue and the most used natural material in the field of TE. It can be synthetized from cells or extracted from human or animal body parts but also derived from different sources such as marine organisms, bacteria or plants. It has been used and processed for various purposes, from regeneration [46] to promote formation of a model of human capillary-like network [47]. There are 16 types of collagen in the human body but around 90% of the body collagen consists of type I, II and III.
One of the distinctive characteristics of collagen is its biological activity in terms of biocompatibility, biodegradability, and low immunogenicity. Besides being the principal component of ECM, it acts as principal mediator in cell adhesion, growth, and differentiation. However, due to inadequate mechanical properties and rapid degradation rate, collagen scaffolds are ordinarily combined with other polymers or cross-linked by covalent bonds that help to preserve the quaternary structure and conformation. Depending on its maturity, source and condition of extraction, the degree of native collagen cross-linking varies. Collagen can be isolated and purified as collagen molecules (soluble collagen) or collagen fibres (insoluble collagen). The fibrillar collagen matrix has a complex structure maintained by the intra- and intermolecular cross-links which make difficult extraction. Solubilization methods use neutral salts, diluted acid with or without enzymes and alkaline solutions but processes can break native collagen in different ways.

Another form of collagen is denatured collagen, called gelatine. Gelatine has a unique characteristic to absorb large amounts of water and this may be considered when using freeze-drying techniques [48]. It is simply the product of collagen hydrolysis derived from sources rich in type I collagen such as bovine, porcine, fish skin, bones, jellyfish, and bird feet. Based on the denaturation hydrolysis process, there are two types of gelatine; type A, which consists of an acid process where the collagen denaturation occurs by thermal hydrolysis of peptide bonds; type B comes from alkali, ionic salts that break the cross-links during collagen heating.

Fibronectin

Fibronectin is another main component of ECM. It possesses binding sites for other components of the ECM such as collagen, fibrin, and heparin, playing a crucial role in cell signalling [49]. Fibronectin also has binding regions for a number of cell-surface receptors but its use is limited because these functions seem to be inhibited by mechanical stretching.

Fibrin

Fibrin is the fibrous protein involved in wound healing. It can be extracted from blood plasma and is widely used in form of glue or gel scaffolds supporting skin cell growth and motility.

Laminin

Laminin is a widely present protein within the ECM and one of the main components of the basal membrane along with collagen IV. Laminin is produced by various cells and it is usually incorporated onto scaffold to improve cell adhesion, migration, differentiation and angiogenesis. This protein may be incorporated in scaffold to create a basement membrane-like, a key element still missing into skin models [50].

Elastin

Elastin gives properties of elasticity to the skin. The difficulty of manipulating elastin *in vitro* is due to the extensive cross-linking and associated insolubility but its addiction to collagen-based scaffold showing a decrease in contraction [51], has made elastin attractive for skin scaffolds.

Glycosaminoglycans (GAGs)

The most important glycosaminoglycans are hyaluronan and chondroitin sulphate. GAGs can be introduced into the composition of the porous scaffolds, in combination with

collagen, chitosan, or other natural biomaterials, to modulate pore size and mechanical properties.

Hyaluronic acid or hyaluronan has been known to promote angiogenesis, facilitate proliferation and migration of fibroblasts and promote scar-less healing in wounds.

Chondroitin sulphate groups increase water retain benefiting from the hydrophilicity of this group and enhance resistance to enzymatic degradation [52].

Chitosan

Chitosan is derived from deacetylation of chitin using alkaline treatment to increase water solubility. Chitin is an almost totally insoluble polysaccharide present in the exoskeleton of shrimp and other sea crustaceans. It is a biomaterial widely used in skin tissue engineering as a wound dressing for its haemostatic and antibacterial properties and as a scaffold for its strength and permeability qualities [53]. Moreover, chitosan can be used on a large scale having a low cost. With a structure similar to GAGs, it does not require aggressive chemical to be dissolved. In the body, lysozymes degrade chitosan into non-toxic products. Chitosan can be combined in porous matrices with other natural biomaterials like collagen and gelatine to enhance their mechanical properties [54, 55].

2.5.3.2 Synthetic materials

Synthetic scaffolds have been investigated for having a defined chemical structure, permitting to tune mechanical and degradation properties. They are usually used either as temporary cover for wounds acting like a skin barrier or combined with natural materials to overcome the lack of cell-recognition signals.

The advantages of synthetic scaffolds over their biological counterparts include the elimination of contamination and disease transmission once implanted, large availability, increased manufacturing uniformity.

Some of commercial, well-known synthetic materials used in skin engineering are:

- ***PGA (Poly (Glycolic Acid))***. It has a low solubility in organic solvents but a glass transition temperature of 35-40°C close to physiological temperature. PGA degrades rapidly in aqueous solutions or *in vivo* due to its hydrophilic nature, losing its mechanical integrity after 2-4 weeks. The most widely used scaffolds derived from this polymer are the nonwoven fibrous fabrics.
- ***PLA (Poly(Lactic Acid))***. It is more hydrophobic than PGA but it has a higher solubility in organic solvents.

PLA scaffolds or implants have remarkably high mechanical integrity *in vitro* or *in vivo* due their slower degradation rate, often taking years to degrade. This is the consequence of the additional methyl group repeating unit in the PLA that makes it more hydrophobic than PGA.

- ***PCL (Poly-ε-caprolactone)***. It is a polymer approved for many applications related to wound care such as sutures. PCL is a slow biodegradable, non-toxic polymer with a clear structure that favours topographical studies [56].

  Its degradation rate is longer than a year making it less attractive for tissue regeneration use. PCL is also hydrophobic but this feature can be improved combining it with natural polymers such as chitosan or collagen that have lower degradation rate and are more hydrophilic.

- ***PVA (Poly(vinyl alcohol))***. Linear poly(vinyl alcohol) (PVA) is a one of the most actively used synthetic polymers for physical hydrogels. Due to its chemical preparation from poly(vinyl acetate), PVAc, it results in a combination of PVA and PVAc. Its physiochemical properties and degree of hydrolysis are determined by the residual ester groups. If the degree of hydrolysis is lower than 90%, it does not form hydrogels.

Table 2. 4 Summary of main characteristics of selected natural and synthetic materials used for skin tissue engineering [2, 43].

Natural	
Collagen	Main component of skin, superior biocompatibility, and cell interaction
Fibronectin	Stimulate migration and cell growth
Fibrin	Source of growth factors
Elastin	Provide elasticity and increase biological activity
GAGs	Increase cell activity and hydrophilicity if combined with other polymers
Chitosan	Biocompatibility, large availability, intrinsic antibacterial nature
Synthetic	
PGA	High tensile strength and hydrophilicity
PLA	Used in blends to tailor mechanical properties
PCL	Unique mechanical properties and biocompatibility
PVA	Highly soluble in water, form hydrogels

2.5.4 Methods of fabrication

The three-dimensional architecture and mechanical properties of skin replacements are completely different to normal skin. This is in part explained by the fact that the manufacturing processes employed are not sophisticated enough to recapitulate the developmental morphogenesis used to create skin naturally. Many methods to design and fabricate scaffold are currently used, most of them based on turning liquid solution to solid state.

2.5.4.1 Freeze-drying

Freeze-drying is a well-known technique to produce scaffold with microstructure architecture and a high level of porosity. Scaffolds are usually produced from an alkaline aqueous solution in which at least one polysaccharide is dissolved by acetic or hydrochloric acid. After homogenization and centrifugation, the emulsion is subsequently frozen in either a specific made-for-purpose mould or using lab plasticware. During freezing stage, the solution forms ice crystals within the structure in function of heat transfer [57]. Keeping material temperature below their transition temperature (*Tg*) is critical to prevent structural collapse [58]. As a consequence of the process, it is clear how strong is the link between scaffold structure and ice crystallization [59]. Ice crystal growth is regulated by the temperature at which solidification takes place. Theoretically, the higher is the temperature gradient and the cooling rate, the smaller is the average pore size in the ice templated structure. Cooling rate also influences the homogeneity of the structure whereas temperature is correlated to the pore size [60]. Thus, the morphology of freeze-dried scaffolds can be tuned by adapting instrumental parameters and solution factors. However, the latter are more convenient to control. For example, it has been demonstrated that controlling the viscosity of solution limits the pore size of scaffolds making the matrix less dependent on cooling rate and thermal gradient [61]. In addition, as well as the cooling rate, lowering the polymer concentration increases the porosity of the constructs [62]. Processing variables need to be controlled carefully in order to synthesize scaffold with desired inner architecture [59]. The last step is to sublimate the solvent within the structure after which the result will be an interconnected porous scaffold. Since no heat is involved in the process, many materials that are sensitive to high temperature can be employed.

2.5.4.2 Electrospinning

Electrospinning is a versatile fabrication method that permits to produce fibrous matrices with a range from macro to nanoscale utilizing a polymeric solution and an electric field (Figure 2.8). A high voltage electrostatic field is introduced between a spinneret (usually a syringe) at a given rate and an earthed collector. At some critical voltage, the surface tension of the polymer is overcome by electrostatic charges and droplets of the solution elongate and stretch into a so-called Taylor cone forming a continuous jet. In order to achieve high-quality fibres without bead formation, it is crucial to maintain a Taylor cone by balancing the electrostatic repulsion, surface tension, and viscoelastic forces. As the jet travels, the solvent evaporates and polymer fibres are formed and collected on the target. Depending on the collector configuration, the morphology of the scaffold can be different. Electrospinning is one of the most used techniques in research studies for scaffold fabrication because of its simplicity and cost-effective process. It allows to obtain substrates with a high surface area to volume ratio, degree of alignment and tuneable porosity. Scaffold characteristics are controlled by numerous manufacturing parameters such as flow rate, collecting distance, electrical voltage and the diameter of the spinneret needle as well as solution parameters (molecular weight, concentration and viscosity of the spinning solution). Electrospun fibres can be also combined with nanoparticles or growth factor in solution or post fabrication expanding the number of potential applications in tissue engineering, from drug delivery to wound healing and dermal regeneration.

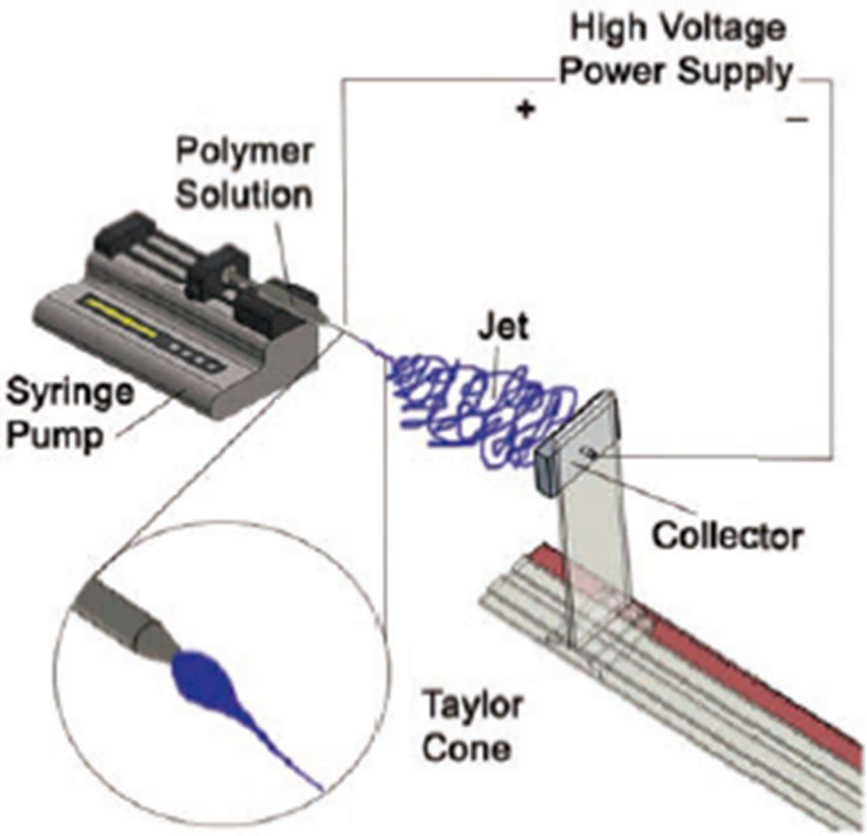

Figure 2. 8 Configuration of electrospinning apparatus [63].

2.5.5 Limitations of skin scaffolds

Designing a model of skin involves considerable challenges. The task of reproducing a fully functional tissue requires evaluation of constraints as many characteristics of normal skin are absent in a model. Solutions are far from being optimal but tailoring specific properties will contribute to investigate different aspects of the skin.

2.5.5.1 Mechanical properties

One of these challenges is the optimization of the mechanical properties of 3D scaffolds. Skin models only approximate true skin organization. The lack of elements such as immune and vascular systems, sweat glands and hair follicles as well as the detachability between layers reduce strength and elasticity in the model. It is in part also explained by the fact that fabrication processes are not enough complex to mimic morphogenesis.

Cross-linking is a technique that can be leveraged to improve mechanical properties, control degradation rate and increase strength and stability. Physical, enzymatic and chemical cross-linking treatments are the most utilized for skin scaffolds.

Physical

- ***Ultra-violet (UV) radiation***. The intensity of the irradiation and duration of exposure determines the extent of cross-linking and denaturation that consequently influence mechanical properties and degradation behaviour. Its use is limited to thin scaffolds and hydrogels.
- ***Dehydrothermal treatment (DHT)***. It is a method whereby the scaffold is exposed to temperatures of 100°-120° C under high vacuum for a time period of 24 h up to 120 h. This step involves condensation reactions that break up water bonds leading to dehydration of the scaffold and resulting in intermolecular crosslinks [64]. It is a lengthy process and may denature the material (20-60%) but at the same time can sterilize the scaffold.

Chemical

- ***1-Ethyl-3-(3-dimethylaminopropyl) carbodiimide (EDC)***. It is a water soluble carbodiimide that permits to crosslink the carboxyl and amino groups of varying residues and improve strength. Even though the small bonds do not influence the scaffold structure, using high levels of this compound is cytotoxic for fibroblast [65] and may lead to an increase in contractility [66]. It is usually used in combination with N-Hydroxysuccinimide (NHS) that improve the activation of carboxylic acid group and thus the crosslinking degree.
- ***Glutaraldehyde (GA)***. It is the gold standard to cross-link tissue and scaffolds used in different applications, mainly transplantations. GA treatment can significantly improve mechanical properties and material durability reacting with amine or hydroxyl functional groups and connecting the biopolymeric chains. However, the functional aldehyde groups are toxic for cells and represent a potential biohazard problem. The concentration of GA and the application method is a determining factor that impact the degree of crosslinking.
- ***Genipin***. It is a green crosslinker being extracted from the fruit of Gardenia jasminoides Ellis. Genipin reacts spontaneously with amino acids because of its multiple active groups, forming blue pigments. Although highly cytocompatible, it is only used in experimental studies due the expensive cost.

Enzymatic

- ***Transglutaminases*** are natural enzymes that catalyse the acyl-transfer reaction between the ε-amino group of lysine and the γ-carboxamide group of glutamines in proteins. Furthermore, it has been shown to facilitate cellular attachment with no reported cytotoxic effects [67]. However, the use of enzymes makes the crosslinking procedure expensive.

2.5.5.2 Lack of vascularization

One of the major issues in skin tissue engineering is the slow process of scaffold vascularization. Ensuring an adequate vascularization remains a challenge. Nowadays, there is no available method that can provide a homogeneous nutrient and oxygen supply to the construct and most of the attempts to create skin scaffold focused on promoting barrier function. In the human skin, nutrients delivery and waste removal occur through diffusion whereas in scaffolds due to inadequate bidirectional porosity, vascularization is not allowed. Therefore, the idea that a bioengineered scaffold may incorporate prefabricated vessels in order to vascularize more rapidly can be a promising strategy. In addition, endothelial cells, vascular cells responsible for vasculature formation, can be integrated in co-culture to better mimic the *in vivo* environment [68].

2.6 Mechanism of cell-scaffold interaction

The success of a tissue engineered scaffold depends upon three factors: cells, scaffold material and scaffold architecture.

Human skin fibroblasts (HSF) and keratinocytes are the most common used in skin tissue engineering application. While keratinocytes are able to proliferate and differentiate spontaneously forming a stratified epithelium, studies have found that HSF exists as subpopulations that is morphologically and functionally heterogeneous, exhibiting distinct gene expressions and functions [69]. For example, papillary dermal fibroblasts display higher growth kinetics and lower contractile properties compared to reticular fibroblasts and are thought to represent an undifferentiated phenotype [70]. One of the main challenges faced in understanding cell-material interactions is that conclusions drawn from one cell type may not be readily applied to another.

Research on how fibroblasts respond to substrates with different mechanical properties and the relationship between cell morphological changes and associated intracellular signalling pathway are topics of great interest [71].

Fibroblasts are anchorage-dependent cells that have the capacity to transmit forces from cytoskeleton to ECM through integrin receptors in connections known as focal adhesions or to other cells by cell-cell junctions. Tensions that form in the cytoskeleton are influenced by chemical and mechanical properties of the material and determine the cell fate. Furthermore, cells can be subjected to mechanical forces such as pressure, shear stress, stretch, compression or combination of those and chemical stimuli from the external environment that can further affect morphology, survival, growth and reorganization (Figure 2.9).

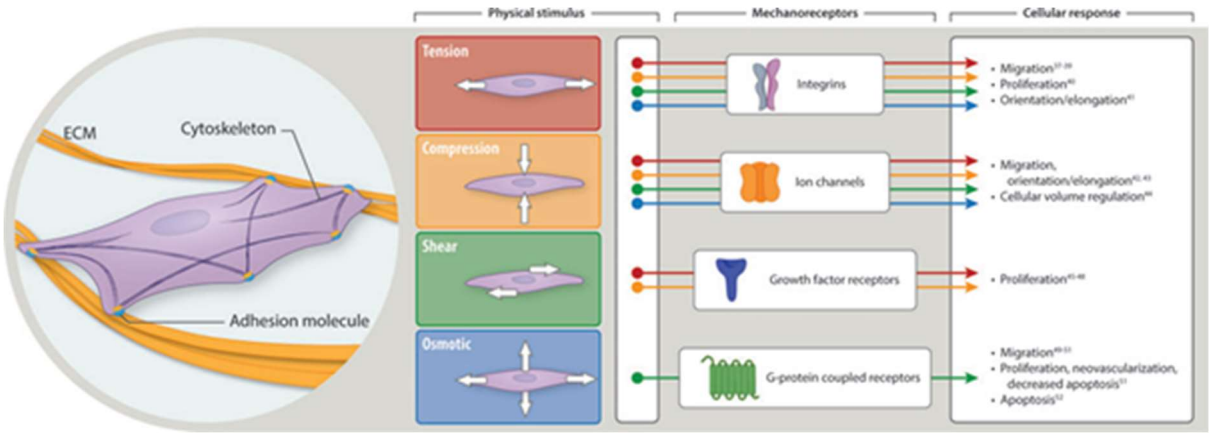

Figure 2. 9 Illustration of cell adhering to adhesion molecules such as integrins and physical stimuli acting on a cell and resulting cellular responses [72].

Topographical features such as pores, fibres or a combination of these play an important part on cell response altering tissue formation and gene expression. Therefore, scaffolds are considered bioactive structures that regulate the mechanism and the extent of cell adhesion. Pore size must be bigger than the cell size that we want to populate the scaffolds but they also have to be interconnected to allow interior cell growth, nutrient supply and waste product exchange. In addition, it was demonstrated that the extension of scaffold contraction can be guided by adjusting the pore size [66].

Fibrous scaffolds have a structure that better resemble natural tissues. In hydrogels, collagen fibrils are dispersed in a solution that forms a gel under specific conditions of temperature and pH. Although cells are easily added to the solution before solidification being embedded in it, these structures represent soft substrates with low mechanical properties. Alternatively, fibrous membranes can be employed to simulate the cellular

microenvironment and match the mechanical properties of the skin. In this case, fibre diameter has to be defined for the specific cell type being direct correlated with the size of pores and therefore influencing cell infiltration [73].

2.7 Bioreactors for 3D culture

In the tissue engineering field, bioreactor refers to a tool that permits to control and accelerate biological processes, providing an ideal environment, controllable and mechanically active. The purpose of a bioreactor is to overcome static system limitations where in a non-homogeneous environment, problems occur with concentration gradients, nutrients supply and other components. Bioreactors are the base of the present and future industrialization of engineered tissues. Currently the use of bioreactors aims to improve cell expansion, dynamically seeding cells within 3D matrices, facilitate the growth of functional 3D tissues and control and regulate tissue development under desired physical and chemical conditions. On the other hand, bioreactor can also be used to investigate and clarify the effect of specific forces and mechanical stimuli in a close and controlled environment. Although there is a wide range of bioreactors that can house cell-seeded scaffolds, they are limited by the lack of specific guidelines that could address different cell culture requirements. Therefore, bioreactors should be chosen and designed based on their specific application.

2.7.1 Design requirements

The biological and mechanical requirements of a bioreactor depend on the specific application and engineered tissue. Nevertheless, fundamental principles should be considered in designing it [74]:

a. Maintain sterility. The material used to fabricate the bioreactor chamber should be suitable for sterilization using traditional methods.
b. Efficient mass transfer and gas exchange to maintain a viable and functional tissue and allow uniform distribution of cells on a 3D scaffold.
c. Suitable for scale up and simple to assemble.
d. Ability to impose physiologically relevant mechanical stimulation to tissues.

2.7.2 Bioreactor for NPWT investigation

In contrast to a large number of studies regarding skin scaffolds there has been little work in the area of bioreactors designed and customized for specific applications.

Bioreactors for skin tissue engineering offer many functions from seeding to maintaining cell cultures or tissue development [75]. However, evaluation of how cells and skin respond to therapies and forces should be the first step before designing a medical device. NPWT investigation has become of great interest not only in wound healing treatment but also in alternative applications such as closing incisional wounds [76] and improving skin graft integration. Veale et al. [77] demonstrated that in *in vitro* study the combination of NPWT and commercial collagen-based matrices, used to accelerate soft tissue regeneration, may lead to sub-optimal delivery of vacuum pressure potentially decreasing the efficacy of the therapy.

NPWT bioreactors have been also developed and tested on several skin models and skin equivalents for various research purposes but there is still not uniformity in regard to how cell should be cultured and studied under negative pressure. Yamashiro and al. [78] proposed a cell culture system capable of real-time monitoring of cells during NPWT treatment whereas Wilkes et al. [14] and McNulty et al. [79] observed cell behaviour interrupting negative pressure treatment. However, all these studies present limitations due to the way medium is supplied to cells and the approach to NPWT delivery. Mass transfer in skin is governed by convective transport and diffusion through the blood capillary system that supply nutrients to tissues which are not more than 100 μm distant. In skin tissue engineering, convective mass transfer is usually replaced by perfusion and from this point of view, a suitable choice of medium flow rate and resulting shear rate applied to cells should be considered. If not well supplied with medium, skin tissue equivalents have shown to undergo apoptosis [80]. Although it can be considered a misrepresentation of *in vivo* conditions, diffusion of nutrients could be also simulated through application of vacuum/negative pressure that would allow the fluid to be drawn towards the surface as investigated by Baldwin et al. [81]. With regards to the NPWT application skin can be thought as compressed and stretched during therapy. A common way to study the effect of stretching on cells involves the culture of cells on substrate exposed to uniaxial or biaxial stretch [13]. With this configuration cells will just adhere superficially and keeping them alive would imply the involvement of shear stresses from the medium. Alternatives to this approach have been made, investigating collagen and fibrin gels populated with fibroblasts

but these models either could not withstand NPWT or the therapy was applied topically by means of needles in small size setup [14, 82] (Figure 2.10).

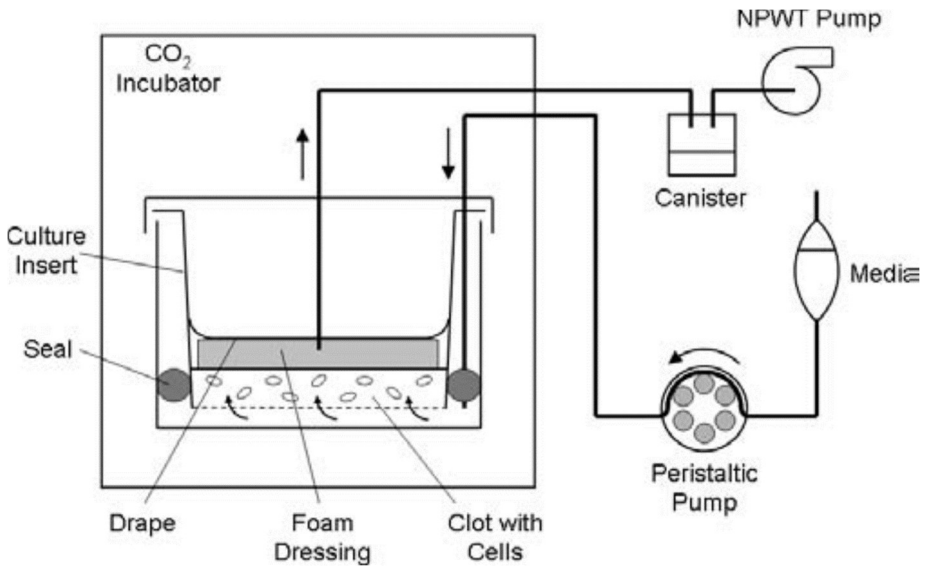

Figure 2. 10 Schematic representation of a single well NPWT bioreactor. Culture insert is placed in well of 6-well plate into cell rings. Medium is introduced into the chamber through a needle and supplied to the cells from the bottom. NPWT is applied through dressing by a syringe needle [14].

Results rely on experiments in which there is heterogeneity and lack of standardization of protocols and methodologies. Developing scaffolds fit for the purpose and a platform suitable to study NPWT would be the first two important steps to advance the understanding of NPWT forces on cells towards the improvement of clinical therapy.

CHAPTER 3 Fabrication of porous scaffolds

3.1 Introduction

During the years, many methods have been employed to produce functional scaffolds suitable for cell behaviour studies [83, 84]. Although there is no definitive method that can closely reproduced mechanical and physicochemical properties of the native extra cellular matrix (ECM), the manufacturing process and materials utilized can influence scaffold porosity, pore size, water absorption and other characteristics that are critical to enhance *in vitro* scaffold bioactivity [85].

In this chapter, collagen-based scaffolds from insoluble collagen type I were fabricated by freeze-drying method with an attempt to standardize the fabrication process, compare combinations of different materials and cross-linking techniques to favour cell arrangements and find an ideal platform for *in vitro* studies.

3.2 Materials and methods

Insoluble fibrillar type I collagen (CL) from bovine Achilles tendon (C9879 Lot SLBG9204V, Lot SLBZ0774, Sigma-Aldrich, UK) was used to make collagen solutions following a protocol adapted from literature [86].

Briefly, collagen was suspended in 0.25 M acetic acid (AA) solution at three different concentration, 0.5% w/V, 0.7% w/V and 0.9% w/V that were chosen after careful literature review. Then, suspensions were mixed with an overhead blender at 15000 rpm for 35 minutes using a container filled with icy water to keep solutions at low temperatures and prevent denaturation of collagen fibres due to casual heating. The resulting homogeneous slurries were degassed under centrifuge at 5000 rpm for 8 min to remove air bubbles and successively pipetted (Single Channel Pipette 0.5-5 ml, Eppendorf Research®) into polystyrene 6-well culture plates (Falcon™, Fisher Scientific) at approximately 5 mm filling height. Lastly, cell culture plates were placed inside a lyophilizer (VirTis AdVantage 2.0, SP Scientific) where shelves temperature was set to -40°C from an initial temperature of 20° C in order to freeze the solutions. After 3 to 4 hours, shelf temperature was raised to 0° C and vacuum was applied allowing sublimination to occur. Scaffolds were left to dry for at least 36 hours and then were removed from the dryer.

After preliminary mechanical and cell culture tests, a concentration of 0.7 % collagen of the first collagen batch was chosen as the most suitable for further experiments. This concentration was eventually changed to 1% for the second collagen batch in order to obtain solutions with same viscosity. During the freeze-drying process, in parallel experiments, collagen solution was pipetted in wells of different size in diameter (12 well plate with well diameter of 22 mm and 24 well plate with well diameter of 15 mm) and the use of freezing temperature of -20°C and -80°C were investigated to examine the impact that they could have on pore size and scaffold structure.

Also, the effect of adding hydrophilic polymers to the collagen solution such as chitosan (CS) 0.7% w/V (LMW, Sigma Aldrich UK), and polyvinyl alcohol (PVA) 5% w/V (86-89% hydrolysed MMW, Alfa Aesar) individually dissolved in 0.25 M acetic acid was evaluated. These polymer solutions were individually mixed with collagen suspension in a percentage of 10% v/v before blending, creating polymers blends. The percentage was chosen after preliminary experiments in which it was determined that higher percentage of chitosan and polyvinyl alcohol would compromise the integrity and the handling of samples in solutions [6].

3.2.1 Characterization of freeze-dried scaffolds

The porous architecture of the scaffolds is a key in determining a suitable biological response in tissue engineering. Although, methods of characterizations vary widely in literature, in this study, some of them were selected for availability and for intent of purpose of the work.

3.2.1.1 Structural characterization and pore size

The choice of using commercially available moulds was made with the aim to standardize the process and obtain reproducible data that might be a starting point for future experiments. In other studies, moulds made from materials having high thermal conductivity such as steel and copper led to rapid freezing of the solution allowing the structure to orientate in a chosen direction [62]. On the contrary, moulds made from materials with low thermal conductivity such as plastic allowed the suspension to freeze at roughly the same rate throughout resulting in a homogenous microstructure [87]. Therefore, freezing samples in thermally insulating moulds is an excellent technique to

have control of the structure, morphology and mechanical properties that are highly important for scaffold fabrication.

The structure of collagen scaffolds was characterized by scanning electron microscopy (SEM) (Cambridge Instruments Stereoscan 360, Oxford Instruments) at different magnifications. The dry samples were prepared sectioning the scaffolds by means of a scalpel. Then, they were carefully mounted onto stubs using carbon adhesive tape and coated with an ultra-thin layer of gold using a gold sputter coater (S150B, Edwards Ltd). This is a standard and needed procedure for analysis of non-conductive materials. In order to measure the pore diameter, analyse and compare the structures, high resolution images of cross-section were recorded and at least 30 apparent pores measured with Fiji-Image J software [88]. Standard deviations of these measurements are represented in graphs by error bars.

3.2.1.2 Viscosity

Viscosity is defined as the measure of the resistance of the fluid deformed by shear stress. The system used to measure this entity is based on the sample type. Generally, polymeric solutions and dispersions behave as non-Newtonian fluid, a substance whose properties does not depend time but on shear stress and temperature.

A viscosity of a solution is an important and critical parameter sometimes neglected and frequently difficult to measure when the product exhibits complex rheological behaviour. Polymer solutions can be considered as a homogeneous system when it is still fluid but at higher concentrations, complex behaviour can be encountered. In this direction goes the choice of using acetic acid that allows disentanglement of collagen molecules favouring mixing and resulting in low viscous and homogeneous solutions [89, 90].

In this study viscosity measurements were taken on various collagen-based slurries at 20°C using a rheometer (Bohlin CVO 120 HR) with a stainless-steel cone/plate geometry (4° cone angle, 40mm cone diameter) and a gap set at 150 μm. Cone-plate measuring system was preferred as it provides constant shear rate across the sample. The aim was to study the rheological behaviour of collagen solutions at different concentrations and between two batches of collagen. They were then plotted as a function of the applied shear rate.

3.2.1.3 Crosslinking

Crosslinking defines a series of techniques that have the purpose to promote bonds between polymer molecules to increase the mechanical properties and stability of scaffolds. As explained in the introductory chapter, it can be achieved in different ways.
In this study, a dehydrothermal (DHT) process was performed in a Gallenkamp Vacuum Oven at 105° C under vacuum for 24 h on scaffolds to overcome shrinkage and biostability problems. In brief, scaffolds were contained in an aluminium foil pouch, sealed on three sides and placed on the shelf in the oven.
After this first step, scaffolds underwent a further crosslinking that consisted of three selected methods:

1) 1-Ethyl-3-(3-dimethylaminopropyl)carbodiimide and N-hydroxysuccinimide (EDC NHS) (6mM) 1:1 in 75% ethanol solution for 24h at room temperature (RT).
2) 0.25% glutaraldehyde (GA) in 75% ethanol solution for 24h at RT.
3) scaffolds were placed on a metallic grid inside a desiccator and exposed to vapour of a 25% glutaraldehyde (GA) water solution for 24h at RT.

Successively, scaffolds from 1) and 2) were extensively washed three times with decreasing ethanol-phosphate buffered saline (PBS) solutions (75% v/v, 50% v/v, 25% v/v) and then freeze-dried for a second time; scaffolds crosslinked through vapours of a 25% GA water solution were left to air-dry at room temperature for further 24h.
The EDC-NHS molarity and molar ratio was chosen based on findings reported in literature. It has been shown that using a 1:1 EDC/NHS molar ratio and concentration up to 10 mM, collagen samples had greater stability and mechanical strength compared to higher molar ratio [91]. After comparing several studies, choices were also made about the concentration of GA and the time of crosslinking [92-94]. Ethanol water solution was the preferred solvent for its ability to preserve the open porous structure of the scaffolds [95].
Moreover, a ninhydrin assay was performed to determine the degree of crosslinking by comparing the percentage of free amino groups in crosslinked and non-crosslinked (NXl) scaffolds adapting a method described previously [96]. In brief, 9 mm disk (n=3) from various scaffolds were cut, weighted and hydrated in 250 µl Milli-Q water (mQ). Then, 1 ml of a solution which contained one part of 4 % (w/v) ninhydrin in ethylene glycol and one part of 200 mM citric acid with 0.16 % (w/v) tin (II) chloride at pH 5.0 in mQ was added. Tubes, protected from light, were immersed in a water bath for 30-35 min at 95-

100°C. In the meantime, solutions of known concentrations of glycine were prepared to generate a standard curve and determine the concentration of free NH_2 groups in the samples. Thus, the samples were cooled to room temperature and 250 µl of 50% isopropanol was added to each sample. After being vortexed, the optical absorbance of the solutions at 570 nm was recorded with a spectrophotometer. The degree of crosslinking of the sample is calculated following Equation (1) in which **NXl NHN** are the reactive amines in non-crosslinked collagen scaffolds and **Xl NHN** are the amines remaining in crosslinked scaffolds.

$$\%\ \text{of crosslinking} = 1 - \frac{\text{Xl NHN}}{\text{NXl NHN}} * 100$$

Equation (1) Percentage of crosslinking degree calculated as a ratio between the difference of reactive ammines in non-crosslinked (NXl NHN) and crosslinked scaffolds (Xl NHN).

3.2.1.4 Attenuated Total Reflection - Fourier Transform Infrared (ATR-FTIR) spectroscopy

Fourier transform infrared (FTIR) spectroscopy is one of the most important techniques of vibrational spectroscopy to evaluate the surface composition of material. Functional groups can be associated with characteristic infrared absorption bands, which correspond to the fundamental vibrations of the functional groups.

ATR-FTIR spectra of CL-based scaffolds was obtained at room temperature in a spectral range from 4000 to 600 cm^{-1} using Nicolet iS5 FT-IR spectrometer (Thermo Scientific) and equipped with an iD5 ATR accessory with diamond crystal. Each spectrum was recorded at a resolution of 4 cm^{-1}, scanned 64 times, and analysed using the OMNIC™ Software. All spectra were represented with wavenumber (cm^{-1}) as abscissa unit and absorbance as ordinate unit. ATR-FTIR was also used to characterize polymer blends and crosslinked scaffolds.

3.2.1.5 Porosity and water swelling

In tissue engineering, porosity and water swelling are two commonly adopted measurements used to characterize scaffold structure and affinity with liquids, respectively. These methods are conceptual models that have been used to represent the system based on their definitions. Therefore, if the definition of porosity is the amount of void space confined by solid surfaces in a finite volume, it is possible to define porosity

as the ratio between volume void and total volume. Based on this concept, water swelling or absorption is the property of water (or any other liquid) to infiltrate inside the structure, fill the void space and be retained or absorbed by the material.
Various techniques and formulas have been utilised to measure these properties, mainly based on variation in volume or weight [97].
In this study, cylindrical scaffolds of 9 mm in diameter and approximately 4 mm in height were obtained punching them out from disks of 35 mm in diameter. To determine the porosity (ε) and the absorption of water (WU), scaffolds were submerged with liquids using micropipette and left at room temperature for 24h, after being initially weighted. Then, scaffolds were removed, gently dripped and the percentage of water uptake was calculated using Equation (2), where ***Ws*** and ***Wd*** represent the weights of hydrated and dried samples (n=3), respectively.

$$\mathrm{F}\ (\%) = \frac{\mathrm{Ws}}{\mathrm{Wd}} * 100$$

Equation (2) Percentage of WU represented as a ratio between the weight of hydrated scaffolds (*Ws*) and the initial scaffold weight in dry conditions (*Wd*).

Although the equation used is the same for both measurements, liquids and method were different. In particular, for porosity measurement pure ethanol, instead of water, was used as fluid and vacuum was applied inside each vial that contained the scaffold by means of a needle connected to a vacuum pump. In this way, air contained in the scaffold pores was removed allowing the infiltration of ethanol within the pores.
As the sponge expanded under vacuum, further investigation to assess the integrity of the microstructure was undertaken using a Cryo-SEM (Zeiss EVO60). The samples imaged on the SEM were scaffolds DHT-treated.

3.2.1.6 Mechanical tests

The mechanical properties of scaffolds were assessed via tensile and compression tests.
For tensile testing, specimens with a dog-bone shaped size (Figure 3.1) were cut out of a 35mm disk using a scalpel with the aid of a cut-to-size paper guide (Figure 3.1c).
They were tested (n=3) in dry and wet conditions to failure using a tensile machine (Lloyd Material Testing LS1) with a load cell of 100 N at a strain rate of 1 mm/min. Scaffolds were immersed in 70% ethanol solution overnight and then washed three times with PBS

solution. The liquid was partly removed using filter paper before mounting the specimen in the tensile machine.

Sandpaper was attached to the grips to avoid slippery of the specimens during testing. Then, Young's modulus (E), maximum stress (σ_{max}) and elongation at break ($\%\varepsilon$) were determined by fitting the experimental data of stress (σ) and strain (ε).

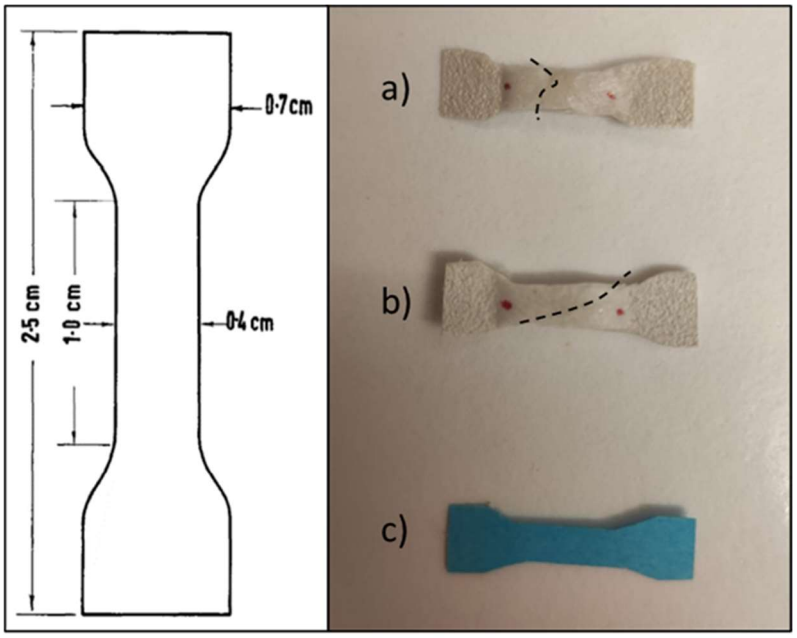

Figure 3. 1 Dimension of specimens used for mechanical testing on the left. On the right, two fractured samples (a) and (b) and the paper guide used to cut the specimens (c).

Scaffolds were also evaluated mechanically in compression. Compressive elastic modulus was determined using a dynamic mechanical analyser (DMA Q800, TA Instruments) machine that measured the thickness of the samples (n=3) automatically. After being hydrated in a 70% ethanol solution for 24h, rinsed and soaked overnight in PBS at room temperature, 9-mm disc-shaped scaffolds were compressed with an initial contact force of 0.02 N at a ramp rate of 0.005 N/min to 0.1 N. Elastic modulus was calculated as the slope of the stress-strain curve over the initial strain regime. Furthermore, measurements of creep-recovery were performed on DMA compressing the specimens of 30% strain and measuring the percentage of shape recovery in one minute.

3.2.1.7 Statistical analysis

For each experimental condition, a sample number of n=3 or more was used, as noted. Data are expressed as mean ± sample standard deviation, represented by error bars. Statistical analysis was carried out, when possible and necessary, using t-test in which a maximum of two groups was used per analysis. Differences were considered significant when $p<0.05$.

3.3 Results and discussion

Results are presented and discussed under various sections.

3.3.1 Preliminary experiments

At the beginning of this study, it was essential to assess the source of collagen to find the appropriate concentration of material in solution for scaffolds fabrication that could be used as skin substitutes. Three concentration of collagen 0.5%, 0.7%, 0.9% w/v in 0.25M acetic acid solution were selected to produce freeze-dried collagen sponges and their structure was analysed using SEM images.

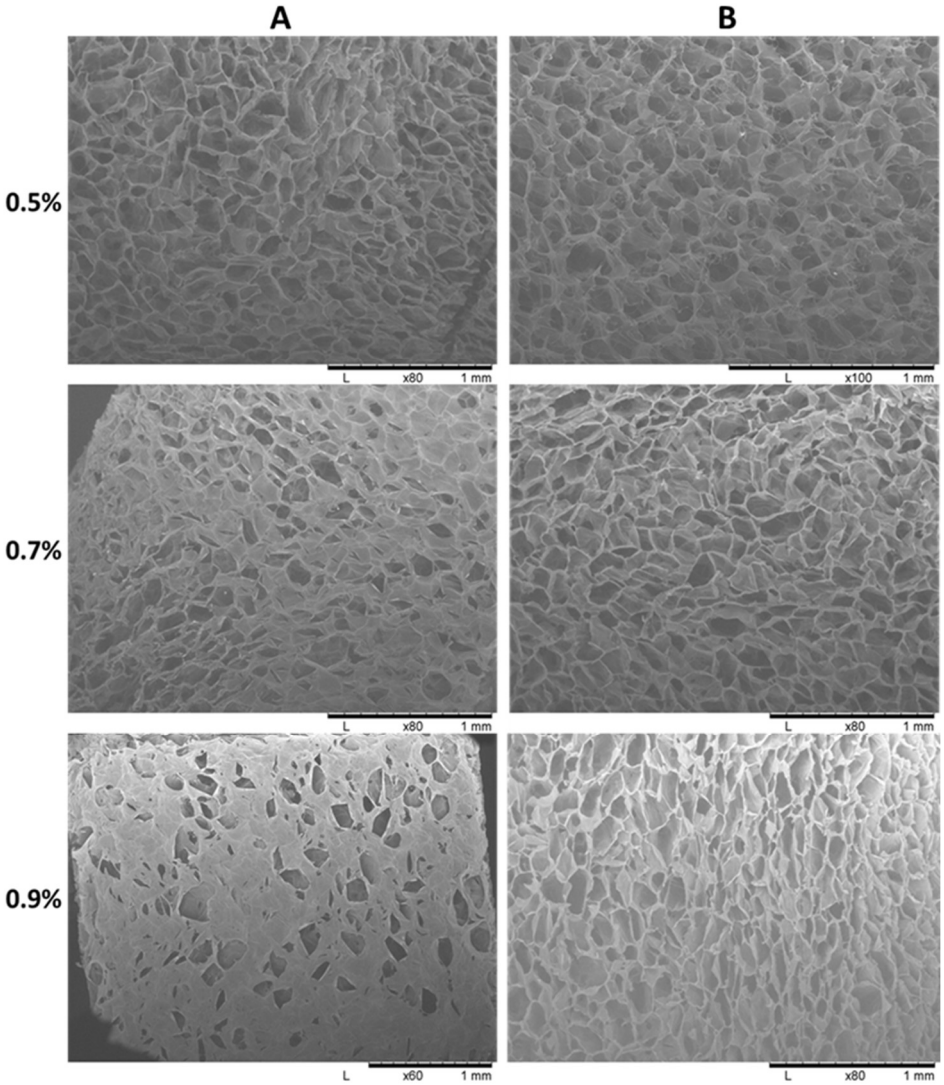

Figure 3. 2 (A) Top surfaces and (B) vertical cross-section of CL scaffolds with different concentration (w/v%) freeze-dried in 6-well plates at -40°. Scale bar = 1 mm.

As shown in Figure 3.2 A as the concentration of CL increases in the solution, porosity on top of the scaffolds seems to decrease and pores to be occluded. This was likely due to an increase of viscosity and surface tension that was too high to overcome sublimation forces during the freeze-drying process. It can be also noticed on Figure 3.2 B that collagen pore walls are thicker at higher concentrations explaining the decrease porosity and water absorption. Although the shape of the pores appears O-shaped for 0.5% and for some extent also for 0.7% and 0.9%, it seems that at higher concentrations the shape of the pores is more elongated, almost elliptical. Despite a variation in appearance, the experiments performed using 0.5% to 0.9% concentrations did not show a relevant change in pore dimensions. To evaluate the effect of lower freezing temperature, solutions at noted concentrations were poured in 6 well plates and frozen in a -80°C freezer for 4-5 hours and then dried in the lyophilisator. The process formed layered structure with irregular shapes (Figure 3.3) that were considered not useful for the purpose of fabricating a structure with definable pores of regular dimensions. However, this result was only obtained when 6 well plates were used as moulds at -80°C.

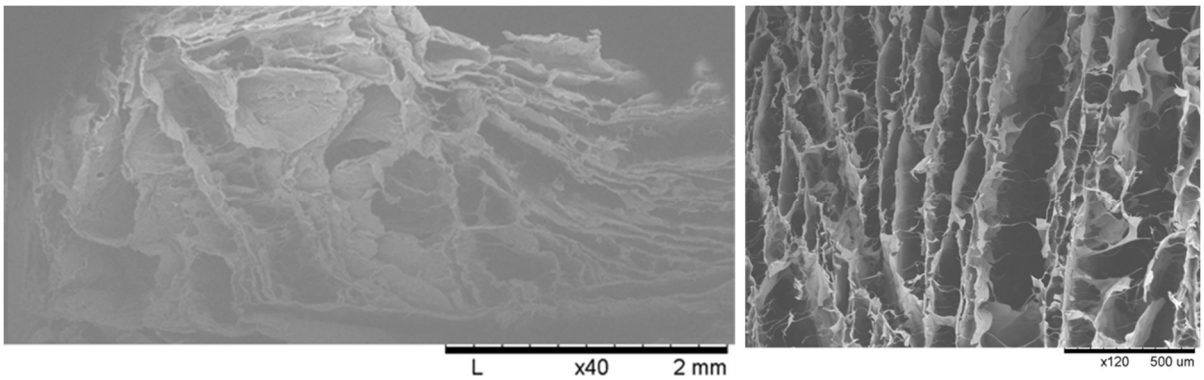

Figure 3. 3 Vertical cross-sectional images of freeze-dried scaffolds at -80°C with irregular and layered structure. Scale bars = 2 mm (left) and 500 µm (right).

The layered structure was not homogenously distributed throughout the height which indicates that scaffolds did not freeze under constant conditions. Presumably, the undefinable structure was caused either by collapse occurred during the drying process or due to flash-freezing that is widely acknowledged to produce smaller ice crystals with a poor network not allowing pore formation [58, 87, 98]. As explained by Schoof et al. [99] during the solidification process there are dynamics at solid-liquid interface that can entrap or repel collagen aggregates depending on the ice front velocity facing the scaffolds. If the ice front velocity, that is the speed at which the solution freezes from the bottom to the

top, exceeds a critical value, a planar ice structure grows through the collagen suspension. Moreover, a break-down of this morphology can be caused when acetic acid is added in the solution. Therefore, with the aim to produce samples with a defined porous structure that could be used for further characterization and experiments, the option to freeze samples at -80°C was discarded. Collagen slurries were frozen and dried in the lyophilaser VirTis AdVantage 2.0, SP Scientific that could reach a maximum freezing temperature of -50°. Based on preliminary experiments that evaluated pore size, water uptake and shrinkage in solution (not reported), it was decided to select 0.7% w/v of collagen in 0.25M of acetic acid solution as concentration to use in further experiments.

3.3.2 Appearance and pore measurement

Mean pore size is an essential aspect of scaffolds for tissue engineering applications. With regards to cells, small pore size can limit liquid diffusion and cell migration towards the centre of the construct [100]. Although the relationship between cells and pore size is controversial and within literature there are conflicting results on the optimal pore size needed for skin engineering scaffolds, a range between 50 and 200 μm is generally accepted as the optimal one [101]. There are different techniques and methods to obtain pores of several sizes [99]. In this study it was investigated the influence of two freezing temperature and the use of moulds with decreasing diameters. Theoretically, the higher the temperature gradient, the faster the freezing rate and the smaller is the ice templated pore sizes [102]. As shown in Figure 3.4, there was a decrease in pore size for scaffolds with a concentration of 0.5% and 0.9% when solutions were frozen at lower temperatures (-40° C). On the other hand, an intermediate concentration of 0.7% did not follow the same tendency as the mean pore size can be considered similar (139.47 ± 24 μm for -20° C, 136.7 ± 29 μm for -40° C).

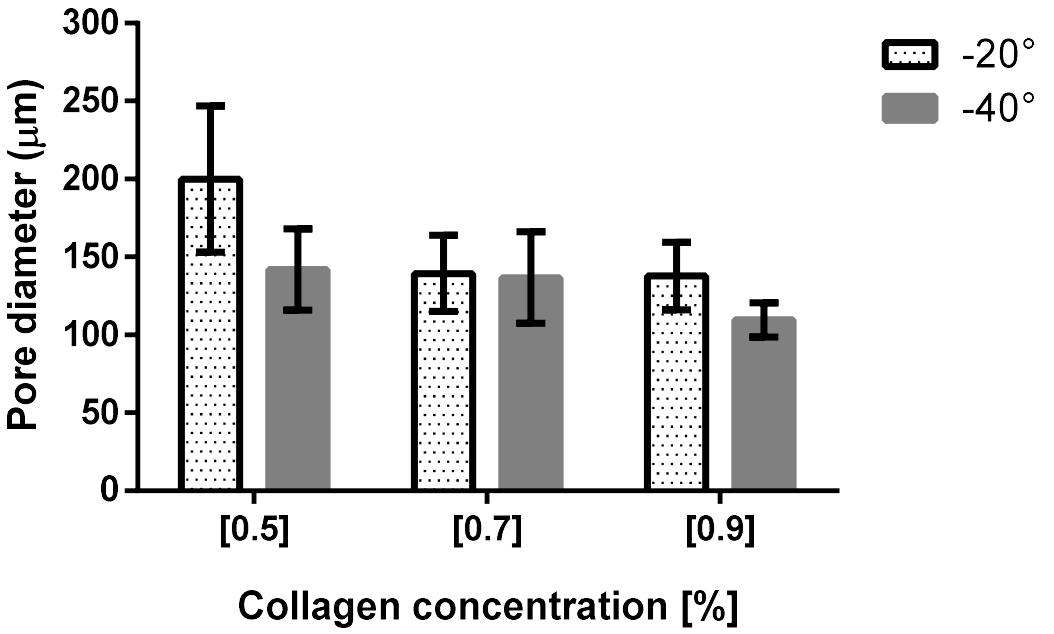

Figure 3. 4 Comparison of mean pore size for scaffolds (n=3) fabricated from solutions with different collagen concentration frozen at -20° C and -40° C in the freeze-dryer.

It is possible to assume that this behaviour depends on the rheological properties of the solution which as reported later in this chapter, are related to the concentration.

However, all pore size measurements had a considerable small standard deviation achieving the objective to restrict the pore size range and obtain a homogenous structure.

Following these results, another study was conducted to demonstrate the impact that the use of mould with smaller size has on the mean pore diameter. Scaffolds with same height had smaller pore size as the diameter of the mould decrease (Figure 3.5).

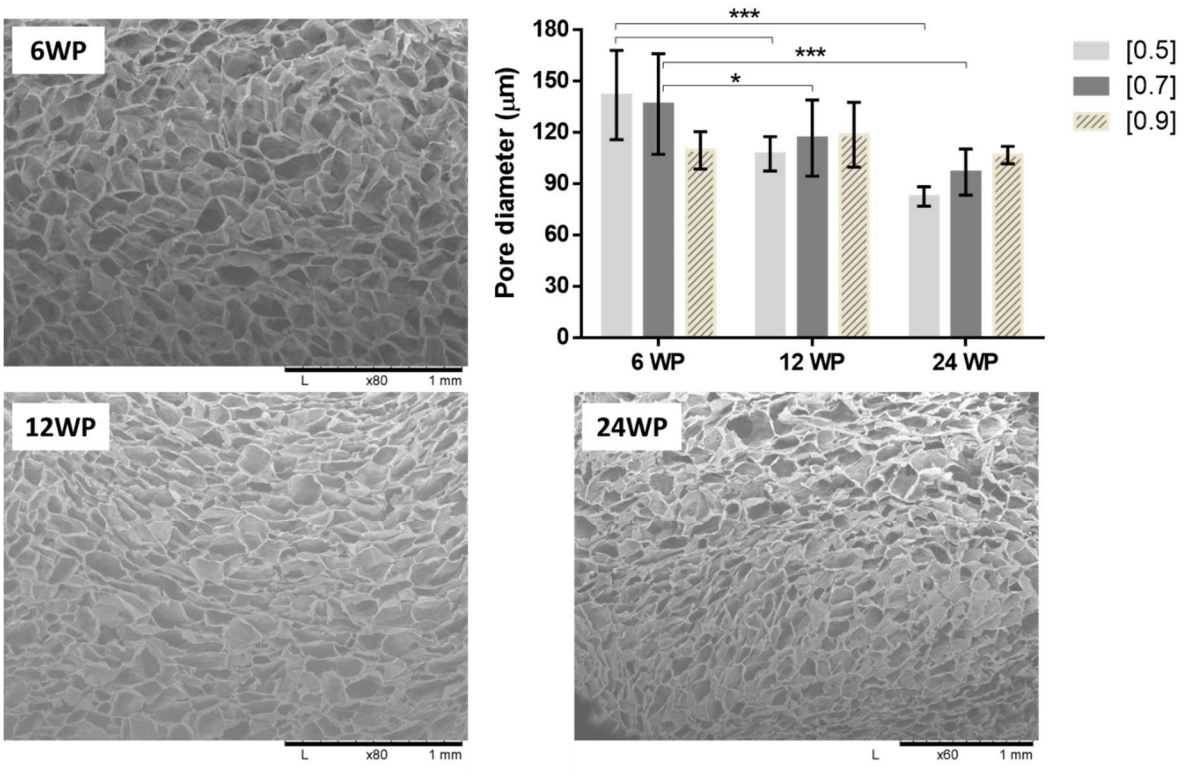

Figure 3. 5 Graph of mean pore size for collagen scaffolds (n=3) obtained from solutions frozen in 6 well plate (6WP, wells with size of 35 mm in diameter), 12 well plate (12WP, wells with size of 35 mm in diameter) and 24 well plate (24WP wells with size of 15 mm in diameter) at -40°C and vertical cross-sectional SEM images of scaffolds with concentration of 0.7%. Scale bar = 1 mm. *= p≤0.05; ***=p≤0.001.

The graph also shows that for smaller mould diameter, the trend is for the pore size to be slightly increase in dimension. This could be due to a difference in the viscosity of the solution, hence liquid density and chemical composition, which can influence the freezing rate leading to a change in pore size for smaller volumes of solution. The hypothesis was, to some extent, demonstrated in a recent study in which researchers found that an increase of collagen percentage in a solution can result in larger pore diameter up to a certain concentration after freeze-drying [93]. Nevertheless, for all the scaffolds observed, the use of plastic moulds at -40°C led to the formation of pores with regular shape. After having investigated the influence of concentration and mould size on the fabrication of scaffolds with a defined, homogenous pore structure, the effect of cross linking on pore size was assessed for scaffolds produced using a collagen concentration of 0.7%, frozen at -40°C in 6 well plates. The choice of these parameters was based on physiochemical and biological preliminary experiments that showed a higher cell affinity and greater stability in solutions than the others. The process of scaffold crosslinking resulted in a 10%-15% shrinkage of the structure in diameter and in colour change (Figure 3.6).

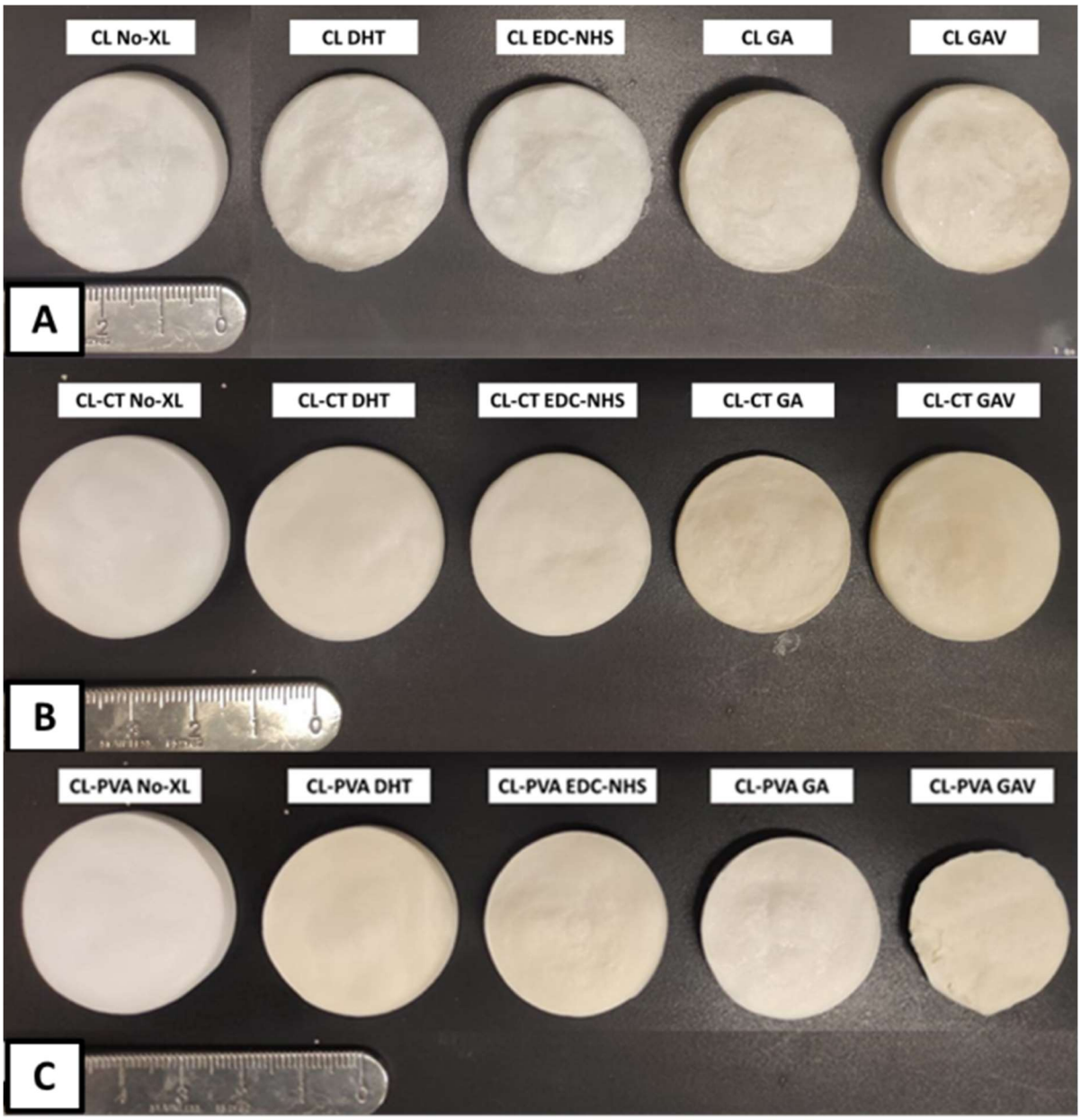

Figure 3. 6 Representative digital photographs of the macromorphology of unmodified (A) collagen (CL No-XL); (B) collagen-chitosan (CL-CT No-XL); (C) collagen-PVA (CL-PVA No-XL); and treated scaffolds.

The surface appearance of each sponge seems not to differ among the various treatments for CL scaffolds, whereas for CL-CT and CL-PVA the initial smoothness of the surface maintained after DHT, was disrupted by further treatments. Roughness to different extent for various scaffolds is visible in Figure 3.6. In addition, the colour of the scaffolds turned yellowish after being crosslinked. The change in colour appears to be more evident for CL-CT scaffolds and for all the scaffolds that were treated with glutaraldehyde due to chemical reactions [103, 104]. To further investigate these alterations, vertical cross-section pore structure was imaged (Figure 3.7) and average size and standard deviations

calculated on 30 measurements (Figure 3.8). After crosslinking by DHT, as no remarkable morphology alteration was observed in Figure 3.6, also the mean pore size measured remained similar. However, the removal of water molecules and increased stiffness caused some reversable flattening in the pore size of these materials. Contrarily, in the commercial dermal template MatriDerm, pore size was found to be reduced after DHT crosslinking [105], probably favoured by the inhomogeneous structure that shrunk under the effect of vacuum. This may indicate a higher capability of scaffolds fabricated in this study to better withstand compression and retain their initial structure. With regard to EDC-NHS, while the pore size of pure collagen scaffolds was comparable to the untreated one and DHT-treated samples, for polymer blends there was a significant increase probably due to the rehydration and additional freeze-drying step. CL scaffolds that were treated with glutaraldehyde solution (GA) and vapour (GAV) showed the same pore structure with a significant increase in size and a change in pore morphology, if compared to the control (CL-No XL), that appears closed with a sheet-like structure.

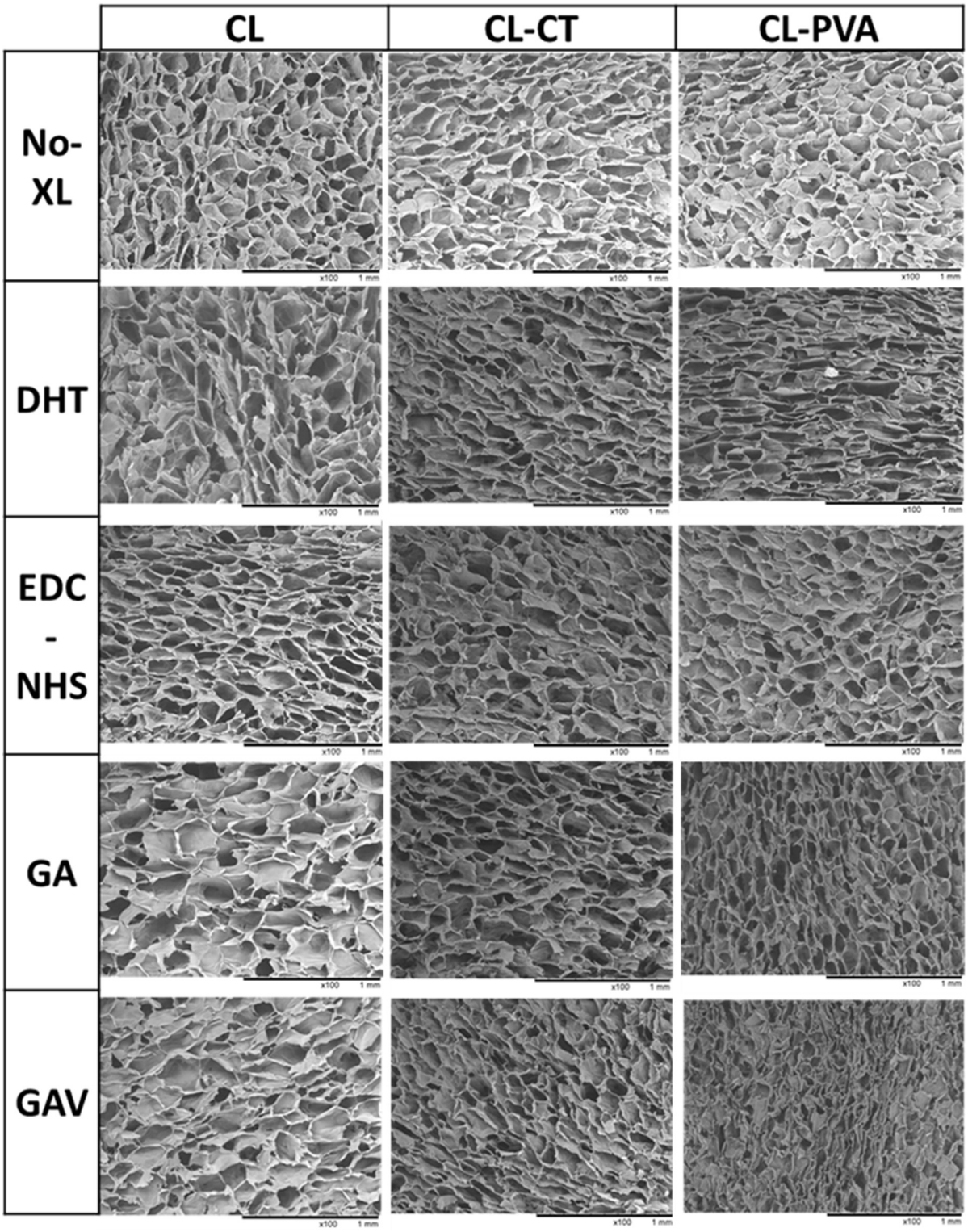

Figure 3. 7 Representation of the cross-sectional SEM images of the analysed scaffolds. Scale bars = 1 mm

On the other hand, glutaraldehyde crosslinking had a different effect on polymer blends, causing a significant decrease in pore size after vapour crosslinking while diameter measurements remained similar to No-XL and DHT treated scaffolds when of glutaraldehyde was used in solution (GA). Long-time exposure and use of a 100% water

solution might have compromised the internal structure, shrinking the pores by 20% in size compared to No-XL treatment, with a more developed and lower-void fraction.

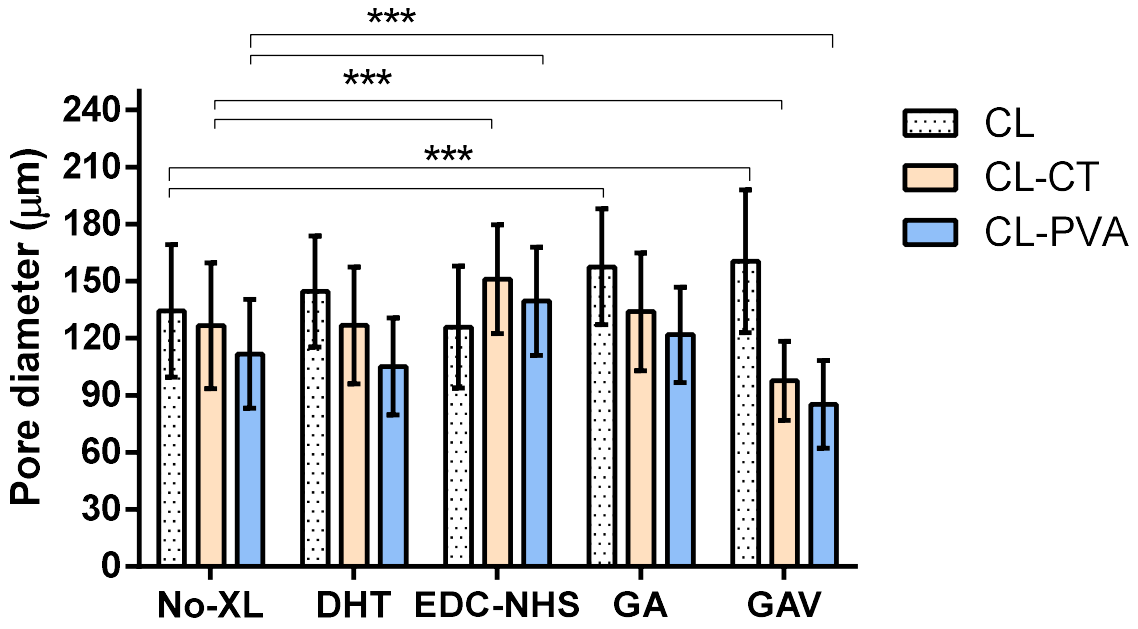

Figure 3. 8 Mean pore size for untreated and treated scaffolds (n=3). ***= p≤0.001.

3.3.3 Viscosity of solutions

The aim of this viscosity study was to explain the choice of increasing collagen concentration to 1% in the solution due to batch-to-batch inconsistency. Differences in texture and mechanical properties were observed during processing of solutions with 0.7% w/v of collagen from the second batch even though the source and manufacturer of the two batches were the same. For this purpose, viscosity measurements of several solutions were compared and results are shown in Figure 3.9.

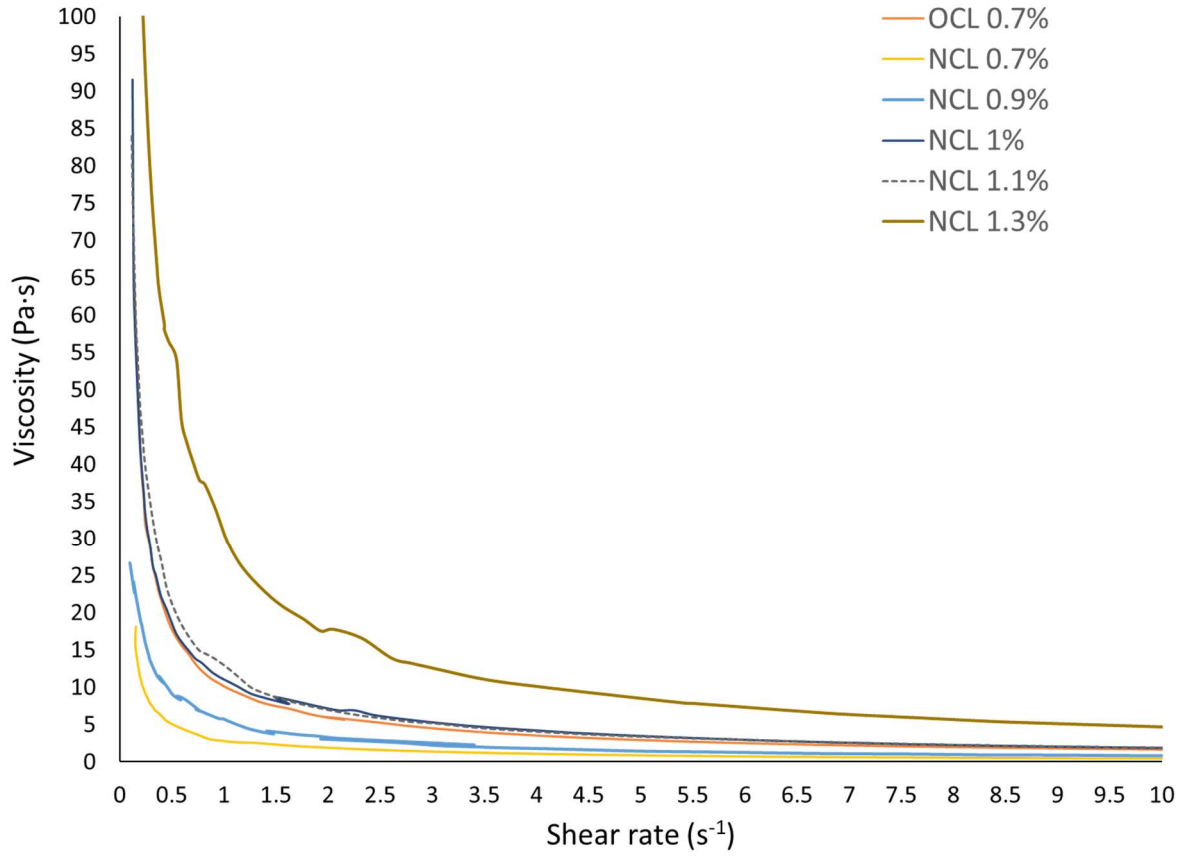

Figure 3. 9 Viscosity of collagen concentrations from first batch (OCL) and second batch (NCL) in function of shear rate.

Results indicate a correlation between collagen concentration and viscosity and inconsistencies in batch-to-batch as already reported in literature [106, 107]. Solutions followed the most common type of non-Newtonian behaviour noted as shear thinning, in which viscosity decreased with increasing shear rate. By measuring and comparing the apparent viscosity of solutions, it was possible to find the matching concentrations between the two batches. In Figure 3.9, it can be observed that the initial apparent viscosity of solutions with a concentration of 0.7% of collagen from the new batch (NCL) is three times smaller than the one from the first batch (OCL) suggesting that the second batch had a lower molecular weight. From Figure 3.10 it is also noticeable that the addition of chitosan and PVA resulted in a significant reduction of the apparent viscosity.

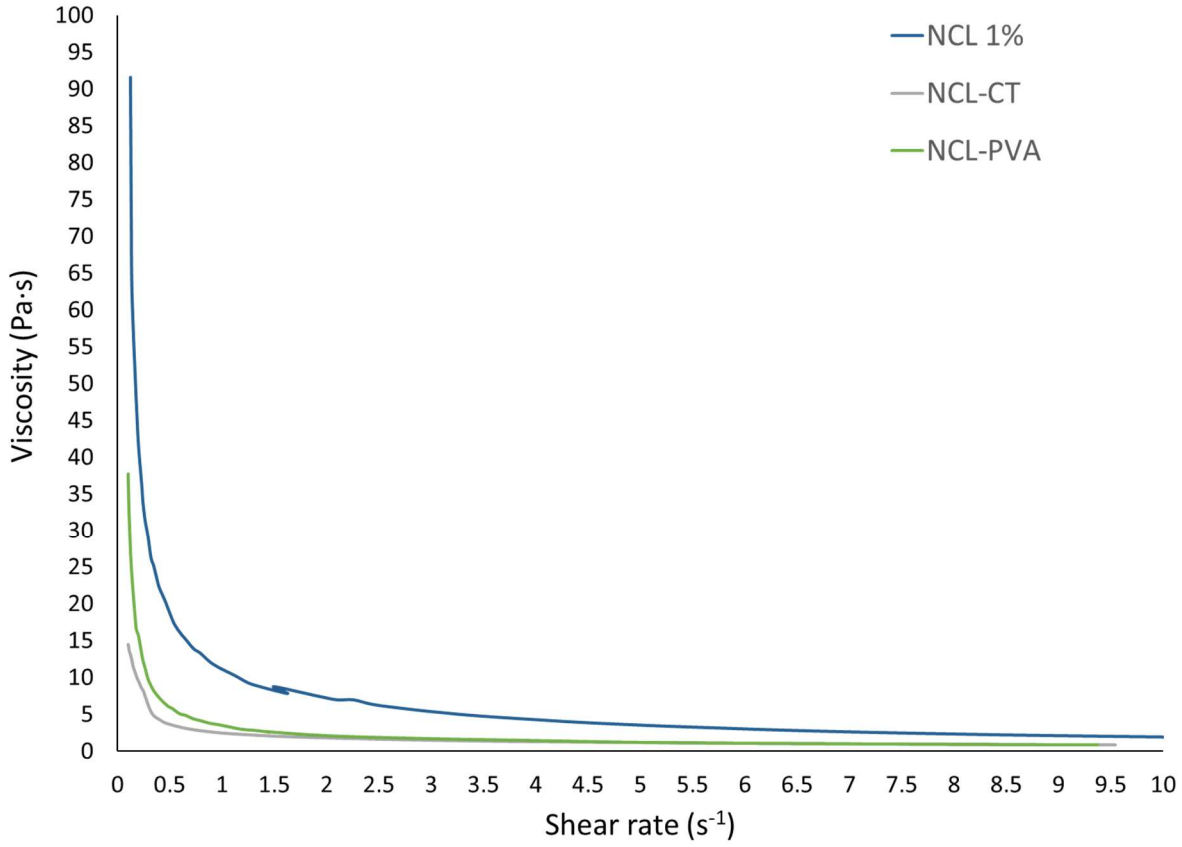

Figure 3. 10 Reduction of apparent viscosity in polymer blends compared to collagen.

Even a small incorporation of shorter and less complex chains as chitosan and PVA, into collagen solutions demonstrated to reduce viscosity and the level of chain entanglement, resulting in a smooth scaffold appearance as discussed in Section 3.3.2.

3.3.4 Degree of cross-linking

Ninhydrin assays was used to assess the presence and the number of free amines groups in scaffolds. Data reported in Figure 3.11 show a high degree of crosslinking (>80%) for all the scaffolds. However, the highest percentages (>95%) were obtained for CL and CL-CT scaffolds treated with DHT, EDC-NHS and GA. Vapour-crosslinked scaffolds exhibited the lowest degree in all three groups. This result can be due to chemical reactions that there might have been during the crosslinking process, increasing the number of free amines. Since samples were not rinsed after crosslinking, these free amines groups may have been detected during ninhydrin assay. Collagen-PVA results could also be influenced

by partial dissolution of PVA in the process as it occurs at high temperatures, higher that 80° C.

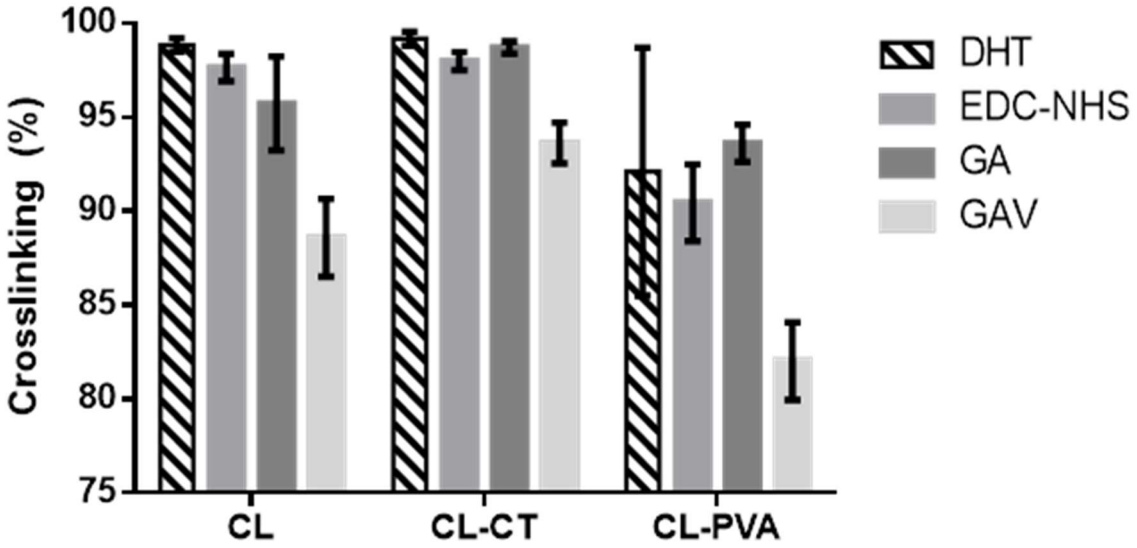

Figure 3. 11 Degree of crosslinking for the three types of scaffolds (n=3).

3.3.5 ATR-FTIR spectrum analysis

Scaffolds were characterized by ATR-FTIR to investigate possible molecular changes occurred after blending collagen with chitosan and PVA, and after crosslinking.

Normalised ATR-FTIR spectra of collagen type I scaffolds, analysed before and after crosslinking, are shown in Figure 3.12. The characteristic absorption bands of amides A, B and I, II, III [93] were observed in all samples. The first two signals are attributable to N-H stretching (3309 cm^{-1}) and C-H stretching, in CH_2 (2923 cm^{-1}) and associated with Amide A for the first and Amide B for the second one. Then, three signals are highlighted in the graph: C=O stretching (1640 cm^{-1}), N-H bending coupled with C-N stretching (1550 cm^{-1}) and N-H bending (1240 cm^{-1}). These are characteristic of Amide I, II and III, respectively. It can be noticed that the peak of amide A (3309 cm^{-1}) broadened after crosslinking, mainly in the CL DHT sample which might be linked to the hydrogen bond interactions [93]. Moreover, changes in intensity happened in scaffolds treated with different crosslinking methods in correspondence of amide B and II bands, in 1712 and 1155 cm^{-1} (red dashed circles in Figure 3.12) where increasing intermolecular bonds due to crosslinking methods, reduced or increased the absorbance [91, 108].

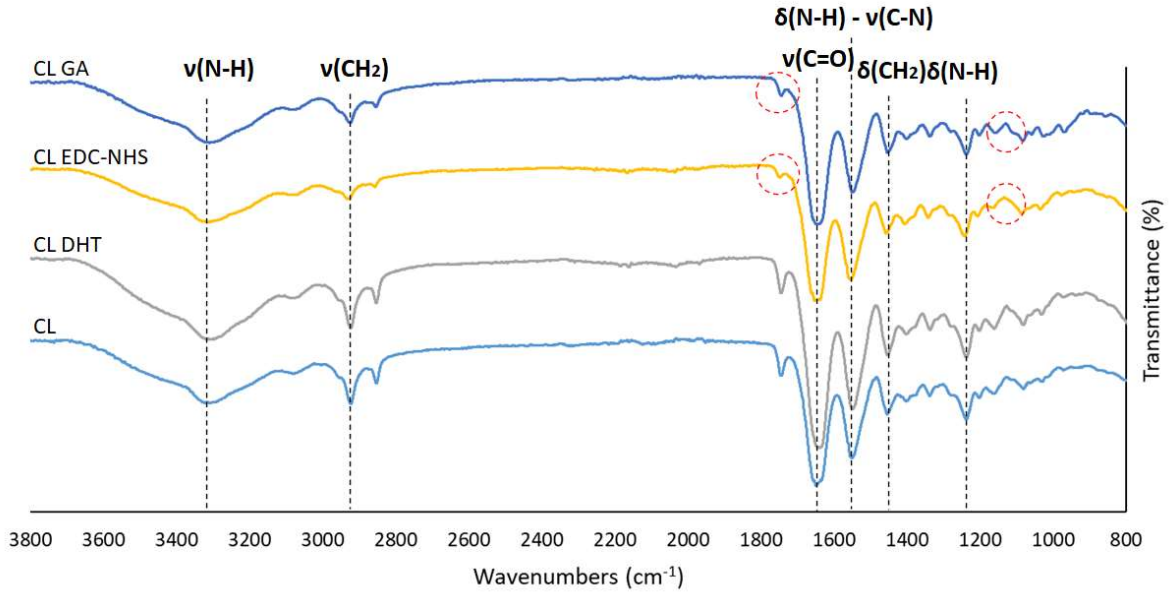

Figure 3. 12 FTIR spectra of collagen samples: non crosslinked collagen scaffold (CL); DHT treated scaffold (CL DHT); EDC-NHS crosslinked scaffold (CL EDC-NHS); GA crosslinked scaffold (CL GA).

As no obvious changes in FTIR spectra were observed, it can be suggested that the collagen structure was not altered after undergoing crosslinking treatments.

ATR-FTIR technique was also used to assess the success of chitosan and PVA bonding to collagen. In Figure 3.13 spectra of untreated collagen, chitosan and PVA were compared with scaffolds in which collagen was blended with chitosan and PVA. Pure chitosan shows a broad peak of weak intensity corresponding to the N-H stretching (Amide A) and characteristic absorption bands of chitosan appear at 1655 (C=O stretching), 1585 (NH_2 bending) and 1380 cm^{-1} (CH_2 bending) [108]. In correspondence of the first band (amide I) the energy C=O stretching from collagen and chitosan contributed to a greater peak in the spectra of collagen-chitosan scaffold. On the other hand, the greater intensity of N-H bending (amide II) in the spectrum of CL-CT means that since N-H bending in collagen molecules is stronger than NH_2 bending in chitosan, the free NH_2 groups in chitosan molecules were changed to N-H groups. Also, peaks that are slightly visible on the graph at 1378 cm^{-1} (CH_2 bending), 1159 (C-O-C stretching), 1079 and 1031 cm^{-1} (C-O stretching) are characteristic of the saccharide structure of chitosan, confirming the presence of chitosan in the collagen structure.

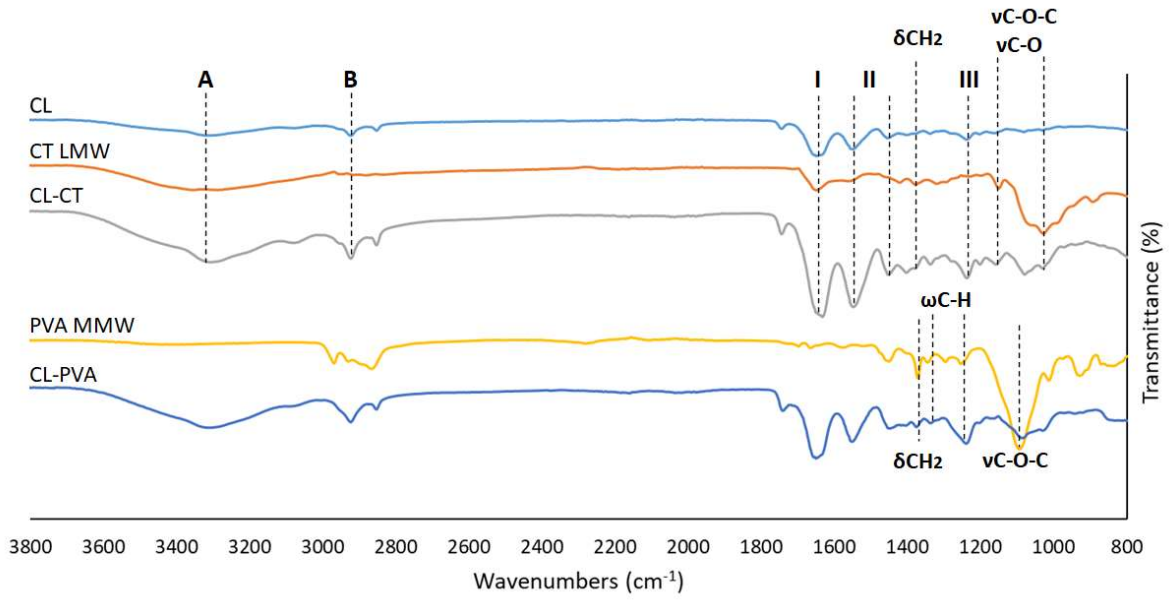

Figure 3. 13 Collagen-Chitosan (CL-CT) and Collagen-PVA (CL-PVA) spectra in comparison with pure collagen (CL), Chitosan low molecular weight (CS LMW) and PVA medium molecular weight (PVA MMW).

The characterization of the PVA structure in the spectrum of collagen-PVA (CL-PVA) through the absorption bands occurs identifying peaks that are not present in the collagen spectrum. As a matter of fact, the two bands with maximum values of 2938 and 2909 cm^{-1} are overlapped by the amide B band of collagen. However, other bands characteristic of PVA in the polymeric chain can be seen at 1424 cm^{-1} (CH_2 bending), at 1372 and 1240 cm^{-1} (C-H wagging) and at 1087 cm^{-1} (O-C-O stretching) (Figure 3.13).
Blending CT and PVA with CL resulted in the breaking of H-bonds and formation of others that can be explained as a change in intensity at absorption bands of Amide A in the range between 1400 and 1000 cm^{-1} of the spectra (Figure 3.13).

3.3.6 Porosity and water swelling

Water uptake and porosity are two important indicators used to determine the suitability and the properties of biomaterials for tissue engineering.
It is crucial for cell attachment and survival that fluid circulation and exchange of nutrients and waste can be promoted through the scaffold. These features are dependent not only on the materials but also on the pore characteristics.

In Figure 3.14, water uptake measurements for all the scaffolds considered in this study are represented as the sample final weight (Wf) after being submerged in water for 24h in function of the sample initial weight (Wi).

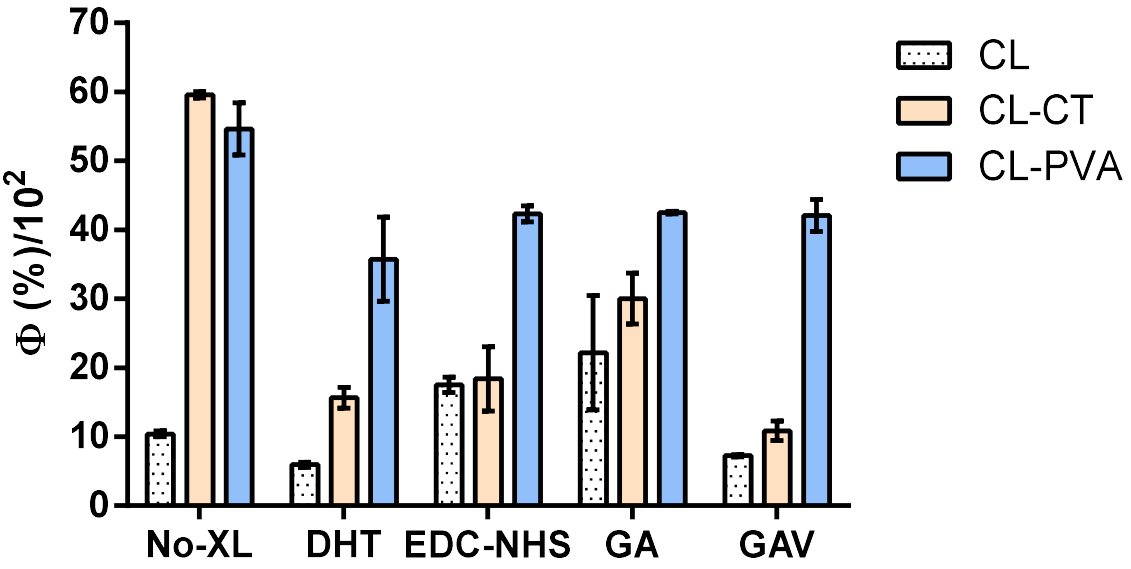

Figure 3. 14 Mean values and standard deviations of water uptake measurements performed on treated and untreated scaffolds (n=3).

The values for polymer blends were six-fold higher than collagen scaffold before crosslinking treatment. It is well known that the higher the concentration of collagen is, the worse the water uptake values get [109], but this experiment demonstrates that adding small amount of hydrophilic material in the scaffold composition can drastically improve the absorption of liquid, contrarily to what Ma et al. [110] found in their research. These disparities in results across studies can be ascribed to the source of collagen used that can present ad different number of hydrophilic groups in its structure. Therefore, it is suggested to characterize every structure individually as the methods, concentration and materials used can extensively vary the characteristics of the scaffolds. In order to give scaffolds more stability and improve degradability time, the use of crosslinking methods is unanimously and undoubtedly needed. Comparing the results, it can be seen a reduction in water uptake after crosslinking for collagen-chitosan (≥50%) and collagen-PVA (~20%) scaffolds with different trends. While values for collagen-PVA scaffolds are comparable across the four treatments, scaffolds containing chitosan reach the highest value after treatment with GA solution.

Overall, the group of scaffolds containing chitosan show similar swelling properties to those of pure collagen. It is worth also to notice that the procedure of freeze-drying partially hydrated the scaffolds after EDC-NHS and GA treatments increasing water uptake ability, hence hydrophilicity. As mentioned above, the water uptake measurement can be strictly correlated to the porosity of the structure. In this study, it was considered necessary to measure porosity with the same method used for water uptake substituting water with ethanol and forcing liquid through the pores by means of a vacuum pump.
As it can be seen from Figure 3.15, liquid absorption using ethanol has greatly increased for CL and CL-CT scaffolds with comparable values pre and post treatments with DHT and GA vapours.

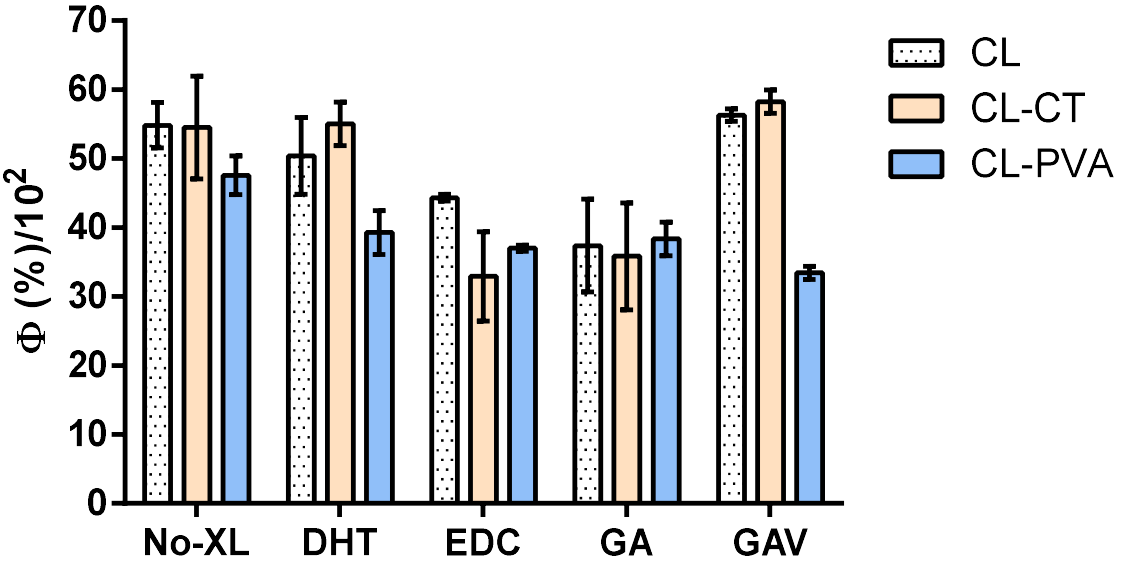

Figure 3. 15 Porosity evaluation of scaffolds immersed in pure ethanol solutions (n=3).

Ethanol was employed because reconstituted porous collagen matrices can be affected by the higher interfacial tension that the two media have, resulting in shrinkage or collapse when in contact with aqueous solutions [111]. In addition, with the aim to investigate the status of the structure in wet status, cryo-SEM images were taken (Figure 3.16). This result indicates that the structure has not changed in morphology after crosslinking treatments and underline the fact that CL-CT behaviour is similar to the collagen scaffolds. On the other hand, if the process of freeze-drying a second time has increased the hydrophilicity of those EDC-NHS and GA scaffolds it may also be the cause of a reduction in porosity.

With regards to CL-PVA, it can be said that the liquid uptake was similar to the previous measurements of water uptake, slightly decreased after crosslinking. Therefore, it can be assumed that for CL-PVA scaffolds the materials employed have a bigger influence on liquid uptake than the pore structure and the media used. The porosity of the scaffold was also measured utilising the liquid displacement method described in literature [112]. The results (not reported) showed that all the scaffolds had a porosity greater than 90% essential to ensure an optimal cell-material interaction. Further, the internal structure of DHT-treated scaffolds in wet status frozen in liquid nitrogen and then sectioned, is showed in Figure 3.16. The appearance of the cross-section surface of collagen scaffold (CL DHT) was widely different from the scaffolds made of polymer blends (CL-CT DHT and CL-PVA DHT). The pores have an open structure and they seem to be interconnected in some points. Moreover, the ice crystals were easily removed using a small vacuum air pump.

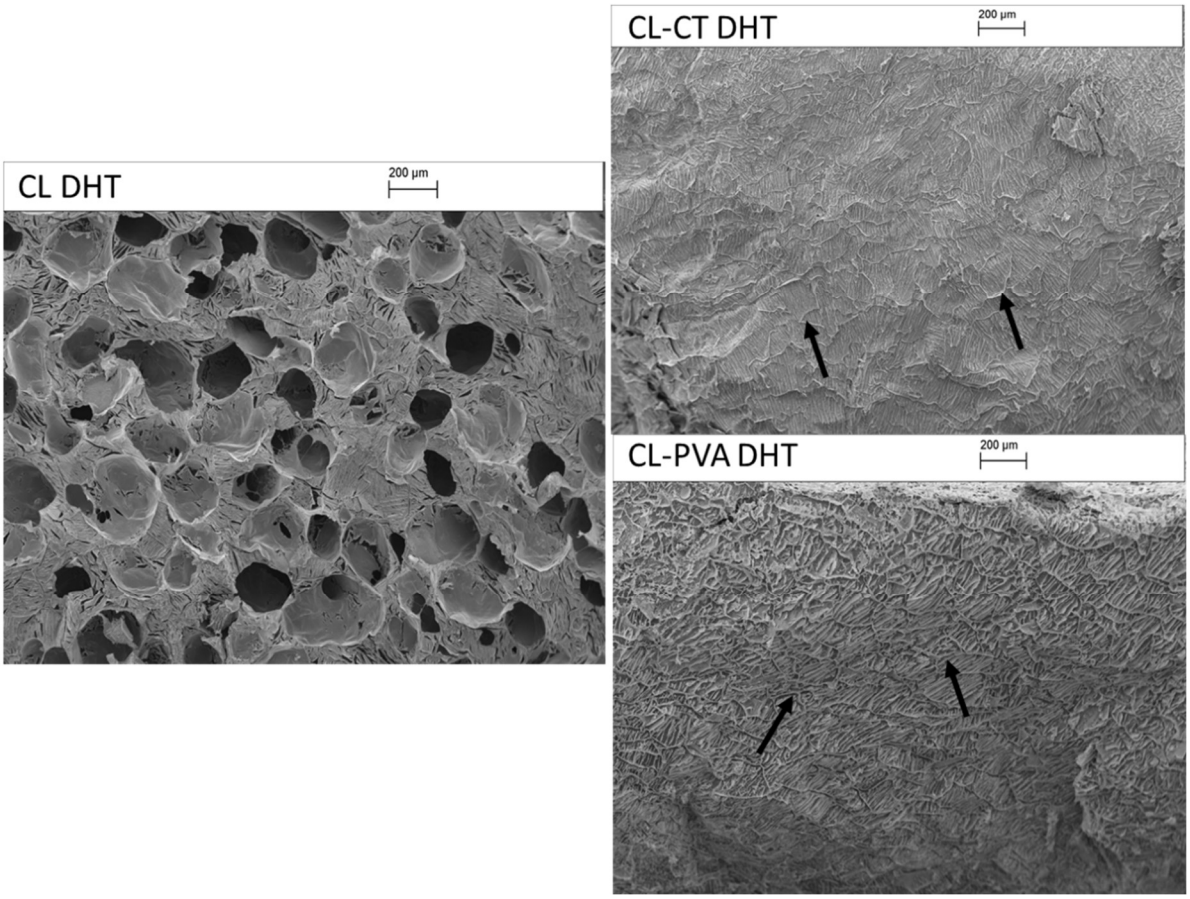

Figure 3. 16 Cross-sectional cryo-SEM images of the DHT-treated CL, CL-CT and CL-PVA scaffolds. The arrows point to the pore rims. Scale bars = 200 µm.

On the contrary, CL-CT DHT and CL-PVA DHT showed a hydrogel-like behaviour where liquid was retained between the pore rims in a well organised ice crystal structure.

However, these scaffolds presented a more brittle behaviour and poor handling probably due to the higher liquid retention. Unfortunately, similar studies that could confirm these hypotheses were not found in scientific literature.

3.3.7 Mechanical tests

Mechanical tests were performed on samples in dry and wet status to determine whether, and to which extent, crosslinking leads to scaffolds with improved mechanical properties. It is well known that the mechanical stability of freeze-dried scaffolds is relatively low because of their porous structure and high thickness [10] and the modulus of elasticity shown in Figure 3.17 for dry scaffolds under tensile tests are confirmation of the data present in literature. In dry status, CL-DHT scaffolds showed an increment in elastic modulus whereas for scaffolds made of polymer blends, CL-CT and CL-PVA, crosslinked with EDC-NHS and GA treatments resulted to have the highest elastic modulus.

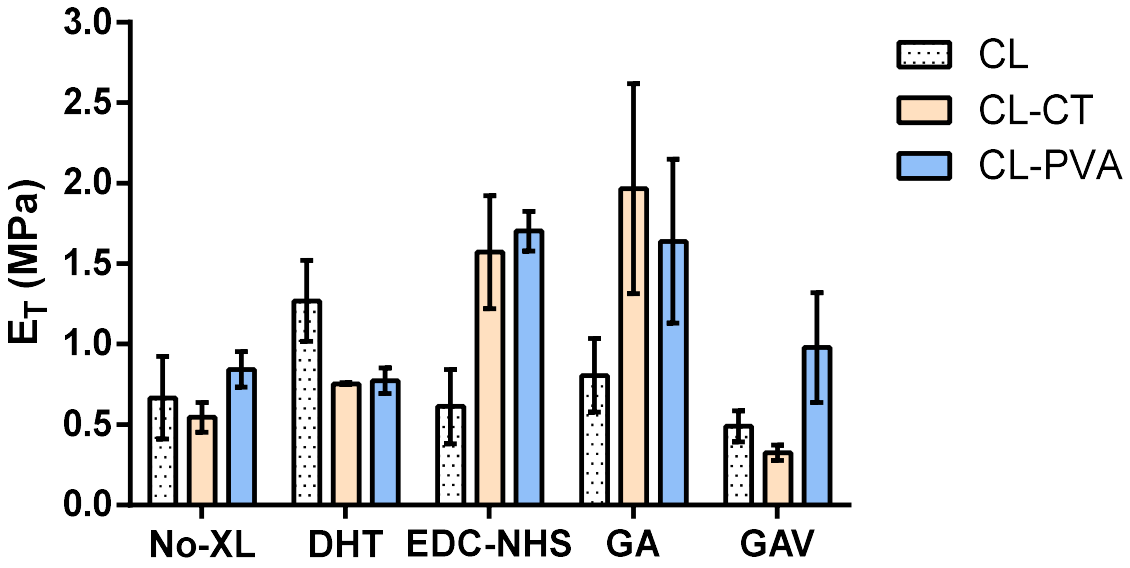

Figure 3. 17 Elastic modulus of dry samples (n=3) derived from stress and strain obtained during tensile tests.

Further, to understand whether these results were also applicable to scaffolds in wet conditions, samples were subjected to compression and tensile tests after being immersed as reported in Section 3.3.6, for 24 hours in a 6 well plate. As shown in Figure 3.18, tensile modulus (E_T) of scaffolds under wet conditions were two orders of magnitude lower than dry scaffolds, with CL-CT samples having the highest elasticity after chemical treatments.

On the other hand, while CL-PVA scaffolds showed the lowest values with slightly improved mechanical properties after crosslinking, results for collagen scaffolds were not significantly different from untreated samples.

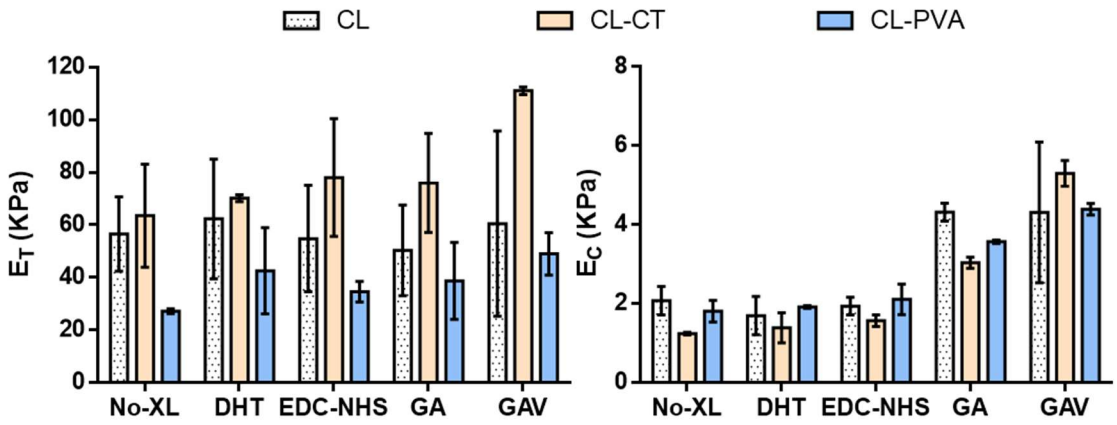

Figure 3. 18 Comparison of elastic moduli of hydrated samples under tensile stress (E_T on the left) and compression (E_C on the right).

However, under compression scaffolds treated with glutaraldehyde performed better than the other categories, especially if crosslinked with vapours, probably due to a greater collagen density linked to a pore size reduction. In addition, analysis of tensile strength and elongation at failure (Figure 3.19) following crosslinking treatment revealed no significant differences across methods. In general, materials that are stiffer tend to have lower elongation and higher tensile strength. Scaffolds made of polymer blends seemed to mechanically be inferior to pure collagen scaffolds in wet conditions for strength and elongation measurements when chemically crosslinked. This can be explained as due to the decrease of polymer matrix mobility that led to a structure more fragile [93].

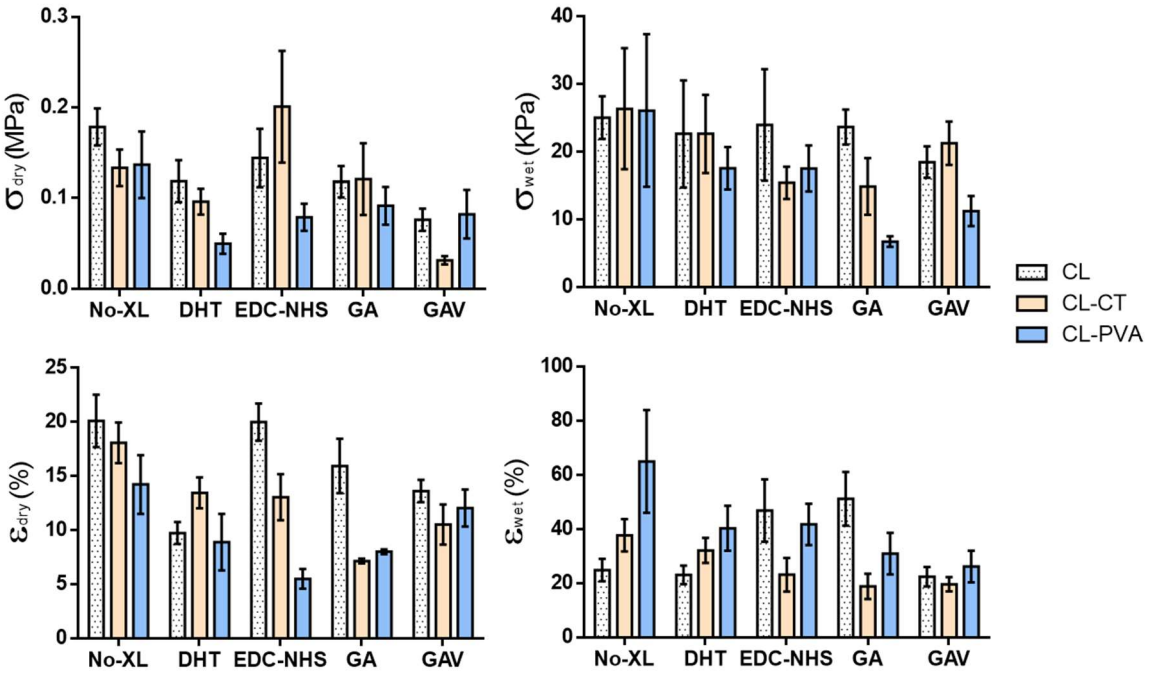

Figure 3. 19 Ultimate stress values (σ) and elongation (ε) of the scaffolds at failure in dry (on the left) and wet (on the right) status after tensile tests.

Similar to what has been presented in a study [113], samples treated with DHT and successively with EDC-NHS present the same compressive modules as the DHT treated scaffolds. All matrices exhibited a similar stress-strain relationship, with 'linear' and 'failure' regions, in which the initial 'toe' tract, characteristic of biological tissues, was not present showing an elastic rather than viscoelastic behaviour. In fact, this feature is common only in fibrous scaffolds in which collagen fibrils start orientating to the direction of stress. As an example, stress and strain curves of the three types of scaffold that were DHT-treated are shown in Figure 3.20.

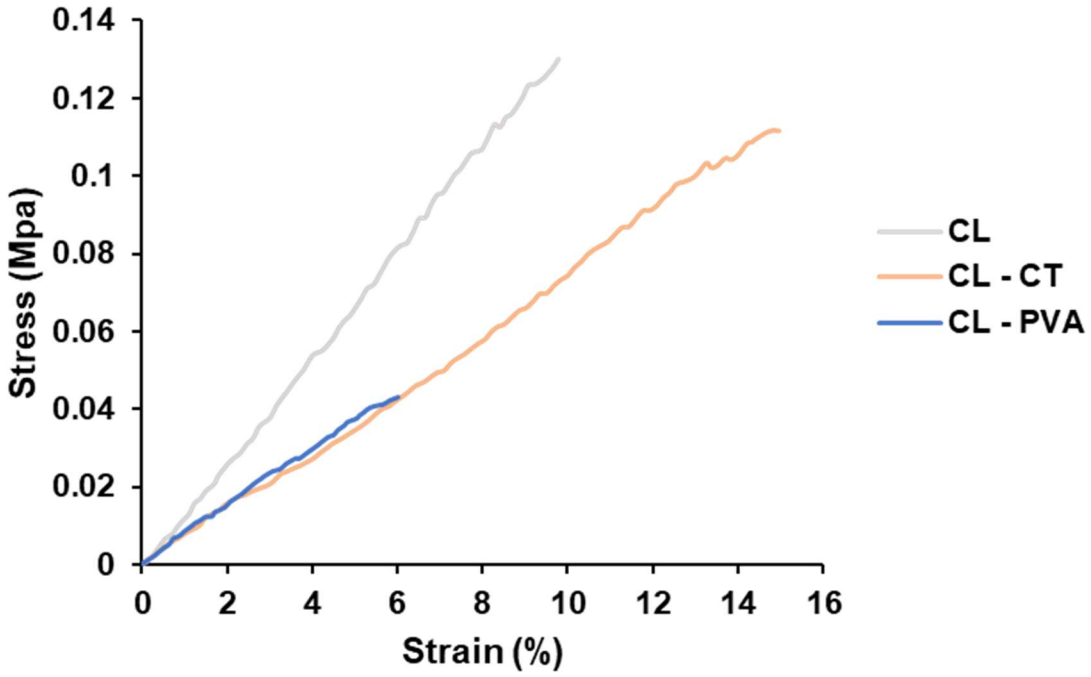

Figure 3. 20 Selected stress-strain curves for DHT-treated scaffolds in dry condition. Curves show the linear region up to the ultimate tensile strength that is equal to fracture stress.

One additional mechanical test, creep-recovery test, was performed on these scaffolds to evaluate shape recovery ability after compression. Looking at the data in Figure 3.21, GA-treated scaffolds showed to have the capability to recover to nearly their initial thickness after 60 seconds. The recovery curves are almost identical among the three types of scaffolds although CL-CT shows a steeper initial tract indicating a higher elasticity of these scaffolds. Regarding the other scaffolds, it is worth to notice that EDC-NHS treatment did not change CL-PVA recovery curve compared to the untreated scaffolds. This may suggest that the method may have very low effect on the scaffolds m. It can also be highlighted that while no-treated pure collagen scaffolds followed the same path as those DHT-treated, non-crosslinked polymer blended scaffolds maintained the thickness imposed under compression showing poor viscoelastic behaviour. The data collected during mechanical tests to some extent confirm the successful crosslinking of the scaffolds.

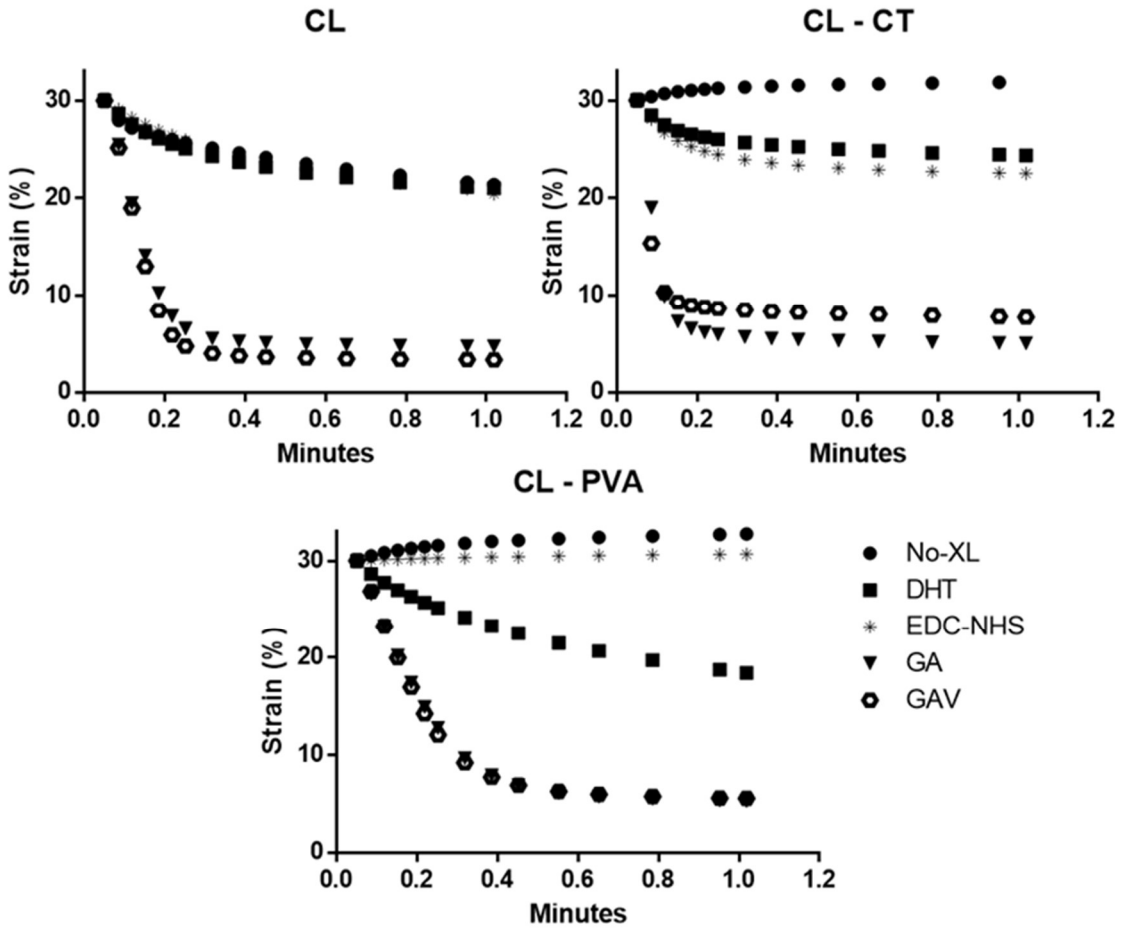

Figure 3. 21 Creep-recovery test from an initial strain of 30%.

3.4 Summary

In tissue engineering, scaffolds can be tailored for the specific application and polymer blending can represent an effective method to obtain the desired result. This study explored and described freeze dried scaffolds discussing and methodically experimenting processes to control and tune their physical properties in order to adapt these templates for various research purposes. Low amounts of hydrophilic materials added to the collagen solution as well as the use of different crosslinking methods showed to influence the structural, chemical, physical characteristics of these scaffolds leading to morphology, hydration and mechanical changes. The optimization of the method to obtain sponge-like scaffolds led to a highly interconnected and homogenous 3D macroporous structure. The distribution of pores was isotropic and size remained relatively constant throughout the scaffolds probably due to amount of solution poured in the mould and the regularity of the mould shape. The use of ethanol showed to preserve the initial structure avoiding shrinkage and

it will later be used as sterilization method for cell culture. Also, it has been shown that crosslinking increases the ability of collagen scaffolds to maintain its physical and chemical integrity but not necessarily improve the mechanical properties. Chitosan provides better elasticity and flexibility than PVA due to longer polymeric chains even though chitosan scaffolds are of poor-handling and more fragile. From a comparison of the three types of scaffolds and the different cross-linking methods applied, glutaraldehyde treated scaffolds generally performed better than any other and EDC-NHS treatment was not much more effective than the use of DHT on its own. The high swelling ratios for collagen-PVA scaffolds across the various crosslinking made these polymer blends a candidate for applications in wound healing where absorption of large amount of nutrients and liquid is essential to support cell growth. Collagen is still the protein of choice for biomaterials preparation and this study has indicated that by varying crosslinking and adding biocompatible materials, porous scaffolds can be fine-tuned to serve specific research purposes and be used for cell culture which suitability will be discussed in Chapter 5.

CHAPTER 4 Fabrication of electrospun membranes

4.1 Introduction

Electrospinning has been used for mimicking the extra cellular matrix (ECM) in skin tissue engineering for many years with great emphasis on cell adherence and stimulation of cell proliferation to promote the healing process [114]. This technology can produce high porosity and high surface-to-area ratio mats from a wide variety of natural and synthetic polymers providing scaffolds with potential morphological features similar to the ECM for their fibrous structure [115]. Furthermore, in view of the results reported in the previous chapter, higher mechanical properties are needed in order to match that of skin and provide mechanical support for cell growth. In this respect, the intrinsic mechanical properties of biomaterials suitable for electrospinning technique can play a part in achieving desirable mechanical properties.
In this chapter, fibrous electrospun mats were made using biocompatible, natural and synthetic materials widely available on the market in an attempt to make this process flexible and potentially available on a bigger scale. While focusing on the optimization of the process, a less explored collector was also developed and adopted with the aim to obtain mats with well distributed and oriented fibres. In addition, differences between nano and microfibrous matrices were investigated in respect to orientation, human dermal fibroblasts (HDF) cell attachment and proliferation.

4.2 Green electrospinning

Green electrospinning is a variant of traditional electrospinning technique that involves the use of weak acid as solvents, solvent-free solutions or water-soluble polymers [116]. This approach has drawn increasing attention because it prevents the inhalation of toxic and user-harmful volatile gases from organic solvents traditionally utilized in the electrospinning process. These solvents pose a risk for the environment and a barrier for industrial scale-up and clinical translation due to the high cost and possible toxicity [117]. However, there are drawbacks and constrains associated to the use of green electrospinning. Restrictions on the choice of polymeric materials for their solubility properties and the complex optimization process due to instability of water-soluble polymers may limit its use.

4.2.1 Materials used in green electrospinning for skin applications

A wide range of natural and synthetic materials have been successfully used to produce electrospun membranes for several skin applications, from skin repairing, wound healing to cell differentiation [118, 119]. Many researchers have favoured blending natural polymers such as collagen, gelatin and chitosan with synthetic ones [120, 121] as natural fibres alone are mechanically weak, while others have investigated the use of pure synthetic polymers [122]. Collagen electrospun scaffolds (CL) have demonstrated to have excellent biocompatibility and to be a favourable environment for cell growth [123, 124]. However, the need of expensive and environmental toxic fluoro-organic solvents such as 1,1,1,3,3,3-hexafluoro-2-propanol (HFP) and 2,2,2-trifluoroethanol (TFE) to dissolve it, with consequent loss of its native structure have restrained its use on commercial scale. Furthermore, collagen is a challenging material to electrospin. Process optimization relies on the source of collagen and on its molecular weight that varies significantly [125], as demonstrated in Section 3.3.3, leading to non-replicable results. Only few studies successfully explored the use of mixture of benign solvents to fabricate collagen electrospun mats [126, 127]. For this reason, in this study, alternative polymeric materials were investigated. Chitosan (CT) is a charged natural polymer that possesses the ability to form covalent or ionic bonds with other chemicals in acid solutions. Although its polycationic nature makes it exceedingly difficult to electrospin into nanofibres [128], addition of other polymers such as polyvinyl alcohol (PVA), Polyethylene oxide (PEO), Polycaprolactone (PCL) and Polylactic acid (PLA) can improve its stability and spinnability [129]. The use of chitosan has been extensively reported in skin tissue engineering for its antibacterial properties and hydrophilicity [130]. Most of the synthetic polymers such as PEO, PVA and PCL are neutral polymers widely studied in the electrospinning process for their biocompatibility and availability in a wide range of molecular weights. A summary of various materials dissolved in benign solvents that were investigated in previous studies, is shown in Table 4.1.

Table 4. 1 List of biomaterials used in green electrospinning for skin applications.

Material	Solvent	Reference
PCL	Acetone	[56]
PCL/PEO –PCL/CT	Glacial Acetic Acid (GAA) - GAA/Formic acid	[121, 131-133]
CT/PEO	GAA/water	[134-136]
PCL/CT	Formic acid - Acetone	[137-139]
Gelatin, PEO/CT, PCL	GAA	[122]
Gelatin/PCL/PEO/CS, PCL/PEO/CT, Gelatin/PCL	GAA/water	[12, 140]
Collagen/PCL, Gelatin/PCL	GAA/water	[120]
Collagen/Nigella sativa oil/Chitosan	Water	[141]
Collagen	PBS/Ethanol – GAA/DMSO	[126, 127]

4.3 Electrospinning system

An electrospinning device was set up by the candidate using existing and new laboratory supplies. In details, the candidate supplied and coordinated the construction of the chamber that contained the apparatus and made use of a syringe pump and high voltage generator that were purchased for a previous electrospinning setup no longer in use. In addition, the candidate designed a low-cost rotating collector for production of aligned fibrous scaffolds. Various polymeric solutions were preliminary tested in order to validate the manufacturing process.

4.3.1 Electrospinning setup

The machine (Figure 4.1) was placed horizontally using a syringe pump and a high voltage generator 40 kV-60 kV (Linari Engineering srl, Italy). Both devices were contained in an in-house built chamber made of acrylic sheets (5 mm thick) that were glued together using acrylic cement by the Mechanical Engineering workshop (University of Hull). The chamber had the purpose to protect the operator from health hazard such as the high voltage but also to limit the influence of external environmental factors that could affect the process (temperature,

humidity, air draughts). In addition, to facilitate access to the pump and collector, a window was created in the middle and connected to a magnetic non-contact safety switch for further protection from injuries due to the high voltage. While the applied voltage could be adjusted using an interface located outside of the chamber, syringe diameter and feed rate had to be set on the pump before starting the experiment. The collection aluminium plate was mounted on a plastic support and the deposition surface was covered with aluminium foil to facilitate the sample collection. A differential voltage was applied from the tip of the syringe needle (+) to collector tray (-) by means of crocodile clips connected to the generator and to earth, respectively. Electrospinning was performed at room temperature (23 ± 5 °C) and at a relative humidity of 25% ± 5% monitored by a thermohygrometer.

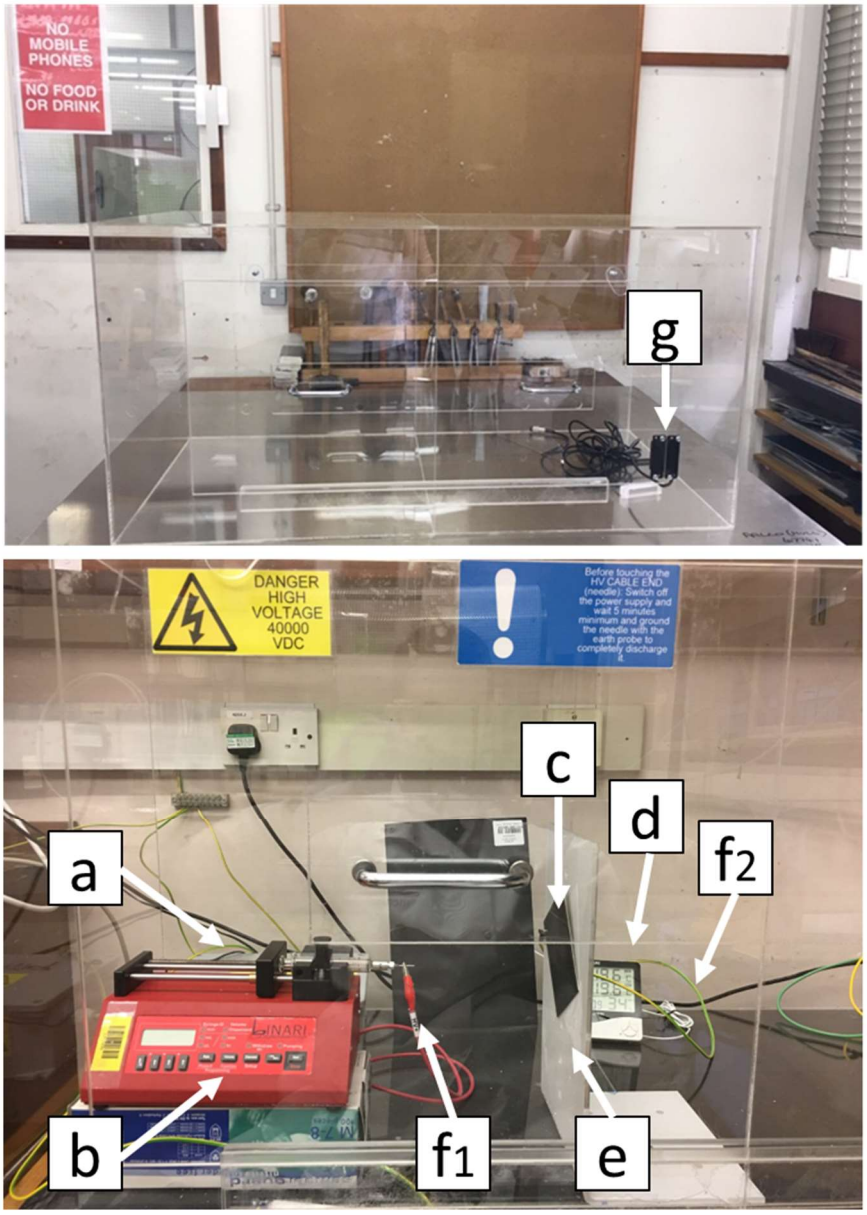

Figure 4. 1 Electrospinning setup in the lab displaying all the parts necessary for the process. a) high voltage power source (behind the pump), b) single channel syringe pump, c) conductive collecting plate, d) thermohygrometer, e) insulated support that holds the plate f1) input cable (+) connected to tip of the needle, f2) output cable (-) connected to the conductive plate and, g) safety switch.

4.3.2 In-house built rotating collector

Different types of collectors can be built to control the morphology of electrospun scaffolds based on their geometry. A recently published study [142] describes the effect of fictitious forces on nickel cobaltite nanofibres during electrospinning comparing a rotating collector (Figure 4.2) with a drum and static collectors. Kumar et al. obtained more uniform and less oriented and agglomerated fibres using the rotating collector. This interesting result combined

with two other related articles found in literature [134, 143] led to the design and development of a rotating disk collector to explore this innovative concept for electrospinning of polymeric solutions and investigate the characteristics of these fibrous scaffolds for skin tissue engineering. The configuration of this collector was also chosen for allowing electrospinning over collagen porous scaffolds fabricating a continuous porous bilayer structure that could better mimic the architecture of the structural organization of the dermis. Results and discussion about this experiment can be found in Section 5.3.

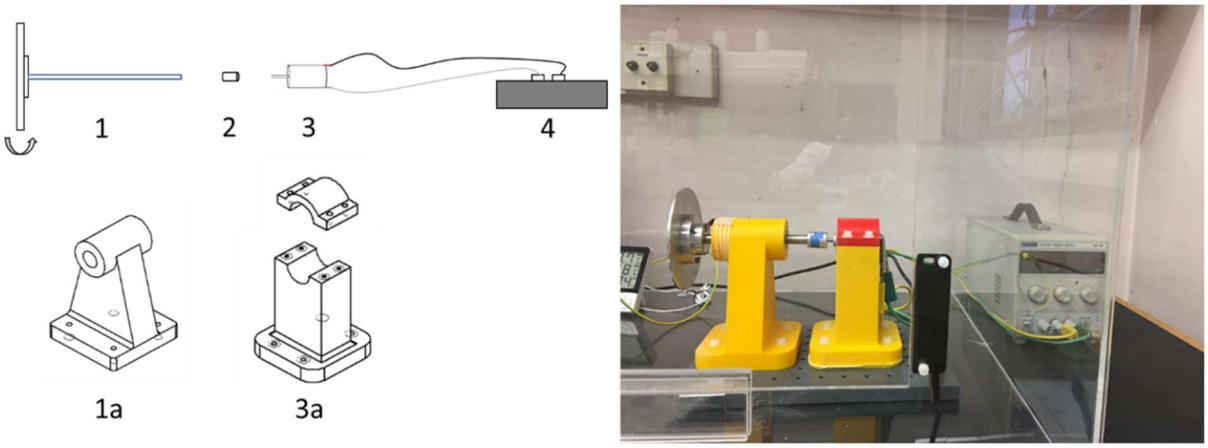

Figure 4. 2 Schematic illustration of the rotating collector components (left) and image of the assembled collector (right). Collector parts: disk connected to a rod (1) and its support (1a), shaft coupling (2), DC motor (3) and its support (3a), power supply (4).

The rotating collector was designed and developed by the candidate. Supporting parts were drawn using SOLIDWORKS software and manufactured in polylactic acid (PLA) using *Ultimaker 2+* 3D printer with the purpose to fit and keep in place the disk and the DC motor. Once assembled supporting parts were anchored to a Teflon modular support by means of nylon screws to electrically isolate the system. Engineering drawings of the supporting parts with details about geometry and dimensions can be found in Appendix I. The metallic parts of the collector composed of an aluminium disk of 120 mm in diameter and an 8 mm aluminium rod were assembled by the Mechanical Engineering workshop (University of Hull). Shaft coupling was obtained from RS components (UK) while DC motor and power supply were provided by the Electrical Engineering department (University of Hull). To allow rotation of the rod, two 8 mm deep grove ball bearings (RS components, UK) were fitted and glued in the extremities of the disk support. A copper bundle was also secured to the 3D printed support by means of cable ties to allow electrical earthing through contact with the disk. The rotational velocity of the collector was

measured in revolutions per minute (RPM) using a laser tachometer. By adjusting the applied voltage, the velocity was regulated upon need.

4.4 Polymer solutions for electrospinning use

Solutions of synthetic and nature-derived polymers in environmental-friendly solvents were employed with the purpose of creating fibrous scaffolds for potential applications in skin tissue engineering and wound healing.

4.4.1 Polyethylene oxide/ Chitosan (PEO-CT) solution

The electrospinning of pure chitosan is impractical due to its polycationic nature and mixing with other polymers is necessary. Polyethylene oxide (PEO) can be used as an auxiliary component to improve chitosan electrospinnability as it increases solution viscosity and surface tension making possible the fabrication of continuous fibres [144].
In the last decades, PEO and Chitosan (CT) blend has emerged as an ideal combination of materials for wound dressing applications. Studies have shown their biocompatibility and antibacterial properties [145] with researchers adding herbal extracts intended to act as an effective treatment for different wound healing mechanisms [146].
On the other hand, less is known of the impact that CT content and their ratio can have on fibre diameter and on mechanical properties of the membranes. Furthermore, the possible dissolution of PEO in solution and stabilisation of CT are underexplored and production of stable process not simple to obtain [135, 147]. For this reasons, different combinations were preliminary tested using amounts that ranged in an interval investigated by Sohi et al.[147] and lastly a solution composed of 3% PEO w/v (900.000 MW, Sigma-Aldrich, UK) and 2% Chitosan (CT) w/v (MMW, Sigma-Aldrich, UK) was chosen. They were mixed overnight in 50% GAA (Fisher Scientific, UK) separately. Solutions of 1:2 and 1:3 PEO-CT were prepared and magnetically stirred for 2 hours before being electrospun. A 5 or 10 ml luer lock syringe was filled with the polymeric solution and connected to a 21G blunt needle (0.8 mm OD, 0.5 mm ID). The applied voltage was 13 KV, with a distance between the needle and the collector of 15 cm. The solution was pumped at rates of 0.2 ml/h ~ 0.4 ml/h since higher feed rate resulted in solution dripping. Changes in fibre diameter were studied increasing the distance from the collector and adjusting the voltage to higher values.

4.4.2 Polycaprolactone (PCL) solution

PCL is a synthetic, degradable polymer commercially used for wound dressing. As a material for skin tissue engineering, it can support fibroblasts and keratinocytes proliferation and exhibits good mechanical properties. In this study, PCL pellets (80000 MW, Sigma-Aldrich, UK) were dissolved in GAA (Fisher Scientific, UK) to produce solutions of 15, 18, 20 % w/v that were intermittently left on a hotplate stirrer at 40°C and ultrasonicated until complete dissolution. The parameters used in the process were: a needle-collector distance of 11 cm, a feed rate of 0.2 ml/h ~ 0.4 ml/h and a high voltage of 9 kV - 12 kV. Temperature and humidity, factors that can have an impact on fibre morphology, could not be controlled but only monitored, since the system utilised was not equipped with an environmental chamber.

4.4.3 Polycaprolactone/ Chitosan (PCL-CT) solution

There are several studies reporting the use of electrospun Polycaprolactone (PCL) and Chitosan (CT) blends for tissue engineering applications since PCL provides mechanical properties to the scaffold while CT can be added to favour wettability, biocompatibility and biodegradation. However, the majority of these studies employs fluoro-organic solvent systems for their dissolution [148, 149] and evaluate resulting membranes biologically for their CT content without discussions how the chitosan can influence the fibre diameter. In this respect, the use of fluorinated solvents shows a narrow deviation in fibre diameter at various PCL-CT ratios [121, 150]. Although, other studies have investigated PCL and CT blends using binary solvent systems with less toxic acids [11, 121, 131, 138], there are still a lack of understanding if the use of a single benign solvent to dissolve the materials can produce a stable and continuous electrospinning jet [151]. Furthermore, the impact that small addition of polar solvent such as water may have on fibre morphology, has not been evaluated. Therefore, the aim of this work was to explore the feasibility of the electrospinning process utilizing PCL dissolved in pure GAA blended with CT dissolved in aqueous acetic acid.

Different combinations with 15%, 18%, 20% PCL w/v in GAA and 1%, 2% MMW Chitosan in 1% GAA with ratio 9 to 1, respectively, were investigated using a static collector. Also, the effect of adding water to PCL solutions was evaluated.

4.5 Physio-chemical methods of characterization

The combinations of polymers presented in the previous section was evaluated using several characterization methods to highlight crucial features in fibrous scaffolds such as morphology and chemical composition.

4.5.1 Morphology and fibre diameter

Electrospun samples were cut out of the aluminium foil used for fibre collection. They were observed using a Bench-top Scanning Electron Microscope (SEM) (T100, Hitachi). and a SEM (Stereoscan 360, Cambridge Instruments) depending on the resolution and information needed. The use of the Stereoscan 360 was necessary to analyse samples at high magnifications. However, this process required an additional step as the non-conductive polymeric samples had to be sputter coated with gold (S150 B, Edwards Ltd) for at least 3 mins to reduce electron charging effect and to be scanned.
The measurement of the average fibre diameter was carried out manually on the image analysis software *ImageJ*, from 30 fibres selected randomly from one image. In order to characterize the alignment of electrospun fibres, analysis using a new developed plugin *OrientationJ* [152] in ImageJ was performed. It automatically creates a visual representation of the fibre orientation plotting its distribution in the image. A more detailed description of the method is presented in Section 4.7.1.3.

4.5.2 Attenuated Total Reflection - Fourier Transform Infrared (ATR-FTIR) spectroscopy

The spectra of bulk materials and electrospun membranes, before and after sterilization, were obtained with a Nicolet iS5 FTIR spectrometer (Thermo Scientific) equipped with an iDR ATR (attenuated total reflectance) accessory. Parameters used are detailed in Section 3.2.1.4. The chemical bonds in PEO, PCL and Chitosan were identified. Also, possible modifications of the chemical structure due to electrospinning and immersion in 70% ethanol solution were investigated. The 70% ethanol solution was chosen as a sterilizing method for membranes prior to cell culture.

4.5.3 Water contact angle (WCA) measurements

The wettability of fibrous scaffolds was evaluated by measuring the water contact angle using sessile drop technique (DSA 100, Kruss Instrument). The samples were directly spun on cover slips attached to the rotating collector with conductive tape. A droplet of water (10 ul) was placed on top of the membranes using a gastight syringe for aqueous samples (Hamilton). The angle was immediately measured by taking pictures of the droplet through the Drop Shape Analysis software (DSA-4). This method determines the contact angle as the apparent contact angle between the calculated drop shape and the baseline using the software polynomial method that is indicated for measuring range between 10° and 180°. Values are calculated as the average of three measurements.

4.5.4 Stabilisation of Chitosan/ Polyethylene oxide (CT/PEO) membranes

The swelling and dissolution of water-soluble electrospinning nanofibres is a common phenomenon that can affect the morphology, structure and applications of the membranes and not often discussed in literature.

Various techniques have been reported to being used on PEO-CT membranes, from chemical and physical crosslinking to environment-friendly solutions with the common goal to promote water stability. PCL and PCL-CT membranes were not investigated to assess morphological changes as PCL is insoluble in water and alcohols. The surface stability was assessed through immersion in several solutions before and after DHT treatment applied for 24h at 105° C under vacuum and the morphology of fibres was studied using SEM.

4.5.5 Mechanical tensile testing

To evaluate the mechanical properties, samples were cut out by means of a scalpel with the same dimension described in Section 3.2.1.6 and detached from the aluminium foil using forceps. In brief, samples size was 25 mm in length, 7 mm in width with a gauge length of 10 mm and width of 4 mm. Two types of PEO-CT and PCL membranes in random and aligned configuration were studied. The tensile properties of the mentioned mats were measured with a Lloyd Material Testing LS1 tensile machine using a load cell of 100N at

strain rate of 1 mm/min. Five samples (n) were tested in dry conditions and the highest and lowest values were discarded in order to have a better representation of the average excluding the extreme values of elastic modulus. Samples from the rotating collector were taken tangential to the rotational axis at 2.5 cm from the centre.

4.6 Cell culture, cell viability and cell morphology

With the purpose to further understand how topography, type of material and substrate stiffness affect cell behaviour, primary human dermal fibroblasts (HSF) isolated from skin specimen collected from different patients were cultured on electrospun substrates.

4.6.1 Primary Human Dermal Fibroblasts Isolation

The following protocol was conducted by collaborators at Daisy building (Castle Hill Hospital, Hull). Tissue samples were initially collected from theatres at Castle Hill Hospital and incubated in holding media, comprised of 500 ml of DMEM (Gibco, Thermo Fisher Scientific, UK), 50ml FBS (Gibco), 10ml of Penicillin-Streptomycin (Gibco) and 10ml Amphotericin B (Gibco). Human skin samples were then defatted using surgical equipment and washed thoroughly in Hank's Balanced Salt Solution (HBSS) (Gibco), while continuously agitated on order to remove any remaining fat. Human samples were then divided into strips and left to incubate in 0.2% dispase (Gibco) for approximately 16 hours at 4°C, maintaining an upwards epidermal orientation. Following an overnight incubation skin was transferred to a sterile petri dish and rinse in DPBS (Gibco) in order to remove residual dispase. Dermal skin was dissected using surgical scalpels into sections measuring approximately 4 x 4 mm. Divided skin sections were then incubated in a designated C tube for approximately 3 hours at 37°C within the specialised enzyme dissociated solution (435µl of buffer L, 12.5 µl of enzyme P, 50µl of Enzyme D and 2.5µl Enzyme A) from the human Whole Skin Dissociation Kit (Miltenyi Biotec, Germany). After incubation, the tube of dissociation enzymes containing the minced skin was diluted using 500µl of cold human dermal fibroblast growth medium (Gibco). The C tube containing the dermal sample was then secured, inverted and attached onto the sleeve of the gentleMACs dissociator (Miltenyi Biotec). Ensuring the sample material was located in close proximity to the rotor, the ‘h_skin_01’ program setting was run. Following termination of the program the C tube was detached from the gentleMACs dissociator and

centrifuged at 400 rpm for approximately 5 minutes to allow the collection of cells at the bottom of the tube. The material was then resuspended in 5ml of human dermal fibroblast growth media and filtered through a 70µm cell strainer. The suspension was then centrifuged at 400 rpm for approximately 5 minutes before resuspension of the cell yield within human dermal fibroblast media. Cells where then left undisturbed at 37°C and 5% CO2 for approximately 48 hours.

4.6.2 Scaffolds sterilization and cell seeding

Fibres were collected directly on 9 mm glass cover slips attached with conductive tape to the disk at 2.5 cm from the center. Before seeding, all scaffolds were sterilized in ethanol 70% (v/v) overnight and washed 3 times with phosphate-buffered saline (PBS). Thus, the solution was removed, and scaffolds were left under UV light (wavelength of 254 nm) for 1 hour. Primary human dermal fibroblasts (HDF) were trypsinized, counted using a haemocytometer and pipetted directly on each membrane (n=3) placed in a 24 well plate in number of $4x10^4$ cells in 100 µl of medium. The plate was incubated for 30 min and after, 400 µl of medium was added in each well and scaffolds were cultured for 2 days at 37° C and 5% CO_2 in an incubator.
Culture medium was Gibco™ DMEM, high glucose, no glutamine, no phenol red supplemented with fetal bovine serum (10% v/v) and streptomycin (1% v/v), all from Thermo Fisher.

4.6.3 Viability assay and cell morphology

The cell-matrix interaction is a major factor that affects cell binding and greatly influences adhesion, proliferation and infiltration of cells. Viability of cells was assessed using MTS assay (CellTiter 96® AQueous One Solution, Promega) while adhesion and proliferation by staining of the cells with a combination of fluorescent dyes diluted in PBS. The MTS tetrazolium compound is converted by reduced nicotinamide adenine dinucleotide phosphate (NADPH), product of enzymes in metabolically active cells, to produce water soluble formazan dye which absorbance intensity can be quantified at 490 nm using a spectrophotometer in a 96 well plate reader after 4 hours of incubation. This method gives an indirect measure of cell proliferation, as the cell mitochondrial activity increases with the number of viable cells. The assay solution was added to the membranes cultured in a 24 well plate in amount of 10% in 100 µl of culture medium at day 3. HDF were also

culture in cell culture-treated plates (Falcon™ 24Well, Corning) following the same procedure to create a calibration curve and be used as control. Using the equation from the calibration curve, the absorbance values recorded for the scaffolds were converted to estimate the number of viable cells in each well. Staining was performed as follow. At day three, constructs were fixed in paraformaldehyde, 4% in PBS. Thus, cells were permeabilized and stained with Rhodamine Phalloidin 1:80 and 4',6-diamidino-2-phenylindole (DAPI) 1:5000 in PBS for F-actin (molecule of cell cytoskeleton) and for cell nuclei, respectively. Both dyes were bought from Invitrogen, Thermo Fisher Scientific. Sample were imaged with an inverted fluorescence microscope (Olympus IX71) and SEM. All tests were performed in triplicates.

4.7 Results and discussion

In this section the feasibility of a steady electrospinning process for solutions described in Section 4.4, was reported. Firstly, the effect of various parameters and of the in-house built rotating collector on fibre diameter and orientation was examined. Secondly, results of chemical and physical characterization were discussed and finally, cell morphology and attachment were presented.

4.7.1 Morphology and topography of electrospun membranes

4.7.1.1 Optimization of spinning parameters for PCL and PEO-CT solutions

Viscosity and conductivity of the polymer solution are considered two of the most influential factors to successfully spin fibres without defects [153, 154]. In this respect, the choice of solvent can greatly influence the process, leading to controversial data in terms of process feasibility if the solution concentrations and spinning parameters are not optimised, particularly for benign solvents such as acetic acid. For instance, Schueren et al. [155] showed that the only use of acetic acid as solvent for polycaprolactone (PCL) was not able to electrospin any fibrous material maintaining the concentration of polymer constant. The addition of formic acid to the solution was necessary to produce bead-free fibres. However, the use of binary solvent systems drastically reduced the average fibre diameter and consequently the macroporosity of the mats that is considered a crucial element for cell infiltration in tissue engineering applications [156]. On the contrary, Liverani and Bocaccini [157] and Kanani and Bahrami [151] were successful in electrospinning concentrations of PCL in pure acetic acid obtaining bead-free membranes. In this study, the aim was to show and confirm that it is feasible to establish a steady jet of PCL in pure acetic acid solution for at least 30 minutes prior to optimization of polymer concentration and applied voltage. In addition, change in fibre diameter with flow rate and distance of the needle from the collector was investigated. Electrospinning process was visually judged by the presence of a stable Taylor cone. Solutions with PCL concentration of 15%, 18%, 20% w/v in pure acetic acid were studied. SEM images of the fibres (Figure 4.3) revealed different morphologies increasing the concentration from 18% to 20%, resulting in homogeneous defects-free fibres. Solution with 15% of polymer was not

possible to electrospin without dripping or sputtering and a stable Taylor cone could not be obtained.

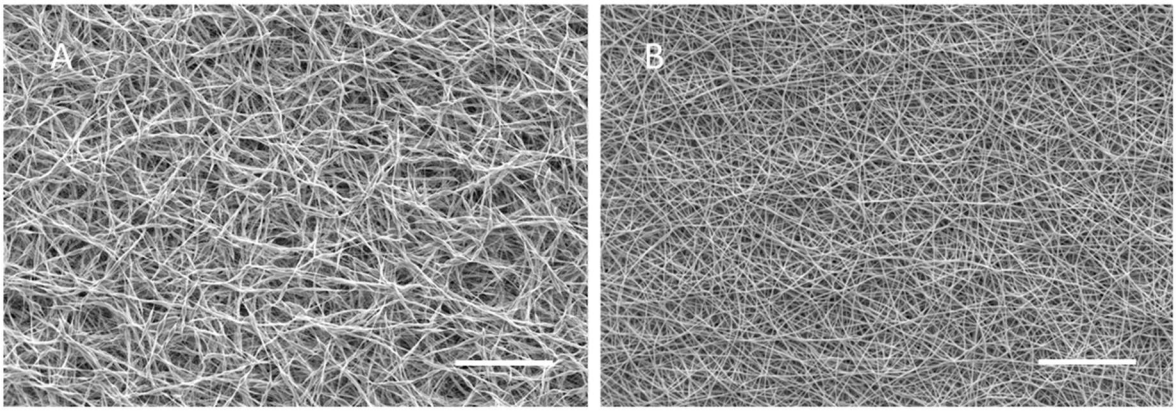

Figure 4. 3 Electrospun scaffolds of PCL 18% (A) and PCL 20% (B). Scale bar = 100 µm.

The average fibre diameters increased with increasing polymer concentration; fibre diameter measurements could not be compared as the use of 18% w/v PCL in solution generated embedded beads resulting in thicker fibres [158].

Change of other parameters such as flow rate and needle-collector distance, was evaluated for 20% PCL and their influence on fibre diameter discussed. As reported in Figure 4.4, it was established that diameter increases steadily from ~1 to 2 µm with higher pumping rate whereas there was no notable change varying the distance in the range between 11 and 15 cm that resulted in stable state. Values of fibre diameters are similar to the one obtained by other researchers [151, 157], which study supported the possibility to use PCL with benign solvents.

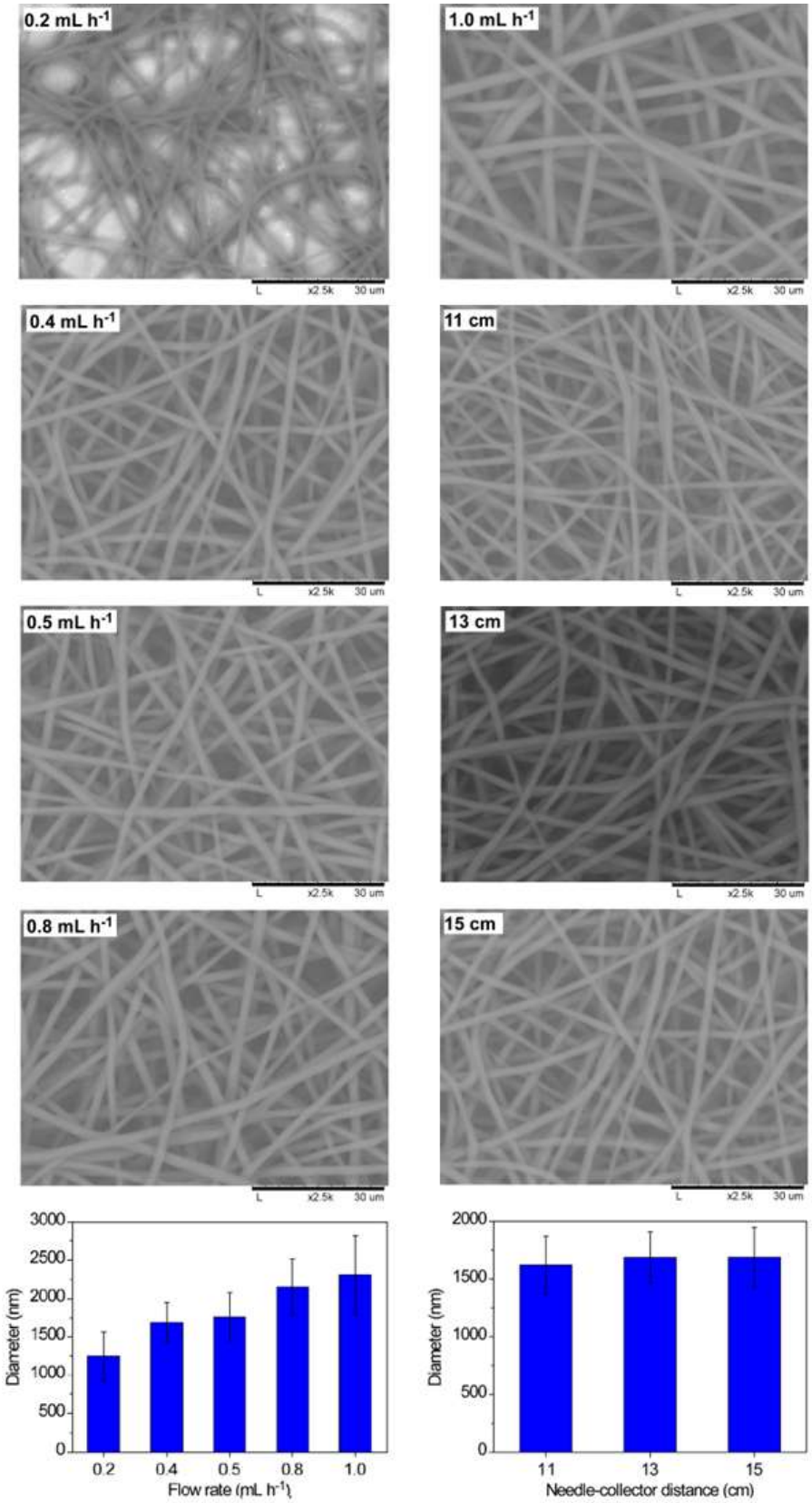

Figure 4. 4 Effect of flow rates and needle-collector distance on fibre diameter from a 20% w/v polymer solution of PCL. Scale bars = 30 µm.

For PEO-CT solutions (Section 4.4.4.1), concentrations were kept constant as well as the flow rate (0.2 ml/h). The latter, when increased, resulted in dripping under certain conditions and for solutions with high amount of chitosan, in which mass-ratio of PEO to CT were over 1:5. The ratio between PEO and CT was evaluated at increasing distance. As shown in the graph (Figure 4.5), it was possible to increase chitosan concentrations up to five times the amount of PEO with a minimal change in fibre diameter at 15 cm.

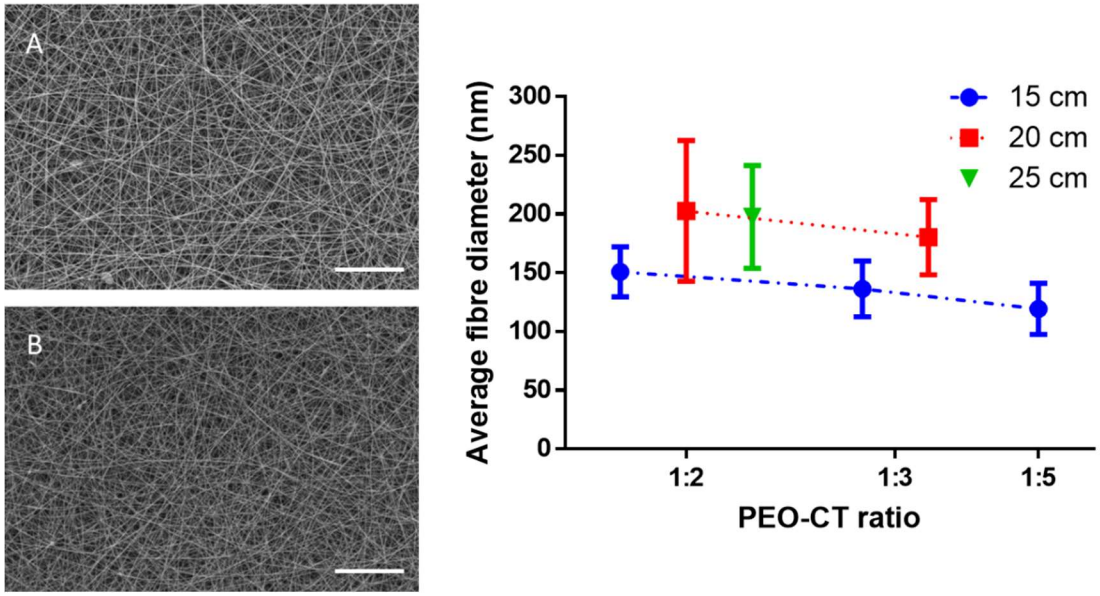

Figure 4. 5 Images of 1:2 PEO-CT (A) and 1:3 PEO-CT (B) membranes and graph representing variations of fibre diameters with needle-collector distance. Scale bars = 10 µm.

When the collector was placed at 20 cm stable conditions were only obtained for 1:2 and 1:3 PEO-CT ratio. Particularly evident is the increasing standard deviation in fibre diameter measurements at longer distances, although this was only possible to be evaluated for PEO-CT 1:2. Measurements of the average fibre diameter resulted in values similar to other studies [135, 147] validating consequently the electrospinning setup and process. However, some discrepancies between current study and literature can be found and might be attributable to the specifics of the materials employed and to the electrospinning setup.

4.7.1.2 Analysis of the effect of rotating collector on appearance and fibre diameter

The use of a rotating disk changes the way fibres are collected as shown in Figure 4.6. While the surface of the static collector was covered randomly (Figure 4.6 A) with the

deposition expanding outwards, rotational movements allowed a well distributed collection of membranes with a more uniform thickness. PCL fibres tended to start arranging at the edge of the collector, spreading towards the centre (Figure 4.6 B); on the contrary, PEO-CT fibres were distributed uniformly on the surface after the same spinning time of 30 minutes (Figure 4.6 C). Distribution of the fibres can vary from micro to nanofibres and can be also associated to different solution conductivity and viscosity (polymer chain entanglement). In support of this hypothesis, Reneker et al [159] reproduced electrically driven bending instability in PCL fibres that resulted in contact and merging while in the "flying" phase, limiting the expansion of the jet path.

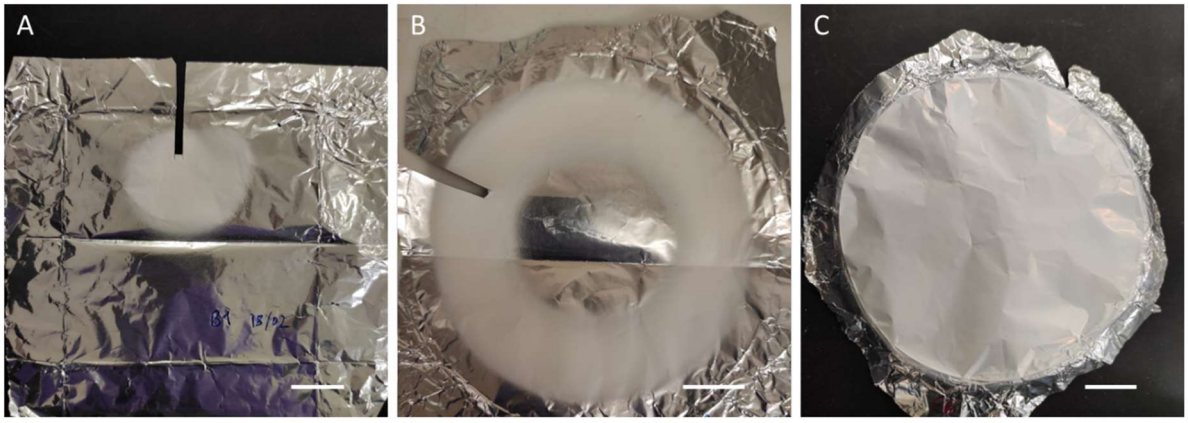

Figure 4. 6 Examples of electrospun membranes obtained with static (A) and rotating collector (B, C) for 20% w/v PCL solutions at needle-collector distance of 11cm (A, B) (B) and PEO-CT 1:2 at needle-collector distance of 15cm (C). Rotating speed for B and C was 500 rpm. Scale bars = 2 cm.

These two parameters not only affect the distribution but also diameter, quality and uniformity of the fibres. Fridrikh et al. [160] demonstrated that fibre diameter can be predicted through a model that consider surface tension, electrostatic charge repulsion, solution conductivity and viscosity. Besides solution properties, topography and morphology of the electrospun fibre mat can also be controlled by collector geometry. A rotating configuration allows to obtain oriented fibres and smaller diameter [161]. As predictable, the in-house built rotating disk at 500 rpm had the same effect on both solutions with a reduction in fibre size between 15 and 20% compared to the static configuration, from 1133.2 ± 243 nm to 925.6 ± 181 nm for PCL and from 151 ± 21 nm to 131.3 ±19 nm for PEO-CT 1:2. Furthermore, it can be observed in Figure 4.7 a slight increase in fibre diameter at higher RPM for PEO-CT 1:2, probably due to partial melting of the fibres.

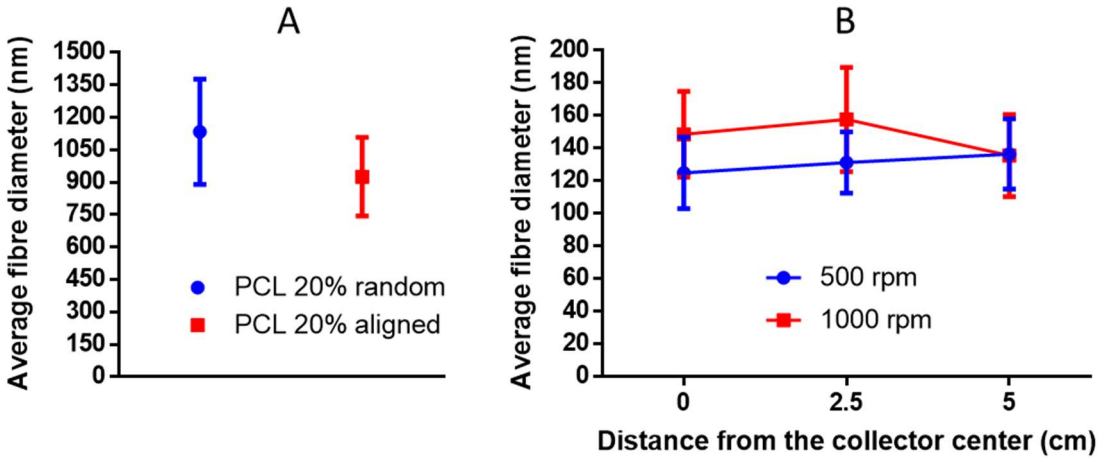

Figure 4. 7 Differences in average fibre diameter (n=30) for 20% w/v PCL in static and rotating (500rpm) configuration (A) and for PEO-CT 1:2 across the deposition surface of rotating disk (B).

Considering that the linear velocity on disk collector depends on the distance from the center [143], PEO-CT 1:2 fibres on the mat were measured at a distance of 0, 2.5 and 5 cm from the center. However, it was not observed a significant increase as also reported by Nitti et al. [134].

4.7.1.3 Fibre alignment analysis

Although it is well known that rotational speed in drum collectors mechanically stretches fibres affecting their diameter and alignment [161] and the effect of high rotational velocity on electrospun mat in a rotating drum have been investigated [134, 143], in this study analysis of SEM images was performed to evaluate fibre alignment and distribution of nano and microfibres at low rotational per minute (500 and 1000 RPM) with the aim to obtain less agglomerated and better distributed fibres. The method use for alignment analysis was based on a new plugin, *OrientationJ* developed in *ImageJ* by the École polytechnique fédérale de Lausanne (EPFL), Biomedical imaging group. The software was employed to characterize the orientation and isotropy of SEM images with a magnification of 3000X. The user specifies the average diameter of the fibre (Structure of Interest, SOI) that the software uses as the size of a Gaussian-shaped window and then the program computes the structure tensor for each pixel in the image. As shown in Figure 4.8 B, orientation properties are visualised as a coloured image with orientation being encoded in a semicircular colour map. A histogram of the degree of orientation (Figure 4.8 D) is then plotted.

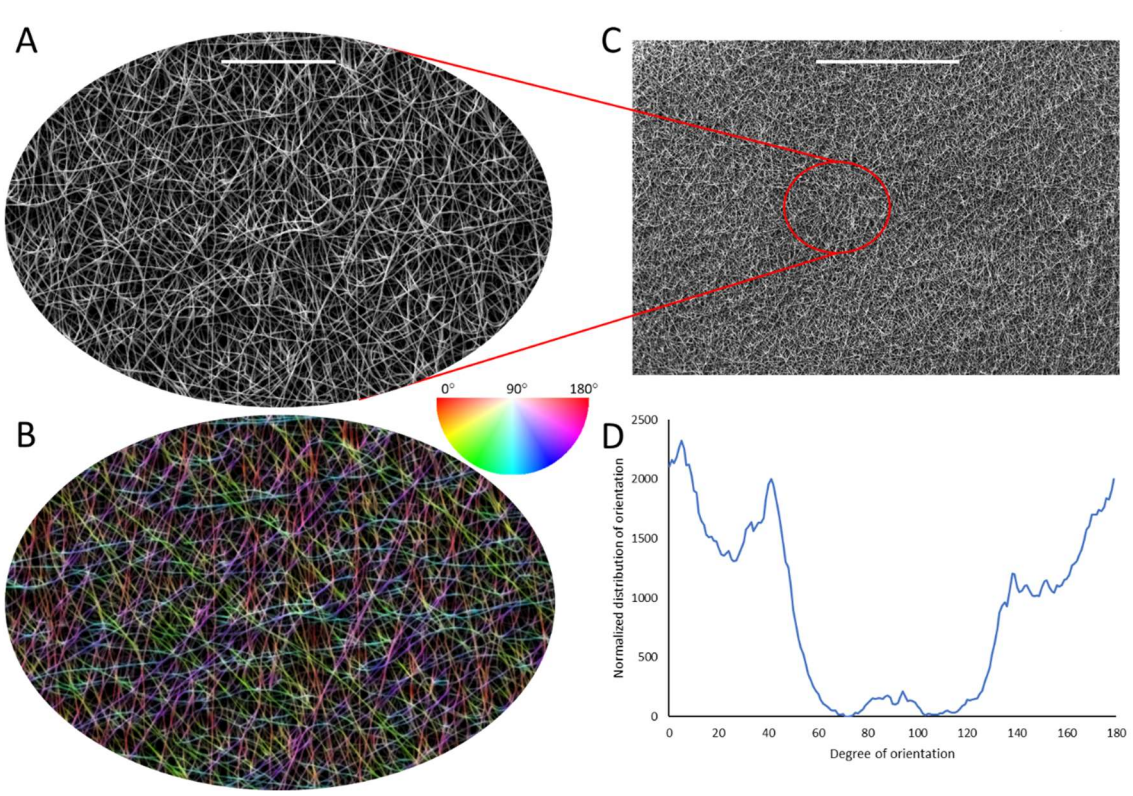

Figure 4. 8 Representative images of *OrientationJ* procedure for PCL fibre at 500rpm; SEM image (A), outputs of the plugin as hue-saturation-brightness (HSB) color-coded map characterizing the orientation of fibres (B) and intensity distribution graph (D) Scale bar of 500 µm for original image (C) and 100 µm for oval image (A).

This method of analysis was reckoned to be more accurate to measure orientation compared to the commonly used two-dimensional fast Fourier transform (2D FFT) approach [162], in which direction and anisotropy are analysed looking for periodic repeats in intensity in the image, giving flat histogram for isotropic content. Also, results are shown without a visible output, precluding adjustment based on the quality of the image. It has been shown that *OrientationJ* is more consistent and representative given results with higher resolution than methods involving Fourier analysis [163].

Figure 4.9 shows PEO-CT 1:2 images used for *OrientationJ* analysis at various positions across the collector at 500 and 1000 RPM and respective histograms that show fibres orientation. The results in each column indicate that as the rotation speed increases and we move away from the centre, the number of orientated fibres is higher and the intensity peak is sharper. Although it is visible from SEM images the presence of fibres in other directions, the analysis seemed to recognise an orientated pattern.

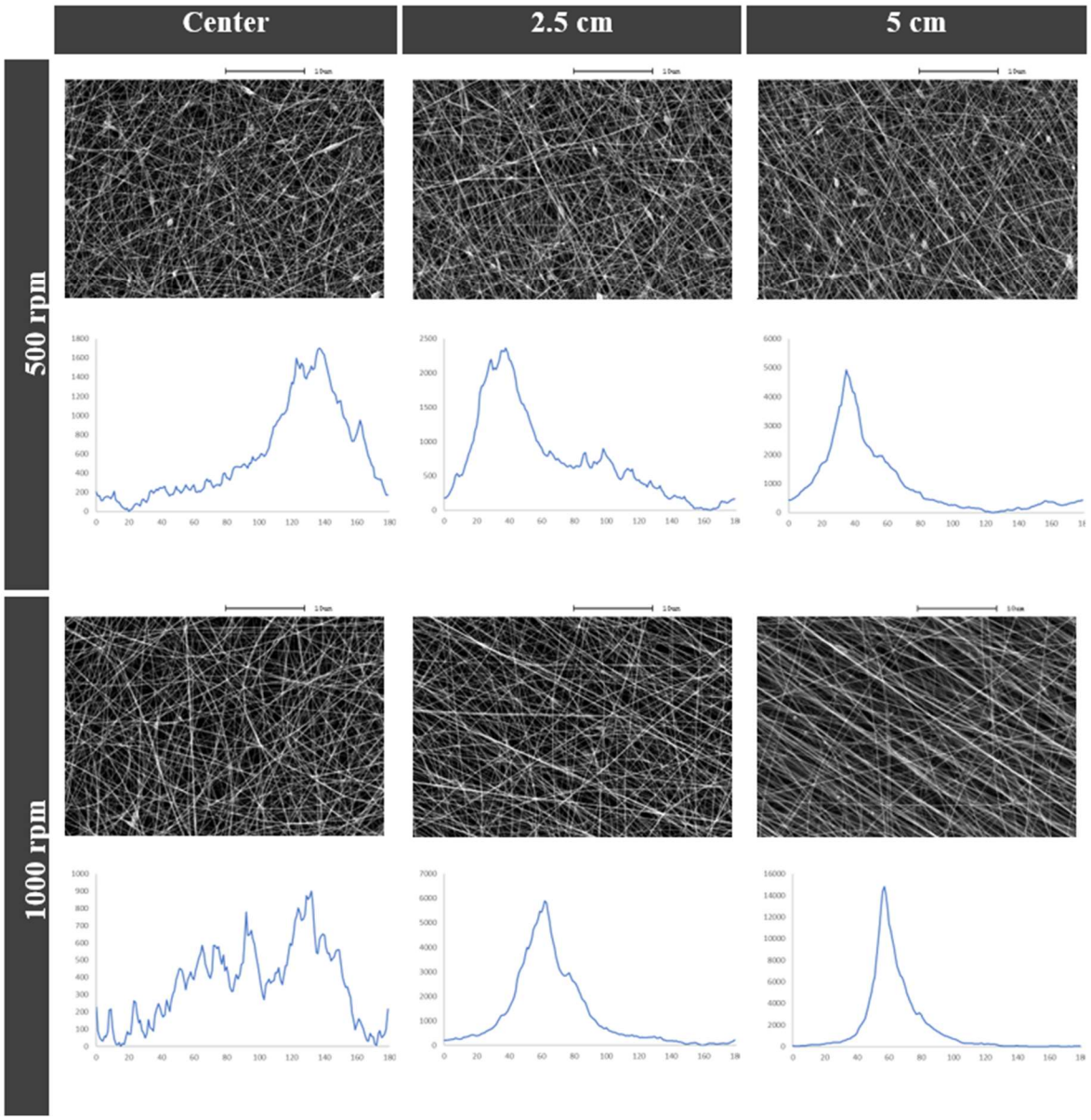

Figure 4. 9 PEO-CT 1:2 SEM images from samples taken at 0, 2.5 and 5 cm from the center at different rotational speed (500 and 100 rpm) and corresponding orientation analysis by OrientationJ representing the normalized distribution of orientation on the y axis and degree of orientation on the x axis from 0° to 180°. Scale bar = 10 µm.

This is consistent with what Nitti et al. [134] presented in their study comparing FFT image analysis to results acquired from tensile mechanical tests. However, it was found that using image processing software, Orientation J, a certain amount of directionality can be also obtained at the centre of the collector.

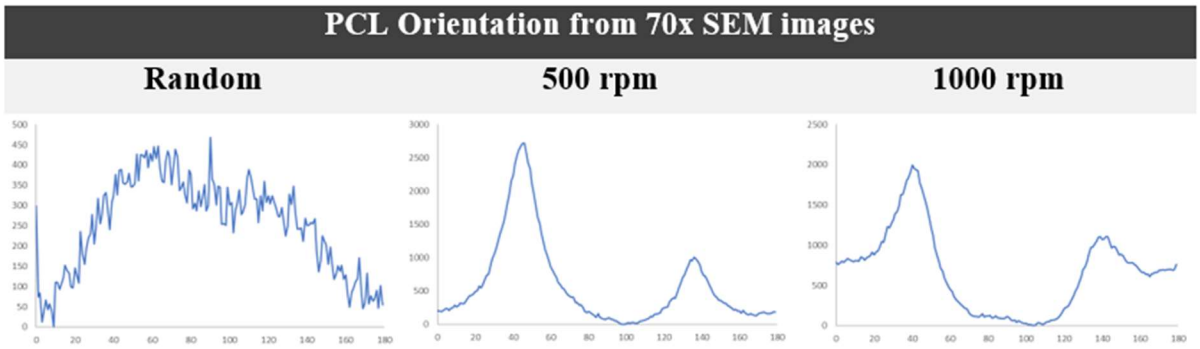

Figure 4. 10 OrientationJ analysis of SEM images of random PCL membranes and aligned membranes at 2.5 cm from centre. The y axis represents the normalized distribution of orientation while the x axis, the degree of orientation from 0° to 180°.

Conversely, intensity distributions for PCL scaffolds showed a different pattern of fibre orientation that, from the images, was not as obvious as for PEO-CT nanofibres. From image analysis (Figure 4.10), two intensity peaks for oriented scaffolds were identified at a distance of 90°-100° from each other suggesting a bimodal distribution, whereas the distribution for random membranes was similar to the PEO-CT 1:2 at the center.

These results might indicate that the rotational disk can align the great amount of PCL microfibres in two distinct directions, perpendicular to each other probably influenced by a phenomenon called charge retention [164]. As the fibres accumulates, there is a drop in the potential difference between the source and the area where fibres have already deposited due to an accumulation of residual charges that presumably affect the electrical field. Although this can negatively impact the alignment of the fibres and prevent fabrication of thick membranes, this fibre distribution may have positive effect on porosity and cell infiltration compared to electrospun mats collected with rotating drums where tightly-packed and aligned fibres induce cellular alignment.

From analysis of SEM images, the use of in-house built rotating collector led to membranes with circumferential and bidimensional aligned fibres. These results will be further validated through mechanical tests.

4.7.1.4 Electrospin feasibility and morphology of PCL-CT blends

A preliminary study to explore the possibility to blend CT with PCL in Glacial Acetic Acid (GGA) was conducted in an attempt to improve biocompatibility, hydrophilicity and degradation time of PCL membranes adding small amount of CT (1%) dissolved in 1% GAA. The feasibility of the process was judged by visually checking the stability of the Taylor cone during a spinning time of 30 minutes and by verifying the absence of defects and beads on SEM images. Using fixed amount of PCL permitted to analyse the effect of CT concentration in solution. Chitosan had a major effect on fibre diameter resulting in much finer fibres when it is added to the PCL solution, as it increases the conductivity and the viscosity of the solution [131].

When 1% of chitosan was used, solutions of 15%, 18%, 20% of PCL could be spun (Figure 4.11 C, D, E). This is in line with a previous reported article [131], in which 14% PCL was used with 1% chitosan in a solution of acetic and formic acid. The average fibre diameter shows a linear increasing trend from 203 nm to 335 nm.

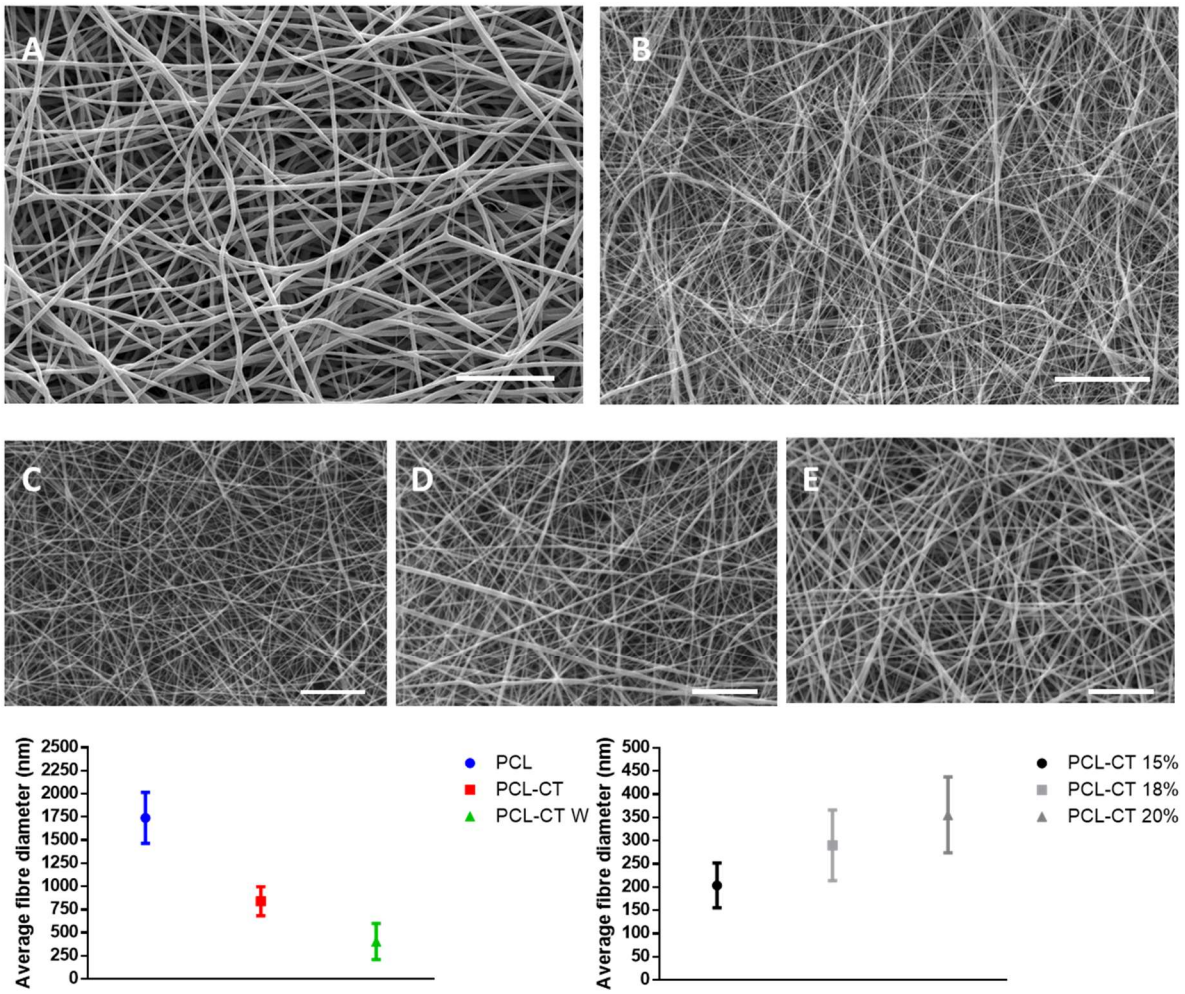

Figure 4. 11 Representative SEM images of electrospun blends of PCL-CT. Graphs compare fibre diameter measurements for (A) 18% PCL - 2%CT (PCL-CT red); (B) 18% PCL in 91/9 GAA/water – 2%CT (PCL-CT W green); (C) 15% PCL - 1%CT; (D) 18% PCL - 1%CT; (E) 20% PCL - 1%CT. Scale bars of 20 µm for A and B and 10 µm for C, D, E

Because of its polycationic nature, the use of higher concentration of chitosan was challenging. Only 2% chitosan in 18% PCL resulted in continuous spinning despite some spitting (Figure 4.11 A). A small increase of 1% in the amount of chitosan led to an increase in fibre diameter from 290 ± 76 nm to 840 ± 156 nm for 18% PCL showing that viscosity as well as conductivity are determining factors in the electrospinning of polymer blend [165]. This has been demonstrated by electrospinning 18% PCL in 91/9 GAA/water solution and 2% CT. By changing electrical properties and viscosity of the solution adding a nonsolvent such as water, the result was a further reduction in fibre diameter, formation of nanofibres with nonuniform size and local thickening of the fibres due to more

entanglement of PCL molecules (Figure 4.11 B) [166]. Likewise, larger fibres obtained with higher amount of acetic acid can be related to a reduction in the solution conductivity. The possibility to use higher ratio of chitosan respect to PCL was also explored. Specifically, PCL-CT 1:2 and 1:3 compositions were evaluated and even though the process of electrospinning was stable leading to membranes with an average fibre diameter smaller the 100 nm, many beads were visible at microscopic level. Due to the presence of defects and fibre entanglement, PCL-CT membranes were not further characterized in this study. Additional improvement of polymer blends in acetic acid may be conducted in the future.

4.7.2 ATR-FTIR spectra analysis

The IR spectral analysis of PEO-CT and PCL was carried out and compared with that of PEO and CT powder and PCL pellets. Based on previous findings [135], PEO is soluble in aqueous medium and its elimination from the scaffold should occur when sterilized in 70%; hence, PEO removal was evaluated after sterilization with 70% ethanol for 24h. Since FTIR peaks of electrospun PCL before and after sterilization compared to pure PCL remained unchanged, the spectra were not reported. Figure 4.12 shows the FTIR spectra of PEO-CT membranes and all characteristic peaks are highlighted in red for CT and in black for PEO. For CT, the broad band centred at around 3300 cm^{-1} (A) corresponds to N-H and OH stretching while bands at 1630 cm^{-1} and at 1550 cm^{-1} (B) are characteristics of amide I (C=O stretching) and II (N-H bending), respectively [167]. There is no notable change in these peaks before and after treatment (AT). Regarding PEO, the band at around 2885 cm^{-1} (CH_2 stretching) is reduced in intensity after immersion in solution as well as other characteristic bands; at 1100 cm^{-1} (III) (C=O stretching) PEO has one of the highest peaks that is smoothed and substituted after immersion in solution by C=O stretching at 1045, characteristic of a polysaccharide structure such as chitosan together with bands at 1150 (C) (anti-symmetric stretching of C=O) [168].

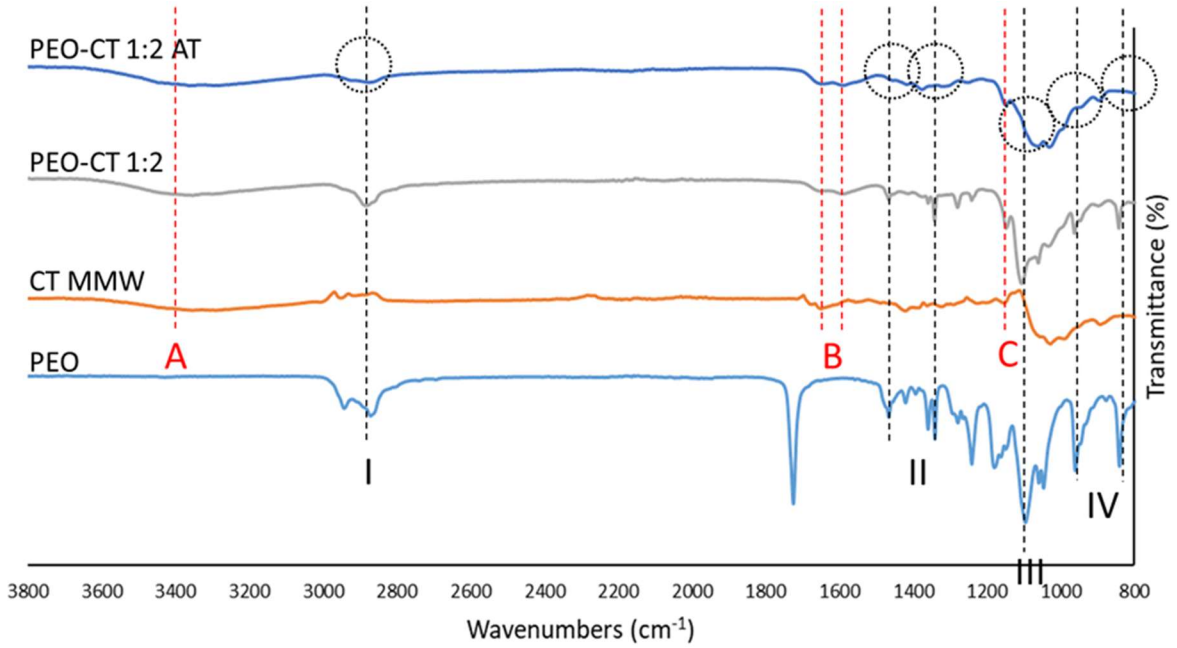

Figure 4. 12 FTIR spectra of pure PEO and Chitosan MMW and electrospun PEO-CT scaffolds before and after sterilization (AT).

Other peaks that can be distinguished in the PEO spectrum but disappeared after immersion are: 850 - 950 cm^{-1} (IV) associated with C=O stretching and 1460-1360 (II), CH_2 deformation. The PEO-CT spectrum with some shifted values respect to the pure materials is an indication of the successful ionic bonds between carbonyl and amino groups in PEO and CT [168]. Results indicate that membranes after immersion are mainly composed of chitosan but small traces of PEO may be still present.

4.7.3 Contact angle measurements for oriented membranes

The hydrophilicity of PCL and PEO-CT membranes was examined using the sessile drop contact angle, capturing the profile of a drop of distilled water on a solid interface and measuring the angle formed.

Contact angle can be described by several equations depending on the solid surface and droplet state. An ideal solid surface is considered smooth, rigid, chemically homogenous and stable. In this case, the contact angle can be predicted measuring the surface tensions of solid and liquid and it is called Young's contact angle. In real applications and in nature, ideal surfaces rarely exist but rather they are heterogenous, chemically and topographically. For this reason, during the years the roughness of a surface was accounted for contact angle measurements and described by Wenzel and Cassie-Baxter states. In the

first one, the apparent contact angle was defined as the contact angle that increases if the surface is roughened while in the second, the focus was on the liquid that does not penetrate small pores leaving air gaps. Although it can be argued that surface chemistry and morphology can influence contact angle, since the current methods of measurement are macroscopic, the only measurable contact angle is the most stable, transitioning from Cassie-Baxter to Wenzel state. In this respect, Gao and McCarthy demonstrated that the interfacial area is irrelevant if the droplet is within the contact perimeter and only the small fraction of the surface probed by the contact line is important in the contact angle behaviour [169]. For rough surfaces, it is generally accepted to consider an average of the apparent contact angle [170]. For contact angles between 0° and 90° the surface is considered hydrophilic. Materials that show angles over 90° are categorized as hydrophobic. Three measurements were performed as described in Section 4.5.3.

PCL scaffolds showed an average contact angle value around 100° (Figure 4.13) which indicates a hydrophobic behaviour. However, possibly due to the use of acetic acid and to the different morphology [156] the measurement was 25% inferior to angles measured in other studies [137]. With regard to the fibrous structure, the different morphology and fibre diameter may have created a surface roughness with less air trapped between interfaces of fibres that result in a more porous structure. Besides the surface chemistry, the topography has a strong influence on liquid-solid interface [171]. However, this result can be a measure of apparent contact angle that differ from the actual contact angle [172].

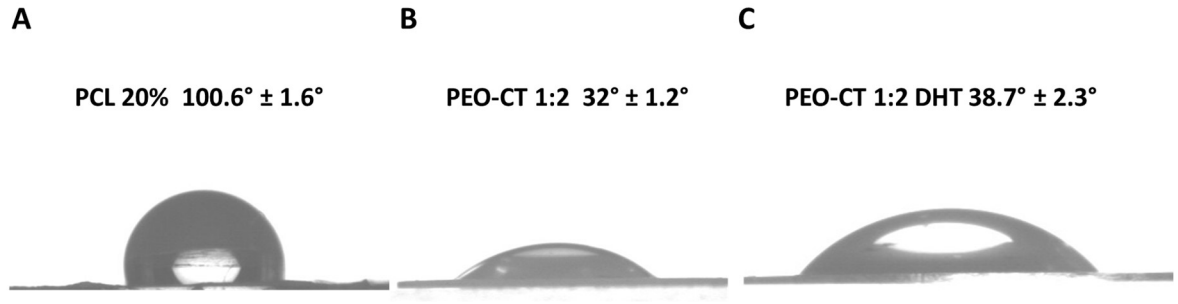

Figure 4. 12 Contact angle images on PCL (A) and PEO-CT scaffolds samples taken at 2.5 cm before (B) and after DHT treatment (C) using water.

On the contrary, PEO-CT membranes showed hydrophilicity with angle of 32° that rose to ~39° after being DHT-treated. This may be a consequence of the fibre swelling and fusing post treatment as shown in Figure 4.13. Remarkably, contact angle measurements for PEO-CT in literature were found to be 25% higher compared to this study [173]. This

could be a further indication of the improved morphology with higher porosity achieved with the rotating disk configuration. This hypothesis needs to be validated in the future by comparing these results with measurements obtained on membranes collected with a static configuration.

4.7.4 Stabilization and physical cross-linking effect on membrane morphology

Various treatments were conducted to check the influence of solutions on the stability of PEO-CT nanofibres that was analysed with SEM images. Overall, after being immersed in liquid the morphology of all samples drastically changed (Figure 4.14).

Crosslinking the membranes by DHT caused fusion at the crossing points and thickening of the fibres resulting in packed and dense membrane with almost no visible porosity. On the other hand, this treatment strengthened the stability of the fibres preserving some features while undergoing partial dissolution when immersed in 1 M Potassium carbonate (K_2CO_3). A salt, in this case potassium carbonate, was used with the objective to neutralize the net charge of chitosan, obtaining insoluble chitosan and extract the acid left from the electrospinning process resulting in a reaction that gives a potassium acetate, water and carbon dioxide. This dissolution manifested further when non-treated fibres were exposed to K_2CO_3 solution. This result was not expected as Lemma et al. [135] proposed and demonstrated the efficacy of this method for stabilization of PEO-CT membranes. However, this can be associated with the specific source of chitosan which can cause partial chitosan dissolution when in contact with salts as discussed by Hirase et al [174]. Despite a partial swelling of the protonated chitosan after PEO removal was expected when in contact with aqueous solutions, neutralization of chitosan in 70% ethanol (EtOH), a non-solvent of chitosan, seemed to be the most suitable for preserving the nanofibre structure in agreement with previous findings [135]. Overall, the size of the nanofibres increased through swelling in all the samples, whether DHT-treated or not, whilst preserving the fibrous morphology except in the case of K_2CO_3 solution. Nevertheless, 70% ethanol solution was selected as membrane stabilizer because it could also be used as method to sterilize the surface before proceeding with cell culture.

For PCL scaffold the surface remained comparable to that one before immersion, because of its hydrophobicity.

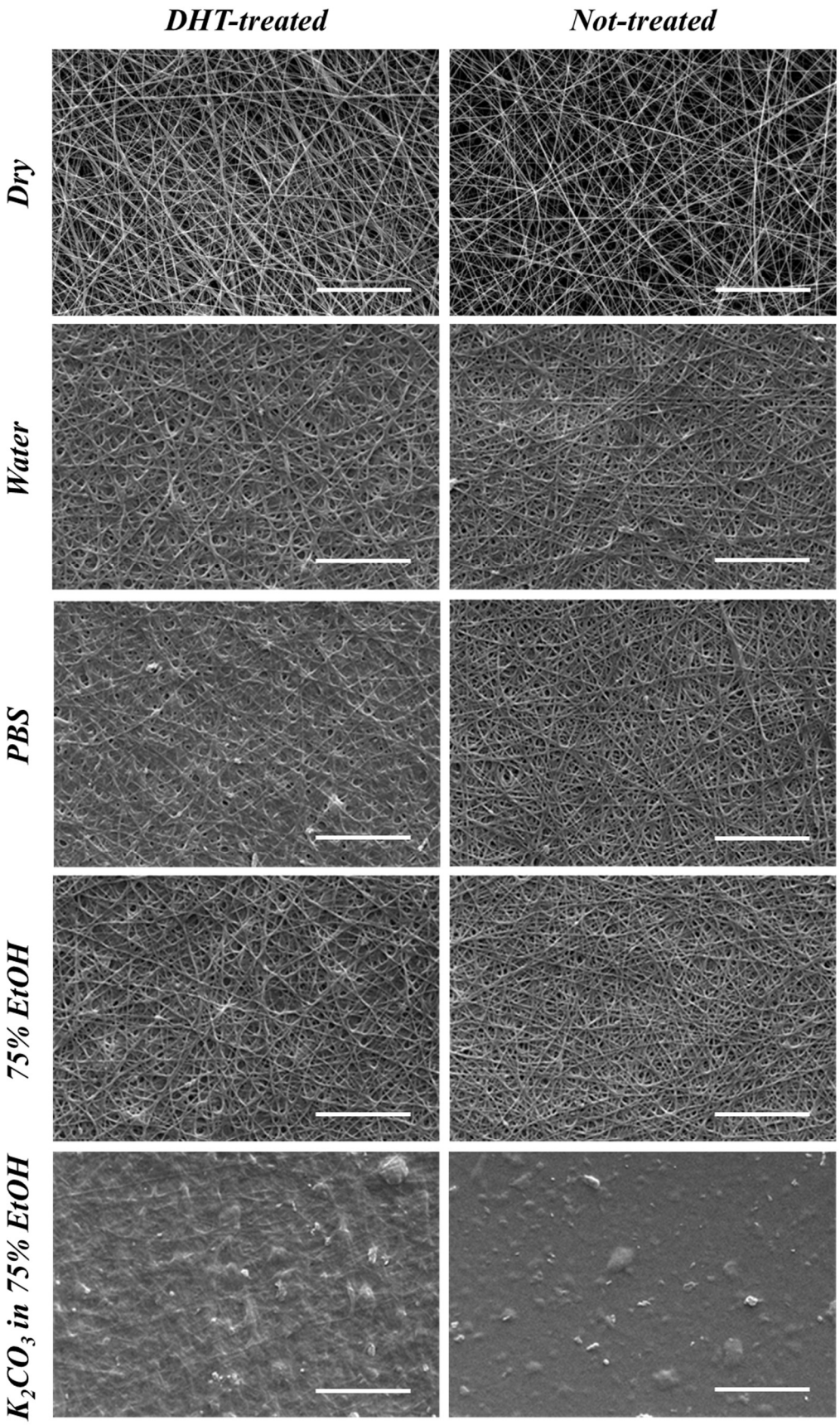

Figure 4. 13 Effect of different solutions to evaluate the stability and morphology of PEO-CT nanofibres before and after DHT crosslinking. Scale bars = 10 µm.

4.7.5 Mechanical properties of electrospun mats

Tensile tests were performed on fibrous membranes to verify that alignment of the fibres occurred and to understand if the mechanical properties of these electrospun mats were suitable for skin tissue engineering applications. As the electrospinning process can influence the characteristics of the membrane, and the time of collection can determine fibre deposition and distribution, a time of three hours was established to collect fibres that were spun at 0.4 ml/h pump rate. Results in Figure 4.15 shows that mechanical properties are dependent on fibre orientation. This is particularly evident for PCL membranes that displayed a 50% increase in Young's modulus (*E*) and higher value of maximum stress from 0.76 MPa to 1.8 MPa (B). These results are comparable with elastic modulus values obtained in other research papers in static configuration [122, 143, 157, 175].

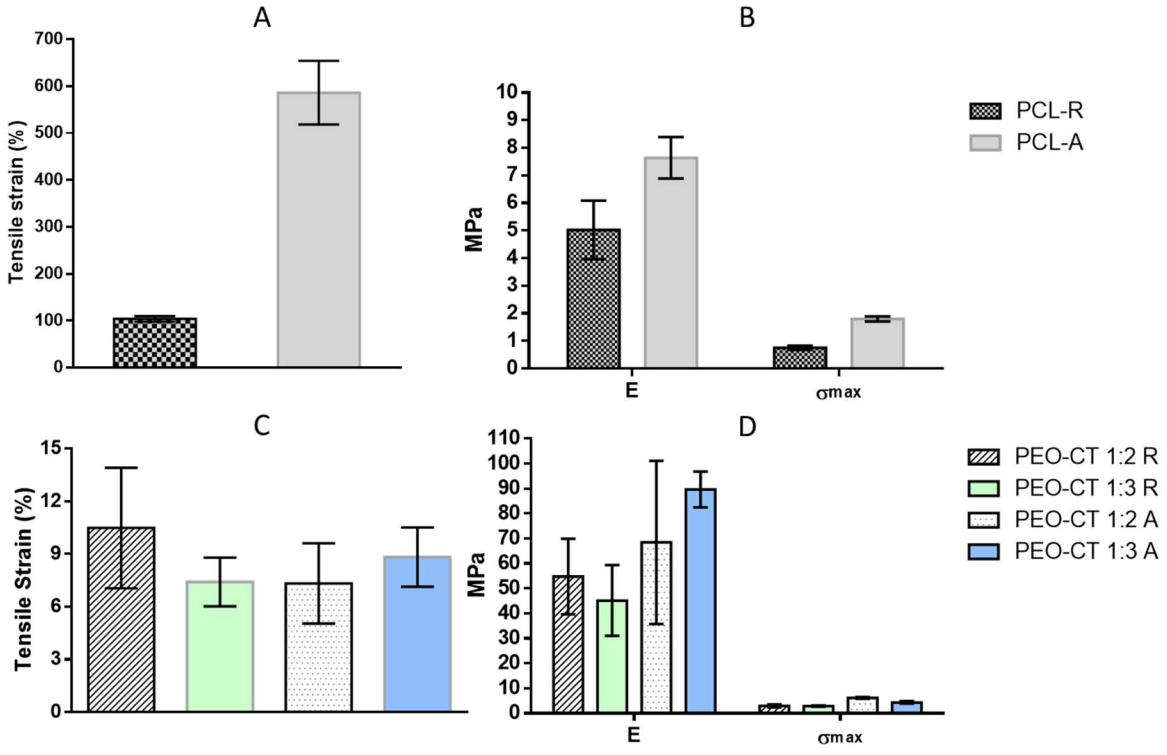

Figure 4. 14 Elongation measurements (A, C) for PCL and PEO-CT random (R) and aligned (A) and respective elastic modulus (E) and maximum stress (σ_{max}) (B, C). n=3

Interestingly, in this study, mechanical properties, i.e., E and σ_{max}, of aligned PCL membranes do not vary greatly from those of random membranes. This finding supports the hypothesis of a continuous but spatially varying fibre orientation without much fibre

drawing towards the direction of rotation [143]. With respect to the percentage of tensile strain at break (Figure 4.15 A), values vary in literature. Silva et al. [122, 175] reported maximum elongation above 600% for random fibres whereas Liverani and Bocaccini [157] found values comparable to this study in which oriented membranes could be stretched six times more than random mats, confirming successful fibre alignment.

Similar to previous studies [176, 177], values of elastic modulus for random PEO-CT fibres with ratio 1:2 were around 50 MPa with a decrease of 10% when the amount of chitosan was increased (1:3) (Figure 4.15 D). While CT is known to be a brittle material that would increase tensile strength, PEO content can alter the mechanical properties of the blended materials adding flexibility. Mechanical tests on aligned membranes confirmed these assumptions, with an overall increase in maximum stress for PEO-CT 1:2 (6.2 ± 0.3 MPa) compared to PEO-CT 1:3 (4.4 ± 0.5 MPa). Similar values for PEO-CT were shown by Nitti et al. [134] when a rotating drum was used for fibres deposition further demonstrating the alignment of the fibres obtained with the rotating disk. However, analysing the mechanical parameters (Young's modulus, tensile strength and elongation at break) for aligned and random PEO-CT membranes, differences in trends are worth to be further discussed. In Figure 4.15 C, the tensile strain decreases with increasing CT ratio for random membranes whereas it slightly increases for aligned samples. The same trend occurs for the elastic modulus in Figure 4.15 D but with higher values for aligned fibres compared to random samples. On the other hand, values of tensile strength are higher for membranes with lower amount of CT but higher for aligned mats. The reason for different trends in tensile strength and elasticity for random and aligned fibers is not completely clear. It can be assumed that orientation improves the material resistance to deform elastically and have a bigger influence than chitosan content. Nonetheless, in aligned fibers, an increase of chitosan content might have enhanced the intramolecular and fiber interactions leading to improved mechanical properties.

From these results, it can be said that while PCL membranes showed characteristics of elasticity and ductility, PEO-CT membranes resulted more brittle and stiffer with values of Young's modulus and ultimate tensile stress that fall in the range of the mechanical properties of the skin [178, 179]. Results are summarised in Table 4.2.

Table 4. 2 Young's modulus (E), stress at break (σ_{max}), and elongation at break of electrospun mats fabricated with static and rotating collector.

Samples	Young's Modulus (MPa)	Tensile strength (MPa)	Tensile strain (%)
PCL-R	5.02 ± 1.06	0.76 ± 0.08	103.94 ± 6.02
PCL-A	7.64 ± 0.75	1.80 ± 0.09	586.22 ± 67.93
PEO-CT 1:2 R	54.78 ± 15.12	2.99 ± 0.53	10.49 ± 3.43
PEO-CT 1:3 R	45.18 ± 14.15	2.85 ± 0.27	7.42 ± 1.39
PEO-CT 1:2 A	68.39 ± 32.62	6.20 ± 0.35	7.33 ± 2.28
PEO-CT 1:3 A	89.6 ± 7.13	4.39 ± 0.52	8.83 ± 1.69

Mechanical tests together with results obtained in the previous chapters, suggested that complex interactions between fibres collected on a rotating disk may exist and that an evaluation of the mechanical properties in multiple directions is needed. Furthermore, a combination of the materials studied may be explored to mirror the mechanical proprieties of the skin.

4.7.6 Cell culture studies

While physical and mechanical properties can be customised adjusting the material ratio, understanding the interaction between the substrate topography and the cells is essential for the design of scaffolds that are suitable for the required biomedical application. In this section, primary human dermal fibroblasts (HDF) behaviour on PCL and PEO-CT membranes was evaluated.

4.7.6.1 Cytotoxicity

Cytotoxicity was analysed using MTS assay under similar culture conditions. Although this assay indirectly measures the cell number converting an absorbance measure using a calibration curve (Figure 4.16), it is a quick method to compare viability and cellular activity across different substrates.

Figure 4.16 shows an estimate of the average number of viable cells attached to the membranes and to the plastic substrate of the culture-treated well plate (CTRL) after 48h. Results indicated that none of the samples cytotoxic and in all cases, HDF cells adhered

to the respective surfaces. However, values for scaffolds were below control probably as a consequence of a slower cell metabolic activity and a slightly smaller area available for seeding and migration, since the diameter of a 24-plate well is ~12mm, 3 mm larger than electrospun samples. Nevertheless, the number of cells attached to membranes was found to be related to the number of cells that were seeded ($4x10^4$). This shows the importance of cell seeding density to populate the scaffold avoiding confluence after few days.

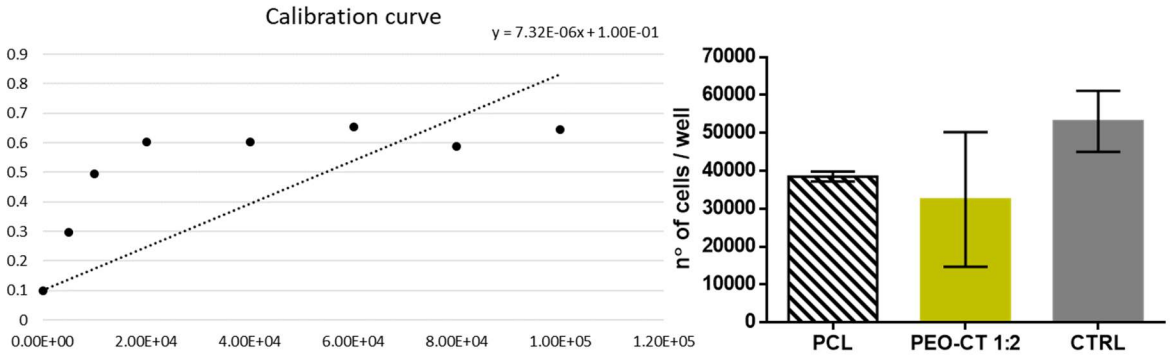

Figure 4. 15 Calibration curve and MTS assay at Day 3 on PCL, PEO-CT membranes and on culture plate (CTRL). n=3

It can be also observed that despite differences in fibre diameter and material, cell attachment is relatively uniform in the scaffolds.

4.7.6.2 Visualisation of cell adhesion and orientation

Despite extensive research, the *in vitro* behaviour of cells in contact with macro and nanofibres is still not well understood, as cell response, besides being affected by many factors such as material and mechanical properties, is also cell line specific [180].
With the aim to understand how fibre morphology influences cell attachment, scaffolds were first fixed in 4% formaldehyde and then imaged by SEM (Figure 4.17). Even though MTS assay showed a similar number of cells attached to the scaffolds, cell topography was completely different. The denser and fibre-packed surface of PEO-CT scaffold promoted the formation of focal adhesions (Figure 4.17 A) and clusters of cells (arrows in Figure 4.17 C) resulting in rounded cells shape upon adhesion and in absence of cell migration. Cells with spherical shape are generally not considered a good indication of cell spreading because implies that cells are not effectively interacting with the substrate. Cell spreading refers in fact to a process by which cells attached to a surface and extend their

cytoplasmic process to create a flattened and extended shape. Although, CT membranes favourably interact with cells and promote cells adhesion because of its cationic nature and hydrophilicity showing signs of activity (cell division, arrow in Figure 4.17 A), CT may not support a high degree of cell adhesion and spreading compared to PCL. Researchers have demonstrated that the degree of acetylation of CT and possible charge distribution at the surface can be linked with cell behaviour to grow in clusters and maintain a spherical shape [122, 181].

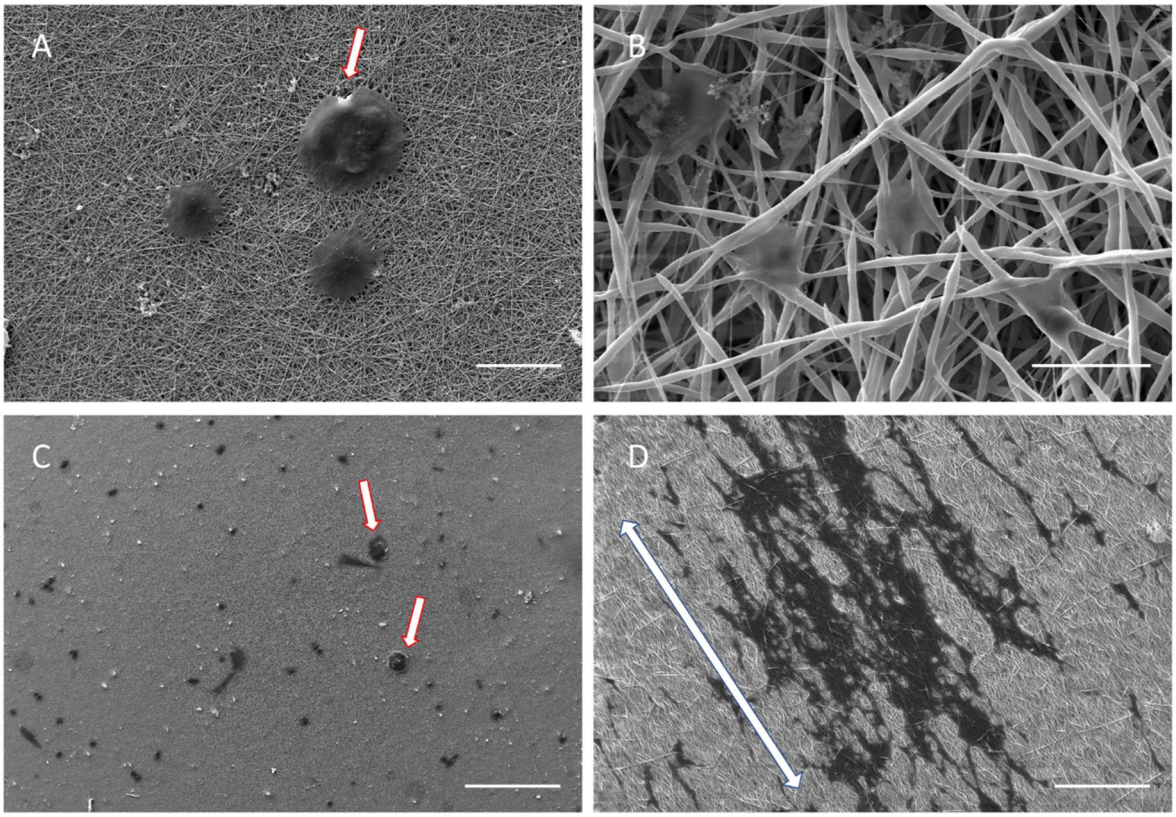

Figure 4. 16 SEM images of HDF attachment on PEO-CT (A) and PCL (B) membranes after 48h at higher (A, B) and lower (C, D) magnification. Scale bars of 20 µm for A, B and 200 µm for C, D

In this respect, HDF cells on PCL fibres resulted in high proliferation and dispersion within the fibrous mats despite the hydrophobic nature of this polymer. It can be seen from Figure 4.17 B that cells exhibited uniform distribution of actin stretched within the fibres. While cells were unable to infiltrate in PEO-CT membranes, on PCL scaffolds cells seemed to move into the structure giving an indication of a compatible pore size for fibroblast migration. These observations are consistent with literature findings in which cell infiltration was facilitate in scaffolds with a distinct bimodal fibre distribution and with fibre diameter in a range between 400 and 1000 nm [122, 182]. It is worth noticing that

from lower magnification images (Figure 4.17 D) cells seemed to proliferate and migrate in the direction of circumferential oriented fibres.

As confirmation of these findings, scaffolds were also imaged under inverted fluorescence microscope after being cultured for 48h, fixed with 4% formaldehyde and stained with DAPI and phalloidin rhodamine. HDF cell-to-cell contact with numerous cytoplasmatic processes corresponding to actin development were observed on PCL membranes (Figure 4.18).

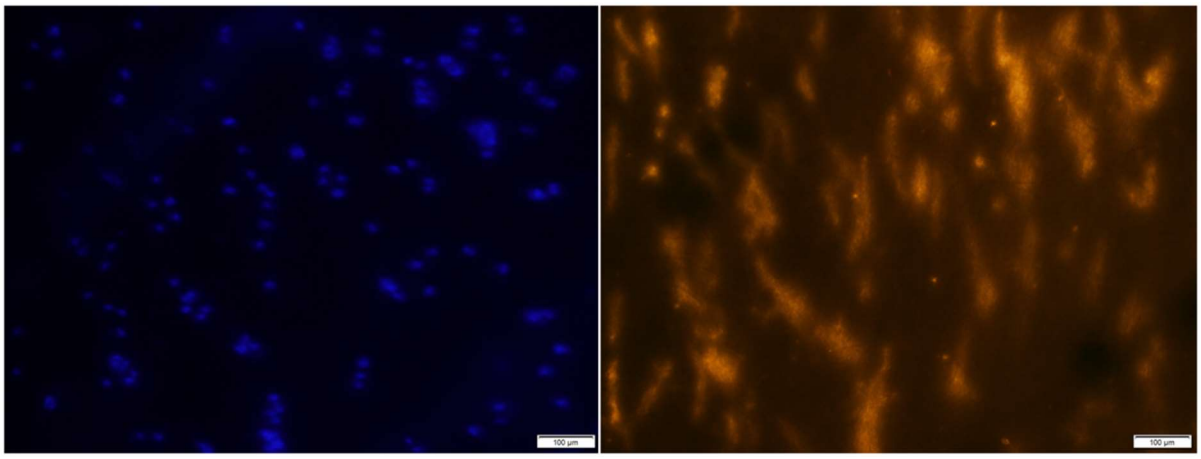

Figure 4. 17 Fluorescent labelling of nuclei (blue) and actin (orange) of HDF cells cultured on PCL membranes. Scale bars of 100 µm

Spherically shaped cells were instead seen on PEO-CT membranes (Figure 4.19), with some of them clustered into spheroid-like cellular aggregates that may also hinder individual cells from spreading. This behaviour on PEO-CT mats could be due to substrate quality, such as stiffness that may have inhibited cell proliferation and migration and roughness that has been demonstrated to be a crucial factor in guiding cell attachment and cytoplasmic spreading [183]. In addition, Nagiah et al. [184] found that hydrophilic surface may have a negative impact on dermal fibroblast proliferation and that substrates with intermediate wettability are preferred by cells. Therefore, further studies of PCL-CT blends and comparison with PCL membranes are necessary to understand if a surface with hybrid wettability can positively affect cell proliferation [149].

However, PCL membranes fabricated in this study showed already good biocompatibility with cells well attached and spread while PEO-CT membranes performed poorly regarding cell adhesion and proliferation. The reasons of these results can be mainly attributed to the features of PCL membranes such as a pore size larger than cell size (~10-15 µm) and the average fibre

diameter suggesting that a value of approximate 1 µm allows HDF growth and orientation as showed also by Liu et al. [185].

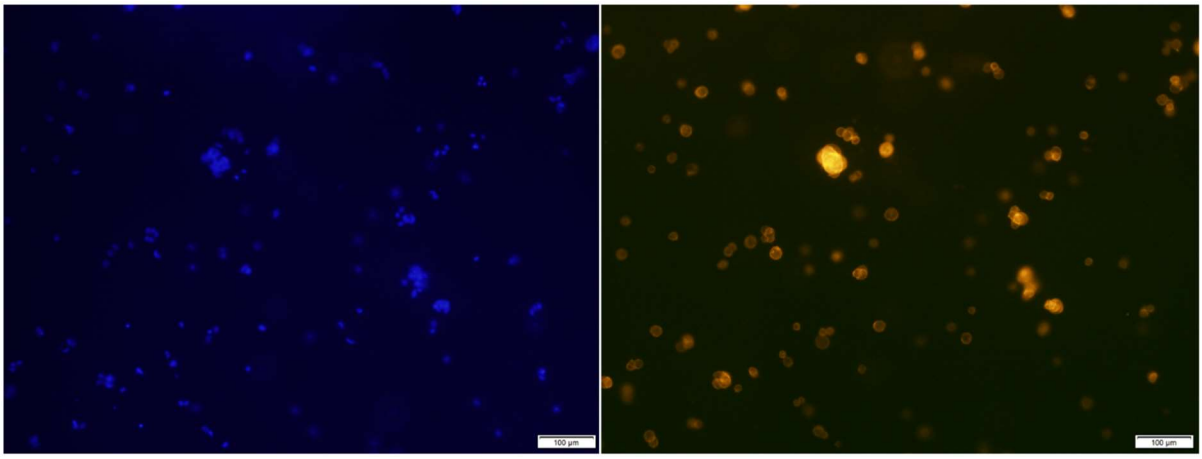

Figure 4. 18 Fluorescence microscopy images of HDF seeded on PEO-CT membranes stained with DAPI and Phalloidin (Day 3). Scale bars of 100 µm

In conclusion, it is possible to state that surface chemistry and topography played an important role for HDF attachment and spreading on electrospun membranes.

4.8 Summary

In the past years, many medical companies have emerged offering electrospinning-based products and trying to translate promising lab findings into commercial products. For this reason, new strategies to fabricate affordable and sustainable fibrous structures similar to the extra cellular matrix (ECM) that are intended to be used as *in vitro* cell culture substrates or for tissue engineering applications, have to be investigated.

In this chapter, the use of green solvents, the optimization of spinning conditions and the development of less-explored method for fibres deposition were explored. The in-house built collector was developed to examine the effect of rotational forces on fibres collection and analyse the behaviour of primary human dermal fibroblasts (HDF) cultured on nano and microfibres. As the electrospinning process is influenced by various inter-related and independent variables, an optimization of spinning parameters was necessary to standardise and validate the process before successfully fabricate PEO-CT, PCL and PCL-CT membranes. Analysis of SEM images showed a decrease in the average fibre diameter using the rotating configuration compared to the static collector. Regarding the PEO-CT fibres, image processing confirmed that fibres were orientated and aligned towards the rotational direction, having a better orientation moving outwards from the centre and with

increasing rotational velocity. Contrarily, oriented PCL fibres showed little difference in morphology not evident alignment in comparison with those produced using static electrospinning. However, mechanical testing and analysis of SEM images demonstrated a fibre deposition in a cross-aligned morphology. Furthermore, blends of PCL and CT in glacial acetic acid were investigated. They were observed by SEM to produce fibre entanglement and beads within fibres. Although the combination of the two materials seemed promising, further work will be performed to optimize the spinning process. To examine the effect that electrospun membranes had on cells, cell assays, staining and imaging were performed. Results showed that PEO-CT membranes were not suitable for HDF cell culture contrary to PCL mats whose morphology positively affected cell attachment and proliferation. Different adhesion patterns were observed and those could be linked not only to the topography but also to the membrane pattern and roughness. To summarise, by using a rotating disk collector the orientation and distribution of the fibres changed, obtaining a more homogenous substrate. This circumferential pattern needs to be further studied as it could be used to reduce contraction during wound-healing.

Ductile PCL electrospun nanofibres collected with this configuration showed promising results that could be relevant for future *in vitro* skin tissue engineering studies, providing better cell infiltration and accelerating surface-wound healing. However, different materials combinations need be tested to better match the mechanical properties of the skin and improve biomimicking.

CHAPTER 5 Scaffold upscaling and proof-of-concept bioreactor to *in vitro* test NPWT devices

5.1 Introduction

Cell culture on plates is a conventional method that provides an unnatural environment and conditions for cell growing [186]. Although it is well recognized and acknowledged that three-dimensional microenvironments similar to the native tissues can help in obtaining better cell physiological responses, cell culture and cells analysis have to be customized and optimized for each specific structure [69, 187].

In this chapter, methods used to study fibroblasts survival and proliferation on porous scaffolds were illustrated and discussed. Also, the possibility to fabricate a bilayer scaffold combining the techniques described in the previous chapters, to better mimic the skin structure was evaluated. Furthermore, a proof-of-concept platform to apply Negative Pressure Wound Therapy (NPWT) on these sponges was developed and tested. To the current knowledge, this study was the first of its kind that was designed to upscale the surface of scaffolds for application and testing of NPWT devices *in vitro*.

5.2 Cell behaviour on porous scaffolds

In order to understand the impact that different physical and chemical features can have on cell interaction and proliferation within a three-dimensional environment, cell culture studies were conducted on porous scaffolds described in Chapter 3. Disks of 9 mm-diameter were punched out of 35-mm-diameter x 4-5-mm-thick scaffolds, obtained by freeze-drying collagen-based solutions in 6 well plates, using a metallic biopsy punch (Figure 5.1).

Figure 5. 1 Example of collagen sample punched out of a 35 mm porous scaffold. Scale bar = 10 mm.

Then, following a similar procedure used for electrospun scaffolds (Chapter 4), porous scaffolds were sterilized for 24h in 70% ethanol solution and successively rinsed with decreasing ratio of ethanol/PBS (50/50; 25/75, 0/100).

Before cell seeding, PBS was removed from the wells and scaffolds were left under UV light (wavelength of 254 nm) for 1 hour. Thus, an estimation of $4x10^4$ human dermal fibroblasts (HDF) cells in 100 µl, counted using a haemocytometer, were pipetted on the surface of the scaffolds and incubated for 30 minutes to allow adhesion. Wells were then topped up with 400 µl of Dulbecco medium and placed again at 37° C and 5% CO_2. After 48h of incubation, viability and proliferation were evaluated by (5-(3-carboxymethoxyphenyl)-2-(4,5-dimethyl-thiazoly)-3-(4-sulfophenyl) tetrazolium (MTS) assay (CellTiter 96® AQueous One Solution Cell Proliferation Assay, Promega). Amount of 10 µl of reagent for 100 µl of cultured medium were pipetted into each well and plates were incubated for 4 h at 37°C in 5% CO_2 atmosphere. Then, 100 µl from each well was sampled and transferred into a 96-well plate where absorbance at 490 nm was recorded. The number of cells was calculated using the standard curve described in Section 4.7.6.1. This test is a simplification of MTT assay, is easy to use and does not require an organic solvent to solubilize the formazan product reducing handling steps and errors in the process. In addition, it is a straightforward method to check cytotoxicity as it can visually detected by a change in colour.

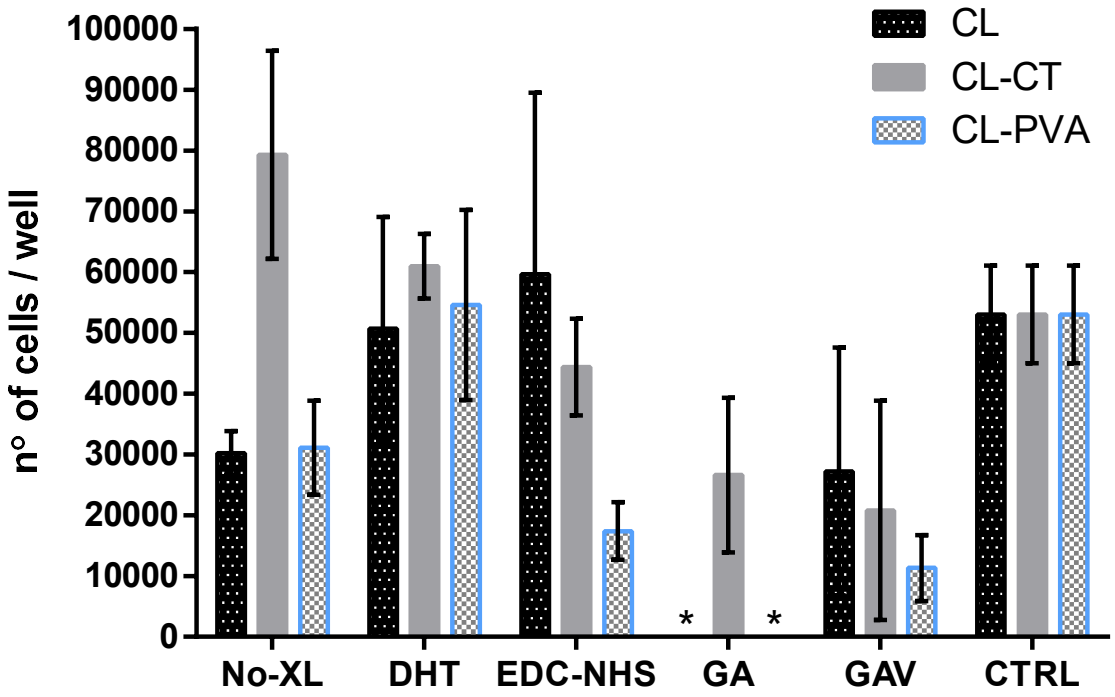

Figure 5. 2 Viability of HDF cells cultured on porous scaffolds differently treated after 48h. Asterisks * indicate no presence of colour change in the solution linked to absence of cell viability. n= 3.

As observable from the graph in Figure 5.2, cell viability was only affected by GA treatment in solution. It is known that residual GA in scaffolds can be a source of high cytotoxicity [188] and the MTS test may have confirmed the role played by GA in cell mortality. Viable cells were not detected for CL and CL-PVA samples, contrarily to CL-CT that showed a number of cells similar to the samples treated with GA vapours. This result may suggest that independently of the material utilised for scaffold fabrication, GA in solution is not easily washed off after crosslinking. Further treatments such as oven-drying [189] and glycine washings [190] have shown to reduce traces of GA in the scaffolds and may be a solution to improve cell survival. *In vitro* cytotoxicity is often overlooked in studies focused on mechanical properties of scaffolds and *in vivo* animal implantation. For example, during *in vivo* studies it may happen that an initial inflammatory response at implant site will eventually neither compromise scaffolds integration in the tissue nor result in rejection [110]. On the other hand, results in Figure 5.2 showed the effectiveness of GA vapour in cell culture that may be used as a substitute of GA solutions for collagen sponges crosslinking as the use of solutions can disrupt the structure and require additional steps to remove GA traces [191]. With regard to CL-PVA scaffolds, the number of estimated cells was the lowest among all the samples tested and

compared to CL and CL-CT. This data could have been altered by the absorption properties of the scaffold that may exchange fluid slower than CL and CL-CT scaffolds [4, 192]. Another possible explanation that can suggest this hypothesis was showed later in Section 5.3. CL-CT scaffolds showed the highest proliferation when un-crosslinked, doubling the initial number of seeded cells, ~ $8x10^4$, and having an estimated 50% more cells when DHT treated than control (CTRL). As DHT crosslinking resulted in a similar proliferation rate for all the scaffolds with relatively low variability and it is known it was therefore selected for the experimental studies presented in following sections. In addition, this choice was made to retain the biomaterial chemistry preserving the cell-binding activity.

It is indeed worth noticing that the proliferation trends varied depending on type of scaffold, meaning that different treatments cannot only influence physical properties but also have an impact on cell growth. For example, Bax et al. [193] studying cellular recognition on EDC-NHS collagen-treated scaffolds, found out that alternated structure decreases cellular spreading, survival and growth. As support to this thesis, a recently published research study [194] reported that HDFs may be driven by mechanical cues for short-term proliferation but long-term proliferation is correlated to levels of integrin-specific binding. To endorse results obtained with the MTS assay and study fibroblast morphology, cell viability was evaluated at day 3 by means of nuclei and actin filaments staining, using DAPI (Invitrogen, Grand Island, NY) 1:5000 in PBS and Rhodamine Phalloidin (Invitrogen, Grand Island, NY) 1:80 in PBS respectively, after being permeabilized and fixed in formaldehyde, 4% in PBS.

In Figure 5.3, examples of fluorescent microscope images of CL-PVA and CL-CT DHT-treated scaffolds are shown. It was found that HDF cells adhered to all the sides of the scaffold showing the same morphology reported in the images. Although, some details may result blurred and out of focus, important characteristics of the cells can be seen.

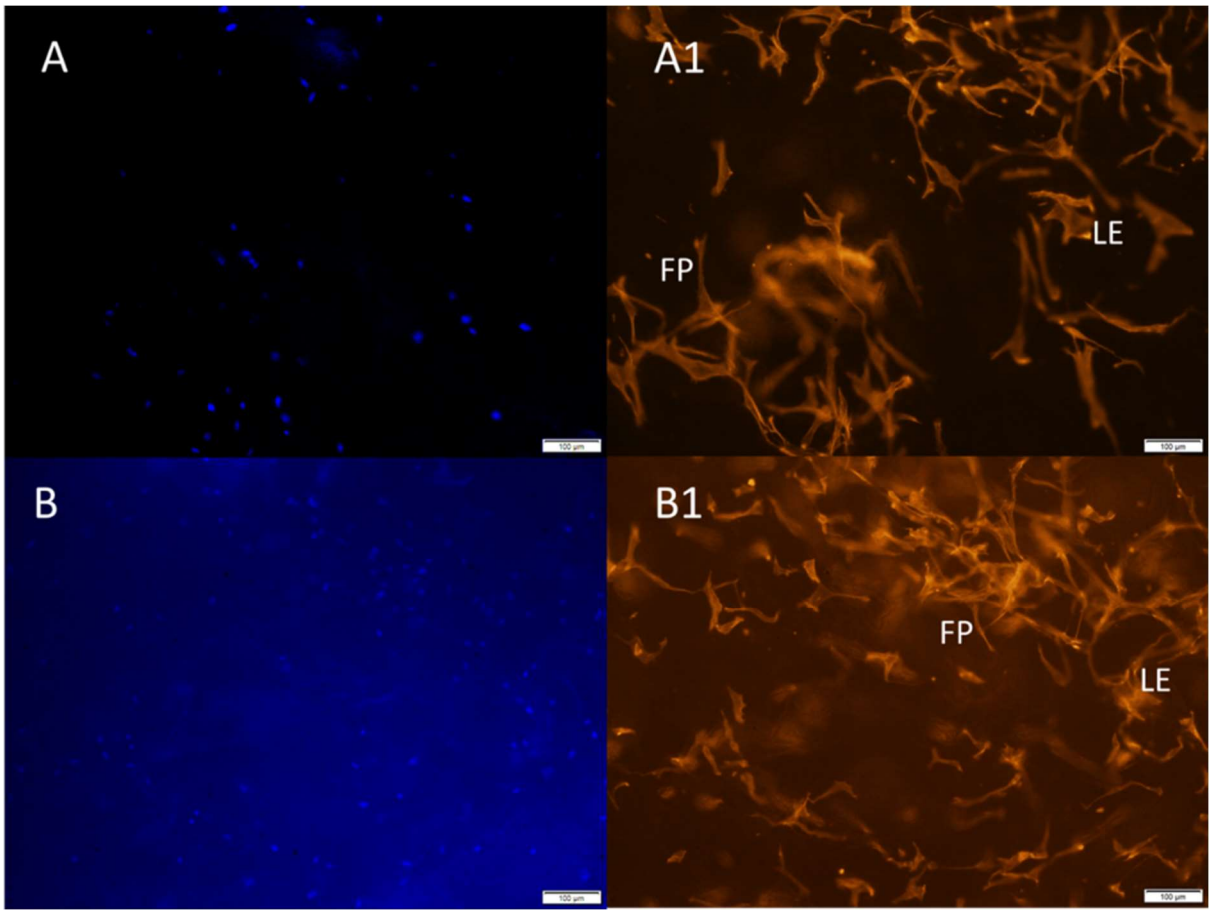

Figure 5. 3 CL-PVA top side (A) and CL-CT lateral side (B); Orange: Phalloidin (actin) (A1, B1); Blue: DAPI (nucleus) (A, B). Examples of lamellipodia (LE) and filopodia (FP) are shown in A1 and B1. Images for DAPI staining were slightly modified in brightness and contrast using ImageJ. All scale bars are 100 um.

Cells presented cellular projections that appeared thinner and longer compared to the fibroblasts shape developed within fibres (Figure 4.18 - 4.19).

As Wong et al. showed in a study [195], fibroblasts tend to use filopodia (FP) for sensing and testing substrate rigidity around the cell body before spreading and establishing stable adhesion. This can be the reason explaining the scarcity of lamellipodial extensions (LE) in the images compared to those when fibroblasts interact with fibres. Fibroblasts spreading in collagen-based matrixes appeared to be similar to that of neurons which form dendritic extensions. It has been demonstrated that these extensions contain microtubule cores and have actin-rich tips that can only form at low tension state [196]. Other than in two dimension or with collagen coated culture surfaces, cases in which fibroblasts develop numerous stress fibres and lamellipodia are under conditions of wound repair and fibrosis when they can differentiate into myofibroblasts [197].

It is crucial that cells seeded in scaffolds contract and elongate coupling their cytoskeletal filaments to exert tensile traction on the surrounding material as it occurs in the dermis [82, 198]. While it is known that these porous scaffolds can only perform as pseudo-3D support for cells [199], changing the material properties and the composition may affect the way cells spread and behave.

5.3 Bilayer scaffolds

In skin tissue engineering, attempts to prepare multilayer scaffolds have already been done using and adapting several techniques for various purposes with the common goal to simulate natural full thickness skin [200, 201]. Although the use of electrospinning to deposit fibres on an insulated material have been shown to be possible [202, 203], some of the issues that may be encountered such as layer separation or membrane thickness have not been addressed. In this study, freeze-dried DHT-treated collagen scaffolds presented in previous sections, were mounted with double side adhesive conductive carbon tape (Agar Scientific) on the rotating aluminium collector (2.5 cm from the centre) and polymer solutions (Sections 4.4.1 and 4.4.2) were electrospun on top of the disks with a pump rate of 0.2 ml/h for 3 hours.

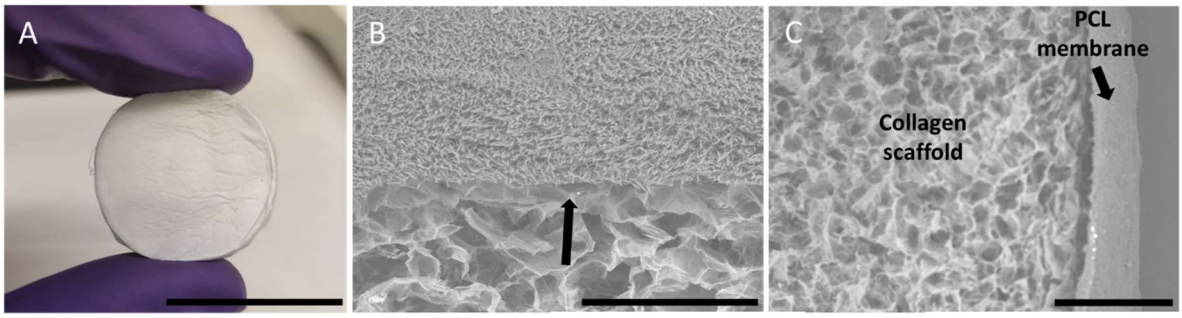

Figure 5. 4 Macroscopic picture of PEO-CT/CL bi-layered scaffold (A) and cross-section of SEM images of PCL-CL scaffold (B, C). Scale bar of 35 mm in (A), 500 µm in (B) and 1mm in (C).

As it can be seen from different angles in Figure 5.4, the two-layer scaffold was successfully created and electrospun fibres adhered and covered uniformly the surface. However, following the use of a scalpel to section the structures for SEM analysis, it was noticed that tension forces caused disruption of the adhesion layer at the cutting point, specifically in the case of the hydrophobic PCL fibrous mat (arrow in Figure 5.4 B, C). This partial detachment, technically called delamination, may have been also influenced

by the insolubility of collagen substrate in acetic acid solutions and to the membrane thickness that required higher forces to be sectioned. The use of soluble collagen would allow partial dissolution of the scaffold surface allowing better fibres adherence to the disk. Despite Uzunalan et al. [204] used soluble collagen isolated in their lab from rat tail and a highly toxic solvent (1,1,1,3,3,3 hexafloro-2-propanol) to electrospun fibres on top of a freeze-dried collagen scaffold, they did not address this potential issue.

To increase the stability and strengthen the bond between the two layers, GA vapor and solution crosslinking has also been used [204, 205] but its efficacy was not successfully demonstrated. Nevertheless, the integrity of bilayer scaffolds was tested and visually inspected after submersion in solution and undergoing cell culture. They were sterilized in 70% ethanol solution and then seeded with $1x10^5$ HDF cells following the procedure described in Section 5.2. Thus, they were incubated for 7 days refreshing the medium every 2 days and the viability was assessed using MTS assay. Compared to the experiment described in Section 5.2, the scaffolds use this time consisted of two layers and had a size of 35 mm in diameter. Unexpectedly, the results were null (Figure 5.5) as no change in colour was detected in any of the scaffolds after the assay.

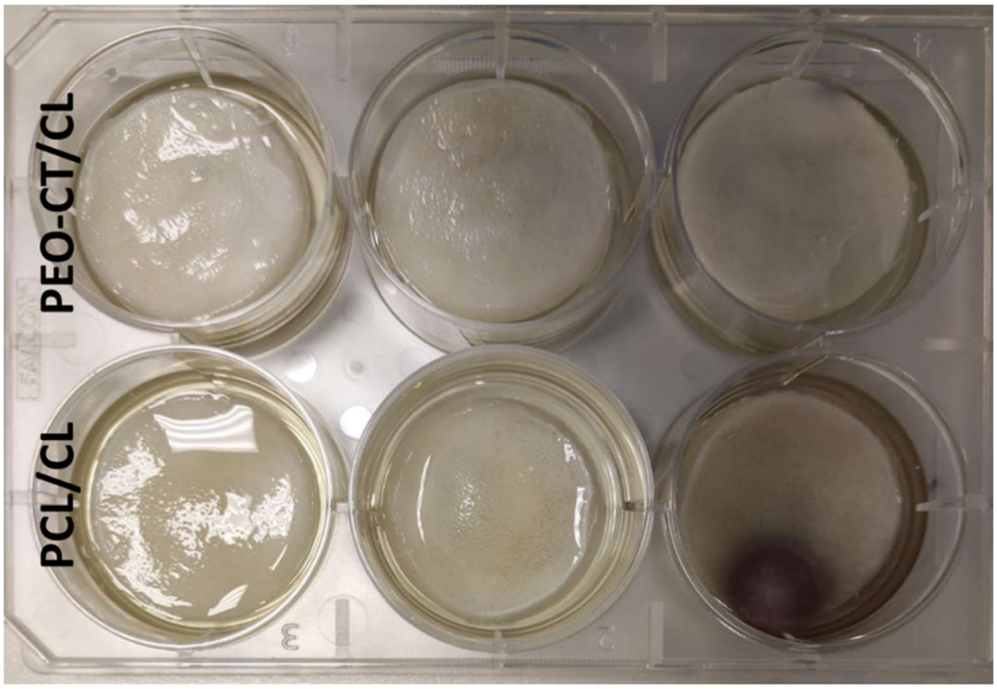

Figure 5. 5 Bilayer scaffolds, on a 6 well plate after MTS assay, showed no purple colour change. Blue spots that appeared on PCL/CL scaffolds after 17 hours of incubation were identified as possible fungal moulds.

It is undoubtable that these materials are biocompatible and suitable for tissue engineering as they are commonly used commercially and in laboratory research [3, 118] and experiments carried out in Section 5.2 supported the hypothesis of the cytocompatibility for the scaffolds fabricated in this work. For this reason, cell assays were questioned and discussed in Section 5.3. In addition, it is possible to notice that the fibrous membranes did not separate from the porous freeze-dried structure underneath after a week immersed in solution, showing the feasibility of the method describe above for creating a bilayer scaffold without further use of crosslinking. Some blue stains, identified as fungal mould, were visible on samples where PCL fibres were deposited. Presumably, this may have been due to a chemical reaction after MTS assay that could not be explained.

Although the possibility to combine the two techniques gave positive results in this preliminary study, in order to increase the stability at the interface between the two layers, the use of a biocompatible adhesive such as gelatine might be considered in the future [206]. Gelatine can be spread on top of the freeze-dried scaffold before performing electrospinning. In this way, while gelatine is cooling and reaches a semi-solid state, fibres can be better integrated and strongly adhere to the lower structure.

5.4 Limitations of viability assays on porous scaffolds

During the years, many assays have been developed to evaluate viability and proliferation of cells [207]. These methods are usually classified according to the measurement type of end points and a proper choice is crucial to evaluate the status of cells at the end of the experiment. The most used techniques to measure cell viability and proliferation on scaffolds are colorimetric methods such as MTT or MTS assays based on metabolic activity of the cells and fluorometric assays such as alamarBlue® and CFDA-AM, both membrane permeable dyes that are converted in fluorescent compounds by the live cells.

Despite its destructive consequences on samples, the decision to analyse cell viability with MTS was initially made to obtain a response in a time of 1 to 4 hours adding the reagent straight to the cell culture plate. This process would have avoided misleading results due cells or media manipulation and would have given rapid answer about the presence of living cells. Although it revealed to be a valid test on small porous samples and electrospun membranes, doubts about its reliability when scaffolds were scaled up to provide a larger surface area for cell attachment arose following the results described in Section 5.2.

MTS assay was repeated, this time on a single-layer porous scaffolds of 35 mm in diameter DHT-treated preventing any possible interference that electrospun membranes might have had on the outcome.

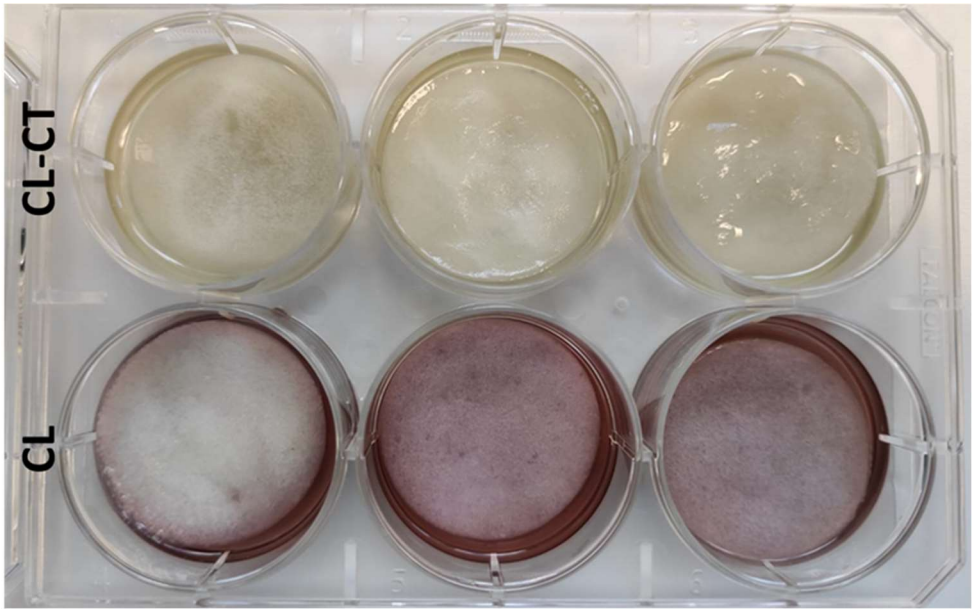

Figure 5. 6 Change in colour on porous scaffolds cultured in a standard 6 well plate after MTS assay.

Figure 5.6 shows that a positive response (colour change to purple) was only obtained for collagen scaffolds, after 5 days of cell culture. To further investigate the reliability of MTS test on these scaffolds, a resazurin-based assay was also performed to follow and measure the proliferation of HDF. While MTS used an intermediate electron receptor and not readily enters viable cells, resazurin-based assays work by a different mechanism. Resazurin is a blue and non-fluorescent compound that is reduced by dehydrogenase enzymes in living cells to form a red fluorescent dye, called resorufin (Figure 5.7), which is visible to the naked eye. Resazurin sodium salt is used in the fluorimetric assay alamarBlue® and has many advantages over MTS [207]. It is more sensitive requiring less cells for reproducible results and it is a non-destructive assay so that measurements can be taken over several time periods.

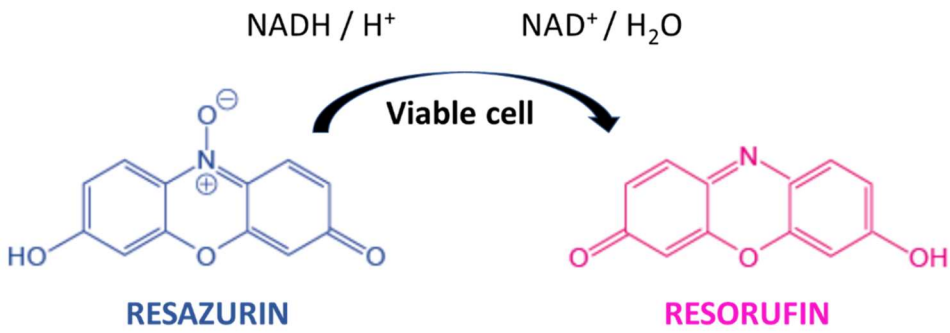

Figure 5. 7 The working principle of resazurin salt and resorufin product from reduction in viable cells Adapted from [208].

Using the same protocol explained in 5.2, scaffolds were sterilized, seeded with 1.25 x 10^4 cells and cultured for 24 hours. A stock solution of 5 mg/ml resazurin sodium salt (SigmaAldrich, UK) was prepared in PBS and successively diluted 1:100, with a final concentration of 0.2 mM. This amount was chosen based on previous studies [209] in order to avoid possible cytotoxic effect on cells due to an incubation time longer than 4 hours. Then, the solution was filter-sterilized trough a 0.2 µm filter into a sterile tube.

After 24 hours, the resazurin solution was added to the scaffolds and to the CTRL (cells cultured in plastic well plates) and incubated at 37° and 5% CO_2. Scaffolds that contained no cells were used as negative control (MCTRL).

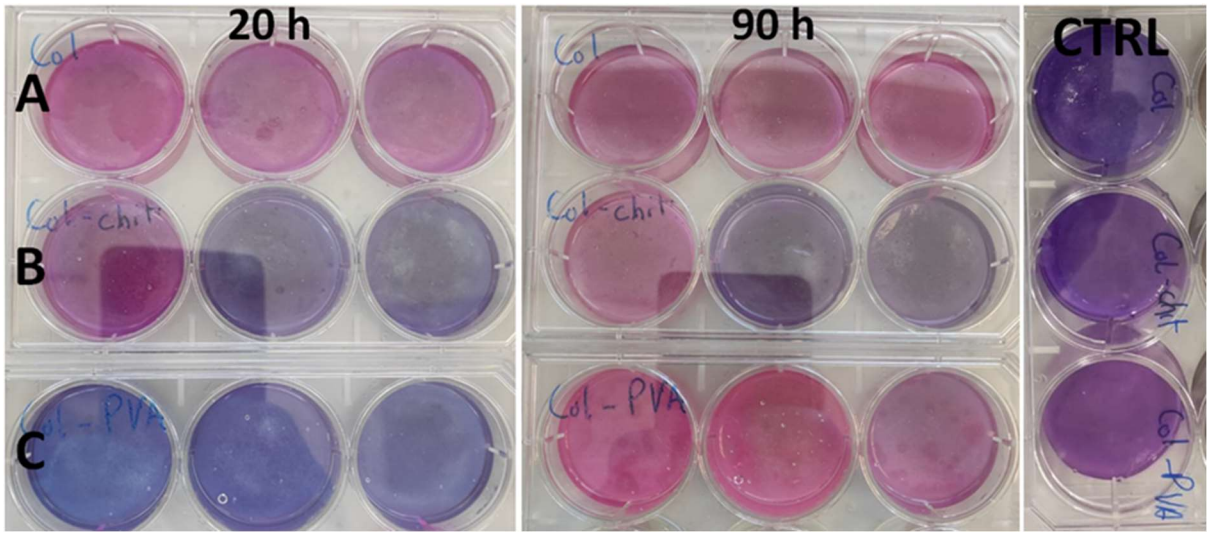

Figure 5. 8 Effect of resazurin incubation time on CL (A), CL-CT (B) and CL-PVA (C) compared to the material control (MCTRL).

The colour change of the media was visually monitored. In contrast to expectations, there was no resazurin reduction after 4 hours for scaffold samples, but a colour change appeared following overnight incubation (20h) (Figure 5.8). This was a signal of the presence of viable cells in CL scaffolds and in one CL-CT scaffold. The absorbance of the medium was then read at 570 nm for resorufin and at 590 nm for resazurin in a microplate reader (Multiskan™ FC Microplate Photometer, Thermo Scientific™) and converted by a calibration curve in an estimated number of cells. Results shown in Figure 5.9 suggest that protocols, in future studies, need to be adapted for the specific material and 3D structure in order to avoid misleading results obtained from resazurin-based assays. The uptake of the scaffolds and the material itself affected the outcome of the test. From the graph, it is possible to notice that measurements of absorbance in absence of colour response (4h and 20h Blu) were comparable to values obtained for acellular scaffolds after 24h (MCTRL), whose medium turned purple. There is also a large discrepancy in the readings between cells cultured on a two dimensional 6-well tissue culture plate (CTRL) and on a 3D scaffold.

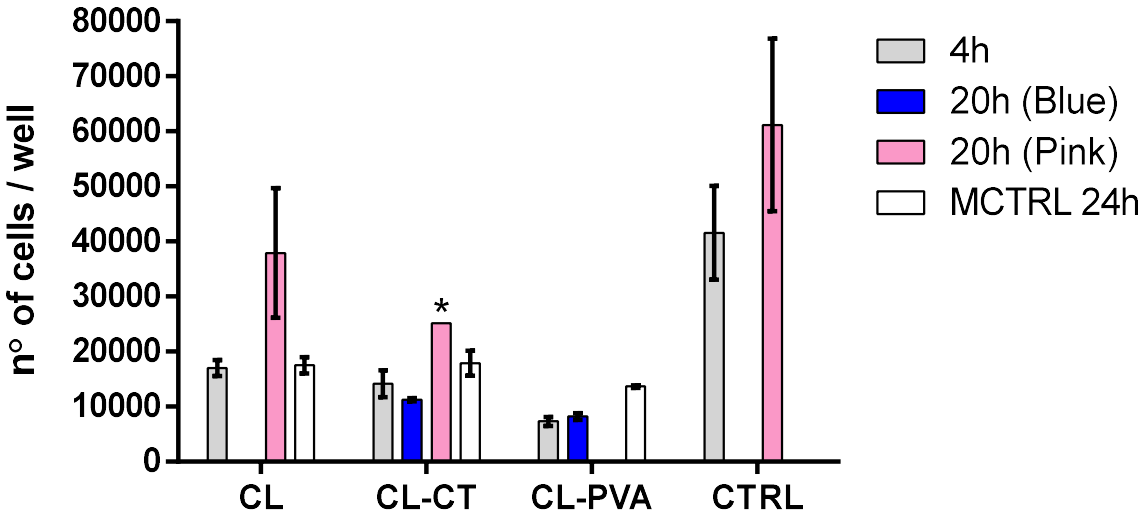

Figure 5. 9 Estimated average number of cells in each scaffold after conversion from absorbance readings using a calibration curve. These results are meant to represent that interaction of resazurin-based assay with the material can affect absorbance readings. T-test revealed no statistical significance differences between samples (p>0.05). * Only one data point.

Following 48h of cell culture medium was removed and scaffolds were washed extensively with PBS before adding fresh media. Whilst the test was deemed non-destructive for the cells, the nature of the scaffolds meant that the dye was retained and thus negating

subsequent testing making further absorbance readings irrelevant. Contrarily, Gong et al. [209] demonstrated in their study that a resazurin-based assay performed on small PLA porous scaffolds (triangles with sides of 8 mm) was successfully washed off, measuring an absorbance value of nearly zero. These differences suggest that material and size of the scaffolds may affect cell-based assays. Nevertheless, scaffolds were maintained in culture over the weekend adding fresh media with the purpose to fix the fibroblasts at day 7 for cell morphology analysis. Remarkably, CL-PVA showed a change in colour at day 5 (90h) in all the samples as shown in Figure 5.9. This supports the thesis that different uptake kinetics may apparently result in absence of cell viability [210]. It is possible to suppose that cells in these scaffolds proliferate slower and that the exchange of liquid occurs gradually as also experienced during PBS washings to remove the dye. Studying resazurin concentration during scaffold cell culture, Gong et al.[209] showed that absorbance increases linearly up to 24h and then begin to slightly deplete. They also observed in a time window of 96h that for low cell density (1.56-6.25 x 10^4) colour may change slowly from blue to dark purple whereas when scaffolds have a high cell density (>25 x10^4) colour turns from dark pink to bright pink progressively with the time. These findings can help to explain the dynamics of colour change in this work indicating a high cell proliferation in those scaffolds which medium turned pink after 90h.

A list of issues encountered in this study regarding MTS and resazurin-based assays on porous collagen-based scaffolds with possible causes and solutions for future studies, have been collected in Table 5. Particularly, the nature of the material and the scaffold structure, the cell density per surface area and the ratio between reagent and volume of medium can greatly impact the results of colorimetric and fluorometric assays. These observations can also be applied to other viability tests. However, it is important to specify that depending on the cell line, different proliferation rate and interaction cell-matrix can be acknowledged [69].

Table 5. 1 List of limitations, causes and potential solutions experienced during cell culture testing 3D scaffolds for availability and proliferation with commercially available assays.

Limitations	Potential cause	Potential solution	Ref.
Cell seeding	• Difference in structure • Culture conditions	• Scaffold precondition and removal of media in the well before seeding • Seeding on both sides covering the entire surface • Establishment of cell density per ml of culture medium	[211]
Estimate of cell number	• Cell attachment to the base of culture plates following seeding • Different cell interaction in 3D (scaffolds) compared to 2D environment (standard curve) • Incubation time for each material • Interaction between reagent and material	• Use of another well plate after seeding • Optimization of incubation time and readings of absorbance at several time points for both scaffolds with cells and without. • Extension of incubation time beyond the recommended	[211, 212]
Assay sensitivity	• Low reagent / volume ratio • Low cell number • Slow diffusion of liquid in the structure • Short incubation time	• Measure of the volume absorbed by the scaffold • Optimization of cell density to obtain colour change • Increase assay working solution or consider dilution factor	[210, 213]
Residual signal after first assay (resazurin-based)	• Dye absorbed by the material	• Measurement of amount of liquid needed to rinse the dye off • Use of smaller samples	[209]

5.5 SEM analysis of cell attachment and morphology

With the aim to verify the presence of fibroblasts across the thickness of the structure, at day 7 post-seeding, cells were fixed as outlined in Section 5.2 on a 35 mm scaffolds. They were consequently dehydrated using freeze-drier, sectioned in samples that were gold-coated and analysed by SEM. The effectiveness of this procedure in preparing cells on 3D scaffolds for SEM examination has been demonstrated in another study [214], in which

authors found no significant difference in cell morphology when scaffolds were dehydrated with freeze-drying compared to chemical standard methods. Cellular infiltration within the sponge as well as cell attachment and morphology were observed and discussed. SEM images (Figures 5.10, 5.11) showed cell attachment throughout the examined samples predominantly on CL scaffold compared to the other polymer blended scaffolds as partially revealed by viability assays in Section 5.3. The advantage of seeding fibroblasts on artificial porous scaffolds over decellularized human dermis consists in obtaining cell infiltration into the structure even when seeded statically on the surface [212], allowing a homogenous distribution of cells. This was confirmed by detecting images of fibroblasts at different heights along the cross-section of the scaffold.

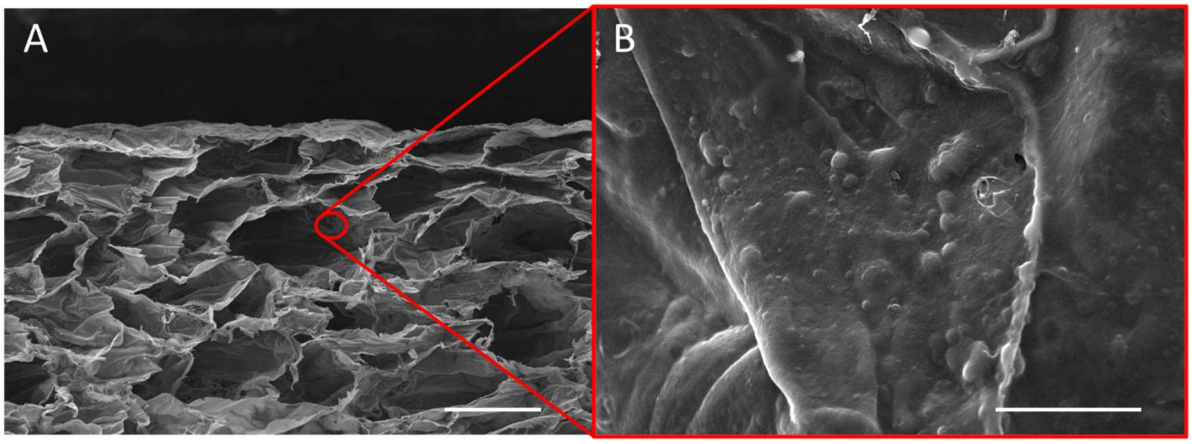

Figure 5. 10 Cross-section of CL scaffold (A) and a zoomed area at the depth of 200 µm under the surface to observe a cluster of cells. Scale bars of 200 µm for A and 20 µm for B.

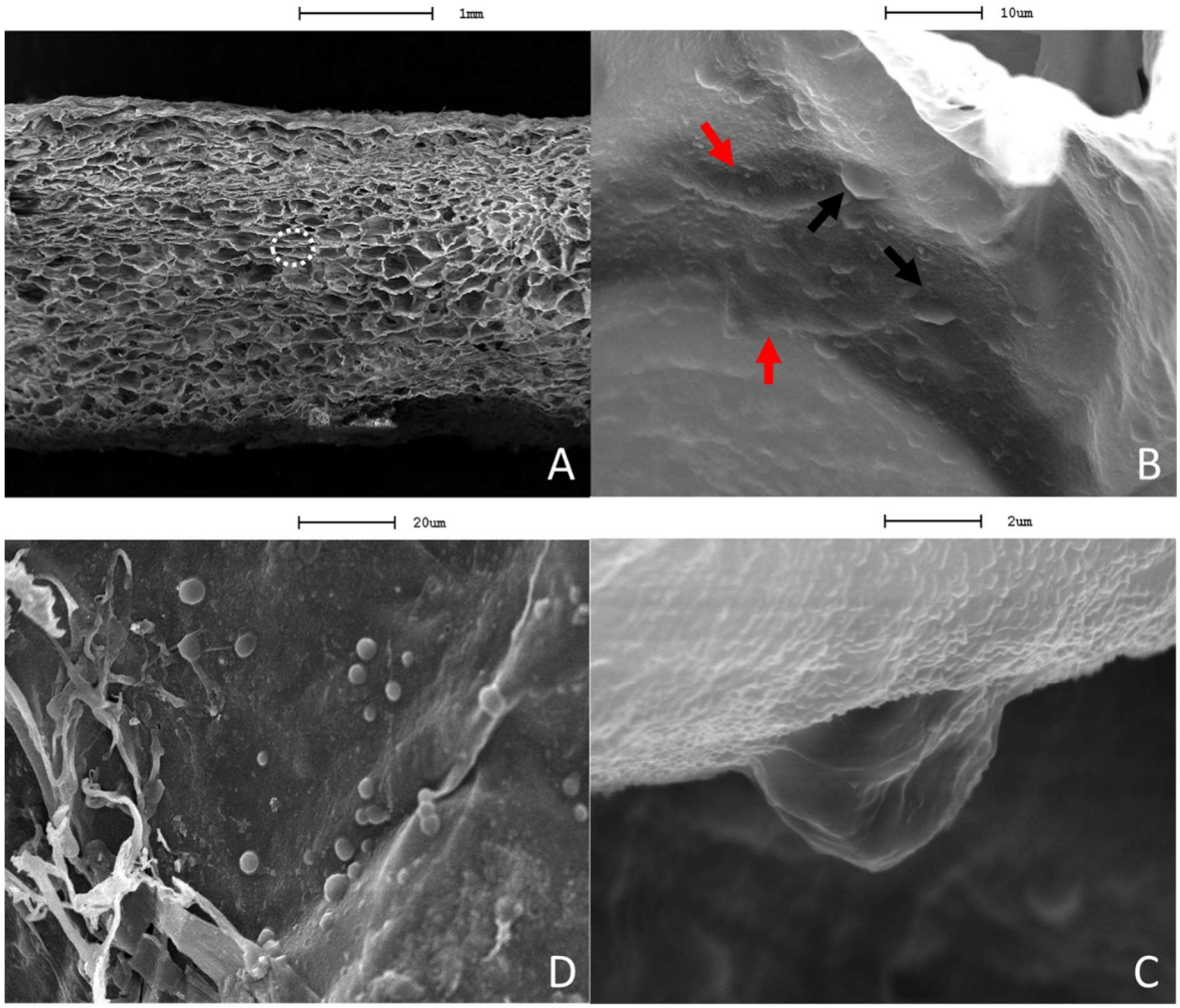

Figure 5. 11 A) Representative cross-section SEM image of CL scaffold B) Spread (red arrows) and rounded (black arrows and C) fibroblasts at day 7 and D) fibroblasts imaged after 48h in culture.

Close examination of the porous structure showed samples with a complex morphology in which fibroblasts were identified and imaged. They can be interpretated as fibroblasts based on their size which slightly differ due to the way they attach to the surface. Elongated and spread morphology (red arrows in Figure 5.11 B) indicate that cells could proliferate after attachment while round-shape cells (black arrows in Figure 5.11 B and Figure 5.11 C) may suggest an unwillingness to spread. However, multiple cytoplasmic processes of attachment and intracellular interactions in early stage were found in these rounded cells. Compared to cells pictured after 48h in Figure 5.11 D, they seemed to be flattened and incorporated into the surface.

Based on literature review, it was found that this behaviour is common when cells are only cultured on porous structures for 7 days [214, 215]. Cells initially adhere to the surface with short filopodia that eventually extend into dendritic extensions. This behaviour may

be influenced by many factors, such as the nature of the fibroblasts [69], the amount of time period in cell culture and the medium used in cell culture. In particular, it has to be said that the initial prolonged incubation time required to generate a signal and resazurin compound residuals in the culture medium might have interfered with the cell's metabolic activity [216, 217]. The potential consequences that resazurin-based assay may have on the cell survival rate and on cell morphology need to be addressed and investigated. It cannot be excluded that alterations in cytoskeleton especially in intermediate filaments and information about the cell-interaction material and cell morphology may have been lost.

Despite scaffolds being extensively washed and freeze-dried, fibroblasts were shown to be strongly anchored onto the pore surface likely indicating cell viability before fixation. Also, the complex morphology of the scaffolds made it laborious to image unambiguously the presence of spread fibroblasts on the surface [218]. In the future, haematoxylin and eosin stain (for cell nuclei and cytoplasm, respectively) can give valuable information about cell distribution and number, while adding specific protein stains such as β tubulin for microtubules and Phalloidin for F-actin can help to visualize the cytoskeleton.

5.6 Platform for NPTW device application

The use of negative pressure has been largely accepted to be beneficial for wound healing, promoting formation of granulation tissue, stimulating angiogenesis and reducing wound exudate [219-221]. However, there is little knowledge about the effect of biochemical changes in response to this force on a cellular level. First attempts to apply cyclic compression and tension forces in vitro by means of vacuum dated back to 1985 when Banes e al. [13] deformed a plastic Petri dish in which chicken-tendon cells were plated. During the years, scientists have investigated several types of cells in two dimension using stiff substrates as plastic or glass [222, 223] or flexible materials such as silicone [81]. Only in the last decades, continuous interest has grown in studying the effects of negative pressure on cells cultured in three dimensional environments in which complex responses that occur from cell-matrix interactions can be reproduced. Although collagen and fibrin gels have been the most commonly used matrix for 3D cell culture [79, 224], their low mechanical stiffness and shrinkage make them unsuitable to replicate the characteristics of skin and to withstand the application of NPWT through the dressing. Therefore, this study aimed to investigate the possibility to test NPWT devices on porous scaffolds

cultured with fibroblasts. Specifically, the single-use negative pressure wound therapy device PICO 7 (TJ Smith and Nephew Ltd) [225] (Figure 5.12 A) that was recently showed in an *ex vivo* study, to cause less damage to the wound edge compared to traditional application [220]. The culture platform (Figure 5.12 B) (Appendix II) was designed and then manufactured in the mechanical workshop (Department of Engineering, University of Hull) from polycarbonate rather than acrylic due to its durability and higher resistance to crack under stress. Also, this material allows visual monitoring of experiment and is suitable for several physical and chemical sterilization methods, in autoclave as well as by means of ethanol solution. The wells were designed to precisely fit the scaffold and guarantee perfusion through the channels. Pump gas permeable tubing (Cole-Parmer, UK) were fitted and connected to a peristaltic pump (IPC, Ismatec part of Cole-Parmer, UK).

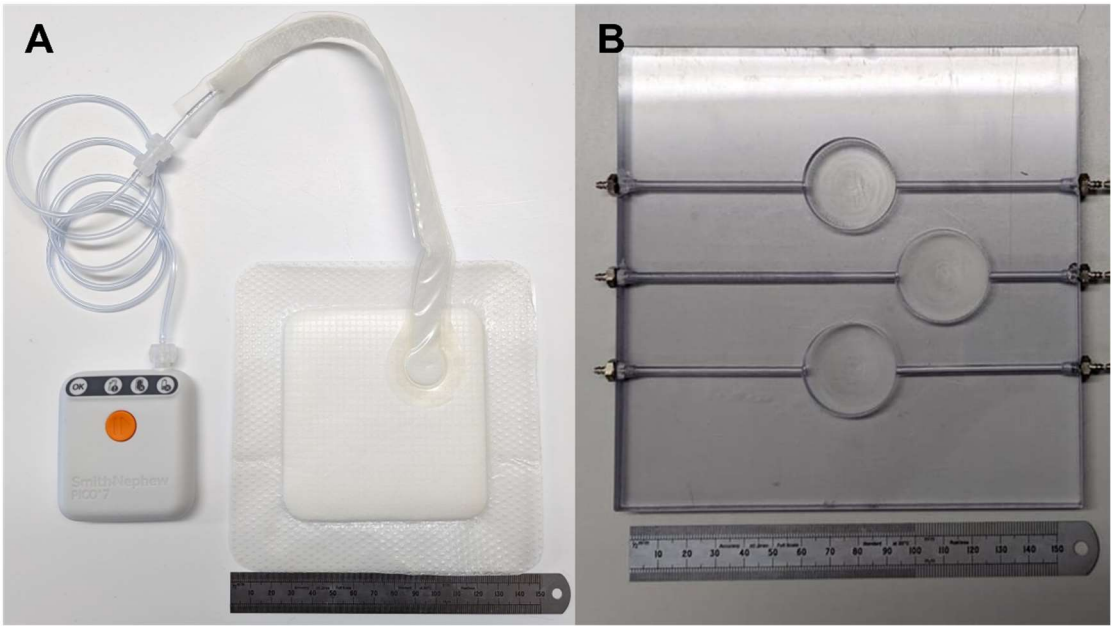

Figure 5. 12 PICO 7 device that applies Negative Pressure through the dressing (A) and the culture platform with 35 mm wells designed to precisely fit the scaffolds(B).

The information provided by the company manufacturer of PICO gave indications about the device and the dressing. The system is intended for wounds with size that should generally be no more than 25% of the dressing pad area and where the level of exudate is low (0.6 g/cm^2/day) to moderate (1.1 g/cm^2/day). The dressing is composed of 4 layers: a flexible perforated adhesive layer in contact with the scaffold, bonded to an airlock layer and an upper fluid absorption structure responsible of delivering negative pressure and exudate removal; it also aids the evaporation through the top film layer that has a high moisture vapor transmission rate [219]. With the purpose to mimic the conditions of

exudate flow rate for wounds, this data could be translated to peristaltic pump setting of 15.6 µl/min for low exudate rate and 28.6 for moderate pump rate. In the testing platform, given the size of the channels, flow rate was set at the minimum value applicable that was 28 µl/min, therefore falling into a range that allowed a moderate absorption of culture medium (Gibco™ Dulbecco's Modified Eagle Medium, DMEM, high glucose, no glutamine, no phenol red, Thermo Fisher) during the experiment. To preliminary test the bioreactor system, flow rate and scaffold perfusion were investigated on DHT-treated CL and CL-CT scaffolds using a solution of PBS tinted with blue food dye with a flexible silicon layer sealing the top surface (Figure 5.13). After 24h, CL scaffold visually showed to be better perfused from a marked blue colour throughout the structure, especially in proximity of the inlet and outlet. Contrarily, as expected from previous experiments, CL-CT had a paler blue colour, probably due to low permeability and longer time needed to exchange fluid.

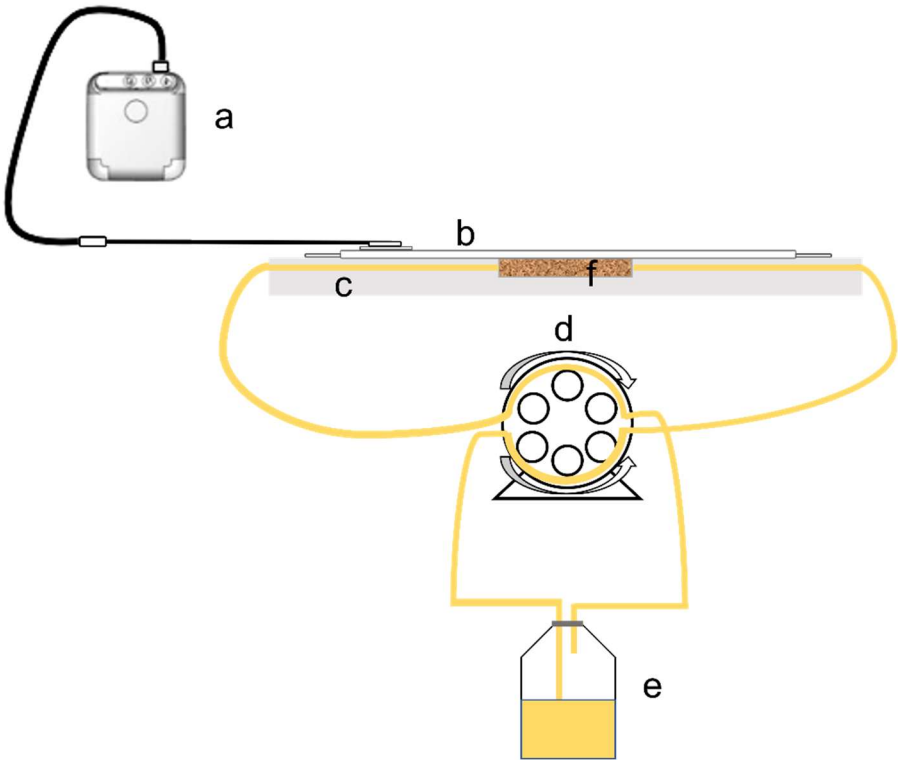

Figure 5. 13 Schematic representation of bioreactor system. a) NPWT device; b) NPWT dressing; c) Culture platform; d) peristaltic pump; e) medium reservoir; f) scaffold

Following these primary experiments, three DHT-treated CL scaffolds were sterilized, seeded with $6x10^4$ HDF using the same procedure described in Section 5.2 and incubated in a 6 well plate for 7 days, replacing the medium every 48 hours.

The platform and tubes were cleaned with ethanol (70%) and air-dried under UV light (wavelength of 254 nm) in a laminar flow cabinet also used for cell culture. Then, scaffolds were transferred from the 6 well plate to the platform and PICO dressing was applied to adhere to the acrylic sheet (Figure 5.14).

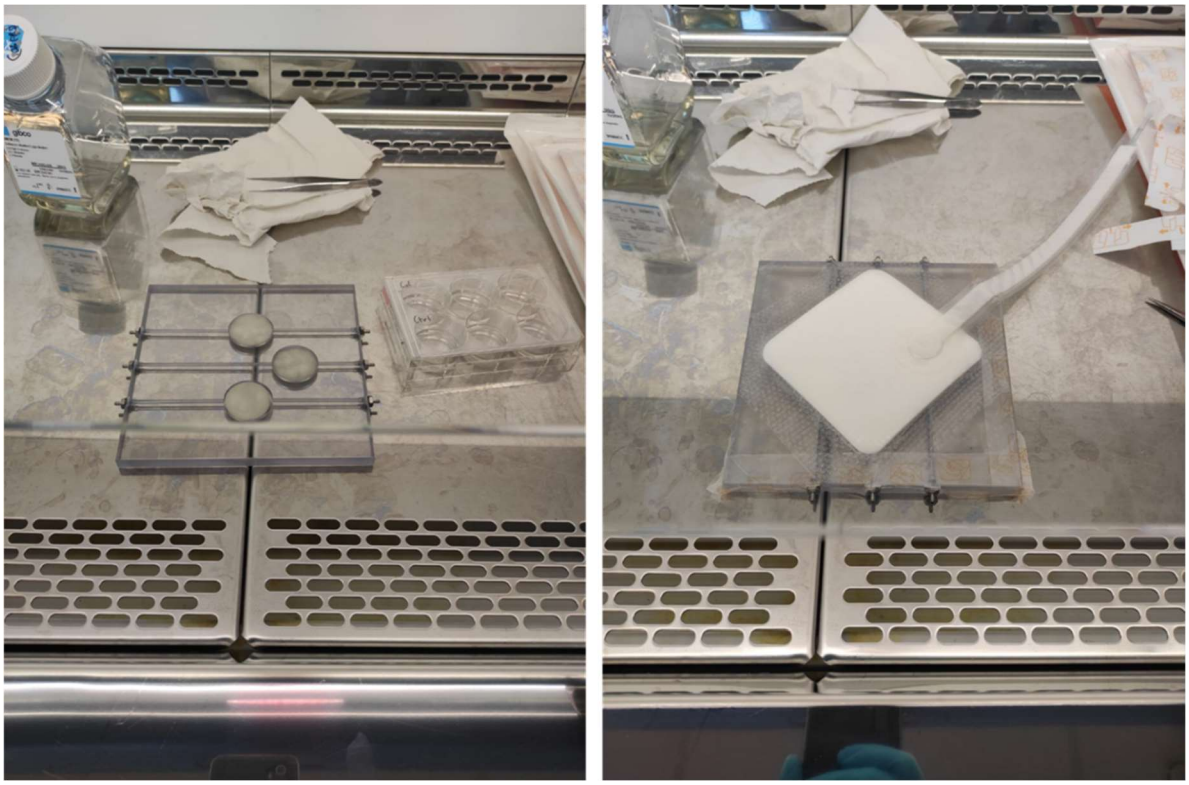

Figure 5. 14 Images of scaffolds in the culture platform and PICO dressing application.

PICO device was turned on and the platform placed in a cell culture incubator (Figure 5.15). It was verified that application of negative pressure on scaffolds occurred for few hours (red arrow in Figure 5.15) and then the device was left in function for 24h. Tubes were connected to a sterile reservoir containing culture medium (white arrow in Figure 5.15).

Figure 5. 15 Setup of bioreactor system for negative pressure application on scaffolds inside a cell culture incubator at 37° C and 5% CO_2.

5.7 Effect of NPWT on porous structure

The vacuum pump delivered a continuous nominal negative pressure of 80 ± 40 mm Hg (based on manufacturer information [225]) equivalent to ~10 ± 5 KPa, on the collagen scaffolds for 24h. After this temporal window, the dressing saturated due to large medium uptake. Therefore, it was not possible to continue the experiment for longer times. The fact that incubators have a tray filled with sterile distilled water that is placed at the bottom to generate a highly humid atmosphere inside, preventing the cultured cells from drying out over time, may have restrained the evaporation rate of the liquid. Also, the cell culture medium has a different viscosity compared to the exudate [226] facilitating water uptake from the dressing. The dressing was consequently removed, scaffolds were fixed in 4% formaldehyde for further SEM analysis. After being rinsed, they were freeze-dried and sectioned in the middle of the scaffold using a scalpel (Figure 5.16 B)

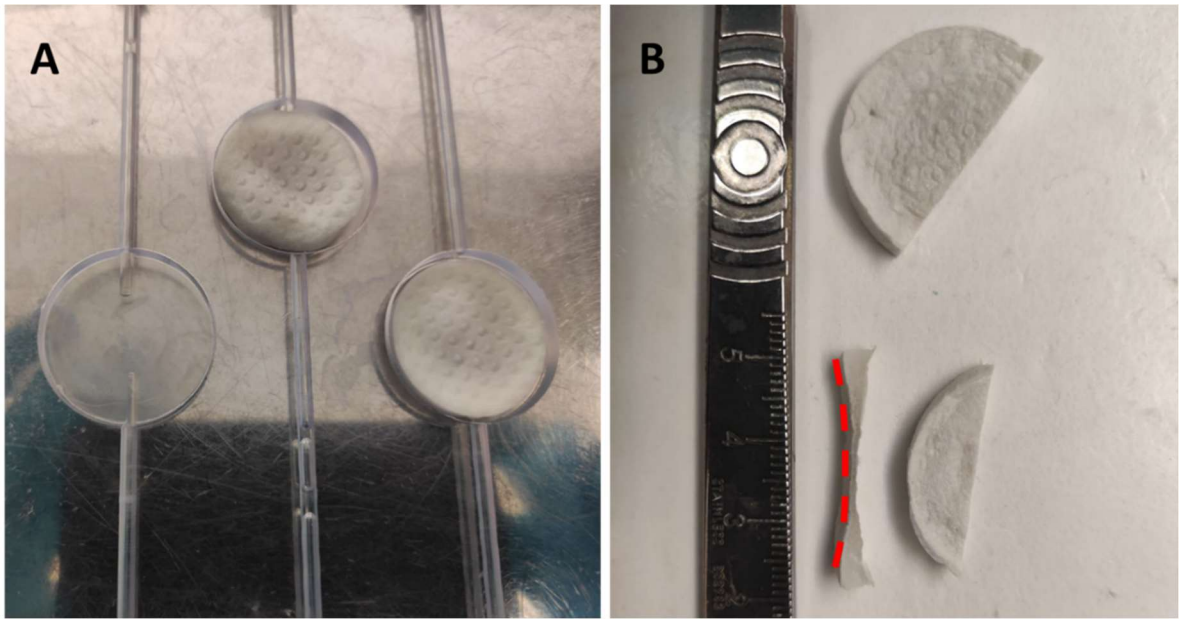

Figure 5. 16 CL scaffolds after dressing removal (A) and freeze-dried CL scaffold sections after cell fixation (B). Red dashed line indicates bending on the side of the scaffold in contact with the culture platform.

Figure 5.16 A shows a pattern on top of the CL scaffold as a consequence of the contact with the lower perforated layer of PICO dressing witnessing that the application of negative pressure occurred across the whole surface. The vacuum drawing is crucial for effectiveness of negative pressure wound therapy because removes exudate and induce microdeformation and this result positively showed the possibility to apply therapeutical negative pressure *in vitro* to a tissue model.

Scaffolds compression was greater moving from the edge towards the centre (Figure 5.16 B) due to the round, rigid edges of the wells that prevented the collapse of the structure. It is also evident from a macroscopic view (red dotted line, Figure 5.16 B) a minimal concavity in the inferior side of the scaffolds after freeze-drying. Presumably, this may be due to the scaffolds being lifted during application of negative pressure, causing an irreversible deformation of the structure. Part of the process improvement could be to anchor the scaffold to the bottom of the well or to a substrate to tackle this issue.

SEM analysis was undertaken to have a better picture of structure alterations and to verify the presence of HDF (Figure 5.17).

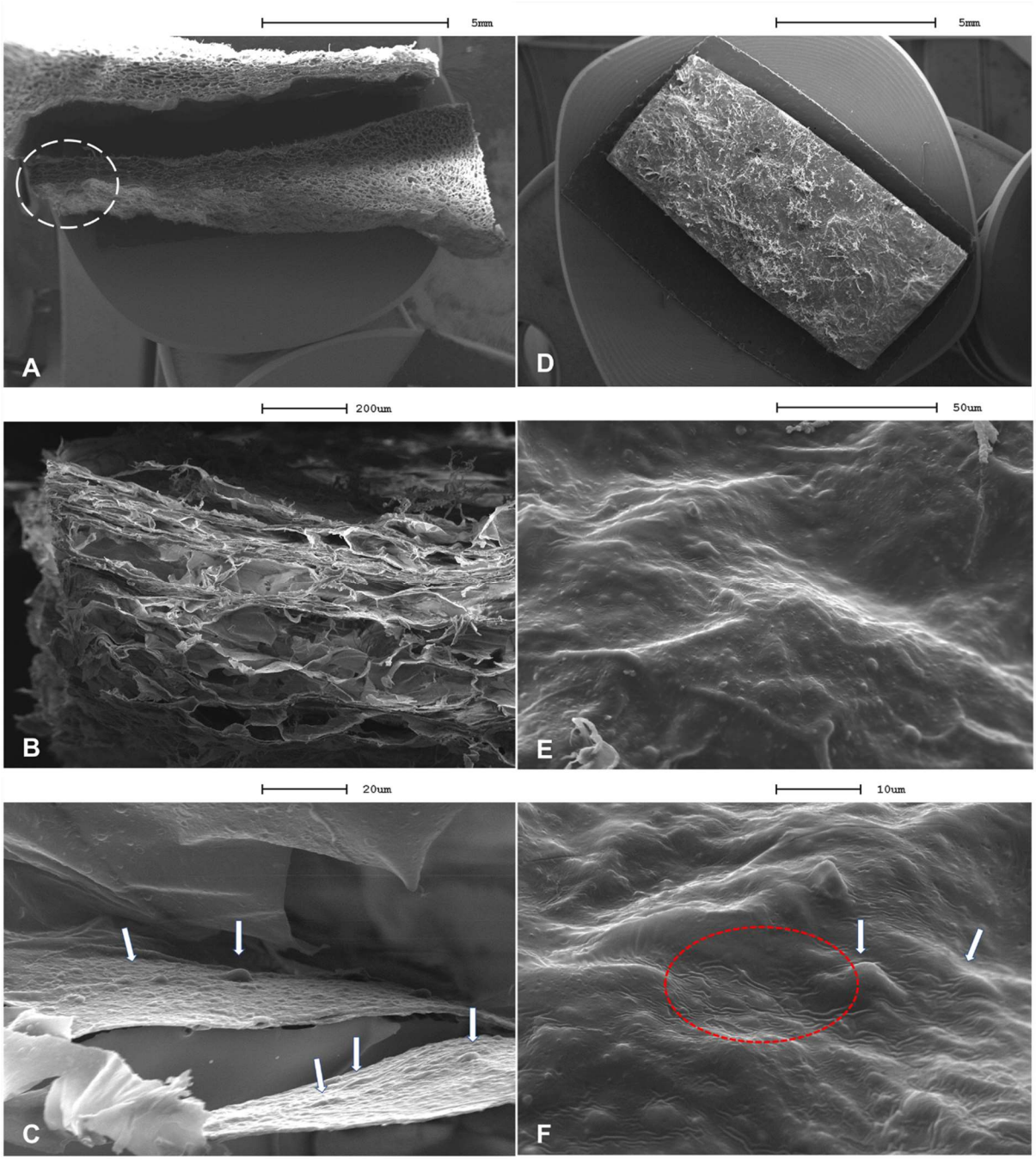

Figure 5. 17 SEM images of DHT-treated scaffold after NPWT application. A), D) Macroscopic views of cross-section and top surface, respectively. B), C) Different magnifications of cross-section edge and E), F) top surface with white arrows pointing at HDF.

Inevitably, the initial porous architecture resulted compressed in the middle part with limited presence of open pores (Figure 5.17 B) that were on the contrary almost intact at the edges. Likewise, the compression on top of the surface led to a rough and irregular collagen layer with absence of pores.

In addition, small ripples were noticed on the top surface (dashed red circle in Figure 5.17 F) probably connected to the delivery of negative pressure through the dressing. This

would imply the possibility to study the effect of micro-deformation on the morphology of fibroblasts cultured and integrated in a 3D scaffold. Indeed, studies showed that fibroblast can transduce mechanical forces into biomechanical signals utilizing differential gene expression and protein secretion [224, 227]. Other research studies [33, 79] found that cells respond differently to the characteristic of the materials used to apply negative pressure. Matrix remodelling by compression and traction has already been shown to be beneficial for cell proliferation of fibroblasts in collagen gels [228], since substrate stiffness as well as elasticity are important mechanical characteristics that determine cell fate. Similarly, it has already been theorized that microdeformation of skin structure caused by negative pressure application can promote cell proliferation through mechanotransduction pathways [229]. However, according to the literature review performed in this work, the application of therapeutical negative pressure to study fibroblast proliferation in a 3D collagen porous scaffold has not been tested yet.

In this study, collagen-based scaffolds have been shown to support cell growth and withstand negative pressure wound therapy application, suggesting a potential use of *in vitro* platforms as preclinical wound healing models. Also, the fact that the scaffolds remained wet throughout indicate that a fluid exudate-like removal would be possible in a clinical setting.

5.8 Summary

Given the fact that *in vitro* cell culture methods are accepted worldwide as a tool that could effectively contribute to further understanding cellular and molecular biology, this chapter describes the integration of fibroblasts in 3D porous collagen scaffolds that could potentially be used *in vitro* for the observation and study of cell development after NPWT application. In particular, it has been shown that a NPWT device can be directly applied on these scaffolds using a bioreactor system. Initially, cell culture experiments on collagen and polymer blended scaffolds of small size did not raise any concern as results were in line with expectations, demonstrating that GA vapour crosslinking can biologically be a valid alternative to the use of GA solution. However, DHT-treated scaffolds were chosen for the following experiments due to their better biocompatibility as a result of MTS test (Figure 5.2). Afterward, seeking to recreate a structure that could closely mimic the dermis, with an upper layer fibrous and well populated similar to the reticular layer and a more porous sublayer as papillary, the combination of methods described in Chapter 3 and

4 was attempted with controversial results due to possible delamination between the two layers and lack of response from cell viability assay. Further experiments confirmed and showed that using scaffolds four-fold bigger in diameter can represent a challenge when cell viability and proliferation are analysed through commercial standard cell assays. Therefore, optimization of cell viability assays for each individual material and size is required in future experiments in order to determine cell concentration. A list of potential solutions to solve common problems was presented in Table 5.1. The use of microscopic techniques such as SEM and fluorescence microscopy was selected as an alternative to colorimetric methods to examine the presence of cells in the scaffolds. Furthermore, they can give information about the spatial distribution and morphology of the cells. Although SEM analysis allowed to detect profiles that were interpreted as cells, the complex morphology of the sample will require further investigation to state unambiguously and determine the presence of cells in the scaffolds after NPWT treatment. Nevertheless, while fibroblasts profiles were recognised throughout the thickness of the collagen porous microstructure, it posed greater challenges to detect cells in scaffolds made of polymer blends. In addition, SEM images showed that these collagen porous structures can withstand negative pressure forces applied by a NPWT device for 24h, and that profiles linked to spread cells were still present in the structure. This work and system can be considered a starting point for studying the effect of NPWT on cell structures and eventually for examination of changes in the production of chemotactic signals. However, further studies are required to confirm and quantify the presence of cells after NPWT application on the scaffolds. Potentially, this bioreactor setup could also be used to investigate the effect of negative pressure on other cells and processes involved in wound healing such as endothelial cells for angiogenesis.

CHAPTER 6 General discussion

In skin tissue engineering, scaffolds can have a myriad of uses, from stimulating regeneration avoiding wound contraction to releasing therapeutical agents, biomedical signals as well as cell carriers [230]. In general, they function as three-dimensional templates for cell adhesion and proliferation with material, surface and mechanical properties to determine the modality of cellular interaction [231]. However, this concept of structure designed for cell growth, has evolved around the principle that scaffolds should be realized for the specific application. One of the main goals of this thesis was to establish reproducible laboratory methods to generate scaffolds that could mimic characteristics of the skin and could be utilized for wound healing studies withstanding the application of therapeutical negative pressure. Methods of fabrication were selected based on strategic choices with the objective to possibly reproduce and validate these predictive structures using industrial production processes. For these reasons, freeze-drying and electrospinning were employed to generate highly porous and fibrous scaffolds, respectively, with characteristics that could partly resemble the skin architecture and be functional for the final purpose. These structures were chemically and physically characterized and then morphological interaction with primary human fibroblast cells, isolated from skin specimens, was evaluated. Accumulating evidence shows that fibroblasts isolated from different tissues in the body are morphologically and functionally heterogeneous as a result of a "positional identity or memory" [69]. In some tissue engineering studies, referenced in this thesis, different immortalised cell line, derived from humans, animals or cancer have been used to investigate cell-material interactions. Although cell lines may retain stability in phenotype and function, they can suffer from dysfunctions such as adapted growth in culture, reduced cell-cell interaction and decreased protein secretion leading to a possible misinterpretation and variability of results. Consequently, in the development of clinically relevant *in vitro* models, cell choice is not negligible and as important as the material. Freeze dried scaffolds were initially analysed in this thesis as detailed in Chapter 3. The high porosity of these structures allowed cell distribution providing a suitable environment for fibroblast secretion of extra cellular matrix (ECM). In addition, fluid transport through the pores could supply cells with nutrients during cell culture and potentially simulate exudate in wound healing studies.

Collagen type I was the material of choice as it is the main component of the ECM in many human tissues and the most commonly used for engineered skin. Mainly attributed to their composition, collagen-based scaffolds have found success in several skin applications. However, the extraction and the source of collagen along with structural differences due to processing parameters can considerably influence cell response and structural outcome [232]. As reported in Section 3.3.3, it was also experienced that collagen varied from batch to batch, suggesting that viscosity or rheology studies should be always included in the fabrication of collagen-based scaffolds. Collagen was used on its own and blended with chitosan and polyvinyl alcohol (PVA) in ratio 9:1 searching for scaffolds with improved physical and mechanical properties comparing the three groups. Previous studies have already shown the potential of tailoring scaffold composition for tissue engineering applications using various collagen and chitosan ratio [6, 192] and collagen and PVA ratio [4, 8]. However, a systematic comparison of the two blends to understand and assess their influence in scaffold composition and the feasibility of their use in NPWT *in vitro* applications has not yet been reported. These biocompatible water-soluble materials could be added to the collagen-based solution without causing any material precipitation, thus allowing reproducible and controlled fabrication of a porous structure. On the contrary, when collagen solution is mixed with glycosaminoglycans (GAGs) to fabricate dermal template for skin regeneration, part of the product precipitates after centrifugation generating liquid-phase separation and discontinuity in the final structure (Figure 6.1).

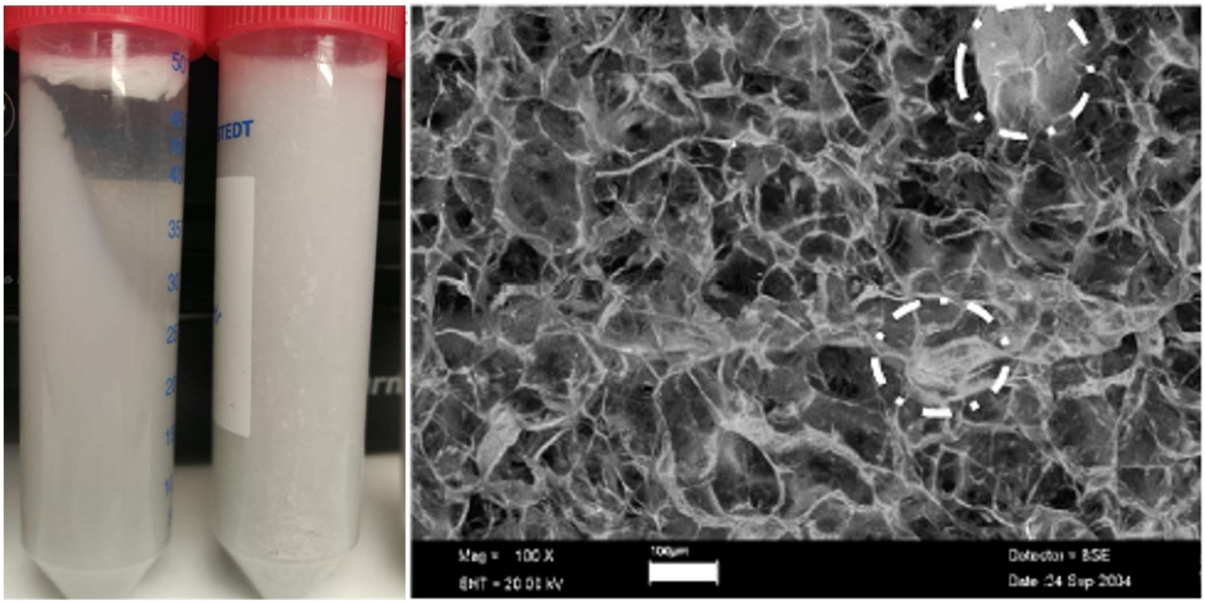

Figure 6. 1 A) Digital images of Collagen-GAG solution before (right) and after centrifugation (left). B) SEM images of Collagen-GAG with non-uniform solid content distribution, adapted from [233].

In addition to the possibility to strengthen mechanical properties, chitosan was added as a potential substitute of GAGs since it has been showed that the N-acetylglucosamine moiety in chitosan is structurally similar to GAGs [5]. Therefore, it could have added the same bioactivity and control hydration to the scaffold. On the other hand, PVA is often used in dressing for wound applications resulting in stiff foams in dry state but soft under wet conditions with liquid that plasticises the polymer backbone. PVA foams are used where rigidity is essential to maintain the form without compressing or collapsing under pressure [234]. These features together with the strong interactions with collagen at low PVA concentration [7] and high hydrophilicity made these scaffolds worth of being studied for negative pressure wound therapy (NPWT) applications. During freeze-dried porous scaffold fabrication, it was found that size and mould filling height cannot be overlooked along with the freezing process. The use of a temperature-controlled shelf was essential to determine the effect of freezing process on pore size as detailed in Sections 3.3.1 and 3.3.2. According to Clearfield and Wei [58], the use of a low shelf temperature (≤ 40° C) and suspensions with relative low pH (≤ 0.5M acetic acid) is effective in maintaining the product temperatures under glass transition temperature thereby preventing collapse. From pore size measurements, it was possible to suppose that the shelf freezing rate had a major impact on the average pore size compared to the final freezing temperature. As reported by O'Brien et al. [60] and showed in Figure 6.2, the

cellular structure of the scaffold produced at constant cooling rate (Figure 6.2 B) appears more homogeneous than the scaffold produced using fast freezing i.e quenching (Figure 6.2 A). To better understand the freezing dynamics of collagen slurries, a modulated differential scanning calorimetry analysis could also be performed.

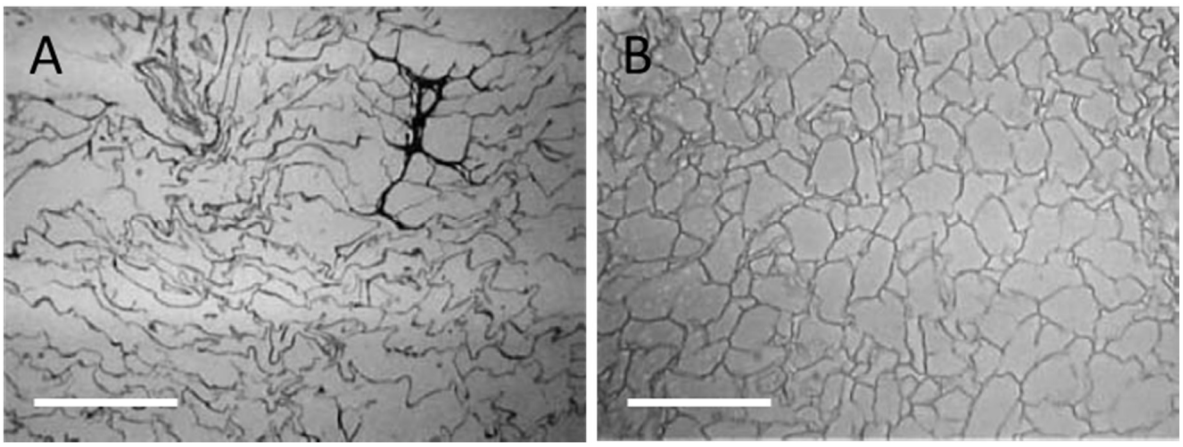

Figure 6. 2 Cross-section images of collagen scaffolds using quenching (A) and constant cooling rate (B), adapted from [60]. Scale bars =300 µm

Despite differences in viscoelastic behaviour of the blends, with collagen-chitosan exhibiting a more fluid-like performance while collagen-PVA a more solid-like (Section 3.3.3), pore size was limited to a range that was suitable for fibroblast seeding and culture. This appropriate range was also maintained after scaffolds crosslinking. DHT treatment was applied to all the scaffolds with the aim to provide a better stability in solution causing a minimum reduction in size. Further carbodiimide (EDC-NHS) and glutaraldehyde (GA) treatments reduced the scaffolds size and slightly modified the pore size. An increase in pore size was attributed to ice-induced damage during the second freeze-dried step, necessary to remove residual cross-linker, but also chemical modification could be accountable for that. Regarding GA vapour treatment, polymer blended scaffolds experienced a significant shrinkage in pore size that could be explained with long incubation time and high hydrophilicity. However, the determination of the exact pore size by analysis of SEM images might be inaccurate due to sample sectioning and handling, thus a comparison with a micro-computed tomography analysis and/or cryo-SEM could be helpful to confirm these results. Chemical characterization of the scaffolds showed an elevated degree of crosslinking demonstrating the effectiveness of the different treatments that translated into specific physical and mechanical properties. Contrarily to reports in literature [97], key measurements such as porosity and water uptake were measured based on

the percentage of increase in mass. Methods established on relative density or relative variation in mass were not considered useful for a proper interpretation of results. The approach taken, allowed the comparison of scaffolds properties based on several factors. The volume of water absorbed was dependent on the degree of hydrolysis and porosity for collagen and collagen-chitosan scaffolds while collagen-PVA showed a constant liquid uptake across all measurements indicating a possible correlation with the collagen/PVA ratio that composed the scaffold. Results showed in Section 3.3.6 of water uptake measurements suggested that DHT cross-linking can dramatically reduce the hydrophilicity of collagen-chitosan scaffolds making it almost comparable to the pure collagen structure. It would have been interesting to measure hydrolytic and enzymatic degradation of these scaffolds to further investigate the effectiveness of the various crosslinking methods. Experiments to test the porosity involved the application of vacuum that permitted the expansion of the structure and fluid entrance into the pores. During the evaluation of how vacuum forces affected the scaffolds, cryo-SEM analysis revealed that polymer blended structures under wet conditions behaved similarly to hydrogel (Figure 6.3) retaining a great amount of water, feature that was not expected based on SEM analysis and mechanical tests.

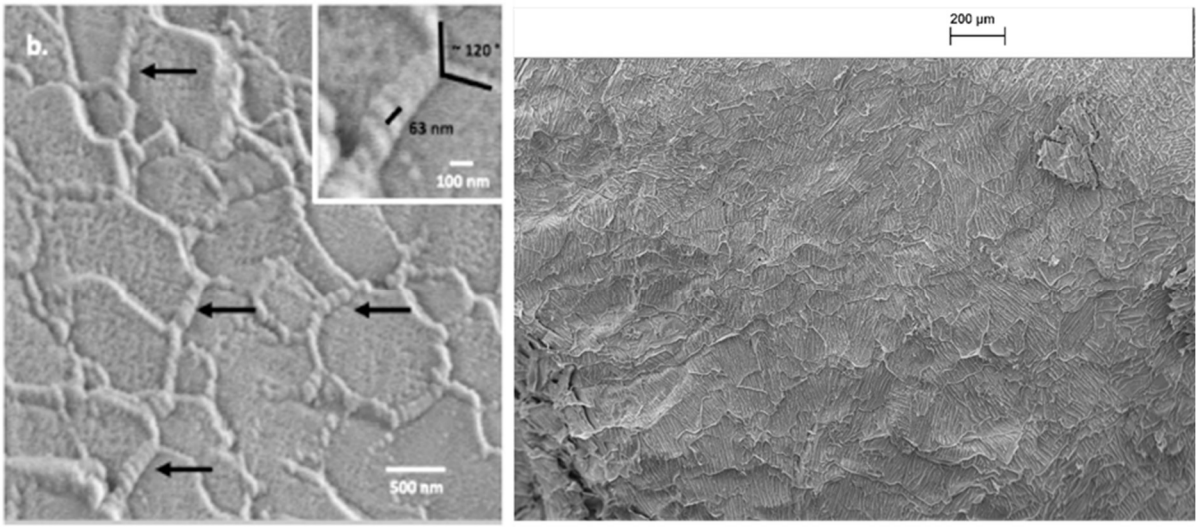

Figure 6. 3 Cryo-SEM pictures of A) 0.5 mg/ml gelatin hydrogel from [235] and B) Collagen-Chitosan 9:1 scaffold fabricated in this thesis with pores swollen by water phase.

Mechanical tensile tests of crosslinked scaffolds did not show any relevant improvement in properties compared to the non-crosslinked samples, and results discussed in Section 3.3.7 were in line with those reported in several research findings. It has to be said that matching the mechanical and physical properties of biological tissues is one of the obstacles in tissue

engineering that scientists have tried to overcome for decades with limited success. However, analysis of creep recovery in compression tests showed that GA treated scaffolds were able to recover to almost the initial thickness when a strain of 30% was applied, while the other crosslinked scaffolds experienced a certain level of permanent deformation. Whilst these results could suggest that GA scaffolds were more suitable for the thesis purpose, cell culture studies reported in Section 5.2 indicated that residual toxicity and increased stiffness may interfere with fibroblasts survival and proliferation. For these reasons, it was decided to use DHT-treated porous scaffolds as 3D structure to test negative pressure wound devices since cell survival was prioritized over mechanical properties. Although collagen sponges are well-established materials and have been used as dermal substitutes they are considered "pseudo-3D culture platform". As a consequence of large pore size, cells mostly grow with a pattern similar to that on 2D surfaces. Electrospinning was a technique that would have provided the possibility to fabricate cues acting in all three directions, comparable to the ECM.

In Chapter 4, electrospun mats were fabricated using a less explored collector in the search of a more homogeneous and well distributed pattern with increased pore size. As the thickness of electrospun scaffolds is limited to hundreds of micrometres, a combination with the porous scaffolds was a promising research concept to develop 3D tissue models. The electrospinning market is extensively growing and the aim of finding sustainable solutions to fabricate medical devices, is drawing particular attention to the use of water/weak acid soluble biomaterials. There is an urgent interest in replacing highly toxic solvents with relatively environment-friendly solvents to industrialize the electrospinning process, especially in the biomedical field for applications such as wound healing, drug release, and tissue engineering. In many studies [236], chitosan (CT) has been used as an alternative substrate to collagen in artificial skin models. In this work, it was combined to biocompatible materials such as polyethylene oxide (PEO) and polycaprolactone (PCL) to facilitate its spinnability and increase mechanical properties. Mats were successfully obtained with static and rotating configuration. Through image analysis, average fibre diameters were measured, and mats categorized in nano and micro scaffolds. There was a substantial difference between PEO-CT and PCL mats not only in terms of size but also in fibre organization. Although it was shown that using the developed rotating collector, fibres could be aligned at rotational speed as low as 500 rpm, the two scaffolds were revealed to have different patterns (Figure 6.4).

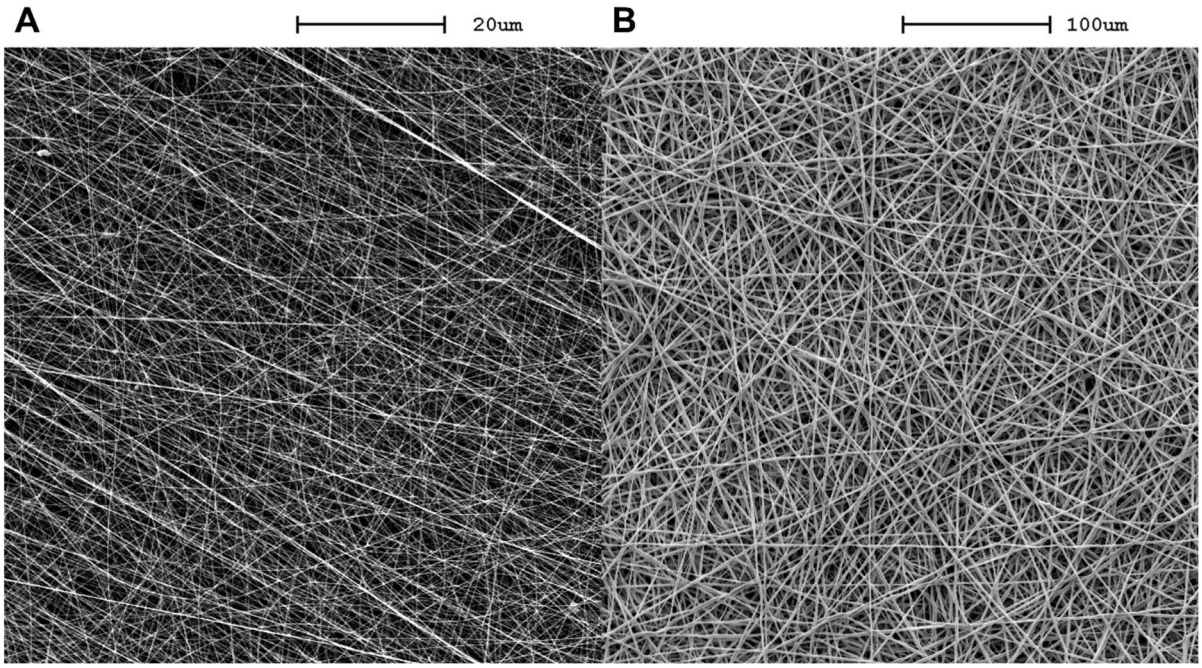

Figure 6. 4 SEM images A) PEO-CT nanofibres and B) PCL microfibres collected on rotating disk.

While PEO-Chitosan showed nanofibres aligned in a specific direction that was more evident with higher speed and at increased distances from the disk center, PCL microfibres had a bimodal distribution that allowed greater pore size and less fibre agglomeration. Most studies carried out using drum collectors showed aligned fibres tightly packed with absence of spacing between them (Figure 6.5). This particular and innovative configuration has demonstrated not only an improvement in mechanical properties of the scaffolds and a reduction in fibre diameter, but it has also provided spacing between the aligned fibres.

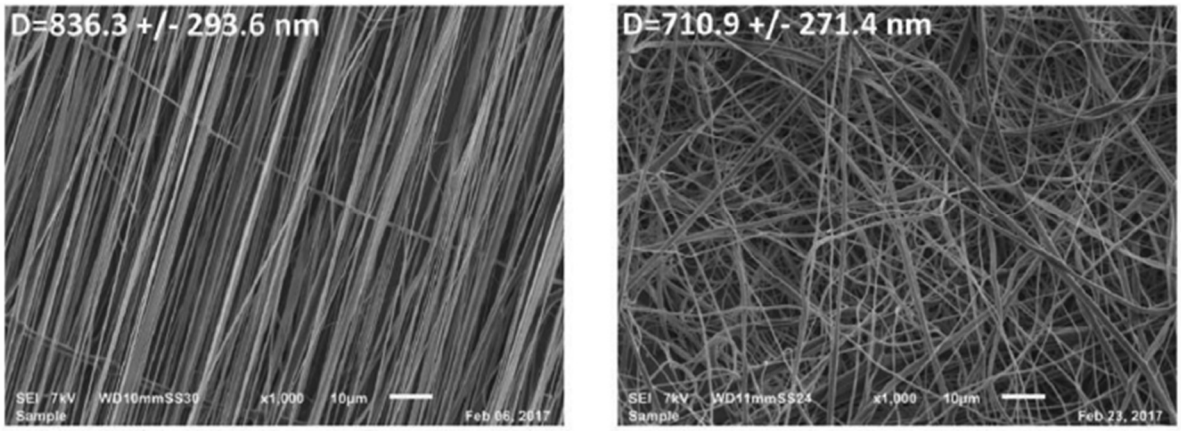

Figure 6. 5 Aligned by drum collector and random electrospun PCL fibres. Adapted from [237]. Scale bars = 10 µm

A distribution study with fibre diameters in the range of ~400-700 μm could potentially be explored to understand the reproducibility of this novel pattern. The result was attributed to the combination of electrostatic forces that accumulated on the fibres and to the rotational movement of the collector. However, the combination of these two phenomena was unexpectedly observed only on PCL mats presumably because bigger fibres retained higher electrostatic forces. Further demonstration of this hypothesis was given by contact angle analysis in Section 4.7.3 which surprisingly showed 25% lower contact angle values than measurements found in literature. The possibility to obtain membranes more hydrophilic by means of a simple collector could open opportunities in several fields since this technology does not alter any of the fundamental variables of electrospinning and can be apply to a wide range of polymers. In addition, mechanical tests showed tensile strength and modulus well within the range of human skin for PEO-CT while PCL mats had 10-fold lower elastic modulus. These results suggest that an appropriate polymers combination such as PCL-CT could be ideal to match skin properties as fibres size for PEO-CT were not suitable for fibroblast proliferation. Generally, fibres of electrospun scaffolds are deposited in the x and y-planes with virtually no fibres oriented across the z-direction. In this respect, the use of other techniques, in addition to the rotating collector, can be applied to increase the void space.

Many approaches can be taken to face this problem from the use of low temperature electrospinning and ultrasonication to dual electrospinning [238]. As reported by ATR-FTIR analysis in Section 4.7.2 PEO can be easily washed away by ethanol/water rinsing so that simultaneous spinning of PEO and another solution might intertwine fibres and be beneficial to create structure with high porosity and void space between layers. Electrospinning can be considered a precursor of 3D printing in which operators can commonly adapt the setup but have limited and challenging control on the final structure. During this study, it was also experienced that reproducible results cannot easily be obtained as too many factors negatively influenced the spinnability process with temperature of the solution and chamber humidity that were found to be critical for reproducibility. Furthermore, a key consideration in electrospinning for cell applications is the duration of spinning. Based on fibre diameter, the electrospinning period can affect pore size and scaffold thickness that consequently will impact cell infiltration and behaviour. To understand skin cells interaction within three-dimensional architecture in the context of the specific structure, fibroblasts were cultured on PEO-CT, PCL and freeze-dried scaffolds. Pore size and fibre diameter had a significant influence on the ability of the cells to infiltrate into the scaffolds. On PEO-CT,

fibroblasts maintained a rounded shape after 3 days in culture but attached well to the surface while PCL showed actin filaments engaged to different fibres with pore size that appeared to be suitable for cell infiltration into the structure. These results also proposed that electrospinning studies should not only focus on mimicking the fibre size of native tissues but rather direct the attention on obtaining pores broader than the cell size of interest. Although, cell studies over a longer period are needed to address cell growth and proliferation, it can be said that PEO-CT membranes could be used for cell attachment and as bacterial barrier for wound healing applications rather than 3D tissue structures. Histological haematoxylin and eosin staining, along micro-CT analysis of scaffolds could be useful to determine how deep cells infiltrated in PCL membranes obtained in random and rotating configuration and to evaluate differences in porosity. On the other hand, the analysis of cell morphology and proliferation on freeze-dried scaffolds resulted to be more complicated particularly in the attempt to upscale the size of the scaffolds. Analysis of cellular activity within the scaffolds produced good results in terms of cytoskeleton protrusions and survival rate. Even though, glycine rinsing might have been utilized to remove GA traces from the scaffolds, GA vapour treatment revealed to be advantageous over GA solution providing the same mechanical properties and ensuring cell survival. Yet, these scaffolds showed lower cell proliferation then the other crosslinking methods. During crosslinking, incubation time may have little effect on material stiffness that mostly depends on polymer concentration, but rather crosslinking change the inner structure and hydration that can interfere with cells interaction since adhesion and proliferation depends on surface characteristics such as chemistry, wettability, and topography. Microscopic inspections helped in the analysis of morphological differences between cells cultured on porous and fibrous scaffolds. It was found that fibroblasts can take longer to spread out on collagen struts compared to PCL fibrous matrices. Cells with rounded morphology could be easily seen and those may indicate a reduced interaction between cells and topographic features as well as they may need longer period of incubation to grow and adapt to a substrate that differ from a plastic layer. Eventually, the aim would be to image cells that are well-spread and integrated on the structure, able to synthesize collagen and proliferate. Even though SEM analysis allowed to identify cells across all the structure, imaging was laborious for lack of contrast and uneven surfaces that made focusing on various depths particularly challenging. As remarked for fibrous scaffolds, a haematoxylin and eosin staining (Figure 6.6) would be suitable to image cell distribution within the scaffolds. Based on the expertise acquired, this method would be

the most reliable for analysis of collagen porous sponge, since confocal images can only reach few hundred micrometres in depth. However, these scaffolds turned out to be quite fragile when sliced by means of a microtome. In this study, wax embedding was unsuccessful as the porous structure crumbled apart when sliced, while cryo-sectioning could work only if vacuum is used to fill up inner pores of the structure with medium before cell culture.

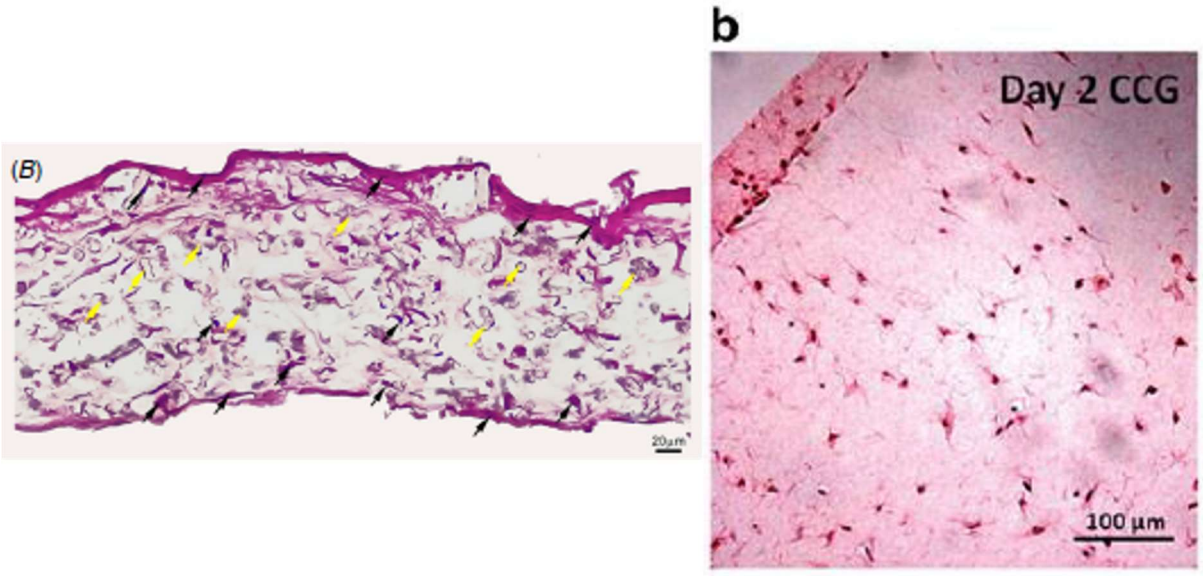

Figure 6. 6 Haematoxylin and eosin staining of cross-sections of PCL electrospun membranes [239] (left) and collagen porous matrix [240] (right) cultured with fibroblasts.

Fibrous and porous scaffolds were identified as possible 3D models designed to mimic native tissue and targeted for Negative Pressure Wound Therapy (NPWT) investigation. Since one of the limitations of electrospinning is the difficulty in building up scaffold thickness, a combination of electrospun matrices and freeze-drying porous scaffolds was explored to make use of the advantages offered by both techniques and serve the purpose. The process of electrospinning on porous structure was straightforward but doubts were raised about attachment of the fibrous structure on the upper porous surface upon application of cutting forces by scalpel. Potential solution for stronger attachment could be the application of a thin layer of gelatine right before the electrospinning process that will perhaps allow fibres to be better integrated. Further development of this structure was limited by issues encountered during cell culture that involved the use of colorimetric assays to evaluate cell viability on scaffolds. Scaling up cell culture means that cell growth should remain consistent as the size of the scaffold increases. Regrettably, many issues were discovered along the process that did not make possible to determine viability nor to

track cell proliferation at various time points. Potential causes and solutions were identified but the timeline did not permit optimization of the process. Since collagen scaffolds were the only samples to show decent viability, they were selected to be tested under negative pressure. For this specific intent, a custom-made bioreactor chamber was designed and fabricated to experiment and support what at the beginning was a research idea as detailed in Section 5.5. It was made of polycarbonate to facilitate the attachment of NPWT device adhesive layers, for ease to be sterilized and because of the possibility to embed fluid channels into the structure. While the use of polydimethylsiloxane is not recommended on studies of this scale, it could be integrated in the system as scaffold support. Even if the fluid flow was maintained as low as possible, a preliminary study showed diffusion of fluid inside the collagen scaffolds after 24h (Figure 6.7).

Figure 6. 7 Digital image of 24h preliminary experiment to assess fluid diffusion in collagen scaffolds.

This would suggest that mechanical stimuli were applied to some extent to the cells by the medium along with the negative pressure. Due to dressing saturation the experiment was stopped after 24h leading to some reflections to be made. Firstly, it is suggested not to run the experiment in triplicates or considering the likely possibility that dressing needs to be changed regularly. Secondly, if compatible with tube fittings and manufacturing process, channels diameter should be smaller in size to meet a low exudate rate. Lastly, as the dressing is designed to absorb exudate, it is recommended to use a medium with higher

viscosity. Finally, this work highlighted the feasibility to apply therapeutical NPWT to tissue engineered scaffolds for the first time. It has to be specified that with the term "therapeutical" is intended the application of NPWT as a whole, in which dressing and pressure are combined to produce deformations to the tissue on micro and macro scales. As a matter of fact, these forces contribute to the acceleration of wound healing under NPWT. SEM analysis showed that DHT scaffolds can tolerate the treatment and interconnection of pores can still be observed after permanent deformation of the scaffolds that was partly anticipated by compression tests. While studies have showed that collagen scaffolds with average pores size of 150 μm have high fluid permeability even when compressive strain are applied [241], fluid transport and diffusion on the resulted structure should be investigated since they have influence on cellular survival and degradation of the scaffold. Nevertheless, this work has demonstrated the possibility to transfer mechanical signals from an external environment to the cells via the scaffolds and that a series of structure variants such as electrospun mats could also be studied to gain knowledge about the effects of NPWT on skin cells.

CHAPTER 7 Conclusions and future directions

7.1 Summary

In this thesis, models of engineered skin that hold specific features were fabricated using conventional and advanced techniques and materials that are cost effective and largely used in industry with the aim to translate this research into an industrial application for research and development purposes. The work was focused on optimizing the fabrication process, improving scaffold properties and understanding the influence of scaffold architecture on cellular function and behaviour. In addition, a proof-of-concept bioreactor system was developed to provide NPWT forces on porous scaffolds. Previous NPWT *in vitro* studies presented limitations with regard to application of negative pressure and the use of small-scale skin equivalents or artificial skin that were not specifically designed for this purpose. This work explored the possibility to create reproducible and durable scaffolds that could withstand high stresses and in which cells could easily infiltrate and be adherent to the substrate. In this way, cells can experience the same level of stretch and forces sensed *in vivo*.

In Chapter 3, the fabrication of highly porous collagen-based scaffolds using a freeze-drying method resulted in a homogeneous pore structure suitable to host skin cells. Results showed that blending water-soluble components i.e., chitosan and PVA in the collagen dispersion before freeze-drying affected the physical of the scaffolds while minimally altering the morphology and mechanical properties. Addition of limited amounts of these materials resulted in scaffolds that could retain amounts of water 6 times higher than those made of pure collagen. However, after cross-linking treatments, water retention capacity of blended collagen scaffolds diminished drastically for CL-CT varying with cross-linking method while a small decrease of around 10% was measured for CL-PVA independently of the treatment. These results may imply that PVA interact strongly with collagen during mechanical blending resulting in a material with innovative physical properties. On the other hand, crosslinked CL-PVA scaffolds showed mechanical properties similar to collagen scaffolds when tested in dry conditions and slightly inferior in hydrated state. This finding further suggests that PVA do not prevent cross-linking agents to react with amino acid residues of collagen, but due to its fluid retention capacity the rigidity of the scaffold can increase when hydrated. On the contrary, elastic modulus of CL-CT scaffolds

in hydrated state was higher than CL and CL-PVA across all the groups. These results confirmed that addition of chitosan in collagen blends can enhance scaffold elasticity. With respect to the proposed application, GA treatments, either in solution or through vapour phase, allowed to obtain scaffolds that showed high compression strength and almost total recoverable elastic deformation for all types. Although, these scaffolds had superior mechanical properties, low fibroblast viability was assessed in cell culture studies possibly attributable to the presence of toxic GA residual in the structure.

While a porous structure was chosen to meet biological and mass transport needs, fibrous scaffolds were designed to match skin mechanical properties and architecture. With the aim to improve the complexity of the skin model and to produce fibrous structures that better resemble the native tissue, in Chapter 4 a planar rotating disk was designed and used to collect fibres in the electrospinning process. This configuration had an impact on the membrane morphology that resulted to be mainly orientated in the direction of spinning for PEO-CT fibres with diameters smaller than 200 nm. On the contrary, the use of the developed collector during electrospinning of PCL dissolved in GAA produced fibres with diameters of around 1 μm that were arranged in a cross-aligned morphology. Further investigation demonstrated an improved hydrophilicity of these scaffolds that could potentially increase passive cellular infiltration. These results confirmed that interactions between material, solvent and system could lead to the development of membranes with unique properties that are not yet reported in research. Furthermore, these PCL membranes showed excellent fibroblast proliferation contrarily to PEO-CT membranes that appeared to inhibit the growth of fibroblasts. Cells formed cellular spheroids and cellular agglomerates although attached to the substrate. This behaviour can be ascribed to the composition of the membranes that after dissolution of PEO in solution were made of pure chitosan. The combination of the freeze-dried and electrospun scaffolds with the aim to realize a bilayer structure that could better mimic the skin was investigated in Chapter 5. Experiments led to the understanding of complications in obtaining the final structure and related problems in scaling up the scaffold size that have not been addressed in existing studies. For instance, the weak interaction between the two structures was attributed to the different nature and physical characteristics of the polymers. Also, lack of standardisation and dosage of assay reagents to test cell viability led to questionable results due to absence of colour change or interaction with the scaffold material. Considerations and consequential solutions were proposed in Table 5.1 with the aim to improve the reproducibility of these methods. Furthermore, a basic bioreactor was successfully

developed and was found to be capable of delivering NPWT under physiologically relevant conditions to study cell behaviour in *in vitro* investigation.

7.2 Conclusions

The central theme of this thesis was to advance the understanding of Negative Pressure Wound Therapy (NPWT) mechanisms by developing bioartificial scaffolds with improved properties that could be used as skin models in bioreactor systems designed for NPWT device studies. By replicating therapeutical conditions as closely as possible and providing a more accurate representation of cellular behaviour, researchers will be able to investigate and understand the mode of action of differing NPWT technologies limiting the need of *in vivo* testing.

This study contributed to new knowledge providing insights in the area of scaffolds for skin engineering *in vitro* applications. The investigation of the freeze-drying technique demonstrated that blending water-soluble components with collagen in 1:9 ratio did not change the main scaffold structure, which was mostly driven by the viscosity of the solution and parameters of the freeze-drying process. On the other hand, material blending affected physical and mechanical scaffold properties as well as the response of cultured fibroblasts. Those properties could be further altered by crosslinking methods. In this respect, results from this work led to the conclusion that dehydrothermal crosslinking is the most suitable method for this specific application, leading to an overall higher cell survival rate compared to the other crosslinking methods. Furthermore, although chitosan has been employed in many skin tissue engineering applications, its use in combination with collagen resulted to be impractical in this work and inferior to PVA as shown by cell culture results reported in Chapter 5, due to reduced cell viability.

Similarly, the use of electrospinning with a novel rotating collector enabled the creation of fibrous scaffolds and provided critical insights into the behaviour of fibroblasts in response to the unique scaffold microenvironment. Particularly, the use of PCL in Glacial Acetic Acid (GAA) solution, that was confirmed to be successful only for specific polymer concentration as described in literature, led to a bimodal fibre distribution not previously reported in other studies. The formation of this structure was attributed to the rotating collector and its interaction with the polymer solution that allowed a better distribution of the fibres modifying their density and orientation. This finding suggests that cellular infiltration of electrospun membranes could be enhanced without applying physical

manipulation or combining other techniques. It was discovered during evaluation of cell interaction and viability that fibroblasts were well spread and could infiltrate into the scaffold showing that pore size and fibre diameter of around 1 μm are crucial features for fibroblast attachment and proliferation. In fact, the use of Chitosan-PEO resulted in membranes with fibre-packed surface that prevented cell ingrowth and promoted only formation of focal adhesion and cluster of cells. These results contribute to the understanding of the effect of fibre diameter on skin cells growth suggesting that electrospinning fibres with diameter below 200 μm are not suitable for human dermal fibroblast proliferation and infiltration.

Moreover, one of the key contributions of this research lies in the development of a proof-of-concept bioreactor system specifically designed for NPWT investigations, introducing a novel approach. This bioreactor enabled the application of negative pressure forces on scaffolds, simulating the conditions of NPWT. The study showed the feasibility of investigating human dermal fibroblast survival, proliferation and morphological changes by subjecting the dehydrothermally treated collagen scaffold to such forces. The integrity of the porous scaffold after application of such therapy was confirmed by microscopy analysis.

Overall, this thesis provides a comprehensive investigation of the intricate interplay between scaffold architecture, cellular behaviour, and therapeutic NPWT. The fabrication of innovative 3D skin models, the thorough evaluation of their properties, and the successful development of a bioreactor system for NPWT investigations collectively underline the potential of this research and lay a foundation for further advancement in bioartificial scaffold design with the ultimate goal of studying negative pressure wound therapy in a controlled and reproducible environment.

7.3 Future work

Promising findings were obtained in this work, but further research is undoubtedly needed to solve experimental problems and confirm and ameliorate the results.

With regards to collagen-based porous scaffolds, future work would be focused on (i) analysing more in detail the permeability and fluid-exchange of collagen-based scaffold with particular interest in collagen-PVA that showed to have unique capacity of fluid retention; (ii) standardizing a protocol for cell viability assays based on the size and dye-material interaction of these scaffolds or using other proposed methods such as separation

of cells from materials; (iii) extending cell culture incubation time. Since a scaffold can be considered physiologically relevant if it contains 'mature' cells, analysis of change in cell morphology and long-term viability are crucial; (iv) allowing fibroblast interaction with keratinocytes, endothelial and inflammatory cells that have important roles in the wound healing process. The outcome of this research also recommends future continuation of the work on the electrospun membranes obtained with the rotating collector. Firstly, it will be necessary to investigate the effectiveness of the fibre alignment method for other blends such as PCL-Chitosan or PCL-gelatin, targeting specific fibre diameter ranges suitable for human dermal fibroblasts. Secondly, further analysis of cell infiltration and consequent comparison with random and drum-aligned membranes will demonstrate the preliminary results of this study and help to advance the production of electrospun products that are speedily growing in industry. To achieve this objective, the new developed collector system should be integrated in a fully automated and standardized process in which control over environmental and process parameters will diminish variability and increase reproducibility. Lastly, additional use of these membranes in wound healing applications such as for antibacterial purposes should be explored with particular attention to liquid permeability / vapor evaporation and degradation of nanofiber structures.

Meanwhile, bonding between the porous structure and electrospun layers should be improved in order to produce a uniform and complex 3D model of skin in which the upper electrospun layer provides mechanical support while the lower, more porous substrate is designed to facilitate cell and fluid infiltration. Measurements of delamination forces and attempts to strengthen the link between the layers could be investigated. Applying an adhesive layer on the porous surface exposed to electrospinning process could be a valid solution in order to obtain a bilayer scaffold. Nevertheless, these developed bioartificial scaffolds were designed to be coupled with a bioreactor to study therapeutical Negative Pressure and consequent mechano-transduction response of cells, in particular of fibroblasts that is the most mechanoresponsive skin cell population. Future work would be directed in the optimization of this testing platform. Several ideas can be applied and integrated:

I. measurements of the optimal flow rate and dressing uptake to perform continuous experiments over 3-4 days without interrupting the experiment
II. use of sensors to control pressure around the structure and fluid flow in inlet and outlet. Even though fluid rate can be set up on the peristaltic pump, drawing forces

from the negative pressure devices could influence the amount of medium that circulate in the system

III. use of soft material such as polydimethylsiloxane (PDMS) to host the scaffold and mimic the mechanical properties of tissues such as adipose tissue that is connected with the dermis.

Eventually this *in vitro* system will allow to study and investigate the cause-effect relationship between mechanical signals from NPWT and biological outcomes. Furthermore, the bioreactor could be utilized to compare and characterize diverse types of skin substitutes for skin tissue engineering applications. Once again it must be acknowledged that engineered tissue integrated in a testing platform is a model of complex living system and beyond these studies there are bound to be limitations. However, the methodology described in this thesis that led to the development of an *in vitro* testing platform could be implemented in order to help and forward the development of NPWT devices.

References

[1] A. C. Panayi, T. Leavitt, and D. P. Orgill, "Evidence based review of negative pressure wound therapy," *World Journal of Dermatology*, vol. 6, no. 1, p. 1, 2017, doi: 10.5314/wjd.v6.i1.1.

[2] A. Sionkowska, "Current research on the blends of natural and synthetic polymers as new biomaterials: Review," *Progress in Polymer Science (Oxford)*, vol. 36, no. 9, pp. 1254–1276, 2011, doi: 10.1016/j.progpolymsci.2011.05.003.

[3] B. Chevallay and D. Herbage, "Collagen-based biomaterials as 3D scaffold for cell cultures: applications for tissue engineering and gene therapy," *Med Biol Eng Comput*, vol. 38, no. 2, pp. 211–218, Mar. 2000, doi: 10.1007/BF02344779.

[4] Z. Peng, Z. Li, F. Zhang, and X. Peng, "Preparation and Properties of Polyvinyl Alcohol/Collagen Hydrogel," *Journal of Macromolecular Science, Part B*, vol. 51, no. 10, pp. 1934–1941, Oct. 2012, doi: 10.1080/00222348.2012.660060.

[5] O. A. Romanova *et al.*, "Chitosan as a Modifying Component of Artificial Scaffold for Human Skin Tissue Engineering," *Bull Exp Biol Med*, vol. 159, no. 4, pp. 557–566, Aug. 2015, doi: 10.1007/s10517-015-3014-6.

[6] C. Tangsadthakun *et al.*, "The influence of molecular weight of chitosan on the physical and biological properties of collagen/chitosan scaffolds," *J Biomater Sci Polym Ed*, vol. 18, no. 2, pp. 147–163, Jan. 2007, doi: 10.1163/156856207779116694.

[7] N. Barbani, M. G. Cascone, P. Giusti, L. Lazzeri, G. Polacco, and G. Pizzirani, "Bioartificial materials based on collagen: 2. Mixtures of soluble collagen and poly(vinylalcohol) cross-linked with gaseous glutaraldehyde," *J Biomater Sci Polym Ed*, vol. 7, no. 6, pp. 471–484, Jan. 1996, doi: 10.1163/156856295X00544.

[8] G. Lai, Z. Du, and G. Li, "The rheological behavior of collagen dispersion/poly (vinyl alcohol) blends," *Korea Australia Rheology Journal*, vol. 19, no. 2, pp. 81–88, 2007.

[9] S. M. Choi, D. Singh, A. Kumar, T. H. Oh, Y. W. Cho, and S. S. Han, "Porous Three-Dimensional PVA/Gelatin Sponge for Skin Tissue Engineering," *Int J Polym Mater*, vol. 62, no. 7, pp. 384–389, Mar. 2013, doi: 10.1080/00914037.2012.710862.

[10] N. Reddy, R. Reddy, and Q. Jiang, “Crosslinking biopolymers for biomedical applications,” *Trends Biotechnol*, pp. 1–8, 2015, doi: 10.1016/j.tibtech.2015.03.008.

[11] T. Prasad, E. A. Shabeena, D. Vinod, T. V. Kumary, and P. R. Anil Kumar, “Characterization and in vitro evaluation of electrospun chitosan/polycaprolactone blend fibrous mat for skin tissue engineering,” *J Mater Sci Mater Med*, vol. 26, no. 1, pp. 1–13, 2015, doi: 10.1007/s10856-014-5352-8.

[12] Y.-H. Nien, J.-Y. Wang, and Y.-S. Tsai, “The preparation and characterization of highly aligned poly(epsilon-caprolactone)/poly ethylene oxide/chitosan ultrafine fiber for the application to tissue scaffold.,” *J Nanosci Nanotechnol*, vol. 13, no. 7, pp. 4703–7, Jul. 2013, doi: 10.1166/jnn.2013.7199.

[13] A. J. Banes, J. Gilbert, D. Taylor, and O. Monbureau, “A new vacuum-operated stress-providing instrument that applies static or variable duration cyclic tension or compression to cells in vitro,” *J Cell Sci*, vol. 75, no. 1, pp. 35–42, Apr. 1985, doi: 10.1242/jcs.75.1.35.

[14] R. P. Wilkes, A. K. McNulty, T. D. Feeley, M. A. Schmidt, and K. Kieswetter, “Bioreactor for Application of Subatmospheric Pressure to Three-Dimensional Cell Culture,” *Tissue Eng*, vol. 13, no. 12, pp. 3003–3010, Dec. 2007, doi: 10.1089/ten.2007.0036.

[15] S. MacNeil, “Biomaterials for tissue engineering of skin,” *Materials Today*, vol. 11, no. 5, pp. 26–35, 2008, doi: 10.1016/S1369-7021(08)70087-7.

[16] M. Pawlaczyk, M. Lelonkiewicz, and M. Wieczorowski, “Age-dependent biomechanical properties of the skin,” *Advances in Dermatology and Allergology*, vol. 5, no. 5, pp. 302–306, 2013, doi: 10.5114/pdia.2013.38359.

[17] C. Schulze *et al.*, “Stiffening of Human Skin Fibroblasts with Age,” *Clin Plast Surg*, vol. 39, no. 1, pp. 9–20, Jan. 2012, doi: 10.1016/j.cps.2011.09.008.

[18] A. V. Rawlings, “Ethnic skin types: are there differences in skin structure and function?1,” *Int J Cosmet Sci*, vol. 28, no. 2, pp. 79–93, Apr. 2006, doi: 10.1111/j.1467-2494.2006.00302.x.

[19] R. Wong, S. Geyer, W. Weninger, J.-C. Guimberteau, and J. K. Wong, “The dynamic anatomy and patterning of skin.,” *Exp Dermatol*, vol. 25, no. 2, pp. 92–8, Feb. 2016, doi: 10.1111/exd.12832.

[20] M. D. Ridge and V. Wright, “Mechanical properties of skin: a bioengineering study of skin structure.,” *J Appl Physiol*, vol. 21, no. 5, pp. 1602–6, Sep. 1966, doi: 10.1152/jappl.1966.21.5.1602.

[21] F. H. Silver, J. W. Freeman, and D. DeVore, “Viscoelastic properties of human skin and processed dermis.,” *Skin Res Technol*, vol. 7, no. 1, pp. 18–23, Feb. 2001, doi: 10.1034/j.1600-0846.2001.007001018.x.

[22] H. Joodaki and M. B. Panzer, “Skin mechanical properties and modeling: A review.,” *Proc Inst Mech Eng H*, vol. 232, no. 4, pp. 323–343, Apr. 2018, doi: 10.1177/0954411918759801.

[23] S. Avril and S. Evans, *Material Parameter Identification and Inverse Problems in Soft Tissue Biomechanics*. in CISM International Centre for Mechanical Sciences. Cham: Springer International Publishing, 2017. doi: 10.1007/978-3-319-45071-1.

[24] M. Meyer, “Processing of collagen based biomaterials and the resulting materials properties,” *Biomed Eng Online*, vol. 18, no. 1, p. 24, Dec. 2019, doi: 10.1186/s12938-019-0647-0.

[25] M. Ottenio, D. Tran, A. Ní Annaidh, M. D. Gilchrist, and K. Bruyère, “Strain rate and anisotropy effects on the tensile failure characteristics of human skin,” *J Mech Behav Biomed Mater*, vol. 41, pp. 241–250, Jan. 2015, doi: 10.1016/j.jmbbm.2014.10.006.

[26] W. Paul and C. P. Sharma, *Advances in Wound Healing Materials : Science and Skin Engineering*, no. June. 2015.

[27] C. Huang, T. Leavitt, L. R. Bayer, and D. P. Orgill, “Effect of negative pressure wound therapy on wound healing,” *Curr Probl Surg*, vol. 51, no. 7, pp. 301–331, Jul. 2014, doi: 10.1067/j.cpsurg.2014.04.001.

[28] O. Borgquist, R. Ingemansson, and M. Malmsjö, “The influence of low and high pressure levels during negative-pressure wound therapy on wound contraction and fluid evacuation.,” *Plast Reconstr Surg*, vol. 127, no. 2, pp. 551–559, Feb. 2011, doi: 10.1097/PRS.0b013e3181fed52a.

[29] T. Isago, M. Nozaki, Y. Kikuchi, T. Honda, and H. Nakazawa, “Effects of Different Negative Pressures on Reduction of Wounds in Negative Pressure Dressings,” *J Dermatol*, vol. 30, no. 8, pp. 596–601, Aug. 2003, doi: 10.1111/j.1346-8138.2003.tb00441.x.

[30] Xia, C. Y., Yu, A. X., Qi, B., Zhou, M., Li, Z. H., & Wang, W. Y., “Analysis of blood flow and local expression of angiogenesis-associated growth factors in

infected wounds treated with negative pressure wound therapy," *Mol Med Rep*, vol. 9, no. 5, pp. 1749–1754, May 2014, doi: 10.3892/mmr.2014.1997.

[31] S. Lalezari *et al.*, "Deconstructing negative pressure wound therapy," *Int Wound J*, vol. 14, no. 4, pp. 649–657, Aug. 2017, doi: 10.1111/iwj.12658.

[32] M. Malmsjö and R. Ingemansson, "Effects of green foam, black foam and gauze on contraction, blood flow and pressure delivery to the wound bed in negative pressure wound therapy," *Journal of Plastic, Reconstructive & Aesthetic Surgery*, vol. 64, no. 12, pp. e289–e296, Dec. 2011, doi: 10.1016/j.bjps.2011.06.023.

[33] R. Wilkes, Y. Zhao, K. Kieswetter, and B. Haridas, "Effects of Dressing Type on 3D Tissue Microdeformations During Negative Pressure Wound Therapy: A Computational Study," *J Biomech Eng*, vol. 131, no. 3, p. 031012, Mar. 2009, doi: 10.1115/1.2947358.

[34] P. Daigle, M.-A. Despatis, and G. Grenier, "How mechanical deformations contribute to the effectiveness of negative-pressure wound therapy," *Wound Repair and Regeneration*, vol. 21, no. 4, pp. 498–502, Jul. 2013, doi: 10.1111/wrr.12052.

[35] S. Ud-Din and A. Bayat, "Electrical Stimulation and Cutaneous Wound Healing: A Review of Clinical Evidence," *Healthcare*, vol. 2, no. 4, pp. 445–467, Oct. 2014, doi: 10.3390/healthcare2040445.

[36] R. Balint, N. J. Cassidy, and S. H. Cartmell, "Electrical Stimulation: A Novel Tool for Tissue Engineering," *Tissue Eng Part B Rev*, vol. 19, no. 1, pp. 48–57, Feb. 2013, doi: 10.1089/ten.teb.2012.0183.

[37] F. Gottrup, M. S. Agren, and T. Karlsmark, "Models for use in wound healing research: a survey focusing on in vitro and in vivo adult soft tissue.," *Wound Repair Regen*, vol. 8, no. 2, pp. 83–96, Apr. 2000, doi: 10.1046/j.1524-475x.2000.00083.x.

[38] A. Stamm, K. Reimers, S. Strauß, P. Vogt, T. Scheper, and I. Pepelanova, "In vitro wound healing assays – state of the art," *BioNanoMaterials*, vol. 17, no. 1–2, pp. 79–87, Jan. 2016, doi: 10.1515/bnm-2016-0002.

[39] S. MacNeil, "Progress and opportunities for tissue-engineered skin," *Nature*, vol. 445, no. 7130, pp. 874–880, 2007, doi: 10.1038/nature05664.

[40] A. Rossi, A. Appelt-Menzel, S. Kurdyn, H. Walles, and F. Groeber, "Generation of a Three-dimensional Full Thickness Skin Equivalent and Automated Wounding," *Journal of Visualized Experiments*, no. 96, pp. 1–7, Feb. 2015, doi: 10.3791/52576.

[41] Y. Marquardt *et al.*, "Characterization of a novel standardized human three-dimensional skin wound healing model using non-sequential fractional ultrapulsed

CO2 laser treatments.," *Lasers Surg Med*, vol. 47, no. 3, pp. 257–65, Mar. 2015, doi: 10.1002/lsm.22341.

[42] C. Egles, J. A. Garlick, and Y. Shamis, "Three-Dimensional Human Tissue Models of Wounded Skin," in *Methods Mol Biol.*, K. Turksen, Ed., in Methods in Molecular Biology, vol. 585. Totowa, NJ: Humana Press, 2010, pp. 345–359. doi: 10.1007/978-1-60761-380-0_24.

[43] M. Morshed, N. 'Izzah AG, C. SR, and R. BHI, "The current available biomaterials being used for skin tissue engineering," *Regenerative Research*, vol. 3, no. 1, pp. 17–22, 2014.

[44] C. Migliaresi and A. Motta, *Scaffolds for Tissue Engineering: Biological Design, Materials, and Fabrication*. 2014. doi: 10.4032/9789814463218.

[45] M. N. Nicholas, M. G. Jeschke, and S. Amini-Nik, "Methodologies in creating skin substitutes," *Cellular and Molecular Life Sciences*, vol. 73, no. 18, pp. 3453–3472, Sep. 2016, doi: 10.1007/s00018-016-2252-8.

[46] I. V. Yannas, E. Lee, D. P. Orgill, E. M. Skrabut, and G. F. Murphy, "Synthesis and characterization of a model extracellular matrix that induces partial regeneration of adult mammalian skin.," *Proceedings of the National Academy of Sciences*, vol. 86, no. 3, pp. 933–937, Feb. 1989, doi: 10.1073/pnas.86.3.933.

[47] V. Hudon, F. Berthod, A. F. Black, O. Damour, L. Germain, and F. A. Auger, "A tissue-engineered endothelialized dermis to study the modulation of angiogenic and angiostatic molecules on capillary-like tube formation in vitro," *British Journal of Dermatology*, vol. 148, no. 6, pp. 1094–1104, Jun. 2003, doi: 10.1046/j.1365-2133.2003.05298.x.

[48] F. Zhang *et al.*, "Fabrication of gelatin–hyaluronic acid hybrid scaffolds with tunable porous structures for soft tissue engineering," *Int J Biol Macromol*, vol. 48, no. 3, pp. 474–481, Apr. 2011, doi: 10.1016/j.ijbiomac.2011.01.012.

[49] G. Maheshwari, G. Brown, D. A. Lauffenburger, A. Wells, and L. G. Griffith, "Cell adhesion and motility depend on nanoscale RGD clustering," *J Cell Sci*, vol. 113, no. 10, pp. 1677–1686, May 2000, doi: 10.1242/jcs.113.10.1677.

[50] F. J. Bye, A. J. Bullock, R. Singh, F. Sefat, S. Roman, and S. MacNeil, "Development of a Basement Membrane Substitute Incorporated Into an Electrospun Scaffold for 3D Skin Tissue Engineering," *J Biomater Tissue Eng*, vol. 4, no. 9, pp. 686–692, 2014, doi: 10.1166/jbt.2014.1224.

[51] A. J. Ryan and F. J. O'Brien, "Insoluble elastin reduces collagen scaffold stiffness, improves viscoelastic properties, and induces a contractile phenotype in smooth muscle cells," *Biomaterials*, vol. 73, pp. 296–307, Dec. 2015, doi: 10.1016/j.biomaterials.2015.09.003.

[52] M. Ansari, S. S. Kordestani, S. Nazralizadeh, and H. Eslami, "Biodegradable Cell-Seeded Collagen Based Polymer Scaffolds for Wound Healing and Skin Reconstruction," *Journal of Macromolecular Science, Part B*, vol. 57, no. 2, pp. 100–109, Feb. 2018, doi: 10.1080/00222348.2018.1435617.

[53] P. K. Dutta, K. Rinki, and J. Dutta, "Chitosan: A Promising Biomaterial for Tissue Engineering Scaffolds," in *Chitosan for Biomaterials II*, R. Jayakumar, M. Prabaharan, and R. A. A. Muzzarelli, Eds., Berlin, Heidelberg: Springer Berlin Heidelberg, 2011, pp. 45–79. doi: 10.1007/12_2011_112.

[54] F. Han, Y. Dong, Z. Su, R. Yin, A. Song, and S. Li, "Preparation, characteristics and assessment of a novel gelatin–chitosan sponge scaffold as skin tissue engineering material," *Int J Pharm*, vol. 476, no. 1–2, pp. 124–133, Dec. 2014, doi: 10.1016/j.ijpharm.2014.09.036.

[55] S. D. Sarkar, B. L. Farrugia, T. R. Dargaville, and S. Dhara, "Chitosan-collagen scaffolds with nano/microfibrous architecture for skin tissue engineering," *J Biomed Mater Res A*, vol. 101, no. 12, pp. 3482–3492, 2013, doi: 10.1002/jbm.a.34660.

[56] M. Ottosson, A. Jakobsson, and F. Johansson, "Accelerated Wound Closure - Differently Organized Nanofibers Affect Cell Migration and Hence the Closure of Artificial Wounds in a Cell Based In Vitro Model," *PLoS One*, vol. 12, no. 1, p. e0169419, Jan. 2017, doi: 10.1371/journal.pone.0169419.

[57] N. Davidenko *et al.*, "Biomimetic collagen scaffolds with anisotropic pore architecture.," *Acta Biomater*, vol. 8, no. 2, pp. 667–76, Feb. 2012, doi: 10.1016/j.actbio.2011.09.033.

[58] D. Clearfield and M. Wei, "Investigation of structural collapse in unidirectionally freeze cast collagen scaffolds," *J Mater Sci Mater Med*, vol. 27, no. 1, p. 15, Jan. 2016, doi: 10.1007/s10856-015-5632-y.

[59] K. M. Pawelec, A. Husmann, S. M. Best, and R. E. Cameron, "A design protocol for tailoring ice-templated scaffold structure," *J R Soc Interface*, vol. 11, no. 92, p. 20130958, Mar. 2014, doi: 10.1098/rsif.2013.0958.

[60] F. O'Brien, "Influence of freezing rate on pore structure in freeze-dried collagen-GAG scaffolds," *Biomaterials*, vol. 25, no. 6, pp. 1077–1086, Mar. 2004, doi: 10.1016/S0142-9612(03)00630-6.

[61] S. J. Florczyk, D.-J. Kim, D. L. Wood, and M. Zhang, "Influence of processing parameters on pore structure of 3D porous chitosan-alginate polyelectrolyte complex scaffolds," *J Biomed Mater Res A*, vol. 98A, no. 4, pp. 614–620, Sep. 2011, doi: 10.1002/jbm.a.33153.

[62] M. Madaghiele, A. Sannino, I. V. Yannas, and M. Spector, "Collagen-based matrices with axially oriented pores," *J Biomed Mater Res A*, vol. 85, no. 3, pp. 757–767, 2008, doi: 10.1002/jbm.a.31517.

[63] R. D. Velasco Barraza, A. S. Álvarez Suarez, L. J. Villarreal Gómez, J. A. Paz González, A. L. Iglesias, and R. Vera Graziano, "Designing a Low Cost Electrospinning Device for Practical Learning in a Bioengineering Biomaterials Course," Revista Mexicana de Ingeniería Biomédica, 2016. doi: 10.17488/rmib.37.1.1.

[64] I. V. Yannas, D. S. Tzeranis, B. A. Harley, and P. T. C. So, "Biologically active collagen-based scaffolds: advances in processing and characterization," *Philosophical Transactions of the Royal Society A: Mathematical, Physical and Engineering Sciences*, vol. 368, no. 1917, pp. 2123–2139, Apr. 2010, doi: 10.1098/rsta.2010.0015.

[65] H. M. Powell and S. T. Boyce, "EDC cross-linking improves skin substitute strength and stability," *Biomaterials*, vol. 27, no. 34, pp. 5821–5827, Dec. 2006, doi: 10.1016/j.biomaterials.2006.07.030.

[66] K. Hori, A. Osada, T. Isago, and H. Sakurai, "Comparison of contraction among three dermal substitutes: Morphological differences in scaffolds.," *Burns*, vol. 43, no. 4, pp. 846–851, Jun. 2017, doi: 10.1016/j.burns.2016.10.017.

[67] R.-N. Chen, H.-O. Ho, and M.-T. Sheu, "Characterization of collagen matrices crosslinked using microbial transglutaminase," *Biomaterials*, vol. 26, no. 20, pp. 4229–4235, Jul. 2005, doi: 10.1016/j.biomaterials.2004.11.012.

[68] F. S. Frueh, M. D. Menger, N. Lindenblatt, P. Giovanoli, and M. W. Laschke, "Current and emerging vascularization strategies in skin tissue engineering," *Crit Rev Biotechnol*, vol. 37, no. 5, pp. 613–625, Jul. 2017, doi: 10.1080/07388551.2016.1209157.

[69] G. Sriram, P. L. Bigliardi, and M. Bigliardi-Qi, “Fibroblast heterogeneity and its implications for engineering organotypic skin models in vitro,” *Eur J Cell Biol*, vol. 94, no. 11, pp. 483–512, Nov. 2015, doi: 10.1016/j.ejcb.2015.08.001.

[70] D. Janson, G. Saintigny, C. Mahé, and A. El Ghalbzouri, “Papillary fibroblasts differentiate into reticular fibroblasts after prolonged in vitro culture,” *Exp Dermatol*, vol. 22, no. 1, pp. 48–53, Jan. 2013, doi: 10.1111/exd.12069.

[71] V. W. Wong, S. Akaishi, M. T. Longaker, and G. C. Gurtner, “Pushing back: wound mechanotransduction in repair and regeneration.,” *J Invest Dermatol*, vol. 131, no. 11, pp. 2186–96, Nov. 2011, doi: 10.1038/jid.2011.212.

[72] L. A. Barnes *et al.*, “Mechanical Forces in Cutaneous Wound Healing: Emerging Therapies to Minimize Scar Formation,” *Adv Wound Care (New Rochelle)*, vol. 7, no. 2, pp. 47–56, Feb. 2018, doi: 10.1089/wound.2016.0709.

[73] S. G. Kumbar, S. P. Nukavarapu, R. James, L. S. Nair, and C. T. Laurencin, “Electrospun poly(lactic acid-co-glycolic acid) scaffolds for skin tissue engineering,” *Biomaterials*, vol. 29, no. 30, pp. 4100–4107, Oct. 2008, doi: 10.1016/j.biomaterials.2008.06.028.

[74] C. Kasper, M. van Griensven, and R. Pörtner, *Bioreactor Systems for Tissue Engineering*, vol. 112. in Advances in Biochemical Engineering/Biotechnology, vol. 112. Berlin, Heidelberg: Springer Berlin Heidelberg, 2009. doi: 10.1007/978-3-540-69357-4.

[75] T. Sun, D. Norton, J. W. Haycock, A. J. Ryan, and S. MacNeil, “Development of a Closed Bioreactor System for Culture of Tissue-Engineered Skin at an Air–Liquid Interface,” *Tissue Eng*, vol. 11, no. 11–12, pp. 1824–1831, Nov. 2005, doi: 10.1089/ten.2005.11.1824.

[76] A. Scalise *et al.*, “Improving wound healing and preventing surgical site complications of closed surgical incisions: a possible role of Incisional Negative Pressure Wound Therapy. A systematic review of the literature.,” *Int Wound J*, vol. 13, no. 6, pp. 1260–1281, Dec. 2016, doi: 10.1111/iwj.12492.

[77] R. W. F. Veale *et al.*, “Influence of advanced wound matrices on observed vacuum pressure during simulated negative pressure wound therapy.,” *J Mech Behav Biomed Mater*, vol. 138, no. October 2022, p. 105620, Feb. 2023, doi: 10.1016/j.jmbbm.2022.105620.

[78] T. Yamashiro, T. Kushibiki, Y. Mayumi, M. Tsuchiya, M. Ishihara, and R. Azuma, “Novel cell culture system for monitoring cells during continuous and variable

negative-pressure wound therapy.," *Skin Res Technol*, vol. 29, no. 1, p. e13262, Jan. 2023, doi: 10.1111/srt.13262.

[79] A. K. McNulty, M. Schmidt, T. Feeley, and K. Kieswetter, "Effects of negative pressure wound therapy on fibroblast viability, chemotactic signaling, and proliferation in a provisional wound (fibrin) matrix," *Wound Repair and Regeneration*, vol. 15, no. 6, pp. 838–846, Nov. 2007, doi: 10.1111/j.1524-475x.2007.00287.x.

[80] G. Notorgiacomo, J. Klug, S. Rapp, S. T. Boyce, and S. C. Schutte, "A bioreactor for studying negative pressure wound therapy on skin grafts," *Int Wound J*, vol. 19, no. 3, pp. 633–642, Mar. 2022, doi: 10.1111/iwj.13661.

[81] C. Baldwin, M. Potter, E. Clayton, L. Irvine, and J. Dye, "Topical Negative Pressure Stimulates Endothelial Migration and Proliferation," *Ann Plast Surg*, vol. 62, no. 1, pp. 92–96, Jan. 2009, doi: 10.1097/sap.0b013e31817762fd.

[82] F. Grinnell, "Fibroblast–collagen-matrix contraction: growth-factor signalling and mechanical loading," *Trends Cell Biol*, vol. 10, no. 9, pp. 362–365, Sep. 2000, doi: 10.1016/s0962-8924(00)01802-x.

[83] L. Moroni *et al.*, "Biofabrication strategies for 3D in vitro models and regenerative medicine," *Nat Rev Mater*, vol. 3, no. 5, pp. 21–37, May 2018, doi: 10.1038/s41578-018-0006-y.

[84] Y. E. Yun, Y. J. Jung, Y. J. Choi, J. S. Choi, and Y. W. Cho, "Artificial skin models for animal-free testing," *J Pharm Investig*, vol. 48, no. 2, pp. 215–223, Mar. 2018, doi: 10.1007/s40005-018-0389-1.

[85] R. D. Abbott and D. L. Kaplan, "Strategies for improving the physiological relevance of human engineered tissues.," *Trends Biotechnol*, vol. 33, no. 7, pp. 401–7, Jul. 2015, doi: 10.1016/j.tibtech.2015.04.003.

[86] K. A. Faraj, T. H. van Kuppevelt, and W. F. Daamen, "Construction of Collagen Scaffolds That Mimic the Three-Dimensional Architecture of Specific Tissues," *Tissue Eng*, vol. 13, no. 10, pp. 2387–2394, Oct. 2007, doi: 10.1089/ten.2006.0320.

[87] K. M. Pawelec, A. Husmann, S. M. Best, and R. E. Cameron, "Understanding anisotropy and architecture in ice-templated biopolymer scaffolds.," *Mater Sci Eng C Mater Biol Appl*, vol. 37, no. 1, pp. 141–7, Apr. 2014, doi: 10.1016/j.msec.2014.01.009.

[88] M. Bartoš, T. Suchý, and R. Foltán, "Note on the use of different approaches to determine the pore sizes of tissue engineering scaffolds: what do we measure?"

Biomed Eng Online, vol. 17, no. 1, p. 110, Aug. 2018, doi: 10.1186/s12938-018-0543-z.

[89] J. Ratanavaraporn, S. Kanokpanont, Y. Tabata, and S. Damrongsakkul, "Effects of acid type on physical and biological properties of collagen scaffolds," *J Biomater Sci Polym Ed*, vol. 19, no. 7, pp. 945–952, Jan. 2008, doi: 10.1163/156856208784613505.

[90] H. Yang, L. Duan, Q. Li, Z. Tian, and G. Li, "Experimental and modeling investigation on the rheological behavior of collagen solution as a function of acetic acid concentration.," *J Mech Behav Biomed Mater*, vol. 77, no. September 2017, pp. 125–134, Jan. 2018, doi: 10.1016/j.jmbbm.2017.09.003.

[91] M. Jafari-Sabet, H. Nasiri, and R. Ataee, "The Effect of Cross-Linking Agents and Collagen Concentrations on Properties of Collagen Scaffolds," *Journal of Archives in Military Medicine*, vol. 4, no. 4, Oct. 2016, doi: 10.5812/jamm.42367.

[92] Y. Y. Peng, V. Glattauer, and J. A. M. Ramshaw, "Stabilisation of Collagen Sponges by Glutaraldehyde Vapour Crosslinking," *Int J Biomater*, vol. 2017, pp. 1–6, 2017, doi: 10.1155/2017/8947823.

[93] V. Perez-Puyana, A. Romero, and A. Guerrero, "Influence of collagen concentration and glutaraldehyde on collagen-based scaffold properties," *J Biomed Mater Res A*, vol. 104, no. 6, pp. 1462–1468, Jun. 2016, doi: 10.1002/jbm.a.35671.

[94] L. Ma, "Collagen/chitosan porous scaffolds with improved biostability for skin tissue engineering," *Biomaterials*, vol. 24, no. 26, pp. 4833–4841, Nov. 2003, doi: 10.1016/S0142-9612(03)00374-0.

[95] L. Buttafoco *et al.*, "First steps towards tissue engineering of small-diameter blood vessels: Preparation of flat scaffolds of collagen and elastin by means of freeze drying," *J Biomed Mater Res B Appl Biomater*, vol. 77B, no. 2, pp. 357–368, May 2006, doi: 10.1002/jbm.b.30444.

[96] J. Ward, J. Kelly, W. Wang, D. I. Zeugolis, and A. Pandit, "Amine functionalization of collagen matrices with multifunctional polyethylene glycol systems.," *Biomacromolecules*, vol. 11, no. 11, pp. 3093–101, Nov. 2010, doi: 10.1021/bm100898p.

[97] P. Tomlins, P. Grant, S. Mikhalovsky, S. James, and L. Mikhalovska, "Measurement of Pore Size and Porosity of Tissue Scaffolds," in *Tissue Engineered Medical Products (TEMPs)*, 100 Barr Harbor Drive, PO Box C700, West Conshohocken, PA 19428-2959: ASTM International, 2004, pp. 3–11. doi: 10.1520/STP11629S.

[98] M. Fauzi, S. Chowdhury, R. Idrus, and B. Aminuddin, “Fabrication of collagen type I scaffold for skin tissue engineering,” *Regenerative Research*, vol. 3, no. 2, pp. 60–61, 2014.

[99] H. Schoof, J. Apel, I. Heschel, and G. Rau, “Control of pore structure and size in freeze-dried collagen sponges.,” *J Biomed Mater Res*, vol. 58, no. 4, pp. 352–7, 2001, doi: 10.1002/jbm.1028.

[100] M. C. Varley, S. Neelakantan, T. W. Clyne, J. Dean, R. A. Brooks, and A. E. Markaki, “Cell structure, stiffness and permeability of freeze-dried collagen scaffolds in dry and hydrated states.,” *Acta Biomater*, vol. 33, pp. 166–75, Mar. 2016, doi: 10.1016/j.actbio.2016.01.041.

[101] F. J. O’Brien, B. A. Harley, I. V. Yannas, and L. J. Gibson, “The effect of pore size on cell adhesion in collagen-GAG scaffolds,” *Biomaterials*, vol. 26, no. 4, pp. 433–441, Feb. 2005, doi: 10.1016/j.biomaterials.2004.02.052.

[102] M. G. Haugh, C. M. Murphy, and F. J. O’Brien, “Novel freeze-drying methods to produce a range of collagen-glycosaminoglycan scaffolds with tailored mean pore sizes.,” *Tissue Eng Part C Methods*, vol. 16, no. 5, pp. 887–94, Oct. 2010, doi: 10.1089/ten.tec.2009.0422.

[103] I. Migneault, C. Dartiguenave, M. J. Bertrand, and K. C. Waldron, “Glutaraldehyde: behavior in aqueous solution, reaction with proteins, and application to enzyme crosslinking,” *Biotechniques*, vol. 37, no. 5, pp. 790–802, Nov. 2004, doi: 10.2144/04375RV01.

[104] V. Perez-Puyana, M. Jiménez-Rosado, A. Romero, and A. Guerrero, “Crosslinking of hybrid scaffolds produced from collagen and chitosan.,” *Int J Biol Macromol*, vol. 139, pp. 262–269, Oct. 2019, doi: 10.1016/j.ijbiomac.2019.07.198.

[105] J. Maitz *et al.*, “The effects of cross-linking a collagen-elastin dermal template on scaffold bio-stability and degradation.,” *J Tissue Eng Regen Med*, vol. 14, no. 9, pp. 1189–1200, Jul. 2020, doi: 10.1002/term.3082.

[106] D. Dippold *et al.*, “Investigation of the batch-to-batch inconsistencies of Collagen in PCL-Collagen nanofibers,” *Materials Science and Engineering C*, vol. 95, no. November 2017, pp. 217–225, 2019, doi: 10.1016/j.msec.2018.10.057.

[107] N. Davidenko *et al.*, “Control of crosslinking for tailoring collagen-based scaffolds stability and mechanics,” *Acta Biomater*, vol. 25, pp. 131–142, 2015, doi: 10.1016/j.actbio.2015.07.034.

[108] X. H. Wang *et al.*, "Crosslinked collagen/chitosan matrix for artificial livers.," *Biomaterials*, vol. 24, no. 19, pp. 3213–20, Aug. 2003, doi: 10.1016/s0142-9612(03)00170-4.

[109] A.-M. Haparanta, J. Koivurinta, E.-R. Hamalainen, and M. Kellomaki, "The effect of cross-linking time on a porous freeze-dried collagen scaffold using 1-ethyl-3-(3-dimethylaminopropyl)carbodiimide as a cross-linker.," *J Appl Biomater Biomech*, vol. 6, no. 2, pp. 89–94, 2008.

[110] L. Ma, C. Gao, Z. Mao, J. Shen, X. Hu, and C. Han, "Thermal dehydration treatment and glutaraldehyde cross-linking to increase the biostability of collagen-chitosan porous scaffolds used as dermal equivalent.," *J Biomater Sci Polym Ed*, vol. 14, no. 8, pp. 861–74, Jan. 2003, doi: 10.1163/156856203768366576.

[111] P.-Y. Chen, H.-J. Hsieh, and L. L. H. Huang, "Shrinking mechanism of a porous collagen matrix immersed in solution.," *J Biomed Mater Res A*, vol. 102, no. 12, pp. 4581–9, Dec. 2014, doi: 10.1002/jbm.a.35135.

[112] Q. L. Loh and C. Choong, "Three-Dimensional Scaffolds for Tissue Engineering Applications: Role of Porosity and Pore Size," *Tissue Eng Part B Rev*, vol. 19, no. 6, pp. 485–502, Dec. 2013, doi: 10.1089/ten.teb.2012.0437.

[113] J. Kozlowska, A. Sionkowska, A. M. Osyczka, and M. Dubiel, "Stabilizing effect of carbodiimide and dehydrothermal treatment crosslinking on the properties of collagen/hydroxyapatite scaffolds," *Polym Int*, vol. 66, no. 8, pp. 1164–1172, Aug. 2017, doi: 10.1002/pi.5371.

[114] V. Jayarama Reddy *et al.*, "Nanofibrous structured biomimetic strategies for skin tissue regeneration," *Wound Repair and Regeneration*, vol. 21, no. 1, pp. 1–16, Jan. 2013, doi: 10.1111/j.1524-475X.2012.00861.x.

[115] M. Kun, C. Chan, S. Ramakrishna, A. Kulkarni, and K. Vadodaria, "Textile-based scaffolds for tissue engineering," in *Advanced Textiles for Wound Care*, Second Edi.Elsevier, 2019, pp. 329–362. doi: 10.1016/B978-0-08-102192-7.00012-6.

[116] C. Z. Mosher *et al.*, "Green electrospinning for biomaterials and biofabrication," *Biofabrication*, vol. 13, no. 3, p. 035049, Jul. 2021, doi: 10.1088/1758-5090/ac0964.

[117] R. Krishnan, S. Sundarrajan, and S. Ramakrishna, "Green Processing of Nanofibers for Regenerative Medicine," *Macromol Mater Eng*, vol. 298, no. 10, Dec. 2012, doi: 10.1002/mame.201200323.

[118] L. Bacakova *et al.*, “Nanofibrous Scaffolds for Skin Tissue Engineering and Wound Healing Based on Synthetic Polymers,” in *Applications of Nanobiotechnology*, IntechOpen, 2020. doi: 10.5772/intechopen.88744.

[119] L. Bacakova *et al.*, “Nanofibrous Scaffolds for Skin Tissue Engineering and Wound Healing Based on Nature-Derived Polymers,” in *Current and Future Aspects of Nanomedicine*, IntechOpen, 2020. doi: 10.5772/intechopen.88602.

[120] D. Miele *et al.*, “Collagen/PCL Nanofibers Electrospun in Green Solvent by DOE Assisted Process. An Insight into Collagen Contribution,” *Materials*, vol. 13, no. 21, p. 4698, Oct. 2020, doi: 10.3390/ma13214698.

[121] F. Roozbahani, N. Sultana, A. Fauzi Ismail, and H. Nouparvar, “Effects of Chitosan Alkali Pretreatment on the Preparation of Electrospun PCL/Chitosan Blend Nanofibrous Scaffolds for Tissue Engineering Application,” *J Nanomater*, vol. 2013, pp. 1–6, 2013, doi: 10.1155/2013/641502.

[122] S. R. Gomes *et al.*, “In vitro and in vivo evaluation of electrospun nanofibers of PCL, chitosan and gelatin: A comparative study,” *Materials Science and Engineering: C*, vol. 46, pp. 348–358, Jan. 2015, doi: 10.1016/j.msec.2014.10.051.

[123] J. Jiménez Vázquez and E. San Martín Martínez, “Collagen and elastin scaffold by electrospinning for skin tissue engineering applications,” *J Mater Res*, vol. 34, no. 16, pp. 2819–2827, Aug. 2019, doi: 10.1557/jmr.2019.233.

[124] J. X. Law, L. L. Liau, A. Saim, Y. Yang, and R. Idrus, “Electrospun Collagen Nanofibers and Their Applications in Skin Tissue Engineering,” *Tissue Eng Regen Med*, vol. 14, no. 6, pp. 699–718, Dec. 2017, doi: 10.1007/s13770-017-0075-9.

[125] A. Hernández-Rangel and E. S. Martin-Martinez, “Collagen based electrospun materials for skin wounds treatment,” *J Biomed Mater Res A*, vol. 109, no. 9, pp. 1751–1764, Sep. 2021, doi: 10.1002/jbm.a.37154.

[126] B. Dong, O. Arnoult, M. E. Smith, and G. E. Wnek, “Electrospinning of Collagen Nanofiber Scaffolds from Benign Solvents,” *Macromol Rapid Commun*, vol. 30, no. 7, pp. 539–542, Apr. 2009, doi: 10.1002/marc.200800634.

[127] A. Elamparithi, A. M. Punnoose, and S. Kuruvilla, “Electrospun type 1 collagen matrices preserving native ultrastructure using benign binary solvent for cardiac tissue engineering.,” *Artif Cells Nanomed Biotechnol*, vol. 44, no. 5, pp. 1318–25, Aug. 2016, doi: 10.3109/21691401.2015.1029629.

[128] X. Geng, O.-H. Kwon, and J. Jang, “Electrospinning of chitosan dissolved in concentrated acetic acid solution.,” *Biomaterials*, vol. 26, no. 27, pp. 5427–32, Sep. 2005, doi: 10.1016/j.biomaterials.2005.01.066.

[129] S. Qasim *et al.*, “Electrospinning of Chitosan-Based Solutions for Tissue Engineering and Regenerative Medicine,” *Int J Mol Sci*, vol. 19, no. 2, p. 407, Jan. 2018, doi: 10.3390/ijms19020407.

[130] K. Kalantari, A. M. Afifi, H. Jahangirian, and T. J. Webster, “Biomedical applications of chitosan electrospun nanofibers as a green polymer – Review,” *Carbohydr Polym*, vol. 207, pp. 588–600, Mar. 2019, doi: 10.1016/j.carbpol.2018.12.011.

[131] L. Van der Schueren, I. Steyaert, B. De Schoenmaker, and K. De Clerck, “Polycaprolactone/chitosan blend nanofibres electrospun from an acetic acid/formic acid solvent system,” *Carbohydr Polym*, vol. 88, no. 4, pp. 1221–1226, May 2012, doi: 10.1016/j.carbpol.2012.01.085.

[132] A. Sarasam and S. V Madihally, “Characterization of chitosan-polycaprolactone blends for tissue engineering applications.,” *Biomaterials*, vol. 26, no. 27, pp. 5500–8, Sep. 2005, doi: 10.1016/j.biomaterials.2005.01.071.

[133] I. Steyaert, L. Van der Schueren, H. Rahier, and K. de Clerck, “An Alternative Solvent System for Blend Electrospinning of Polycaprolactone/Chitosan Nanofibres,” *Macromol Symp*, vol. 321–322, no. 1, pp. 71–75, Dec. 2012, doi: 10.1002/masy.201251111.

[134] P. Nitti *et al.*, “Influence of Nanofiber Orientation on Morphological and Mechanical Properties of Electrospun Chitosan Mats,” *J Healthc Eng*, vol. 2018, pp. 1–12, Nov. 2018, doi: 10.1155/2018/3651480.

[135] S. Mengistu Lemma, F. Bossard, and M. Rinaudo, “Preparation of Pure and Stable Chitosan Nanofibers by Electrospinning in the Presence of Poly(ethylene oxide),” *Int J Mol Sci*, vol. 17, no. 11, p. 1790, Oct. 2016, doi: 10.3390/ijms17111790.

[136] P. Kolhe and R. M. Kannan, “Improvement in ductility of chitosan through blending and copolymerization with PEG: FTIR investigation of molecular interactions.,” *Biomacromolecules*, vol. 4, no. 1, pp. 173–80, 2003, doi: 10.1021/bm025689+.

[137] K. T. Shalumon, K. H. Anulekha, K. P. Chennazhi, H. Tamura, S. V. Nair, and R. Jayakumar, “Fabrication of chitosan/poly(caprolactone) nanofibrous scaffold for bone and skin tissue engineering,” *Int J Biol Macromol*, vol. 48, no. 4, pp. 571–576, May 2011, doi: 10.1016/j.ijbiomac.2011.01.020.

[138] O. F. Tursucular, I. Cerkez, M. Orhan, and Y. Aykut, “Preperation and antibacterial investigation of polycaprolactone/chitosan nano/micro fibers by using different solvent systems,” *Tekstil ve Konfeksiyon*, vol. 28, no. 3, pp. 221–228, 2018.

[139] A. Chanda *et al.*, “Electrospun chitosan/polycaprolactone-hyaluronic acid bilayered scaffold for potential wound healing applications.,” *Int J Biol Macromol*, vol. 116, pp. 774–785, Sep. 2018, doi: 10.1016/j.ijbiomac.2018.05.099.

[140] J. C. Silva, “Evaluation of nanofibrous scaffolds obtained from blends of chitosan, gelatin and polycaprolactone for skin tissue engineering,” *Int J Biol Macromol*, 2017, doi: 10.1016/j.ijbiomac.2017.05.004.

[141] Md. R. Alam, S. Alimuzzaman, Md. S. Abdus, Fahmida-E-Karim, and Md. E. Hoque, “Collagen/Nigella sativa/chitosan inscribed electrospun hybrid bio-nanocomposites for skin tissue engineering,” *J Biomater Sci Polym Ed*, pp. 1–22, 2023.

[142] B. Sachin Kumar, S. K. Kalpathy, and S. Anandhan, “Synergism of fictitious forces on nickel cobaltite nanofibers: electrospinning forces revisited,” *Physical Chemistry Chemical Physics*, vol. 20, no. 7, pp. 5295–5304, 2018, doi: 10.1039/C7CP07435B.

[143] M. B. Fisher, E. A. Henning, N. Söegaard, J. L. Esterhai, and R. L. Mauck, “Organized nanofibrous scaffolds that mimic the macroscopic and microscopic architecture of the knee meniscus.,” *Acta Biomater*, vol. 9, no. 1, pp. 4496–504, Jan. 2013, doi: 10.1016/j.actbio.2012.10.018.

[144] T. M. Righi, R. S. Almeida, and M. A. D’Ávila, “Electrospinning of Gelatin/PEO Blends: Influence of Process Parameters in the Nanofiber Properties,” *Macromol Symp*, vol. 319, no. 1, pp. 230–234, Sep. 2012, doi: 10.1002/masy.201100137.

[145] T. T. Yuan, P. M. Jenkins, A. M. DiGeorge Foushee, A. R. Jockheck-Clark, and J. M. Stahl, “Electrospun Chitosan/Polyethylene Oxide Nanofibrous Scaffolds with Potential Antibacterial Wound Dressing Applications,” *J Nanomater*, vol. 2016, pp. 1–10, 2016, doi: 10.1155/2016/6231040.

[146] F. Asghari *et al.*, “Hybrid PCL/chitosan-PEO nanofibrous scaffolds incorporated with A. euchroma extract for skin tissue engineering application.,” *Carbohydr Polym*, vol. 278, no. August 2021, p. 118926, Feb. 2022, doi: 10.1016/j.carbpol.2021.118926.

[147] A. N. Sohi, H. Naderi-Manesh, M. Soleimani, S. Mirzaei, M. Delbari, and M. Dodel, “Influence of Chitosan Molecular Weight and Poly(ethylene oxide): Chitosan Proportion on Fabrication of Chitosan Based Electrospun Nanofibers,” *Polymer*

Science, Series A, vol. 60, no. 4, pp. 471–482, Jul. 2018, doi: 10.1134/S0965545X18040077.

[148] D. Semnani *et al.*, "Evaluation of PCL/chitosan electrospun nanofibers for liver tissue engineering," *International Journal of Polymeric Materials and Polymeric Biomaterials*, vol. 66, no. 3, pp. 149–157, 2017, doi: 10.1080/00914037.2016.1190931.

[149] M. S. Kim, S. J. Park, B. K. Gu, and C.-H. Kim, "Polycaprolactone-Chitin Nanofibrous Mats as Potential Scaffolds for Tissue Engineering," *J Nanomater*, vol. 2012, pp. 1–9, 2012, doi: 10.1155/2012/635212.

[150] E. Bolaina-Lorenzo, C. Martínez-Ramos, M. Monleón-Pradas, W. Herrera-Kao, J. V Cauich-Rodríguez, and J. M. Cervantes-Uc, "Electrospun polycaprolactone/chitosan scaffolds for nerve tissue engineering: physicochemical characterization and Schwann cell biocompatibility," *Biomedical Materials*, vol. 12, no. 1, p. 015008, Dec. 2016, doi: 10.1088/1748-605X/12/1/015008.

[151] A. Gholipour Kanani and S. H. Bahrami, "Effect of Changing Solvents on Poly(-Caprolactone) Nanofibrous Webs Morphology," *J Nanomater*, vol. 2011, pp. 1–10, 2011, doi: 10.1155/2011/724153.

[152] R. Rezakhaniha *et al.*, "Experimental investigation of collagen waviness and orientation in the arterial adventitia using confocal laser scanning microscopy," *Biomech Model Mechanobiol*, vol. 11, no. 3–4, pp. 461–473, Mar. 2012, doi: 10.1007/s10237-011-0325-z.

[153] R. M. Nezarati, M. B. Eifert, and E. Cosgriff-Hernandez, "Effects of humidity and solution viscosity on electrospun fiber morphology.," *Tissue Eng Part C Methods*, vol. 19, no. 10, pp. 810–9, Oct. 2013, doi: 10.1089/ten.TEC.2012.0671.

[154] A. Haider, S. Haider, and I.-K. Kang, "A comprehensive review summarizing the effect of electrospinning parameters and potential applications of nanofibers in biomedical and biotechnology," *Arabian Journal of Chemistry*, vol. 11, no. 8, pp. 1165–1188, Dec. 2018, doi: 10.1016/j.arabjc.2015.11.015.

[155] L. Van der Schueren, B. De Schoenmaker, Ö. I. Kalaoglu, and K. De Clerck, "An alternative solvent system for the steady state electrospinning of polycaprolactone," *Eur Polym J*, vol. 47, no. 6, pp. 1256–1263, Jun. 2011, doi: 10.1016/j.eurpolymj.2011.02.025.

[156] X. Zhu, W. Cui, X. Li, and Y. Jin, “Electrospun fibrous mats with high porosity as potential scaffolds for skin tissue engineering.,” *Biomacromolecules*, vol. 9, no. 7, pp. 1795–801, Jul. 2008, doi: 10.1021/bm800476u.

[157] L. Liverani and A. Boccaccini, “Versatile Production of Poly(Epsilon-Caprolactone) Fibers by Electrospinning Using Benign Solvents,” *Nanomaterials*, vol. 6, no. 4, p. 75, Apr. 2016, doi: 10.3390/nano6040075.

[158] N. E. Zander, “Hierarchically Structured Electrospun Fibers,” pp. 19–44, 2013, doi: 10.3390/polym5010019.

[159] D. H. Reneker, W. Kataphinan, A. Theron, E. Zussman, and A. L. Yarin, “Nanofiber garlands of polycaprolactone by electrospinning,” *Polymer (Guildf)*, vol. 43, no. 25, pp. 6785–6794, Jan. 2002, doi: 10.1016/S0032-3861(02)00595-5.

[160] S. V. Fridrikh, J. H. Yu, M. P. Brenner, and G. C. Rutledge, “Controlling the Fiber Diameter during Electrospinning,” *Phys Rev Lett*, vol. 90, no. 14, p. 144502, Apr. 2003, doi: 10.1103/PhysRevLett.90.144502.

[161] H. He, Y. Wang, B. Farkas, Z. K. Nagy, and K. Molnar, “Analysis and prediction of the diameter and orientation of AC electrospun nanofibers by response surface methodology,” *Mater Des*, vol. 194, p. 108902, Sep. 2020, doi: 10.1016/j.matdes.2020.108902.

[162] C. E. Ayres *et al.*, “Measuring fiber alignment in electrospun scaffolds: a user’s guide to the 2D fast Fourier transform approach,” *J Biomater Sci Polym Ed*, vol. 19, no. 5, pp. 603–621, Jan. 2008, doi: 10.1163/156856208784089643.

[163] T. D. Clemons *et al.*, “Coherency image analysis to quantify collagen architecture: implications in scar assessment,” *RSC Adv*, vol. 8, no. 18, pp. 9661–9669, 2018, doi: 10.1039/C7RA12693J.

[164] G. Collins, J. Federici, Y. Imura, and L. H. Catalani, “Charge generation, charge transport, and residual charge in the electrospinning of polymers: A review of issues and complications,” *J Appl Phys*, vol. 111, no. 4, p. 044701, Feb. 2012, doi: 10.1063/1.3682464.

[165] C. J. Angammana and S. H. Jayaram, “Analysis of the Effects of Solution Conductivity on Electrospinning Process and Fiber Morphology,” *IEEE Trans Ind Appl*, vol. 47, no. 3, pp. 1109–1117, May 2011, doi: 10.1109/TIA.2011.2127431.

[166] W. Li, L. Shi, X. Zhang, K. Liu, I. Ullah, and P. Cheng, “Electrospinning of polycaprolactone nanofibers using H_2O as benign additive in

polycaprolactone/glacial acetic acid solution," *J Appl Polym Sci*, vol. 135, no. 3, p. 45578, Jan. 2018, doi: 10.1002/app.45578.

[167] C. Kriegel, K. M. Kit, D. J. McClements, and J. Weiss, "Electrospinning of chitosan–poly(ethylene oxide) blend nanofibers in the presence of micellar surfactant solutions," *Polymer (Guildf)*, vol. 50, no. 1, pp. 189–200, Jan. 2009, doi: 10.1016/j.polymer.2008.09.041.

[168] T. T. Yuan, P. M. Jenkins, A. M. DiGeorge Foushee, A. R. Jockheck-Clark, and J. M. Stahl, "Electrospun Chitosan/Polyethylene Oxide Nanofibrous Scaffolds with Potential Antibacterial Wound Dressing Applications," *J Nanomater*, vol. 2016, pp. 1–10, 2016, doi: 10.1155/2016/6231040.

[169] L. Gao and T. J. McCarthy, "How Wenzel and Cassie Were Wrong," *Langmuir*, vol. 23, no. 7, pp. 3762–3765, 2010.

[170] A. Marmur, "Solid-Surface Characterization by Wetting," *Annu Rev Mater Res*, vol. 39, no. 1, pp. 473–489, Aug. 2009, doi: 10.1146/annurev.matsci.38.060407.132425.

[171] R. Ghobeira, M. Asadian, C. Vercruysse, H. Declercq, N. De Geyter, and R. Morent, "Wide-ranging diameter scale of random and highly aligned PCL fibers electrospun using controlled working parameters," *Polymer (Guildf)*, vol. 157, no. October, pp. 19–31, Nov. 2018, doi: 10.1016/j.polymer.2018.10.022.

[172] A. Marmur, "Soft contact: measurement and interpretation of contact angles," *Soft Matter*, vol. 2, no. 1, pp. 12–17, 2006, doi: 10.1039/B514811C.

[173] Z. Kharat, M. Sadri, and M. Kabiri, "Herbal Extract Loaded Chitosan/PEO Nanocomposites as Antibacterial Coatings of Orthopaedic Implants," *Fibers and Polymers*, vol. 22, no. 4, pp. 989–999, Apr. 2021, doi: 10.1007/s12221-021-0490-3.

[174] R. Hirase, Y. Higashiyama, M. Mori, Y. Takahara, and C. Yamane, "Hydrated salts as both solvent and plasticizer for chitosan," *Carbohydr Polym*, vol. 80, no. 3, pp. 993–996, May 2010, doi: 10.1016/j.carbpol.2010.01.001.

[175] J. L. Ferreira, S. Gomes, C. Henriques, J. P. Borges, and J. C. Silva, "Electrospinning polycaprolactone dissolved in glacial acetic acid: Fiber production, nonwoven characterization, and In Vitro evaluation," *J Appl Polym Sci*, vol. 131, no. 22, Nov. 2014, doi: 10.1002/app.41068.

[176] C. Tonda-Turo *et al.*, "Non-covalently crosslinked chitosan nanofibrous mats prepared by electrospinning as substrates for soft tissue regeneration," *Carbohydr*

Polym, vol. 162, no. January, pp. 82–92, Apr. 2017, doi: 10.1016/j.carbpol.2017.01.050.

[177] T. T. Yuan, P. M. Jenkins, A. Marie, D. Foushee, A. R. Jockheck-clark, and J. M. Stahl, "Electrospun Chitosan / Polyethylene Oxide Nanofibrous Scaffolds with Potential Antibacterial Wound Dressing Applications," vol. 2016, 2016.

[178] S. Chen, B. Liu, M. A. Carlson, A. F. Gombart, D. A. Reilly, and J. Xie, "Recent advances in electrospun nanofibers for wound healing.," *Nanomedicine (Lond)*, vol. 12, no. 11, pp. 1335–1352, Jun. 2017, doi: 10.2217/nnm-2017-0017.

[179] C. H. Daly, "Biomechanical Properties of Dermis," *Journal of Investigative Dermatology*, vol. 79, no. 1, pp. 17–20, Jul. 1982, doi: 10.1038/jid.1982.4.

[180] J. Pelipenko, P. Kocbek, and J. Kristl, "Nanofiber diameter as a critical parameter affecting skin cell response," *European Journal of Pharmaceutical Sciences*, vol. 66, pp. 29–35, Jan. 2015, doi: 10.1016/j.ejps.2014.09.022.

[181] I. F. Amaral, A. L. Cordeiro, P. Sampaio, and M. A. Barbosa, "Attachment, spreading and short-term proliferation of human osteoblastic cells cultured on chitosan films with different degrees of acetylation," *J Biomater Sci Polym Ed*, vol. 18, no. 4, pp. 469–485, Jan. 2007, doi: 10.1163/156856207780425068.

[182] M. Chen, P. K. Patra, S. B. Warner, and S. Bhowmick, "Role of Fiber Diameter in Adhesion and Proliferation of NIH 3T3 Fibroblast on Electrospun Polycaprolactone Scaffolds," *Tissue Eng*, vol. 13, no. 3, pp. 579–587, Mar. 2007, doi: 10.1089/ten.2006.0205.

[183] A. Ravindran Girija, V. Palaninathan, X. Strudwick, S. Balasubramanian, S. Dasappan Nair, and A. J. Cowin, "Collagen-functionalized electrospun smooth and porous polymeric scaffolds for the development of human skin-equivalent," *RSC Adv*, vol. 10, no. 45, pp. 26594–26603, 2020, doi: 10.1039/D0RA04648E.

[184] N. Nagiah, L. Madhavi, R. Anitha, N. T. Srinivasan, and U. T. Sivagnanam, "Electrospinning of poly (3-hydroxybutyric acid) and gelatin blended thin films: fabrication, characterization, and application in skin regeneration," *Polymer Bulletin*, vol. 70, no. 8, pp. 2337–2358, Aug. 2013, doi: 10.1007/s00289-013-0956-6.

[185] Y. Liu, Y. Ji, K. Ghosh, R. A. F. Clark, L. Huang, and M. H. Rafailovich, "Effects of fiber orientation and diameter on the behavior of human dermal fibroblasts on electrospun PMMA scaffolds," *J Biomed Mater Res A*, vol. 90A, no. 4, pp. 1092–1106, Sep. 2009, doi: 10.1002/jbm.a.32165.

[186] F. Grinnell, “Fibroblast mechanics in three-dimensional collagen matrices,” *J Bodyw Mov Ther*, vol. 12, no. 3, pp. 191–193, Jul. 2008, doi: 10.1016/j.jbmt.2008.03.005.

[187] B. Gantenbein, A. S. Croft, and M. Larraillet, “Mammalian Cell Viability Methods in 3D Scaffolds for Tissue Engineering,” in *Fluorescence Methods for Investigation of Living Cells and Microorganisms*, IntechOpen, 2020. doi: 10.5772/intechopen.93078.

[188] P. Umashankar, T. Kumari, and P. Mohanan, “Glutaraldehyde treatment elicits toxic response compared to decellularization in bovine pericardium,” *Toxicol Int*, vol. 19, no. 1, p. 51, 2012, doi: 10.4103/0971-6580.94513.

[189] Y. Liu, L. Ma, and C. Gao, “Facile fabrication of the glutaraldehyde cross-linked collagen/chitosan porous scaffold for skin tissue engineering,” *Materials Science and Engineering: C*, vol. 32, no. 8, pp. 2361–2366, Dec. 2012, doi: 10.1016/j.msec.2012.07.008.

[190] L. Sun, B. Li, D. Yao, W. Song, and H. Hou, “Effects of cross-linking on mechanical, biological properties and biodegradation behavior of Nile tilapia skin collagen sponge as a biomedical material,” *J Mech Behav Biomed Mater*, vol. 80, pp. 51–58, Apr. 2018, doi: 10.1016/j.jmbbm.2018.01.006.

[191] Y. Y. Peng, V. Glattauer, and J. A. M. Ramshaw, “Stabilisation of Collagen Sponges by Glutaraldehyde Vapour Crosslinking,” *Int J Biomater*, vol. 2017, 2017, doi: 10.1155/2017/8947823.

[192] A. Martínez, M. D. Blanco, N. Davidenko, and R. E. Cameron, “Tailoring chitosan/collagen scaffolds for tissue engineering: Effect of composition and different crosslinking agents on scaffold properties,” *Carbohydr Polym*, vol. 132, pp. 606–619, Nov. 2015, doi: 10.1016/j.carbpol.2015.06.084.

[193] D. V Bax *et al.*, “Fundamental insight into the effect of carbodiimide crosslinking on cellular recognition of collagen-based scaffolds,” *Acta Biomater*, vol. 49, pp. 218–234, Feb. 2017, doi: 10.1016/j.actbio.2016.11.059.

[194] M. Nair, R. K. Johal, S. W. Hamaia, S. M. Best, and R. E. Cameron, “Tunable bioactivity and mechanics of collagen-based tissue engineering constructs: A comparison of EDC-NHS, genipin and TG2 crosslinkers,” *Biomaterials*, vol. 254, no. April, p. 120109, Sep. 2020, doi: 10.1016/j.biomaterials.2020.120109.

[195] S. Wong, W. Guo, and Y. Wang, “Fibroblasts probe substrate rigidity with filopodia extensions before occupying an area,” *Proceedings of the National Academy of*

Sciences, vol. 111, no. 48, pp. 17176–17181, Dec. 2014, doi: 10.1073/pnas.1412285111.

[196] S. Rhee, H. Jiang, C.-H. Ho, and F. Grinnell, "Microtubule function in fibroblast spreading is modulated according to the tension state of cell–matrix interactions," *Proceedings of the National Academy of Sciences*, vol. 104, no. 13, pp. 5425–5430, Mar. 2007, doi: 10.1073/pnas.0608030104.

[197] J. J. Tomasek, G. Gabbiani, B. Hinz, C. Chaponnier, and R. A. Brown, "Myofibroblasts and mechano-regulation of connective tissue remodelling," *Nat Rev Mol Cell Biol*, vol. 3, no. 5, pp. 349–363, May 2002, doi: 10.1038/nrm809.

[198] X. Huang *et al.*, "Matrix Stiffness–Induced Myofibroblast Differentiation Is Mediated by Intrinsic Mechanotransduction," *Am J Respir Cell Mol Biol*, vol. 47, no. 3, pp. 340–348, Sep. 2012, doi: 10.1165/rcmb.2012-0050OC.

[199] R. A. Brown and J. B. Phillips, "Cell Responses to Biomimetic Protein Scaffolds Used in Tissue Repair and Engineering," in *International Review of Cytology*, 2007, pp. 75–150. doi: 10.1016/S0074-7696(07)62002-6.

[200] X. Yang, J. D. Shah, and H. Wang, "Nanofiber Enabled Layer-by-Layer Approach Toward Three-Dimensional Tissue Formation," *Tissue Eng Part A*, vol. 15, no. 4, pp. 945–956, Apr. 2009, doi: 10.1089/ten.tea.2007.0280.

[201] C. Vaquette and J. Cooper-White, "A simple method for fabricating 3-D multilayered composite scaffolds," *Acta Biomater*, vol. 9, no. 1, pp. 4599–4608, Jan. 2013, doi: 10.1016/j.actbio.2012.08.015.

[202] H.-Y. Lin, S.-H. Chen, S.-H. Chang, and S.-T. Huang, "Tri-layered chitosan scaffold as a potential skin substitute," *J Biomater Sci Polym Ed*, vol. 26, no. 13, pp. 855–867, Sep. 2015, doi: 10.1080/09205063.2015.1061350.

[203] J. Pan, N. Liu, H. Sun, and F. Xu, "Preparation and Characterization of Electrospun PLCL/Poloxamer Nanofibers and Dextran/Gelatin Hydrogels for Skin Tissue Engineering," *PLoS One*, vol. 9, no. 11, p. e112885, Nov. 2014, doi: 10.1371/journal.pone.0112885.

[204] H. Lin, W. Tsai, and S. Chang, "Collagen-PVA aligned nanofiber on collagen sponge as bi-layered scaffold for surface cartilage repair," *J Biomater Sci Polym Ed*, vol. 28, no. 7, pp. 664–678, May 2017, doi: 10.1080/09205063.2017.1295507.

[205] G. Uzunalan, M. T. Ozturk, S. Dincer, and K. Tuzlakoglu, "A Newly Designed Collagen-Based Bilayered Scaffold for Skin Tissue Regeneration," *Journal of*

Composites and Biodegradable Polymers, vol. 1, no. 1, pp. 8–15, Jan. 2013, doi: 10.12974/2311-8717.2013.01.01.2.

[206] Y. Shi, L. Ma, J. Zhou, Z. Mao, and C. Gao, "Collagen/chitosan-silicone membrane bilayer scaffold as a dermal equivalent," *Polym Adv Technol*, vol. 16, no. 11–12, pp. 789–794, Nov. 2005, doi: 10.1002/pat.653.

[207] Ö. S. Aslantürk, "In Vitro Cytotoxicity and Cell Viability Assays: Principles, Advantages, and Disadvantages," in *Genotoxicity - A Predictable Risk to Our Actual World*, InTech, 2018, pp. 1–18. doi: 10.5772/intechopen.71923.

[208] "https://www.creative-bioarray.com/support/resazurin-cell-viability-assay.htm."

[209] X. Gong, Z. Liang, Y. Yang, H. Liu, J. Ji, and Y. Fan, "A resazurin-based, nondestructive assay for monitoring cell proliferation during a scaffold-based 3D culture process," *Regen Biomater*, vol. 7, no. 3, pp. 271–281, Jun. 2020, doi: 10.1093/rb/rbaa002.

[210] F. Bonnier *et al.*, "Cell viability assessment using the Alamar blue assay: A comparison of 2D and 3D cell culture models," *Toxicology in Vitro*, vol. 29, no. 1, pp. 124–131, Feb. 2015, doi: 10.1016/j.tiv.2014.09.014.

[211] A. Levin, V. Sharma, L. Hook, and E. García-Gareta, "The importance of factorial design in tissue engineering and biomaterials science: Optimisation of cell seeding efficiency on dermal scaffolds as a case study," *J Tissue Eng*, vol. 9, p. 204173141878169, Jan. 2018, doi: 10.1177/2041731418781696.

[212] N. O. Ojeh, J. D. Frame, and H. A. Navsaria, "In Vitro Characterization of an Artificial Dermal Scaffold," *Tissue Eng*, vol. 7, no. 4, pp. 457–472, Aug. 2001, doi: 10.1089/10763270152436508.

[213] J. S. Uzarski, M. D. DiVito, J. A. Wertheim, and W. M. Miller, "Essential design considerations for the resazurin reduction assay to noninvasively quantify cell expansion within perfused extracellular matrix scaffolds," *Biomaterials*, vol. 129, pp. 163–175, Jun. 2017, doi: 10.1016/j.biomaterials.2017.02.015.

[214] J. T. Y. Lee and K. L. Chow, "SEM sample preparation for cells on 3D scaffolds by freeze-drying and HMDS," *Scanning*, vol. 34, no. 1, pp. 12–25, Feb. 2012, doi: 10.1002/sca.20271.

[215] R. Mad Jin, N. Sultana, S. Baba, S. Hamdan, and A. F. Ismail, "Porous PCL/Chitosan and nHA/PCL/Chitosan Scaffolds for Tissue Engineering Applications: Fabrication and Evaluation," *J Nanomater*, vol. 2015, pp. 1–8, 2015, doi: 10.1155/2015/357372.

[216] T. L. Riss, R. A. Moravec, A. L. Niles, H. A. Benink, T. J. Worzella, and L. Minor, *Cell Viability Assays*. 2013.

[217] A. Idrees *et al.*, "Validation of in vitro assays in three-dimensional human dermal constructs," *Int J Artif Organs*, vol. 41, no. 11, pp. 779–788, Nov. 2018, doi: 10.1177/0391398818775519.

[218] R. A. Kamyshinsky *et al.*, "Environmental Scanning Electron Microscopy of Dermal Fibroblasts on Various Types of Polymer Scaffolds," *Crystallography Reports*, vol. 65, no. 5, pp. 762–765, Sep. 2020, doi: 10.1134/S1063774520050107.

[219] M. Malmsjö, E. Huddleston, and R. Martin, "Biological effects of a disposable, canisterless negative pressure wound therapy system.," *Eplasty*, vol. 14, p. e15, 2014.

[220] H. N. Wilkinson, F. L. Longhorne, E. R. Roberts, V. R. Brownhill, and M. J. Hardman, "Cellular benefits of single-use negative pressure wound therapy demonstrated in a novel ex vivo human skin wound model," *Wound Repair and Regeneration*, vol. 29, no. 2, pp. 298–305, Mar. 2021, doi: 10.1111/wrr.12888.

[221] A. C. Lesiak and A. B. Shafritz, "Negative-pressure wound therapy," *Journal of Hand Surgery*, vol. 38, no. 9, pp. 1828–1832, 2013, doi: 10.1016/j.jhsa.2013.04.029.

[222] Y.-G. Zhang *et al.*, "Effect of Negative Pressure on Human Bone Marrow Mesenchymal Stem Cells In Vitro," *Connect Tissue Res*, vol. 51, no. 1, pp. 14–21, Feb. 2010, doi: 10.3109/03008200902855891.

[223] P. Chen, C. Hsu, K. Yang, C. Wu, and C. Wang, "The effects of negative pressure treatment on the extracellular matrix gene expression and protein production of fibroblasts," *Process Biochemistry*, vol. 50, no. 10, pp. 1662–1668, Oct. 2015, doi: 10.1016/j.procbio.2015.06.014.

[224] F. Lu *et al.*, "Microdeformation of Three-Dimensional Cultured Fibroblasts Induces Gene Expression and Morphological Changes," *Ann Plast Surg*, vol. 66, no. 3, pp. 296–300, Mar. 2011, doi: 10.1097/SAP.0b013e3181ea1e9b.

[225] "https://www.smith-nephew.com/education/resources/literature/us-wound-covid/pico/pico-7-hcp-manual/."

[226] C. Poon, "Measuring the density and viscosity of culture media for optimized computational fluid dynamics analysis of in vitro devices," *J Mech Behav Biomed Mater*, vol. 126, p. 105024, Feb. 2022, doi: 10.1016/j.jmbbm.2021.105024.

[227] B. P. Thampatty and J. H. Wang, “Mechanobiology of Fibroblasts,” in *Mechanosensitive Ion Channels*, A. Kamkin and I. Kiseleva, Eds., Dordrecht: Springer Netherlands, 2008, pp. 351–378. doi: 10.1007/978-1-4020-6426-5_16.

[228] E. Hadjipanayi, V. Mudera, and R. A. Brown, “Close dependence of fibroblast proliferation on collagen scaffold matrix stiffness,” *J Tissue Eng Regen Med*, vol. 3, no. 2, pp. 77–84, Feb. 2009, doi: 10.1002/term.136.

[229] V. Saxena, C.-W. Hwang, S. Huang, Q. Eichbaum, D. Ingber, and D. P. Orgill, “Vacuum-Assisted Closure: Microdeformations of Wounds and Cell Proliferation,” *Plast Reconstr Surg*, pp. 1086–1096, 2004, doi: 10.1097/01.PRS.0000135330.51408.97.

[230] A. Rahmani Del Bakhshayesh *et al.*, “Recent advances on biomedical applications of scaffolds in wound healing and dermal tissue engineering,” *Artif Cells Nanomed Biotechnol*, vol. 46, no. 4, pp. 691–705, May 2018, doi: 10.1080/21691401.2017.1349778.

[231] S. Amado, P. Morouço, Paula Pascoal-Faria, and N. Alves, *Biomaterials in Regenerative Medicine*. InTech, 2018. doi: 10.5772/66233.

[232] S. Böhm, C. Strauß, S. Stoiber, C. Kasper, and V. Charwat, “Impact of Source and Manufacturing of Collagen Matrices on Fibroblast Cell Growth and Platelet Aggregation,” *Materials*, vol. 10, no. 9, p. 1086, Sep. 2017, doi: 10.3390/ma10091086.

[233] B. A. Harley, J. H. Leung, E. C. C. M. Silva, and L. J. Gibson, “Mechanical characterization of collagen-glycosaminoglycan scaffolds,” *Acta Biomater*, vol. 3, no. 4, pp. 463–74, Jul. 2007, doi: 10.1016/j.actbio.2006.12.009.

[234] M. Sambasivam, R. White, and K. Cutting, “Exploring the role of polyurethane and polyvinyl alcohol foams in wound care,” in *Wound Healing Biomaterials*, Elsevier, 2016, pp. 251–260. doi: 10.1016/B978-1-78242-456-7.00012-X.

[235] C. Marmorat, A. Arinstein, N. Koifman, Y. Talmon, E. Zussman, and M. Rafailovich, “Cryo-Imaging of Hydrogels Supermolecular Structure,” *Sci Rep*, vol. 6, no. 1, p. 25495, May 2016, doi: 10.1038/srep25495.

[236] S. B. Qasim *et al.*, “Electrospinning of Chitosan-Based Solutions for Tissue Engineering and Regenerative Medicine,” *Int J Mol Sci*, vol. 19, no. 2, Feb. 2018, doi: 10.3390/IJMS19020407.

[237] R. Ghobeira, M. Asadian, C. Vercruysse, H. Declercq, N. De Geyter, and R. Morent, “Wide-ranging diameter scale of random and highly aligned PCL fibers electrospun

using controlled working parameters," *Polymer (Guildf)*, vol. 157, pp. 19–31, Nov. 2018, doi: 10.1016/j.polymer.2018.10.022.

[238] Ameer, PR, and Kasoju, "Strategies to Tune Electrospun Scaffold Porosity for Effective Cell Response in Tissue Engineering," *J Funct Biomater*, vol. 10, no. 3, p. 30, Jul. 2019, doi: 10.3390/jfb10030030.

[239] B. L. Farrugia, T. D. Brown, Z. Upton, D. W. Hutmacher, P. D. Dalton, and T. R. Dargaville, "Dermal fibroblast infiltration of poly(ε-caprolactone) scaffolds fabricated by melt electrospinning in a direct writing mode," *Biofabrication*, vol. 5, no. 2, p. 025001, Feb. 2013, doi: 10.1088/1758-5082/5/2/025001.

[240] E. García-Gareta, N. Ravindran, V. Sharma, S. Samizadeh, and J. F. Dye, "A Novel Multiparameter In Vitro Model of Three-Dimensional Cell Ingress Into Scaffolds for Dermal Reconstruction to Predict In Vivo Outcome," *Biores Open Access*, vol. 2, no. 6, pp. 412–420, Dec. 2013, doi: 10.1089/biores.2013.0043.

[241] F. J. O'Brien, B. A. Harley, M. A. Waller, I. V. Yannas, L. J. Gibson, and P. J. Prendergast, "The effect of pore size on permeability and cell attachment in collagen scaffolds for tissue engineering," *Technology and Health Care*, vol. 15, no. 1, pp. 3–17, Dec. 2006, doi: 10.3233/THC-2007-15102.

Appendix I

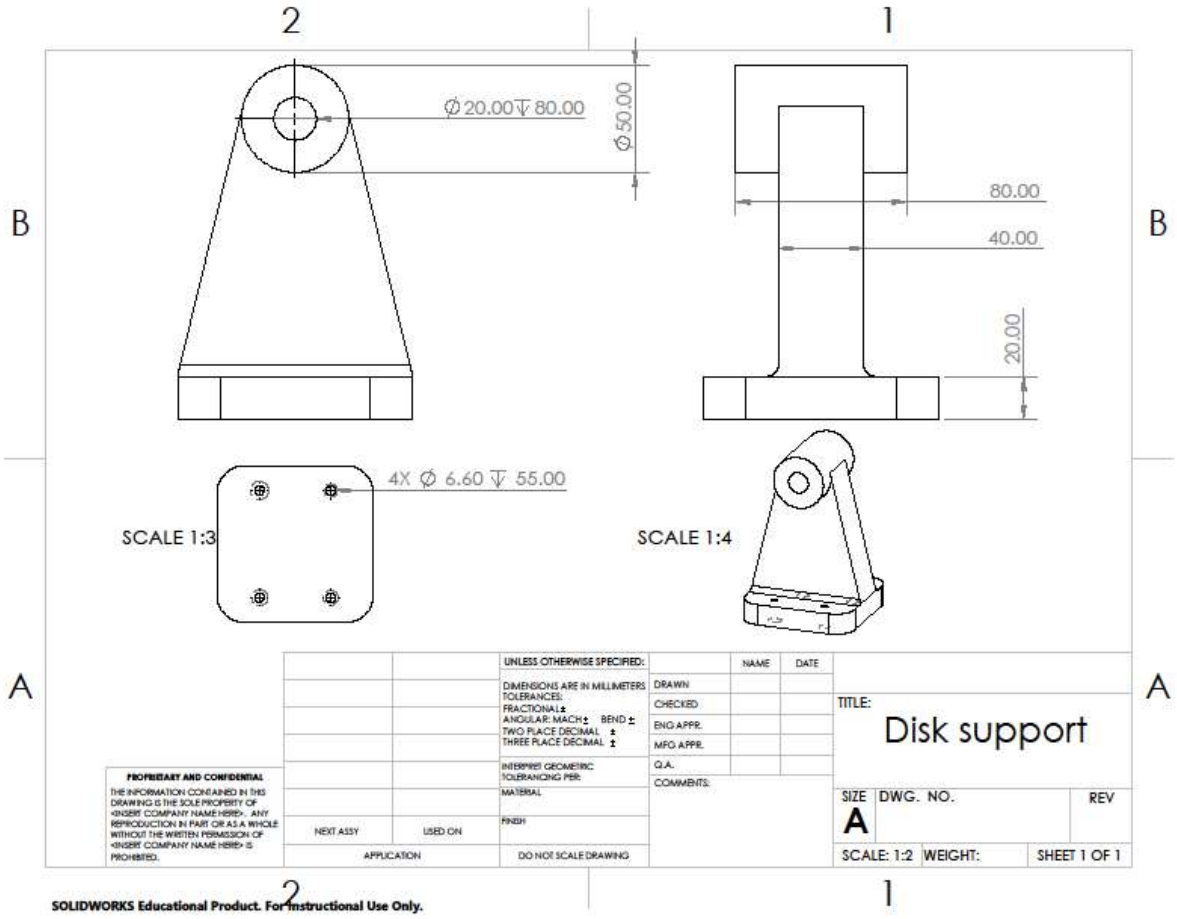
2
1
B
A
Ø 20.00 ↧ 80.00
Ø 50.00
80.00
40.00
20.00
4X Ø 6.60 ↧ 55.00
SCALE 1:3
SCALE 1:4
UNLESS OTHERWISE SPECIFIED:
DIMENSIONS ARE IN MILLIMETERS
TOLERANCES:
FRACTIONAL ±
ANGULAR: MACH ± BEND ±
TWO PLACE DECIMAL ±
THREE PLACE DECIMAL ±
INTERPRET GEOMETRIC TOLERANCING PER:
MATERIAL
FINISH
NEXT ASSY
USED ON
APPLICATION
DO NOT SCALE DRAWING
NAME
DATE
DRAWN
CHECKED
ENG APPR.
MFG APPR.
Q.A.
COMMENTS:
TITLE:
Disk support
SIZE
A
DWG. NO.
REV
SCALE: 1:2
WEIGHT:
SHEET 1 OF 1
PROPRIETARY AND CONFIDENTIAL
THE INFORMATION CONTAINED IN THIS DRAWING IS THE SOLE PROPERTY OF <INSERT COMPANY NAME HERE>. ANY REPRODUCTION IN PART OR AS A WHOLE WITHOUT THE WRITTEN PERMISSION OF <INSERT COMPANY NAME HERE> IS PROHIBITED.
SOLIDWORKS Educational Product. For Instructional Use Only.

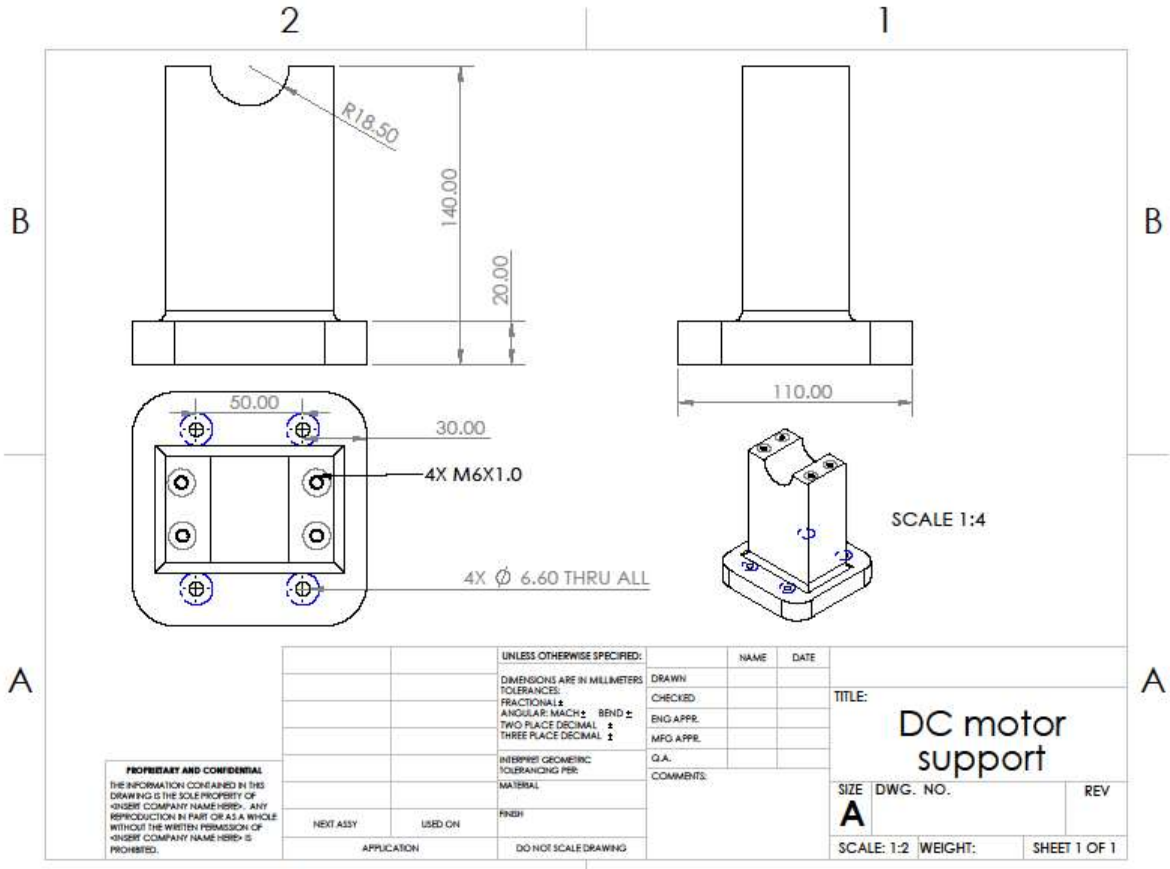

SOLIDWORKS Educational Product. For Instructional Use Only.

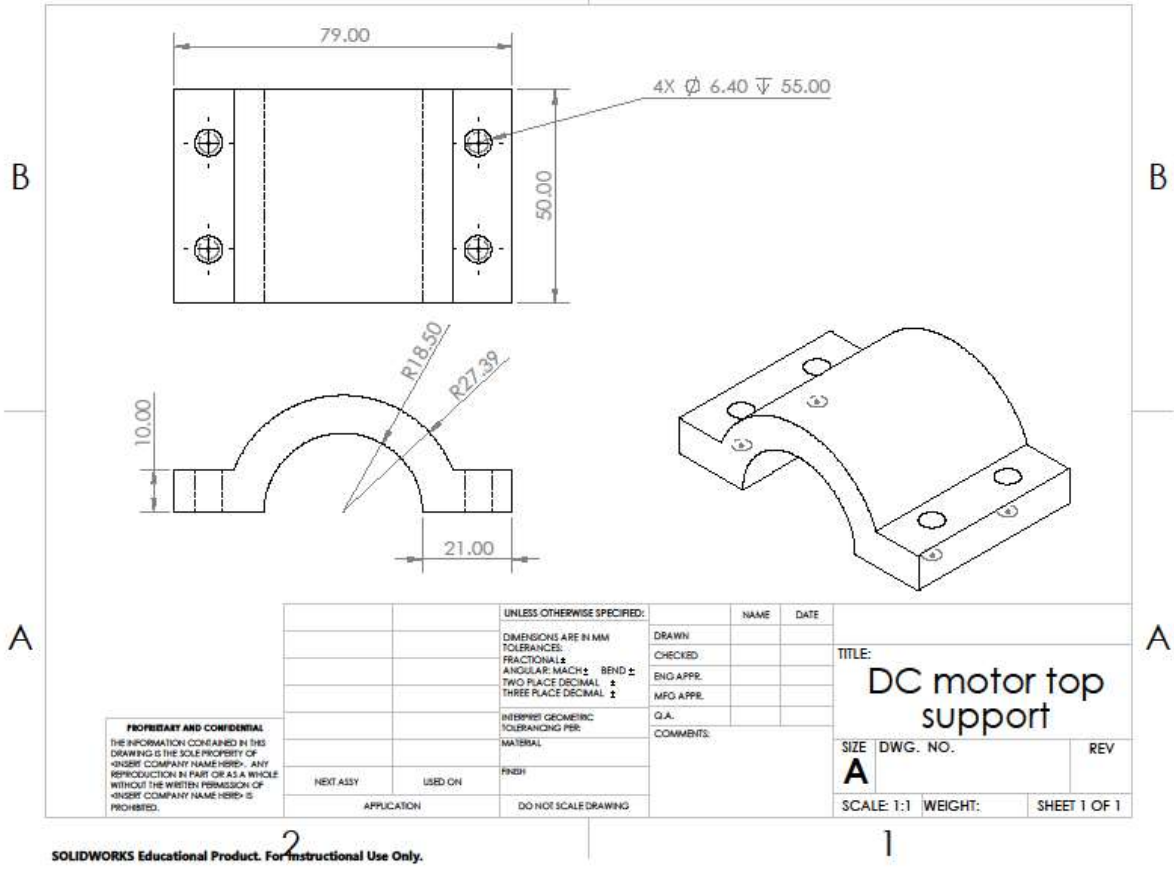

SOLIDWORKS Educational Product. For Instructional Use Only.

Appendix II

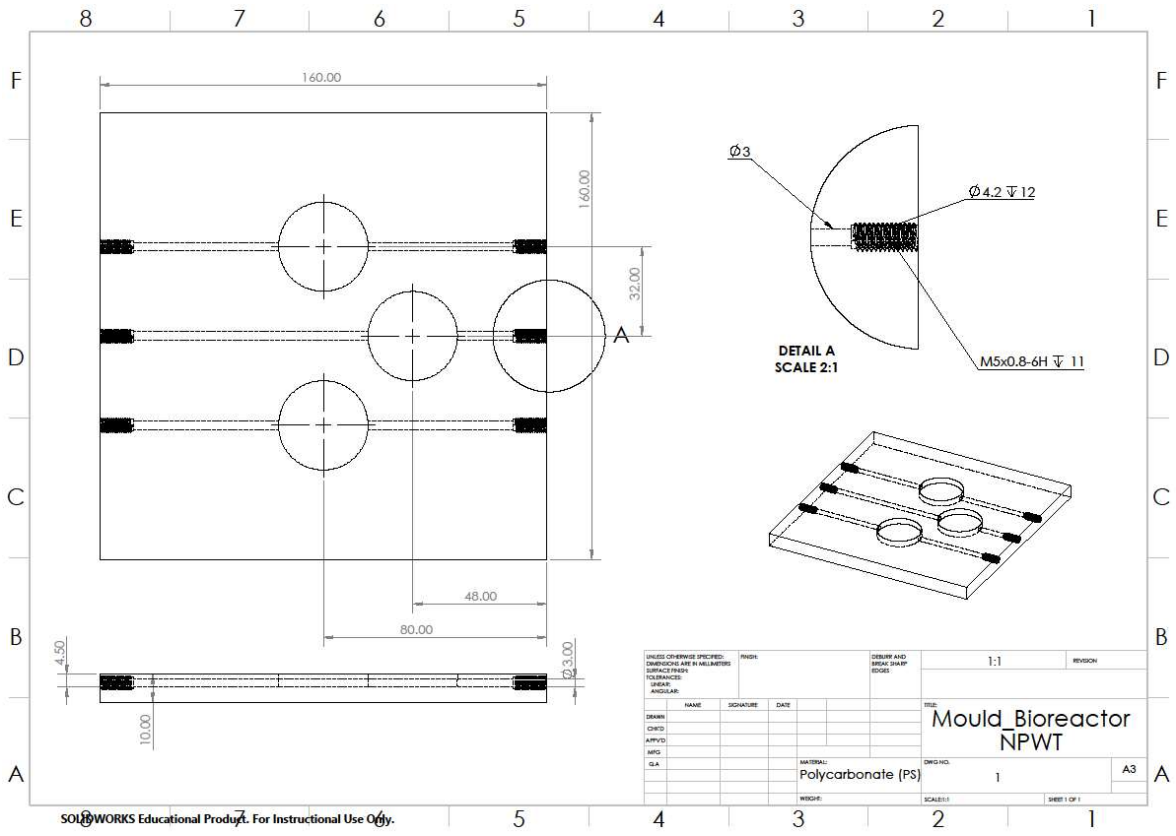
160.00
160.00
32.00
A
48.00
80.00
4.50
10.00
Ø3.00
Ø3
Ø4.2 ↧12
M5x0.8-6H ↧ 11
DETAIL A
SCALE 2:1
1:1
Mould_Bioreactor
NPWT
Polycarbonate (PS)
A3
SOLIDWORKS Educational Product. For Instructional Use Only.